THE STUDY OF CONVECTIVE HEAT TRANSFER FROM A ROTATING DISC WITH SPECIAL EMPHASIS ON THE EFFECTS OF DISTURBING THE BOUNDARY LAYER

by

Robin Wilfred Dennis

A Thesis Presented for the Degree of Doctor of Philosophy

At the University of Aston in Birmingham

January 1970

SUMMARY

Attempts to predict the operating temperatures of disc brakes have shown the need for an investigation into the heat transfer from a rotating disc when the airflow induced by rotation is disturbed in a number of ways, each linked with the conditions of the operating environment.

A survey of previous work revealed that a considerable body of work existed on the basic systems of a disc rotating in still air and a rectangular flat plate in a uniform stream, which aided the understanding of the effects of more complex flow systems on the heat transfer, such as were studied during this investigation.

Experiments were made with an electrically heated rotating disc; measurements were made of the surface temperature and heat input when steady state was reached, and the heat transfer coefficient calculated from these. Experimental data were found for the heat transfer from a disc rotating in still air and in an airflow parallel and adjacent to the disc surface. The effects of masking certain sectors of the disc were found in both of the environments just described. Finally, experiments were made with boundary layer tripping devices and jets of air directed at the disc surfaces to discover the effectiveness of these methods in increasing the heat transfer. The results from the disc rotating in still air agreed with measurements by previous workers and a prediction based on a combination of data for a rotating disc and a stationary surface achieved good correlation with data recorded with the disc rotating in an air crossflow. The other sections of work, with masked sectors, boundary layer trips and air jets, introduced flow patterns which affected the heat transfer in a complex manner. These effects were explained with the aid of flow visualization and general theoretical correlations obtained.

The experimental findings are used in a new approach to predict disc brake operating temperatures, giving reasonable correlation with experimental data from dynamometer tests on a disc brake.

ACKNOWLEDGEMENTS

The author would like to thank his supervisors, Professor A. J. Ede and Mr. C. Newstead, for their help and guidance and the Directors of Girling Limited for providing the research facilities.

CONTENTS

NOMENCLATURE

ROMAN LETTERS		Units
A	area	m^2
Ap	angle subtended by pad from disc centre, degree	
a,b,K,n	constants	
br	rotor thickness	m
Cp, Cv	specific heats, constant pressure, constant volume	$J/g^{\circ}K$
C	caliper horizontal width	m
Cm	moment coefficient (equation 3.02)	
D	caliper vertical height	m
E	energy	J
Em	thermocouple potential	mV
f	friction factor	
F,G,H	non-dimensional velocities	
	$F = u_r/\omega R, \quad G = u_t/\omega R, \quad H = u_z/\sqrt{\nu\omega}$	
h	heat transfer coefficient	W/m^2K
H*	ratio of δ^* to δ^{**}	
k	thermal conductivity	W/m K
K	quantity defined by equations 5.33, 5.34, 5.35	J/K
l	length of plate in direction of stream	m
lb	length of bell (figure 5.02)	m
L	mass of vehicle acting on brake	kg
m	mass of rotor	kg
N	rotational speed	rev/min
P	power	W
Q	rate of heat flow	W

RR	wheel rolling radius	m
R	radius	m
Ro	main disc outer radius	m
Ri	main disc inner radius	m
Rr	guard rim outer radius (applicable to experimental disc only).	m
s,q	functions of z in equation 2.07	
T	temperature	K
Tq	torque	N m
t	time increment	s
U	velocity of stream or vehicle	m/s
u	velocity in boundary layer	m/s
V	velocity of air jet	m/s
v_*	friction velocity = $\sqrt{\tau_w/\rho}$	m/s
x	length from leading edge of plate in direction of stream	m
X	z/δ	
y	distance from leading edge of plate to start of heated section	m
z	distance in normal direction from disc or plate surface	m

GREEK LETTERS

α	thermal diffusivity (k/ρ Cp)	m^2/s
β	volumetric coefficient of isobaric thermal expansion (T = abs. film temp)	$\simeq \frac{1}{T}$
δ	boundary layer thickness	m
δ^*	displacement boundary layer thickness (equation 2.33)	m
δ^{**}	momentum boundary layer thickness (equation 2.34)	m
ε	emissivity	

η	angle of yaw	degree
θ	temperature difference	K
μ	dynamic viscosity	$N\ s/m^2$
ν	kinematic viscosity	m^2/s
ξ	dimensionless axial distance from disc	$z\sqrt{\frac{\omega}{\nu}}$
ξ_δ	dimensionless boundary layer thickness	$\delta\sqrt{\frac{\omega}{\nu}}$
ρ	density	g/m^3
σ	Stefan-Boltzmann constant of radiation	$5.735 \times 10^{-8} W/m^2K^4$
τ	shear stress	N/m^2
ϕ	angle of sector	degree
ω	angular velocity of rotation	rad/s

SUBSCRIPTS

a	ambient condition
b	bulk (average across disc)
be	disc bell parameter
c	caliper parameter
couple, non-couple	appertaining to side of disc with thermocouples without thermocouples
d	disc rotor parameter
free	without external disturbances
forced	with forced convection
i	disc inner radius
in	insulating ring parameter
lin	lining parameter
L	based on overall plate length
m	average value
mo	disc mounting flange parameter
nat	with natural convection
o	disc outer radius

r,t,z	in radial, tangential or axial direction
rim	disc rim parameters
s	parameter of laminar sub-layer
scraper	conditions with scraper on disc
stationary wire	conditions with wire stationary near disc
T	Tufnol mounting
total	total amount
te	thermal boundary layer
w	property at surface or wall
x	property at distance x from leading edge of plate
∞	property distant from surface
1	at beginning of time increment
2	at end of time increment

DIMENSIONLESS GROUPS

Re_o	rotational Reynolds number			$\frac{\omega R_o^2}{\nu}$
Re_t	crossflow Reynolds number			$\frac{U R_o}{\nu}$
$Re_{x,R}$	local Reynolds number	$\frac{U x}{\nu}$	or	$\frac{\omega R^2}{\nu}$
Nu_o	mean Nusselt number	$\frac{h_m R_o}{k}$		
$Nu_{x,R}$	local Nusselt number	$\frac{hx}{k}$	or	$\frac{hR}{k}$
Pr	Prandtl number	$\frac{\nu}{\alpha}$		
Gr	Grashof number	$\frac{g\beta l^3 \Theta}{\nu^2}$		
St	Stanton number	$\frac{Nu}{RePr}$		

LIST OF FIGURES

Chapter 1

INTRODUCTION

1.1 FLUID MECHANICS AND CONVECTIVE HEAT TRANSFER

Convective heat transfer is the process by which heat is transferred between a surface and the fluid in which it is immersed; it is actually conduction in a fluid, the particles of which are in relative motion. Therefore, the analysis of convective heat transfer is fundamentally allied to the study of fluid mechanics; the study of relative motion within the fluid. The flow around a body may be induced by external means, termed forced convection, or may be produced by the temperature difference between body and fluid, which causes buoyancy forces to appear due to the change in density of the fluid, called natural convection.

A summary of some of the pioneering works in this field may make a useful contribution to the understanding of present day methods of approach. The hydrodynamic equations of flow of a compressible viscous fluid were developed by Navier in 1827 and Stokes in 1845, after whom the equations were named. These were not of immediate use in the analysis of fluid mechanics due to the enormous mathematical difficulties of their solution. Around 1870 Reynolds and Nusselt made considerable advances in the field; Reynolds by recognising the two basic types of flow, laminar and turbulent, and Nusselt developed the extremely useful tool of dimensional analysis. At low stream velocities it was observed that the flow travelled in streamlines parallel to one another, with little movement of particles across the stream, called laminar flow.

Then as speed increased the flow became unstable, and eddies formed in the stream causing the fluid particles to move through the stream with a random motion, called turbulent flow.

The first approach to an analysis of the mechanism of convective heat transfer was made by Reynolds in 1874, when he presented his now famous analogy of friction to heat transfer, which enabled a theoretical or empirical description of the friction due to flow over a body to be used to predict the heat transfer. However, the principles of flow over a surface were not fully understood until Prandtl presented his boundary layer theory in 1904. This introduced the important concept that the friction and heat transfer were primarily determined by the behaviour of the fluid in a very small layer adjacent to the surface, wherein the velocity changed rapidly from the stream velocity to that of the surface. This theory allowed the Navier-Stokes equations to be simplified and solved, and Reynolds analogy was modified by Taylor and Prandtl to take account of the boundary layer. Reynolds analogy was then theoretically valid only for fluid of Prandtl number of unity, when the thermal and momentum boundary layers were identical, but in practice reasonable accuracy was obtained in the range $0.5 < Pr < 5$.

The analysis to date had achieved reasonable correlation with experimental data for the friction and velocity distribution for laminar flow, but was less successful with turbulent flow. Prandtl and Von Karman produced a more rigid mathematical analysis for turbulent flow where an intermediate eddy current layer, which had previously been neglected, was allowed for.

The initial work was concerned with the behaviour of flow and heat transfer in pipes and then Von Karman solved the Navier-Stokes equations, after applying Prandtl's boundary layer approximations, for a flat plate in a stream and a rotating disc, in 1921.

A considerable number of later workers presented analyses for the heat transfer by introducing the energy or heat flow equation and solving it in conjunction with the Navier-Stokes equations, or by a less fundamental method, by taking an empirical value for the velocity distribution, substituting it into the energy equation, and integrating to derive the heat transfer coefficient, usually called the Integral method.

From these beginnings a coherent body of knowledge in the field of fluid mechanics and convective heat transfer has developed, and it is worthy of note that this has only taken place in the present century.

1.2 THE ROTATING DISC

The disc and cylinder formed the basis of the study of rotating systems and have been the subject of investigation for a number of years. The flow over a rotating disc was first analysed in 1921, but it was not until much later, in 1948, that Wagner made an attempt to predict the heat transfer. Therefore the processes of fluid flow and heat transfer are well understood, although research into their behaviour under many conditions is by no means complete. The rotating disc plays an important role in the field of forced convection heat transfer as, like the flat plate, an exact solution of the Navier-Stokes equations, with the Prandtl boundary layer approximations, can be found for the fluid flow and heat transfer, permitting comparison with, and evaluation of, less fundamental methods, such as Reynolds analogy or Integral methods.

The experimental measurement of heat transfer and velocity profiles on a rotating disc is not prone to the disturbances encountered on many other systems, such as the flat plate in a stream, and therefore the system is again useful for correlation of experimental data to the various methods of theoretical analysis.

The present study of the heat transfer from a rotating disc was implemented due to the fairly recent introduction of disc brakes as a means of retarding rotating machinery and vehicles, which introduced the disc into environments which had not previously been studied. The behaviour of the flow and heat transfer of a rotating disc has up to now been important only in the fields of turbines and electric machines, where the environment has usually produced conditions symmetric about the rotational axis of the disc, which is not the case for a brake disc.

1.3 THE DISC BRAKE

A disc brake consists of a disc, attached to a rotating component which is to be retarded, and a means of applying one pad of friction material to each side of the disc. The latter device is called a caliper, which usually comprises a housing, bolted to a solid unit to take the torque, and a mechanical or hydraulic means of clamping the two pads onto the disc.

If a prediction could be made of the suitability of a disc brake for a particular application, whilst still in the design stage, a substantial reduction of the development time and cost could be made. To do this it is necessary to predict disc operating temperatures, which affect disc life, lining friction level and pad wear life. A disc absorbs energy created by friction between the pad and disc and subsequently dissipates it by conduction, convection and radiation. Sufficient knowledge exists on conduction and radiation to allow the heat loss along those routes to be calculated, but no data is available on the convective dissipation from a disc, except in still air. Heat transfer coefficients are needed for a disc mounted on a moving vehicle, creating an airflow across it, and with a caliper mounted on the disc, which disturbs the airflow and covers some of the surface.

1.4 PRESENT WORK

The developments just described led to the present investigation of the convective heat transfer from a rotating disc in an air crossflow and with simulated calipers on it. In addition it is desirable to increase the heat transfer from the disc in order to increase the energy absorption or lower the surface temperatures of disc brakes. Thus the effects of disturbing the boundary layer to cause premature turbulent flow, and directing jets of air at the disc have been investigated.

The results of these experiments have been used in a prediction of disc brake operating temperatures, allowing for dissipation of heat from the disc during the braking period. This is of importance during long stops of low energy absorption rate.

Chapter 2

PREVIOUS WORK

2.1 INTRODUCTION

Research into the fluid flow and heat transfer of two systems, the rotating disc and the flat plate in a stream, is of importance to the present work. In both cases early papers generally concentrated on the flow of fluid around the bodies, as this information was necessary before well directed investigations into the heat transfer could be made, a relationship between the two having been established by Reynolds in the early part of this century.

The first publications concerned with a rotating disc dealt with the fluid flow and heat transfer in still air, where flow is created by rotation of the disc only. No temperature difference is needed for this flow to exist and hence it is designated forced convection. As there are a large number of these papers they have been divided into the convenient sections of laminar and turbulent flow to be surveyed. Later papers investigated deviations from the basic system by looking at the effects of forced axial flow, nearby stationary and rotating planes, and flow at the rim, some of which are included in the survey.

Only a small selection of relevant publications on the heat transfer from a flat plate will be described, as this subject is now amply treated in most standard texts. In addition to these, some papers on the effect of separated regions of flow have been studied.

The bibliography is to be found at the end of the thesis. It is referenced in this chapter by the number in square brackets following the name of the author. The bibliography is grouped into areas of

investigation to facilitate further study on a particular topic, whereas in the text the papers are described in historical order.

2.2 ROTATING DISC IN STILL AIR

Two comprehensive surveys of the heat transfer and fluid flow behaviour of a rotating disc have been published, one by Dorfman {1}, and the other by Kreith {2}. These cover much of the work which will be described here, although the survey by Dorfman, 1963, dealt more exclusively with Russian research. Dorfman describes investigations into the heat transfer and hydrodynamic resistance of a rotating disc with laminar and turbulent flow, with a forced axial flow, flow in a confined space and the effects of a viscous fluid. Kreith gave a survey of convective heat transfer in rotating systems, one of which is the disc, in 1968.

LAMINAR FLOW

A considerable body of work, both theoretical and experimental, has been devoted to the study of the flow and heat transfer characteristics of the rotating disc under laminar flow conditions. As in most branches of convection, the basic feature of the theoretical work is the assumption that the heat transfer has no effect on the flow pattern; the fluid flow equations can accordingly be solved independently, and the velocity distribution obtained. Fluid flow data are then fed into the heat flow equation, which is solved to give the temperature distribution. Heat transfer and drag can be deduced from the results, the former being presented in the usual Nusselt equation form.

$$Nu = K\ Re^{a}\ Pr^{b} \qquad (2.01)$$

where K, a and b are constants. Since the heat flow part of the problem can be separated from the fluid flow part, useful information can be

obtained from a number of papers which deal only with flow under isothermal conditions.

Papers are presented which give theoretical predictions of the heat transfer throughout the range of Prandtl numbers, but the majority of the experiments have been made in air, others have used a mass transfer technique and one was made in water.

Survey

The starting point of the theoretical work is to be found in a paper by von Karman {3} , published in 1921. He set up the basic Navier-Stokes equations for flow on a steadily rotating, isothermal disc, together with the continuity equation, which were then reduced to three simultaneous non-dimensional differential equations. This system represented a rare case in which the equations could be solved without neglecting terms. The appropriate boundary conditions, one of which assumed that the radial and tangential velocities at the edge of the boundary layer were zero, were used to give the velocity profiles within the boundary layer, and the drag coefficient. The solution, found by the substitution of an approximate series expansion, gave the dimensionless velocity components shown in figure 2.01*.

Von Karman noted that the axial inflow velocity u_z tended to a finite limiting value as the edge of the boundary layer was approached, i.e. as $z \to \delta$, so that when $z \geqslant \delta$

$$u_z = 0.708 \sqrt{\nu\omega} \qquad (2.02)$$

This represented a steady stream of air drawn axially towards the disc, over the whole surface, to replace the air thrown off radially by the rotation. The solution also indicated another important feature of the

* The figures are to be found on the page immediately following the first place of reference

FIGURE 2.01

Theoretical Equations of Laminar Velocity Profiles on a Rotating Disc in Still Air

Karman [3]

$$F = a\frac{\xi}{\xi_\delta}\left(1-\frac{\xi}{\xi_\delta}\right)^2\left(1+2\frac{\xi}{\xi_\delta}\right) - \frac{1}{2}\left(\frac{\xi}{\xi_\delta}\right)^2\left(1-\frac{\xi}{\xi_\delta}\right)^2$$

$a = 1.026$

$\xi_\delta = 2.58$

$H_\infty = -0.708$

$$G = \frac{1}{2}\left(2+\frac{\xi}{\xi_\delta}\right)\left(1-\frac{\xi}{\xi_\delta}\right)$$

$$H = 2\xi\left[0.31\left(\frac{\xi}{\xi_\delta}\right)^4 - 0.52\left(\frac{\xi}{\xi_\delta}\right)^3 - 0.17\left(\frac{\xi}{\xi_\delta}\right)^2 + 0.51\frac{\xi}{\xi_\delta}\right]$$

Cochran [4] corrected from Karman

$a = 0.19466$

$\xi_\delta = 2.79$

$H_\infty = -0.55$

$$F = a\,\xi_\delta\left(1-\frac{\xi}{\xi_\delta}\right)^2\left(\xi+\frac{2}{\xi_\delta}\right) - \frac{\xi^2}{2}\left(1-\frac{\xi}{\xi_\delta}\right)^2$$

$$G = \left(1-\frac{\xi}{\xi_\delta}\right)^2\left(1+\frac{\xi}{2\,\xi_\delta}\right)$$

$$H = -\left[a\,\xi_\delta\,\xi^2 - \frac{\xi^3}{3} + \frac{1}{2}\frac{\xi^4}{\xi_\delta}(1-3a) + \frac{2}{5}\frac{\xi^5}{\xi_\delta^2}\left(2a-\frac{1}{2}\right)\right]$$

flow on a rotating disc, namely that the boundary layer thickness is independent of the radial distance R. A comparison of Karman's velocity profiles with those developed and measured later is made in figures 2.02, 3, 4, and 5. The boundary layer thickness may be determined from the axial distance at which the radial and tangential components of the velocity of the fluid return to zero, i.e. $\zeta = 2.8$.

The next step forward came, 13 years later, from Cochran {4} in 1934. He examined the equations developed by von Karman and confirmed the correctness of the method, but found a numerical error in the solution, and gave the modified results for the dimensionless velocity profiles as shown in figure 2.01. He also presented an exact numerical solution of the Navier-Stokes and continuity equations which did not bring the velocities to zero at the edge of the boundary layer, but gave two differential systems, one for inside and the other for outside the boundary layer, and obtained a continuous solution for both sets. The resultant velocity profiles are compared with those of von Karman in figures 2.02, 3, 4 and 5, where significant differences can be seen between them, the most marked being the value of the angle of yaw distant from the disc. Von Karman found that this became zero at the boundary layer edge, whilst Cochran brought it to a constant finite value of 35°.

In 1948 Wagner {13} made the first theoretical estimation of the heat transfer from a rotating disc. He resolved the general equation of steady state heat balance for a fluid in motion to that for a rotating disc, giving

$$\alpha \frac{d^2\theta}{dz} - u_z \frac{d\theta}{dz} = 0 \qquad (2.03)$$

Integrating twice gives the temperature distribution in the boundary layer, and the heat transfer coefficient was found from the temperature gradient at the surface as

$$h = \frac{K}{\int_0^{\infty} \exp\left[\frac{1}{a}\int_0^z u_z dz\right] dz} \qquad (2.04)$$

The expression for u_z derived by von Karman, which consisted of two equations, one for inside the boundary layer, and the other for outside,

FIGURE 2.02

Laminar Axial Velocity Profiles

on a Rotating Disc in Still Air

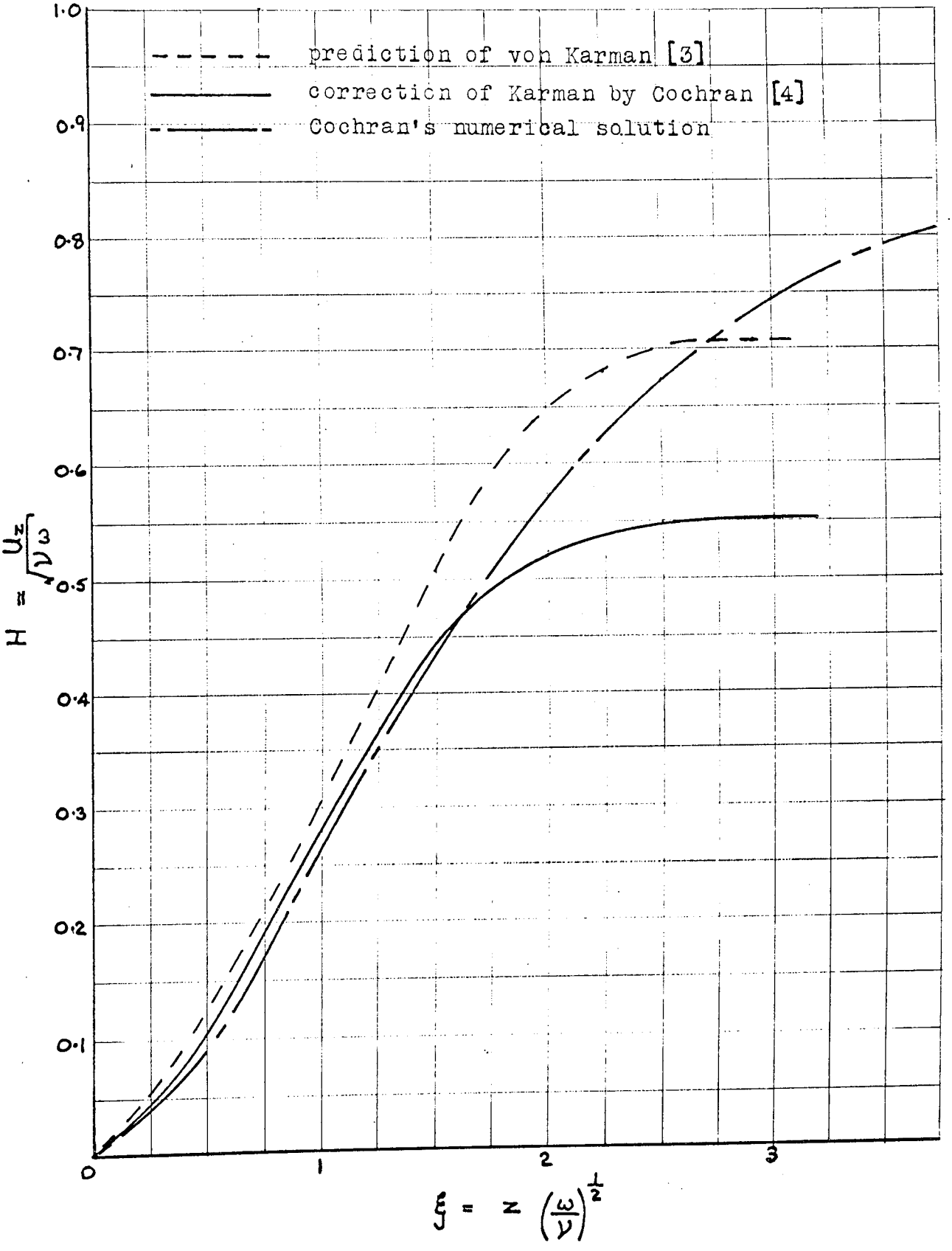

FIGURE 2.03

Laminar Radial Velocity Profile

on a Rotating Disc in Still Air

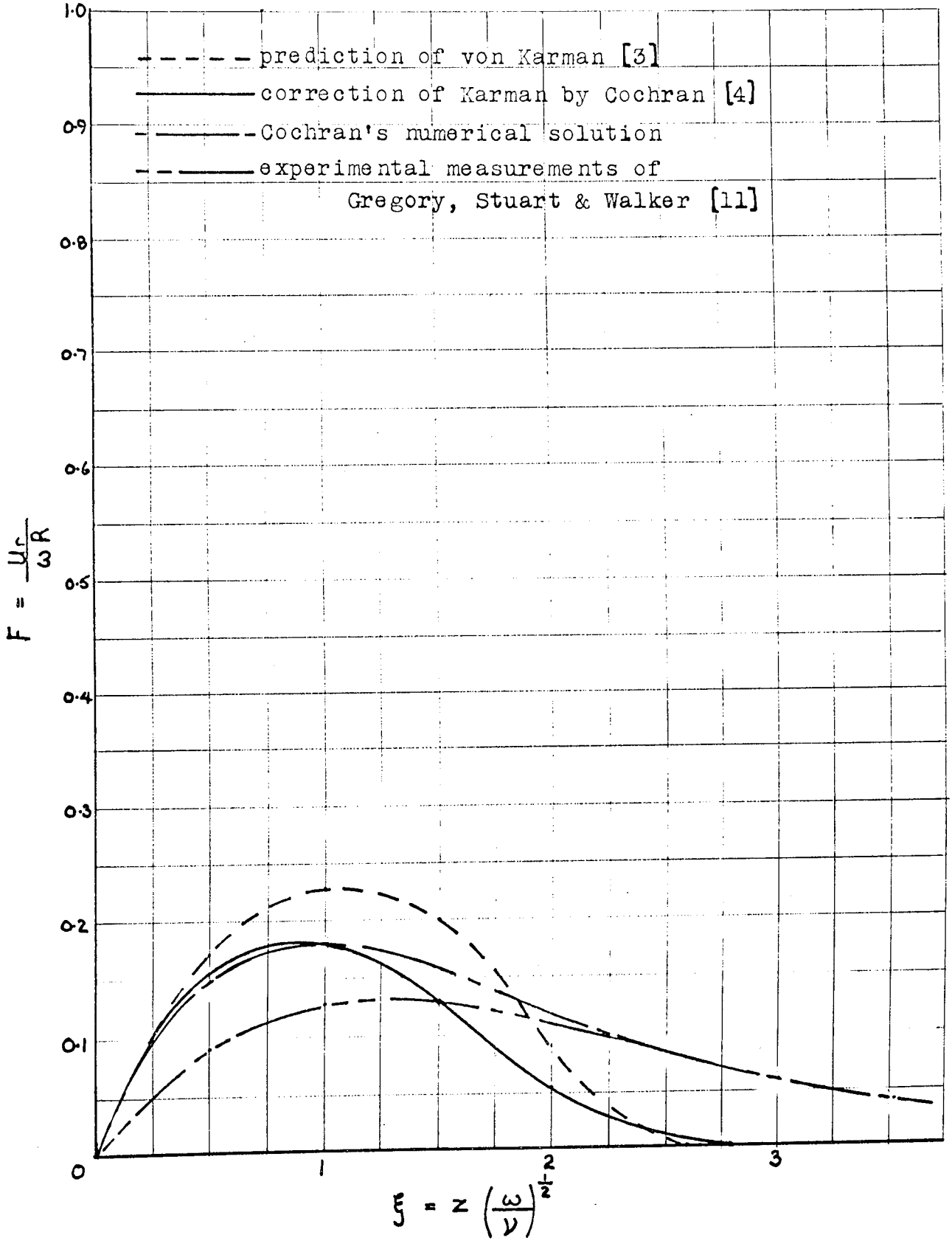

FIGURE 2.04

Laminar Tangential Velocity Profile on a Rotating Disc in Still Air

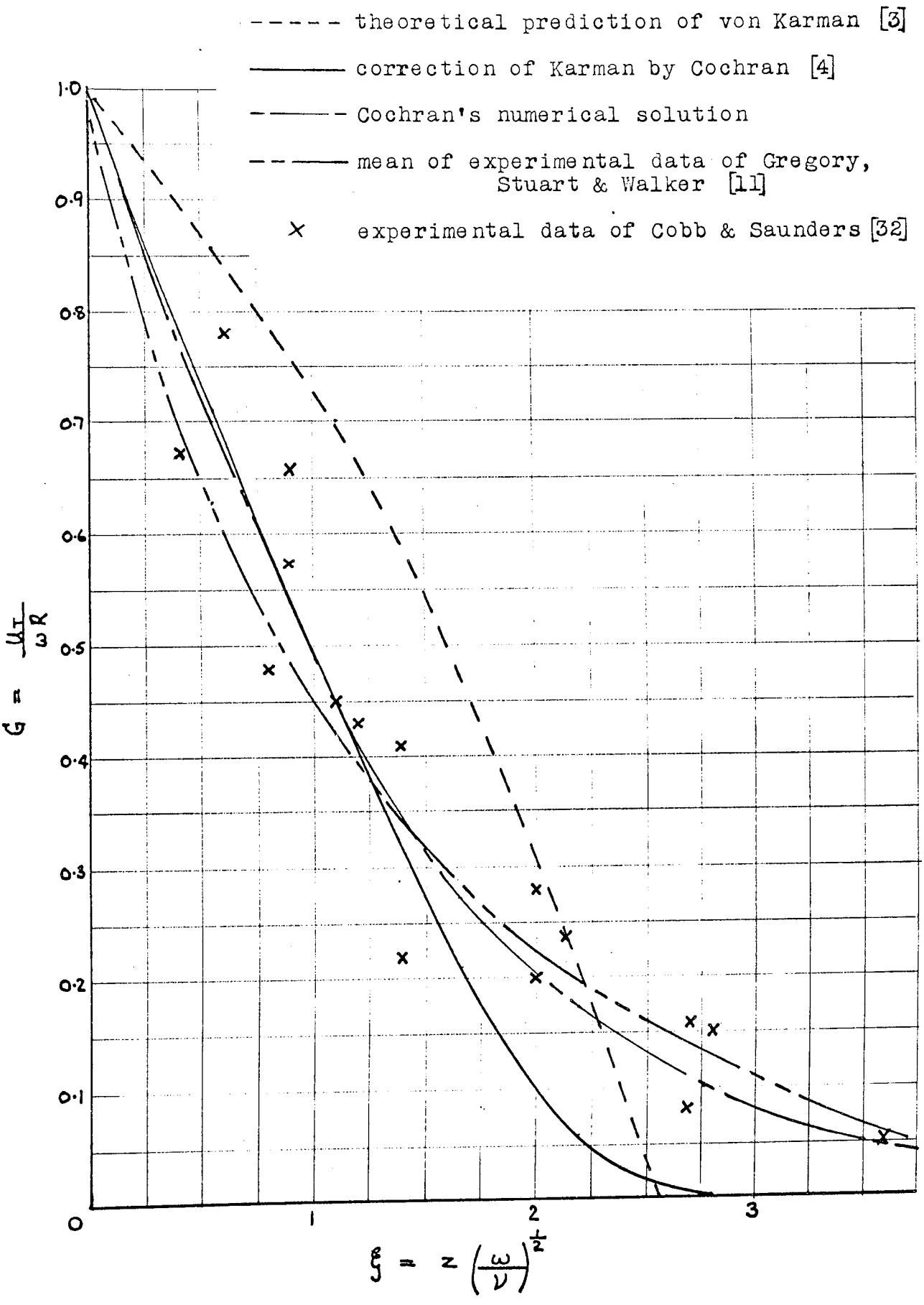

FIGURE 2.05

Angle of Yaw in the Laminar Region on a Rotating Disc in Still Air

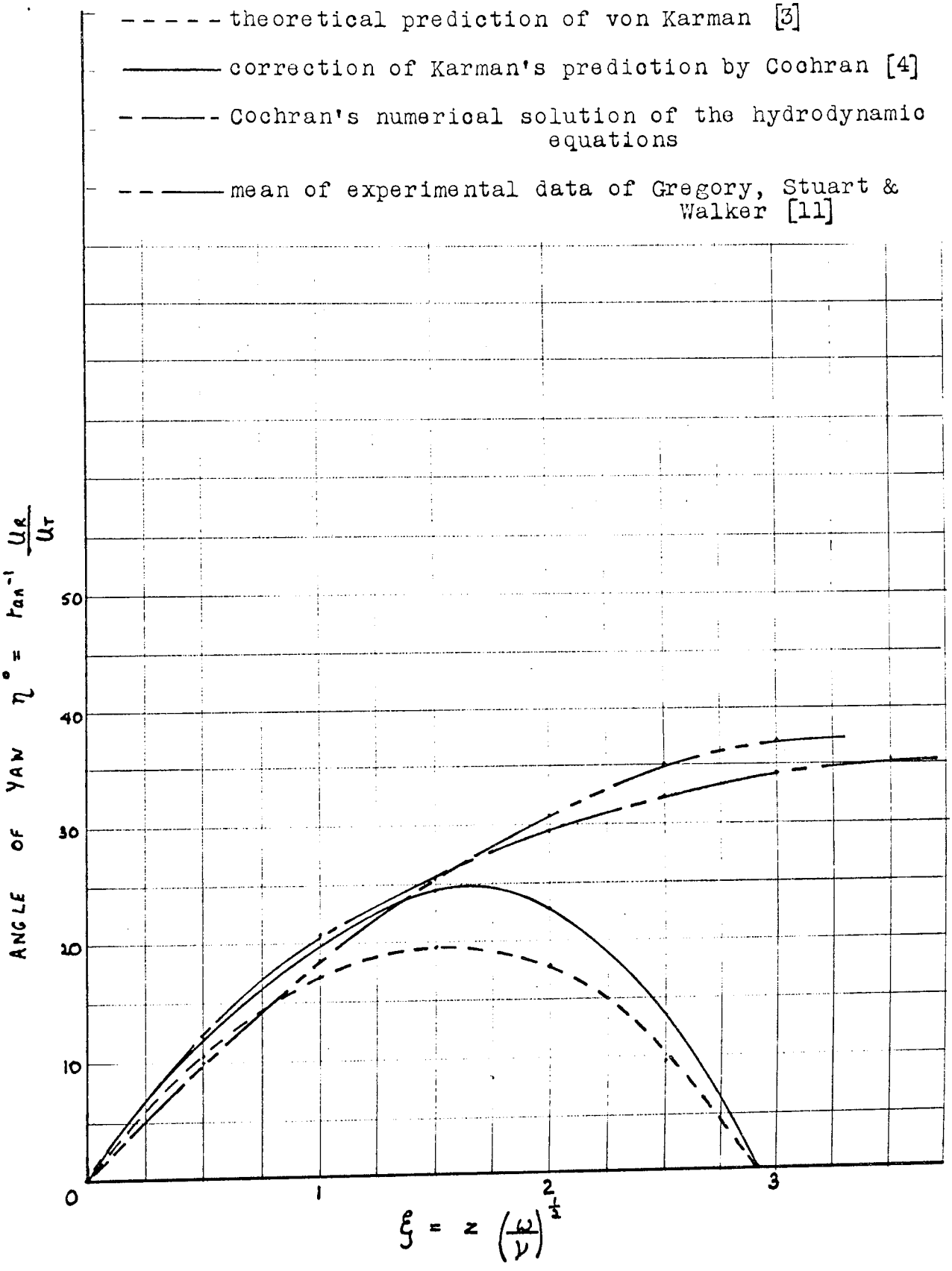

was substituted in equation 2.04. This was then solved numerically to give the relation between the Nusselt and Reynolds numbers, for a Prandtl number of 0.74, as

$$Nu_o = 0.339\ Re_o^{0.5} \qquad (2.05)$$

The solution was repeated by the author with the method shown in appendix I, but the result disagreed with that of Wagner giving

$$Nu_o = 0.389\ Re_o^{0.5} \qquad (2.06)$$

The same expression 2.04 was presented by Kreith, Taylor & Chong {34}, who solved it for a Prandtl number of 2.4. The author used the same method to check their solution as used for that of Wagner and agreed with the result of Kreith, et.al., supporting the result of equation 2.06.

Millsaps & Pohlhausen {15}, 1951, predicted the heat transfer in fluids of Prandtl number from 0.5 to 10, by using the non-dimensional differential equations of heat transfer in conjunction with the hydrodynamic equations already analysed by Cochran {4} to fully describe the thermal system. They obtained the heat transfer equations by assuming that the temperature distribution followed the expression

$$T = R^2 s(z) + q(z) + T_\infty \qquad (2.07)$$

which was substituted for T in the energy equation for the steady motion of an incompressible fluid. The differential equations were then solved by a numerical technique to give the temperature profile within the boundary layer and the heat transfer coefficient. The latter was found to vary slightly with radius, although this was so small that it could be neglected, giving the heat transfer, for Pr=0.72, as

$$Nu_o = 0.28\ Re_o^{0.5} \qquad (2.08)$$

Millsaps & Pohlhausen use a modified Prandtl number in which the specific heat at constant volume was used instead of the specific heat at constant pressure. The reason for this is not clear, but may be because their equations are concerned with viscous dissipation (heat generation due to shear of the fluid within the boundary layer). The constant pressure specific heat is more appropriate to a boundary layer

as it is not constrained in volume, and was subsequently used by Wagner and later workers. Using the method of Millsaps & Pohlhausen with the constant pressure specific heat gives the relation

$$Nu_o = 0.35\ Re_o^{0.5} \qquad (2.09)$$

The temperature profile calculated by Millsaps & Pohlhausen is shown in figure 2.06. Their prediction of the heat transfer, valid in the range of Prandtl number from 0.5 to 10, is plotted in figure 2.07.

In 1954 Young {31} made the first experimental measurements of the heat transfer from a rotating disc in still air. Working with a horizontal disc, insulated on the underside, and taking measurements from the top surface, he found that natural convection affected the heat transfer up to a Reynolds number of 40,000. Beyond this, up to a Reynolds number of 90,000, the heat transfer depended on rotational speed only. In the region affected by natural convection his results differed considerably from the heat transfer predicted by Wagner, whose equation assumed zero heat transfer at zero rotation, hence taking no account of natural convection.

Young obtained the following results by experiment

$$Re_o > 40{,}000 \qquad h = 0.35\omega^{0.38} \qquad (2.10)$$

$$Re_o < 40{,}000 \qquad h = \left[0.195\left(\frac{1-Re_o}{40{,}000}\right)\theta^{0.42} + 0.35\ \frac{Re_o}{40{,}000}\ \omega^{0.38}\right] \times \left[1 - 2.6\ \frac{Re_o}{40{,}000}\ \log_{10}\frac{Re_o}{40{,}000}\right] \qquad (2.11)$$

where h is in $\frac{B.Th.U.}{h\ ft^2\ ^oF}$, ω in r.p.m. and θ in ^oF.

Due to the variation of surface speed with radius, the natural convection heat transfer had a greater effect on smaller radii and hence the heat flux varied across the surface. Young allowed for this by having a series of concentric heaters in the disc which were adjusted to give a uniform surface temperature, this being measured from the resistance of the heater wires. He did not take readings very far into the laminar region as the maximum Reynolds number was 90,000, and later

FIGURE 2.06

Laminar Flow Temperature Profile

on a Rotating Disc in Still Air

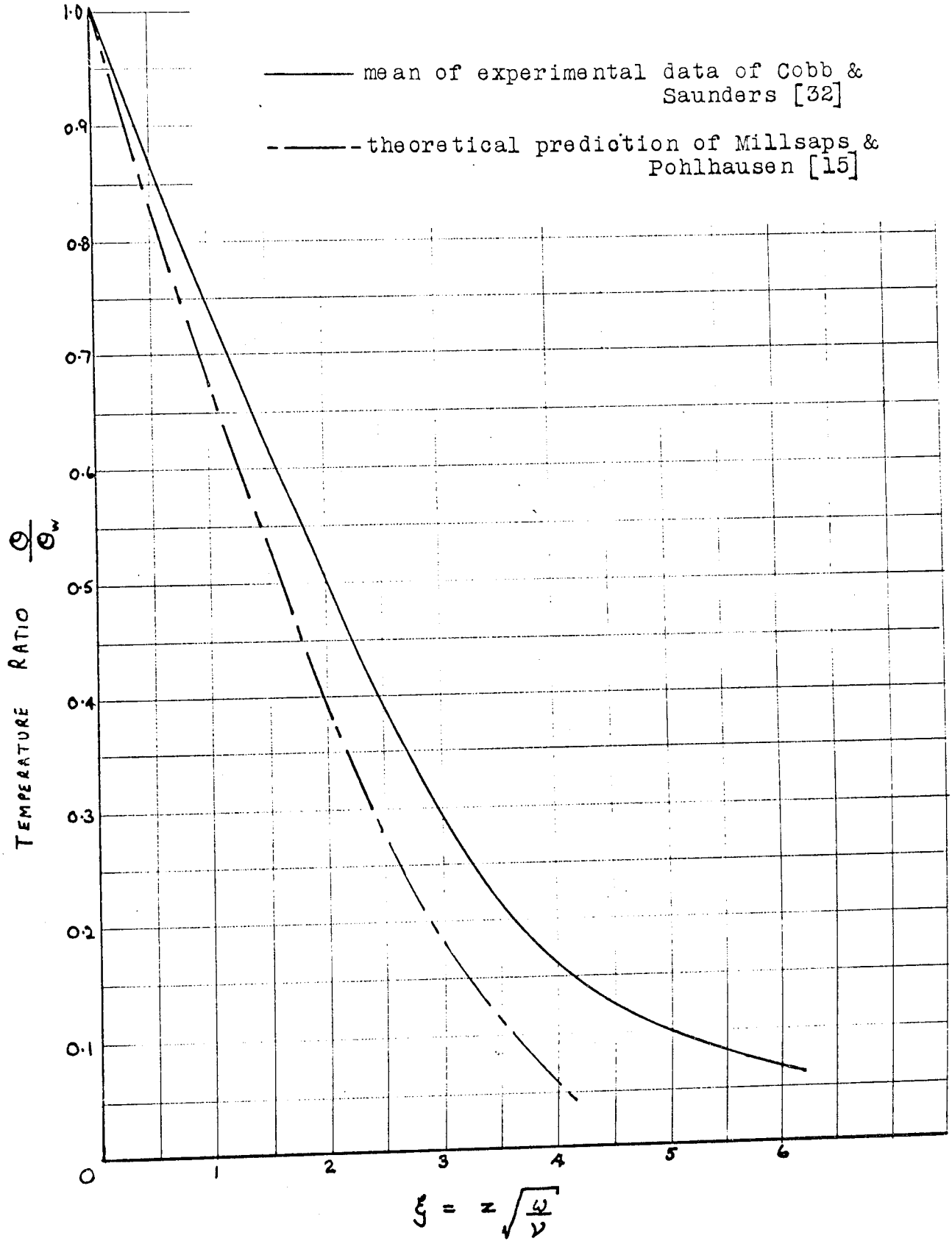

workers found that transition to turbulent flow occurred at

$Re_o = 240{,}000.$

In addition, Young observed that a more accurate result could be obtained from Wagner's {13} analysis if it were calculated at a Prandtl number of 0.70 instead of 0.74 and if the velocity profiles of Karman {3}, corrected by Cochran {4} were used. This gave the result

$$Nu_o = 0.333\ Re_o^{0.5} \tag{2.12}$$

The author had independently made this observation and derived the result, by the method shown in appendix 2.

$$Nu_o = 0.318\ Re_o^{0.5} \tag{2.13}$$

For comparison with other predictions the author also calculated the heat transfer at Prandtl numbers from 0.1 to 100, and the result is plotted in figure 2.07. The discrepancy between equations 2.12 and 2.13 of only 5%, was probably caused by insufficient accuracy in the values of the velocity profile used in one or both of the methods.

Cobb & Saunders {32}, 1956, made experimental measurements of the heat transfer from a vertical disc rotating in still air, throughout the range of laminar flow, and into the turbulent region. They used a single heater in the main disc, providing a uniform heat flux which, as the heat transfer coefficient is independent of radius in the laminar region, gave a uniform surface temperature. Outside this range, the high thermal conductivity of the aluminium disc was sufficient to maintain an adequately uniform surface temperature. Cobb and Saunders did not make such a detailed investigation of natural convection effects as Young, but they did verify that it affected the heat transfer at Reynolds numbers below 40,000. The disc surface temperature was measured with embedded thermocouples and the heat loss from the rim compensated for by having a separate heater around it, adjustable to give zero heat flow from the rim of the main disc. The experimental results in the laminar region followed the line

FIGURE 2.07

Laminar Heat Transfer From a Rotating Disc in Still Air

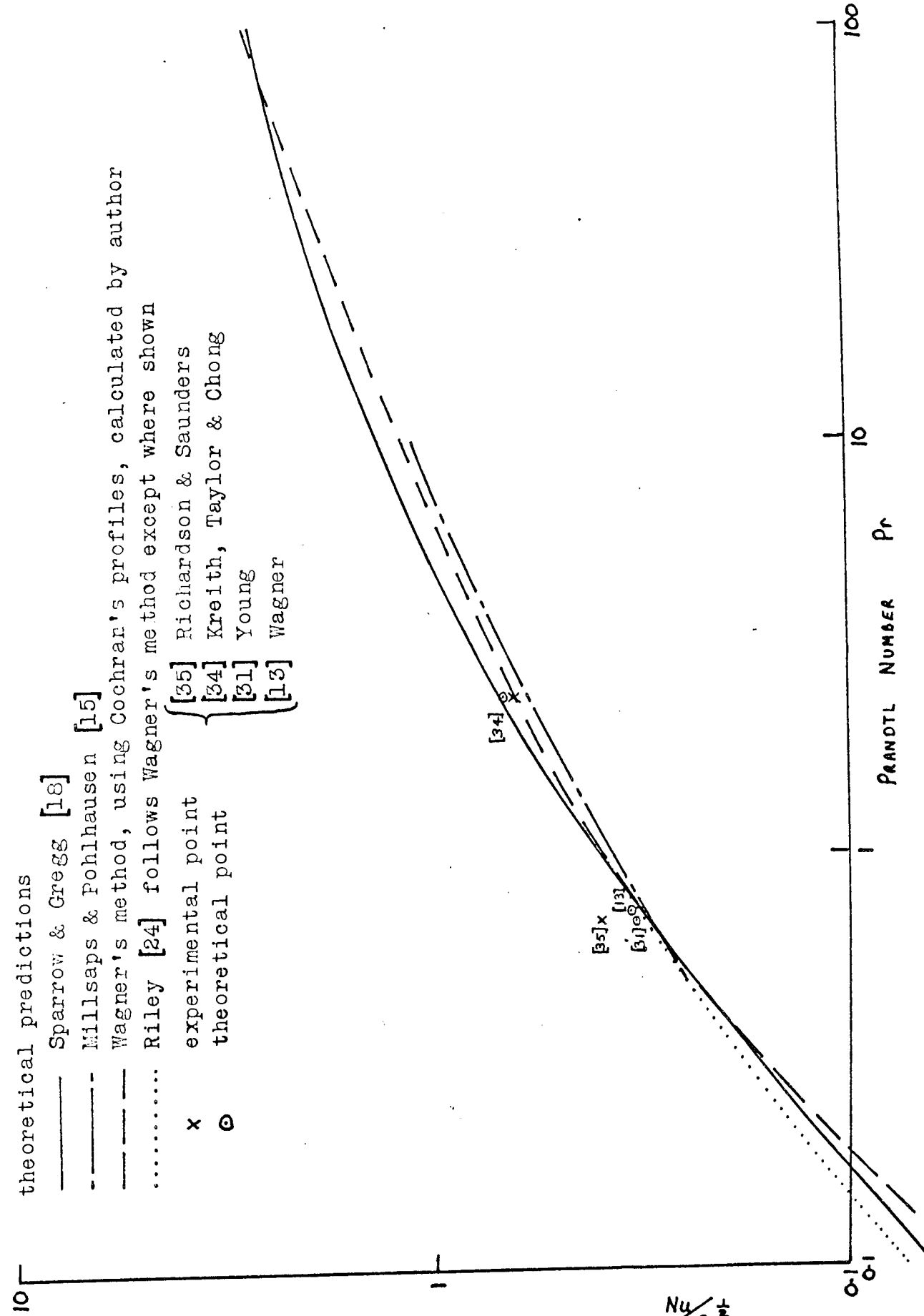

$$Nu_o = 0.36\ Re_o^{0.5} \qquad (2.14)$$

but later work by Richardson & Saunders {35} on the same rig revealed that a 10% error had been made in the measurement of the ambient temperature, amending the result to

$$Nu_o = 0.4\ Re_o^{0.5} \qquad (2.15)$$

Cobb & Saunders also made measurements of the tangential velocity profile and temperature profile, which are reproduced in figures 2.04 and 6, in comparison with those of other workers. The radial profile was not measured due to the velocities involved being too small for accurate results with their equipment. The tangential velocity measurements were well scattered around the prediction of Cochran and the temperatures were higher than predicted by Millsaps & Pohlhausen.

In the same year Gregory, Stuart & Walker {11} described further experiments into the fluid flow around a rotating disc. They made careful measurements of the angle of yaw and the total velocity and from these they calculated the radial and tangential profiles, which have been plotted here in figures 2.03 and 4. Close agreement was reached with the prediction of Cochran for the tangential profile, although there is some discrepancy in the angle of yaw measurements, which Gregory, Stuart & Walker thought due to the possibility that the two tubes of the yawmeter were not aligned to sufficient accuracy. The tangential velocity measurements were taken at two different radii, but with the results plotted non-dimensionally they fell on the same line, proving the theoretical independence of boundary layer thickness and radius.

The analogy between heat and mass transfer was utilized by Kreith, Taylor & Chong {34} in 1959 to determine the heat transfer coefficient of a disc rotating in still air. An aluminium disc coated with napthalene was rotated and the loss of weight measured. The experiments verified that the mass transfer, and hence the heat transfer, was constant across the whole surface, and gave the result at a Prandtl

number of 2.4 of

$$Nu_o = 0.64\ Re_o^{0.5} \qquad (2.16)$$

Kreith, Taylor & Chong described a theoretical evaluation of the heat and mass transfer using the same method as Wagner {13} and obtained the result

$$Nu_o = 0.67\ Re_o^{0.5} \qquad (2.17)$$

As was described earlier, this calculation was repeated by the author in appendix 1, where the same result was found.

Sparrow & Gregg {18}, 1959, continued the numerical solution of Millsaps & Pohlhausen {15} to predict the heat transfer over the full range of Prandtl numbers. By observing that at low Prandtl numbers the thermal boundary layer was much thicker than the velocity one, and the reverse for high Prandtl numbers, asymptotic solutions were obtained for these two extremes. In between, values of the heat transfer were computed at Prandtl numbers of 0.01, 0.1, 1, 10 and 100. From these values a graph was constructed, part of which is repeated in figure 2.07.

Richardson & Saunders {35} used the apparatus of Cobb & Saunders in 1963 to take measurements of the heat transfer in the laminar region, and in the region of relatively high natural convection. These results followed the equation

$$Nu_o = 0.4\ (Gr_o + Re_o^2)^{0.25} \qquad (2.18)$$

in the range of Reynolds numbers up to 2.4×10^5, and Grashof numbers up to 7.6×10^7. It was also found that Young's measurements could be fitted to a similar equation

$$Nu_o = 0.47\ (Gr_o + Re_o^2)^{0.25} \qquad (2.19)$$

Richardson & Saunders thought that the discrepancy was probably due to an experimental error in Young's measurements.

In the Ph.D thesis of Richardson {33} he describes experiments to measure the heat transfer coefficient of a disc rotating in water, of Prandtl number 7.9, but the result was very much lower than predicted

by any of the theoretical evaluations surveyed, giving

$$Nu_o = 0.3\ Re_o^{0.5} \qquad (2.20)$$

Sparrow & Gregg predicted a value of

(See fig.2.07) $$Nu_o = 1.0\ Re_o^{0.5} \qquad (2.21)$$

In 1964 Riley {24} made another prediction of the heat transfer for all values of the Prandtl number. On the assumption that a linear relationship existed between viscosity and temperature the momentum equations were reduced to their incompressible form and the energy equation was solved in the form of a series, to obtain two results, one neglecting and one allowing for viscous dissipation. For the former, two further solutions were found, one for small Prandtl numbers and the other for large ones, with close agreement between the two where they met, in the region of Pr = 0.4. A numerical solution of the energy equation agreed to within 1% of the series solution over the whole range of Prandtl numbers. Figure 2.07 shows the laminar heat transfer for values of Prandtl number from 0.1 to 100. Rileys result deviates from the calculations of the author (using Cochrans profiles in the integral method of Wagner) only in the range of $Pr < 1$.

The most recent work was reported by Iguchi & Maki {37} in 1967, using a mass transfer technique at a Prandtl number of 2.4. A disc coated with napthalene was rotated in the range of Reynolds numbers from 195 to 42,000, covering the whole range of natural convection, but not extending very far into the region of laminar flow. Their results were as follows

With $1.95 \times 10^2 < Re_o < 3 \times 10^4$ $\qquad Nu_o = 1.58\ Re_o^{0.4} \qquad (2.22)$

With $Re_o > 3.5 \times 10^4$ their results agreed with those of Kreith, Taylor & Chong {34}, (equation 2.16)

Summary

Some papers will be presented in later sections which covered the heat transfer from a rotating disc in still air as a side topic, whilst their main one was the effect of some other variable on the system. These were disregarded in this section in order to simplify the description of the many papers already involved.

Cochran used a numerical method to solve the hydrodynamic equations to obtain the velocity profiles, which are therefore preferable to those of von Karman, who used an approximate method of solution with the assumption that the velocities were reduced to zero at the edge of the boundary layer. The experimental measurements of Gregory, Stuart & Walker supported Cochran's theoretical profiles, whilst those of Cobb & Saunders were really too scattered to be conclusive, but nevertheless also followed Cochran's tangential profile.

The first prediction of the heat transfer was made by Wagner, for air (Pr = 0.74) who used the velocity profiles of Karman in the heat flow equation, which was then integrated to give the heat transfer coefficient, called the integral method of solution. Subsequently Karman's profiles were proved to be inaccurate, invalidating this result, although not the method. Young and the author used the profiles as corrected by Cochran for Pr = 0.7 to obtain the result (equation 2.12)

$$Nu_o = 0.33\, Re_o^{0.5}$$

Later papers by Millsaps & Pohlhausen, Sparrow & Gregg and Riley predicted the heat transfer for a range of Prandtl numbers, 0.5 to 10 for the former and all values for the latter two. Figure 2.07 shows that these differ by a maximum of 20% at Pr = 10. The author used the corrected Karman's velocity profiles in the theory of Wagner to calculate the heat transfer from $0.1 < Pr < 100$, also shown in figure 2.07. Although Karman's velocity profiles were shown to be inaccurate by comparison with experiment in the region of the boundary layer edge

the line of $Nu/Re^{\frac{1}{2}}$ differs very little from that of Sparrow & Gregg whose solution of the hydrodynamic equations, if taken separately, would give the same velocity profiles as Cochrans numerical method, which have been shown to be much closer to experimental data. Little deviation occurs because the heat transfer is affected more by the conditions at the wall than at the edge of the boundary layer.

Three measurements have been made of the heat transfer from a disc rotating in air. Young's experiments, whilst being a valuable first attempt, were not far enough into the region of laminar flow unaffected by natural convection to enable a comparison to be made with theoretical predictions. Cobb & Saunders method was found to have a 10% error by Richardson & Saunders, making their results coincide to give, equation 2.18:-

$$Nu_o = 0.4 \left(Gr_o + Re_o^2 \right)^{0.25}$$

This constitutes a 25% increase on the prediction of Sparrow & Gregg, the reason for which has not been found to date.

Kreith, Taylor & Chong and Iguchi & Maki made experiments using an analogous mass transfer technique, at an effective Prandtl number of 2.4, and their results agreed, following equation 2.17:-

$$Nu_o = 0.64\ Re_o^{0.5}$$

This differs by only 6% from the prediction of Sparrow & Gregg, for that Prandtl number.

TURBULENT FLOW

The study of the heat transfer in the region of turbulent flow on a rotating disc is probably of greater importance than that in the laminar region as it occurs more frequently in practical applications. The heat transfer in the laminar regime had been predicted well before experimental correlation was achieved, but due to the complexity of turbulent flow it was first investigated experimentally and, in common with turbulent flow over other bodies, only semi-empirical methods of

analysis have been used to predict the heat transfer. These have used theoretical and experimental values of the moment coefficient and velocity profiles in Reynolds analogy of fluid flow to heat transfer.

Previous experimental work has shown that transition from laminar to turbulent flow in the boundary layer on a rotating disc starts at a local Reynolds number of around 240,000, and fully turbulent flow exists above 400,000. Therefore, at any rotational speed, on a disc of sufficiently large radius, there will be an inner laminar region, then a region of transition, and finally a region of turbulent flow.

The work done in the region of turbulent flow, like that in the laminar region, falls into two parts, the study of the flow profiles and resistance to rotation and the study of the heat transfer. The resistance to rotation, expressed by the value of the moment coefficient, was found from the shear stress at the surface, which also gives the velocity profiles.

Survey

Von Karman {3} made the first theoretical determination of the turbulent velocity profiles, as well as the laminar ones, in 1921. Karman's work formed one of the pioneering approaches to the analysis of turbulent boundary layers and therefore was not only of importance to the study of the flow on a rotating disc, but also to the flow over other bodies. Karman assumed that the velocity distributions near the wall followed a 1/7th power law, derived from an expression for the distribution of the mean velocity u near a smooth wall, where τ_w is the shear stress at the wall.

$$u = 8.7\, v_* \left(\frac{v_* z}{\nu}\right)^{1/7} \qquad (2.23)$$

v_* is the friction velocity, defined as

$$v_*^2 = \frac{\tau_w}{\rho} \qquad (2.24)$$

The friction velocity is a measure of intensity of turbulent eddying

and of the transfer of momentum due to these fluctuations.

Karman obtained an equation for the shear stress at the wall by consideration of the flow of momentum, and hence derived the velocity profile equations shown in figure 2.08, as well as the moment coefficient. The velocity profiles of Karman and later workers are compared in figures 2.09 and 2.10.

Fourteen years elapsed before further investigations were published by Goldstein {5} in 1935. He checked the results of Karman, and corrected his equation for the boundary layer thickness, as shown in figure 2.08. He proposed that the expression (2.23) for the velocity profile upon which Karman's analysis was based had been found valid only for a range of values of $\frac{v_* z}{\nu}$ up to about 600, beyond which the velocity close to the wall, u, was better described by a logarithmic expression

$$u = a v_* \log_e \frac{v_* z}{\nu} + \text{constant} \qquad (2.25)$$

For values of $\frac{v_* z}{\nu}$ below about 30, neither expression agreed with measurements, as the rate of shear was so large that the viscous shearing stress had an appreciable effect on the motion.

Using the logarithmic profile (2.25), Goldstein derived the shear stress at the wall in the same way as Karman, by consideration of the flow of momentum, or, which gives the same result, by integration of the equations of motion, to give the velocity profiles and the moment coefficient.

In 1944 Theodorsen and Regier {10} took measurements of the tangential flow profile and moment coefficient. They found that with maximum surface roughness transition occurred at a Reynolds number of 220,000, whilst for a perfectly smooth disc laminar flow remained up to Re_o = 310,000. In addition, they showed that the moment coefficient was independent of Mach number up to M = 1.69, and dependent only on the Reynolds number.

FIGURE 2.08

Equations of Turbulent Velocity Profiles

on a Rotating Disc in Still Air

Karman [3]

$$F = 0.162 \left(\frac{z}{\delta}\right)^{\frac{1}{7}} \left(1 - \frac{z}{\delta}\right)$$

$$G = 1 - \left(\frac{z}{\delta}\right)^{\frac{1}{7}}$$

where $$\delta = 0.462\ R \left(\frac{\nu}{R^2\omega}\right)^{\frac{1}{5}}$$

Goldstein [5] a) corrected from Karman.

as above except for

$$\delta = 0.526\ R \left(\frac{\nu}{R^2\omega}\right)^{\frac{1}{5}}$$

b) calculations assuming a logarithmic velocity profile

$$F = \alpha \left(1 + \frac{1}{\gamma} \log_e \frac{z}{\delta}\right) \quad \text{for} \quad z < z_1$$

$$F = -\frac{\alpha}{\gamma} \log_e \frac{z}{\delta} \quad \text{for} \quad z_1 < z \leq \delta$$

$$G = -\frac{1}{\gamma} \log_e \frac{z}{\delta}$$

where $\frac{z_1}{\delta} = e^{-\frac{1}{2}\gamma}$, and $\delta = \dfrac{A C \nu \gamma e^{\gamma}}{\omega R \sqrt{1+\alpha^2}}$

and $\dfrac{\omega R^2}{\nu} = Re_R = 3 A^3 C \gamma e^{\gamma} = 0.826\ \gamma e^{\gamma}$

with $A = 1.97$, $B = 6.53$, $C = 0.036$, $\alpha = \frac{1}{3}$

FIGURE 2.09

Turbulent Radial Velocity Profile on a Rotating Disc in Still Air

ω = 220 rad/s
R = 146mm
Re_o = 323,000

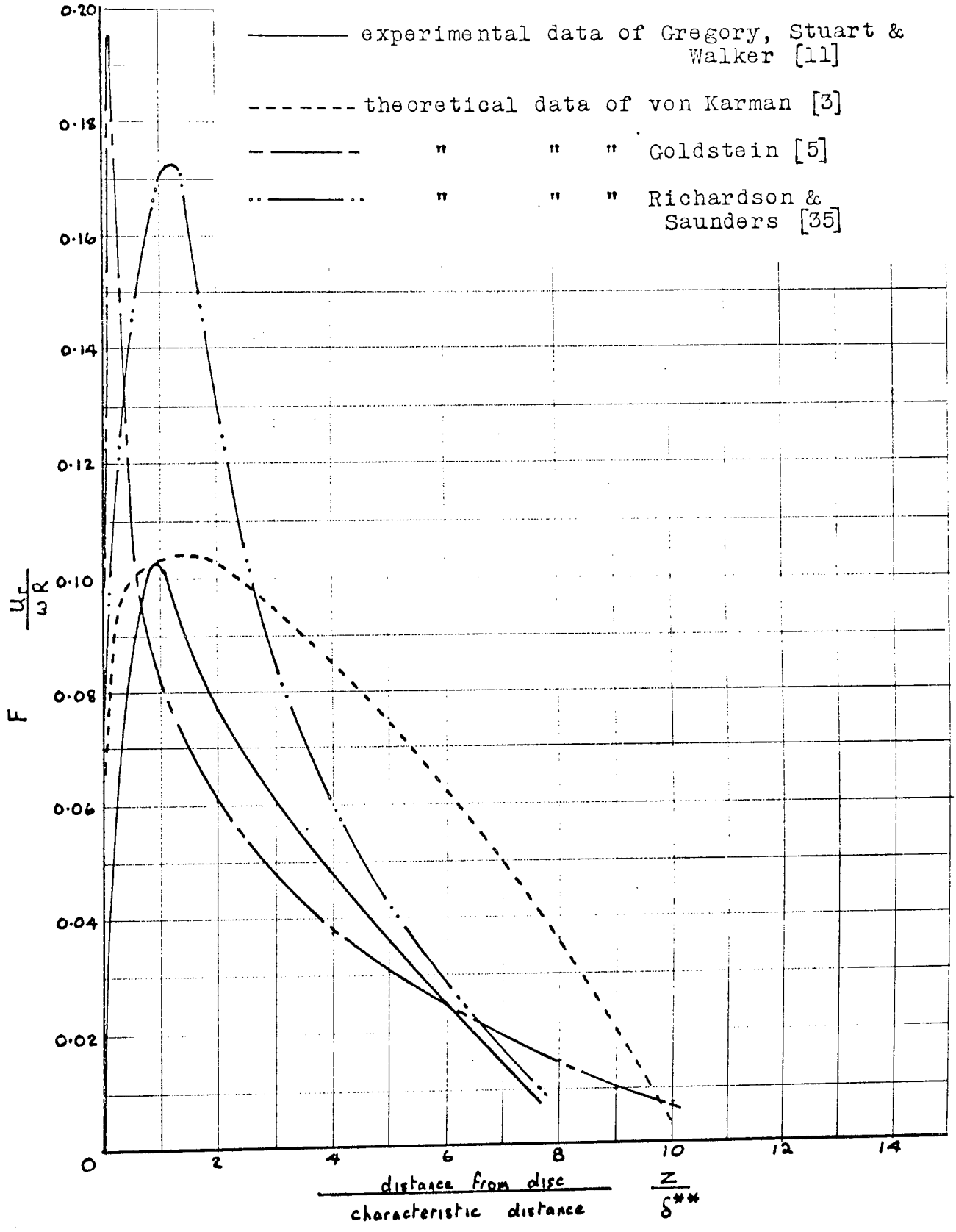

FIGURE 2.10

Turbulent Tangential Velocity Profile on a Rotating Disc in Still Air

ω = 220 rad/s
R = 146mm
Re_o = 323,000

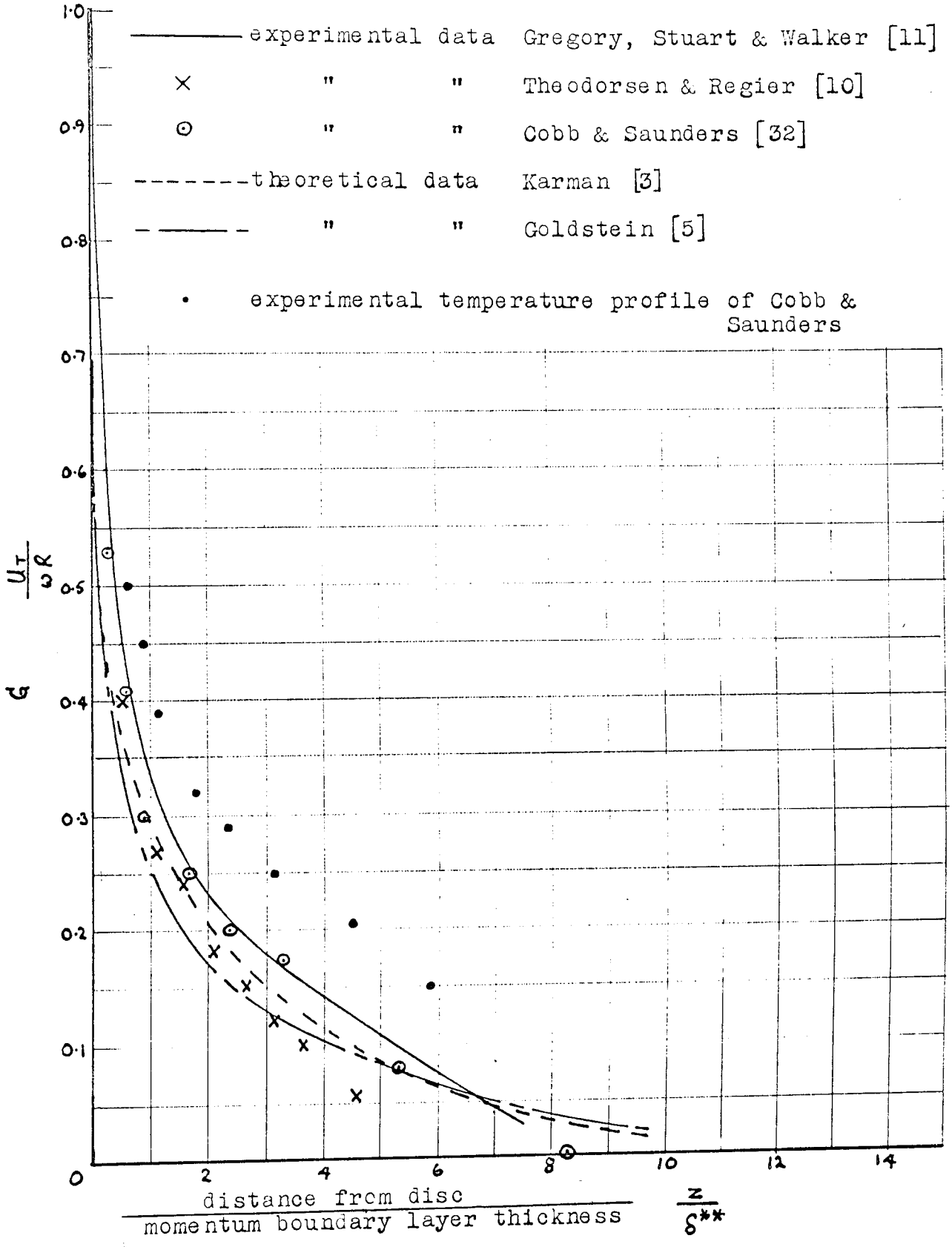

Gregory, Stuart & Walker, 1956, [11] made a further set of experimental observations of the velocity profiles. They measured the total velocity and the angle of yaw, and then resolved these into the radial and tangential components of flow. They also investigated the behaviour of the flow at the onset of instability in the boundary layer of a rotating disc prior to the region of transition. The face of a disc was covered with china clay to indicate the modes of flow. After rotation at a suitable speed the surface of the clay had a pattern of a series of equi-angular spirals, which seemed to indicate the presence of stationary vortices in the boundary layer. This region of instability began at a Reynolds number of 180,000, whereas transition started at a Reynolds number of 280,000. An acoustic stethoscope was also used to determine the critical Reynolds numbers. This consisted of a piece of plastic tube, which, if one end was listened to, while the other was held in the boundary layer, could be used to detect the critical radii, as there was silence in the laminar region, a note of fairly definite pitch when vortices were formed, and a roar in the turbulent region. The critical Reynolds numbers thus found agreed with those deduced from the china-clay method.

In the same year, Cobb & Saunders [32] made the first heat transfer measurements in the turbulent region. Transition occured at a Reynolds number of 240,000 and measurements were taken up to a value of 730,000, where 80% of the disc area was under turbulent flow. Their results are presented as a double logarithmic plot of Nusselt number against Reynolds number in figure 2.11. The region of transition extended beyond the range of their tests due to the continuous existence of a laminar region on the disc, but the line of heat transfer eventually became asymptotic to the line for all the disc under turbulent flow. From their results Cobb & Saunders estimated that if the whole of the disc were under turbulent flow the heat transfer would be

FIGURE 2.11

Heat Transfer from a Rotating Disc in an Open Environment

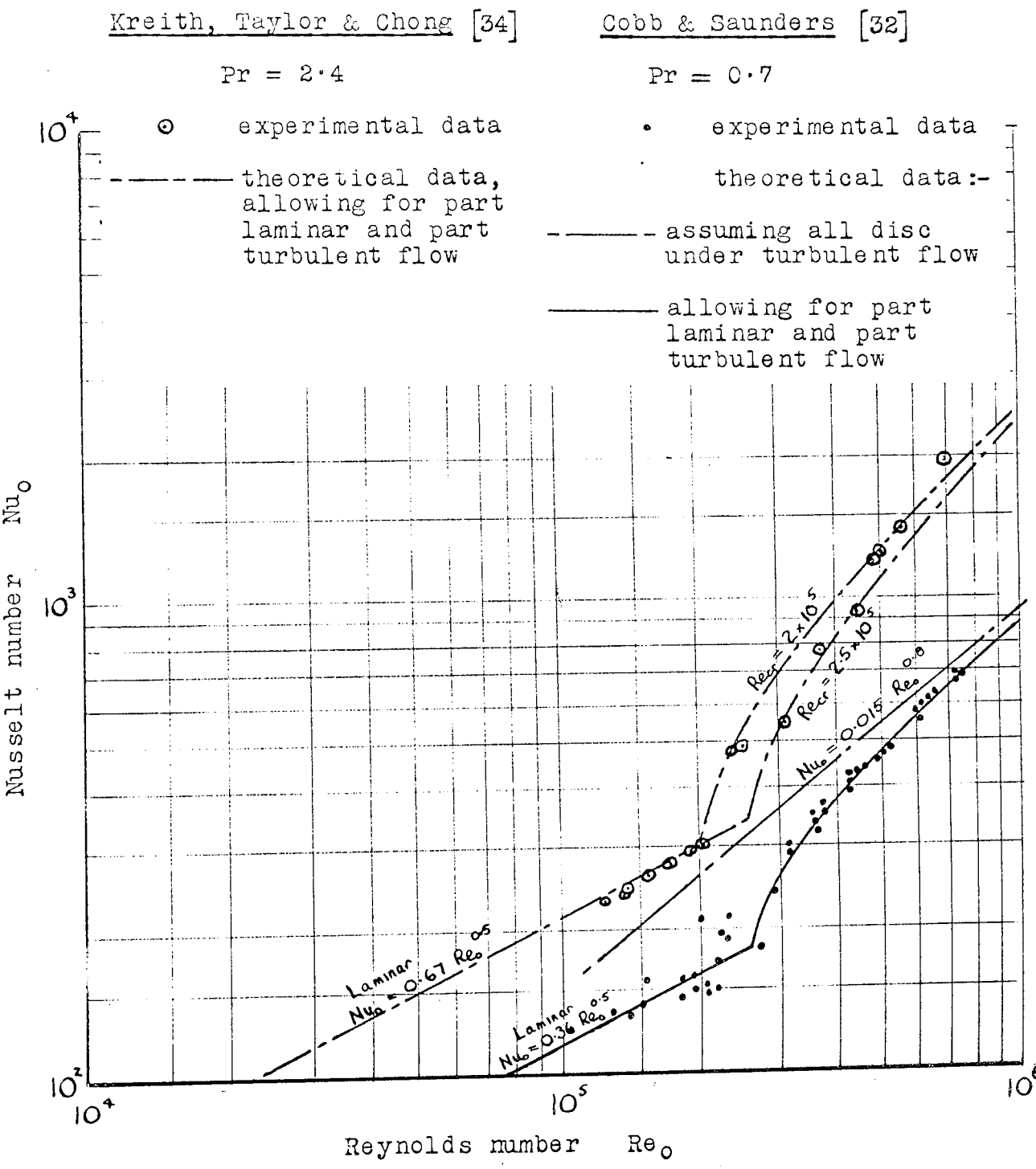

$$Nu_o = 0.015\ Re_o^{0.8} \qquad (2.26)$$

For the region of transition the heat transfer was predicted by assuming that the area under turbulent flow followed equation 2.26 and the area under laminar flow followed the equation for laminar heat transfer (2.14) and the average effect over the disc found by integration. This prediction agreed well with experiment when the radius of change from laminar to turbular flow had a local Reynolds number of 240,000.

Cobb & Saunders made an empirical prediction of the heat transfer by using the analogy of friction torque to heat transfer developed by Reynolds. The local turbulent friction coefficient was taken from the paper of Theordorsen & Regier, and used in the analogy to derive the equation for all the disc under turbulent flow

$$Nu_o = 0.0149\ Re_o^{0.8} \qquad (2.27)$$

They also attempted to predict the turbulent heat transfer by assuming that the temperature profile followed the same law as Karman's turbulent tangential velocity profile. By substituting this in an equation for the heat flow through the boundary layer they achieved the result

$$Nu_o = 0.0095\ Re_o^{0.8} \qquad (2.28)$$

The large discrepancy between this and the measured heat transfer indicated that the temperature profile must depend on the radial, as well as the tangential, velocity components.

Measurements of the velocity and temperature profiles were made by Cobb & Saunders, and these are repeated in figure 2.10. The velocity measurements were close to the profile predicted by Karman, but the measured temperature profile was higher than the velocity profile. This was to be expected with a fluid of Prandtl number less than unity when both velocities and temperatures were plotted relative to the momentum thickness. These results confirmed that the inequality of the profiles was the cause of the inaccurate prediction of equation (2.28).

In 1958 Davies [16] presented a more rigorous theoretical prediction of the heat transfer in the turbulent region. The distribution of the radial component of Reynolds shearing stress in the boundary layer was calculated by an integration of the equation of mean flow, using von Karman's velocity profiles. The distribution of eddy heat diffusivity was evaluated by applying Reynolds analogy in a thin region of flow very near to the surface of the disc, using the approximate similarity of the radial component of disc flow and plate flow to extend the results into the remainder of the inner part of the boundary layer (approximately 16% of the layer thickness). He then used the method developed by Davies & Bourne [45] to evaluate the heat transfer from the disc for a constant surface temperature. Assuming that the disc was rotating sufficiently fast enough to neglect the laminar sub-layer, Davies obtained the result

$$Nu_o = 0.014\ Re_o^{0.8} \qquad (2.29)$$

which is close to the experiments of Cobb & Saunders (equation 2.26).

In 1959 Kreith, Taylor & Chong [34] measured the heat transfer from a rotating disc by a mass transfer analogy technique at a Prandtl number of 2.4. The change in weight of a napthalene disc was found, and in addition the observations of Gregory, Stuart & Walker were verified as the imprints of a stationary vortex system were reproduced on the surface of the napthalene after a test in the region of instability. These vortices were also found to be present, to a lesser extent, in the turbulent region. Transition occurred at a Reynolds number of 2.0 to 2.5×10^5, and the results followed a similar path to those of Cobb & Saunders, rising steeply from the point of transition to become asymptotic to the line of all the disc under turbulent flow, as shown in figure 2.11.

Kreith, Taylor & Chong presented an empirical analysis of the heat transfer in the turbulent region, and combined this with the equation

of laminar heat transfer to predict the behaviour in the region of transition. The analysis of the turbulent heat transfer was based on the experimentally determined drag coefficient of Theordorsen & Regier, which was then used in Reynolds analogy. The predicted heat transfer, shown in figure 2.11, agreed closely with their own experimental results and with the results of Cobb & Saunders at Pr = 0.72, except at high Reynolds numbers when the latter's own theoretical analysis was closer to experiment.

Richardson & Saunders {35} made a prediction of the heat transfer in 1963, using an empirical method. They argued that the discrepancy between experimental radial velocity profiles and theoretical curves suggested that a new profile description was needed. This they found by solving the equation for the laminar radial flow numerically, imposing upon it a tangential velocity distribution following the 1/7th power law. This profile was then integrated with the measured temperature profile to give, for all the disc under turbulent flow

$$Nu_o = 0.0138\ Re_o^{0.8} \qquad (2.30)$$

Dorfman { 1 } , 1963, presented yet another prediction of the heat transfer. He assumed a radial power law distribution of temperature across the disc, $\theta_w = a\ R^n$, with a Prandtl number of unity, to make the velocity and temperature profiles of the same form, and then the problem was solved by Reynolds analogy. For a constant temperature disc surface this gave

$$Nu_o = 0.0151\ Re_o^{0.8} \qquad (2.31)$$

Finally, Kreith {2} , in his survey of rotating systems, presented his own analysis of turbulent heat transfer from a rotating disc. This was a semi-empirical method based on the analogy between the moment coefficient and the heat transfer, and gave the result

$$Nu_o = 0.0174\ Re_o^{0.8} \qquad (2.32)$$

Summary

It was desirable to plot the velocity profiles non-dimensionally as this prevents errors due to units, but this proved rather more difficult for the turbulent profiles than for the laminar ones. At all Reynolds numbers, due to the constant boundary layer thickness in the laminar region, the distance from the disc surface, z, could be made non-dimensional by multiplying by the term $\sqrt{\frac{\omega}{\nu}}$. The profile was then the same for any Reynolds number. In the turbulent region, however, the boundary layer thickness varies with Reynolds number, so the axial distance is compared with the displacement thickness δ^* or the momentum thickness δ^{**}, defined by

$$\delta^* = \int_0^\delta G\,dz \qquad (2.33)$$

$$\delta^{**} = \int_0^\delta G(1-G)\,dz \qquad (2.34)$$

If $H^* = \delta^*/\delta^{**}$ we get, for Karman's power profiles, $H^* = 1.285$, whilst for Goldstein, $H^* = 1.24$ and for Gregory, Stuart & Walker $H^* = 1.4$.

Figure 2.09 shows that neither the theoretical radial profile of Karman or Goldstein are supported completely by the experimental measurements of Gregory, Stuart & Walker, but the profile of Goldstein is better fit to those measurements. The profile calculated by Richardson & Saunders was a similar shape to the measured profile but still reached a much higher maximum value, although it was good enough to give a reasonable prediction of the heat transfer, when used with the measured temperature profile and substituted into the heat flow equation.

Figure 2.10 shows the tangential velocity profiles, where the three experimental profiles and two calculated ones all fall within reasonably close limits, tending to disagree only towards the outer edge of the boundary layer. The measured temperature profile of Cobb & Saunders, when plotted as a ratio of the same momentum thickness as the velocity profile, runs above the velocity profile. This is because the Prandtl

number of air is less than unity, when the thermal boundary layer is thicker than the velocity one. If the temperature profile were plotted relative to the thermal boundary layer thickness the two profiles would be alike. No theoretical temperature profile has been evaluated as it has not been possible to solve the Navier-Stokes continuity and energy equations directly for turbulent flow. The existing predictions of the heat transfer using Reynolds analogy or the use of assumed temperature profiles in the heat flow equation obviously do not yield a predicted temperature profile.

The measurements of the heat transfer (figure 2.11) by Kreith, Taylor & Chong, and Cobb & Saunders both agreed with predictions based on the analogy of friction to heat transfer, using previously measured values of the friction coefficient. The heat transfer in the overall transition region was also accurately predicted by allowing for part of the disc under turbulent flow and the remainder laminar, using the measured Reynolds number of transition to calculate the critical radius. No allowance was made for the actual transition zone on the disc at a fixed speed, so the close correlation between calculated and measured values of the Nusselt number seems to indicate that this region was small. At high Reynolds numbers the laminar zone became insignificant and the heat transfer line approached the line for all the disc under turbulent flow.

All predictions of the heat transfer used semi-empirical methods involving either analogy of friction to heat transfer or the assumption that velocity and temperature profiles were similar. The agreement between these profiles and experiment was extremely good, although these assumptions are only valid for a Prandtl number of one. Experiments in the air, $Pr = 0.7$, are usually well predicted by such methods, but the agreement that was reached at $Pr = 2.4$ must be regarded as somewhat fortuituous, and these methods of prediction certainly could not be relied upon outside this range.

OTHER SUBJECTS OF INVESTIGATION

After the basic system of a rotating disc in an open environment had been fully investigated, research began to extend into the study of the effects of external variables on the fluid flow and heat transfer. These further areas of work have now evolved into:- the non-isothermal disc surface, nearby stationary and rotating planes, and a uniform forced axial flow towards and away from the disc. These are all concerned with turbine applications where the disc has a non-isothermal surface at start and shut down, rotates in a casing (giving nearby stationary planes), and has a forced flow of fluid in the axial direction. In addition, it has been found possible to cool a turbine rotor by introducing an axial stream of fluid through a porous surface, or by air cooling with an axial stream.

None of these topics directly affect the research carried out in this project, except for the effect of nearby stationary planes, which was used in the design of the rig. Therefore, the publications will only be briefly described, just to give some background into how these lines of research have progressed.

Non-isothermal Surface

Cess & Sparrow {20} analysed the heat transfer for a step change in wall temperature, and then produced a general analysis for arbitrary variations of spacially uniform surface temperature with time. The flow was taken as steady and laminar, and results were presented for a linear variation of temperature with time for Prandtl numbers of 0.72, 1, 10 and 100.

Dorfman {1} , in his book, considered the influence of a quadratic and an arbitrary radial distribution of temperature head on a rotating disc in the laminar and turbulent regions of flow.

Nearby Stationary and Rotating Planes

Kreith, Taylor & Chong {34} , in a mass transfer experiment, placed a napthalene covered disc in a shroud and conducted tests in the laminar flow region. They varied the ratio of disc diameter to distance from the shroud and compared the mass transfer ratio to that of a free disc, and obtained the results in figure 2.12. They proposed that when the disc was a sufficient distance from the shroud there were two distinct boundary layers, one on the stationary, and one on the rotating surface, leaving a core of fluid rotating at approximately one half of the disc velocity between them. In this condition it was not expected that the mass or heat transfer would be affected. However, when the clearance was reduced to give interference of the boundary layers the mass and heat transfer was reduced and any further decrease caused a considerable reduction of circulation and eventually a choking of the central core.

Richardson & Saunders {35} repeated the above experiments using a heated disc to measure the heat transfer directly. They differentiated between interference with the flow from the rim and interference with axial flow to the disc. A stationary plane of smaller diameter than the disc did not affect the flow from the rim but did affect the axial inflow, with little effect on the heat transfer. However, if it were close enough, within the order of one disc thickness, a stationary plane of larger diameter than the disc interfered significantly with the axial inflow and the rim jet. As the clearance between the disc and this stationary surface was reduced the flow demanded by continuity requirements had to pass between a decreasing annular gap between them. Eventually the pressure difference across the rim jet caused it to snap onto the plane and gave a partial recirculating motion to the fluid, as shown in figure 2.12. This, as well as reducing the airflow to the disc surface, also increased its approach temperature, hence rapidly

FIGURE 2.12

Effect of a Nearby Stationary Plane on the Heat Transfer from a Rotating Disc in Still Air

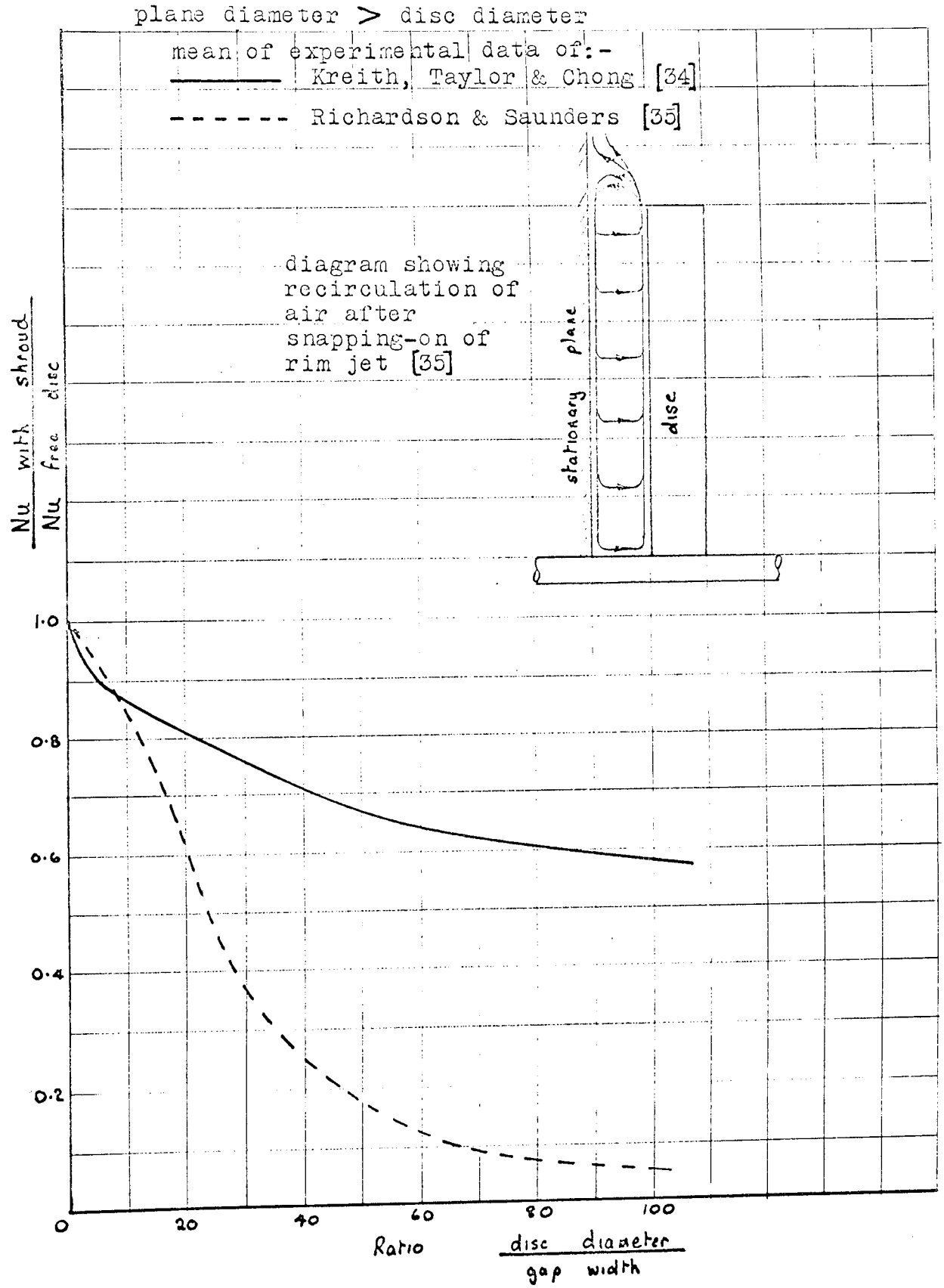

reducing the heat transfer. This accounted for the discrepancy between the results of Kreith, Taylor & Chong and those of Richardson & Saunders, the mass transfer technique could not allow for the increased approach temperature of the entrained fluid.

Dorfman { 1 } devoted a chapter to the discussion of the flow around a disc rotating in a confined space. He made a theoretical approach to the effect of a tight fitting casing on the moment coefficient in laminar and turbulent flow, and investigated the flow in the laminar range between a rotating and a stationary disc of infinite radii, and between two rotating discs. In the casing the fluid was thrown off at the rim of the disc, flowed across the casing edge and inwards towards the rotational axis, along the static wall, to be recirculated along an axial path to the disc.

The heat exchange in the flow between two rotating discs was investigated by Kapinos { 25} , who considered flow both from the centre to the periphery, aided by the rotation, and in the reverse direction, giving a theoretical solution for two conditions. Firstly, if the boundary layers on the discs did not interfere then the core of fluid between them would flow radially outwards and the velocity profiles would be the same as those for an isolated disc. Secondly, if the boundary layers did interfere, then the heat transfer would be reduced, and an analysis was presented for this reduction.

Kreith & Viviand {26 } studied the problem of laminar source flow between a stationary and a rotating disc, which finds an application in disc pumps, spacecraft condensators and seawater condensation plants. The stationary disc had a circular hole at the centre through which the source flow was supplied, it then travelled radially outwards across the disc surface to be ejected at the rim. Kreith & Viviand found a theoretical solution, by perturbation methods, for the heat transfer, assuming a parabolic radial velocity distribution, which agreed with a limited number of mass transfer experiments.

In 1966 Sharma & Agarwal {28} made a theoretical analysis of the heat transfer from an enclosed rotating disc with a small gap between disc and housing. The flow was assumed viscous and the fluid incompressible to find the effects on the temperature profile of radial outflow and inflow through a central source. In addition the Nusselt number on the rotor and stator was found for regions of both recirculation and no recirculation. Solutions for the temperature profiles and heat transfer were presented and it was shown that the rate of heating from the rotor and stator increased with an increase in the net radial outflow and the opposite happened for a net radial inflow.

Axial Forced Flow

The investigation of forced axial flow on a rotating disc lends itself to theoretical analysis as the flow on an isolated disc has its own induced axial flow and it is this velocity component which is varied. Hannah {6} first made a theoretical prediction of the velocity profiles and moment coefficient with a forced axial flow towards the disc in the laminar region in 1947. The disc was show to have two distinct effects on the velocity of the fluid along the axis; it acts as a centrifugal fan by its rotation and hence sucks fluid towards it, and also acts as an infinite plane barrier opposing, by viscosity, the radial flow due to an externally imposed fluid motion. At high rotational speeds relative to axial flow velocity the first function dominates, but when these are reversed the disc becomes a barrier to the flow. Hence for a fixed supply pressure the axial inflow velocity increases with rotational speed.

In 1951 Bachelor {7} studied the system of a rotating disc with the fluid at infinity having an arbitrary uniform angular velocity about the axis of rotation of the disc, as well as a velocity in the axial direction induced by the disc rotation. He described a one-parameter family of solutions for this system and then found a two-parameter.

family of solutions to describe the flow between two parallel discs rotating about the same axis at different angular velocities.

Yamaga [19] determined theoretically the heat transfer from a rotating disc normal to a uniform forced flow in the laminar region. The flow profiles that were found in the process of determining the heat transfer were the same as those found by Schlichting & Truckenbrodt [8], who repeated the work of Hannah. The heat transfer was determined for a range of Prandtl number from 0.1 to 100.

Kreith, Doughman & Kozlowski [21] experimentally investigated the heat transfer characteristics of a partially enclosed rotating disc by means of a mass transfer analogue. Mass transfer rates to air from napthalene coated discs were measured at Reynolds numbers of rotation from 1.5×10^4 to 4.5×10^5 with no source flow, a free source flow and a forced flow of air directed into the centre of the enclosing shroud. The equivalent Prandtl number of the system was 2.4. With no source flow it was found that at certain gap sizes, when the boundary layers on the disc and shroud did not interfere, and before the shroud was so far away that the heat transfer reverted to that of a free disc, the heat transfer was increased beyond that for a free disc. The shroud caused this by hastening the onset of transition for no source flow, whilst with free source flow the onset of transition occurred even earlier. The forced source flow was turbulent at all inlet velocities due to the disturbances it meets in the supply route.

In 1964 Tien & Tsuji [23] made a theoretical determination of the temperature distributions and heat transfer for laminar forced flow against a non-isothermal rotating disc. The surface temperature was assumed to vary according to a power law with the radius and numerical solutions of the boundary layer equations were given for all values of the Prandtl number.

Mabuchi, Tanaka & Sakakibara [29] made a theoretical investigation of the effect of dissipative energy on the laminar heat transfer from a disc rotating in a uniform forced axial stream. For an incompressible fluid with constant physical properties the energy equation was solved exactly for the following; a quadratic variation of surface temperature with radius, an isothermal surface, and an insulated surface.

The addition or removal of mass at a boundary surface is used as a means of controlling the boundary layer. If the layer is liable to separation then mass removal holds it onto the surface whilst mass addition to the boundary layer aids cooling of the surface.

In 1960 Sparrow & Gregg [18] considered the effect of fluid injection and suction through the surface of a rotating disc. They theoretically estimated the heat transfer and flow field for the entire range from large suction velocities to large blowing velocities, and found that the heat transfer increased with the suction velocity. However with fluid injection the heat transfer, described by the Nusselt number, was reduced eventually to zero. This was because the injected fluid had a temperature close to that of the surface, which at high enough rates of mass addition blanketed the surface. This did not mean that the disc was perfectly insulated, but that heat was transported from it by the fluid passing through the surface, and not by forced convection from the surface. Increased blowing caused the surface temperature to approach more and more closely the temperature of supply of the blown fluid.

In 1966 Lee, in a Ph.D. thesis [36], described experiments to measure the effect on the heat transfer of fluid injection and withdrawal through the surface of a rotating disc. This thesis has not been studied sufficiently to compare the results with those of Sparrow & Gregg.

2.3 FLAT PLATE PARALLEL TO A STREAM

A large number of investigations have been made into heat transfer from a flat plate by natural and forced convection. The study of forced convection on a flat plate goes back to the work by pioneers in the fields of boundary layer theory and the mechanism of convection heat transfer. T. von Karman and K. Pohlhausen developed approximate methods of solution of the Prandtl boundary layer equations for the flat plate and other bodies in the 1920's. This yielded the velocity profiles in the boundary layer and the boundary layer thickness for laminar and turbulent flow. The heat transfer by natural convection from a vertical plate was first found by integration of the boundary layer equations by Pohlhausen, in collaboration with E. Schmidt and W. Beckmann in 1930.

Most standard texts now give a comprehensive coverage of the basic systems of free and forced convection on an isothermal flat plate but certain variations on these standard systems have recently been the subject of further investigations. Recent papers on forced convection have investigated leading edge effects including separation of flow, supersonic and hypersonic velocities of flow, non-isothermal surfaces and free stream turbulence. Although the majority of experiments have been conducted in air, some measurements have been made with air of controlled humidity and with water. Free convection heat transfer theory has been extended to allow for variation of fluid properties with temperature within the boundary layer when a large temperature difference exists between the surface and ambient fluid.

When a flat plate is situated parallel to an airstream a boundary layer is created on the plate surface. If the leading edge is smooth enough not to disturb the flow then the flow in the boundary layer is laminar over an initial length of the plate. The boundary layer then

gradually thickens until the disturbances due to irregularities of the surface or flow become sufficiently large so that they are not damped but grow to produce a turbulent boundary layer; where the individual fluid particles execute fluctuating motions around some mean flow path. These fluctuations enhance the convective heat exchange, by transporting heat from one side of the boundary layer to the other, and hence heat transfer in turbulent flow is considerably higher than in laminar flow. When turbulent flow has developed the boundary layer thickens again as the flow proceeds along the plate. The result, on a sufficiently long plate, is that the heat transfer is highest at the leading edge, then gradually decreases until transition to turbulent flow occurs. It then rises rapidly to a maximum and gradually decreases again as the turbulent boundary layer thickens. Exactly the same phenomenon occurs with natural convection.

FREE CONVECTION

Most standard texts pay some attention to free convection on a vertical surface, but a more detailed review was made by Ede {53} in 1967, from which some of the information presented here has been taken. The first successful attempt to predict the laminar heat transfer was made by Pohlhausen, in collaboration with Schmidt and Beckmann. They solved the flow and energy equations by applying Prandtl's boundary layer approximations, and experimental values of the velocity and temperature gradients, obtaining a solution for a Prandtl number of 0.733 of

$$Nu_x = 0.39 \left(Gr_x \, Pr \right)^{\frac{1}{4}} \qquad (2.35)$$

The Grashof number, $Gr = \frac{g \beta \ell^3 \Theta}{\nu^2}$, is a dimensional number which reflects the size of the buoyancy forces affecting the flow in free convection, fulfilling the same function as the Reynolds number in forced convection.

In 1953 Ostrach {54} obtained exact solutions of the Schmidt and Beckmann equations for Pr from 0.01 to 1000, by means of a computer. For Pr = 0.733 the following result was found, which is very close to that found by the approximate method.

$$Nu_x = 0.388 \left(Gr_x \, Pr \right)^{\frac{1}{4}} \qquad (2.36)$$

In experimental work difficulty was found in reproducing the idealized situation assumed by theory, especially that of uniform surface temperature, but it has since been established that the effect of this on the result is less than might be expected. At a Prandtl number of one the ratio of Nusselt number with a uniform heat flux and the Nusselt number with a uniform surface temperature was 1.07. The various experimental results tend to run slightly above the theory, probably due to stray currents of air and disturbances, which always occur to some degree, depending on the amount of care taken during the experiment.

In 1954 Hara {58} calculated the heat transfer from a vertical heated plate, allowing for the variation of fluid properties dependent on temperature. He assumed that the specific heat was constant, and viscosity and thermal conductivity varied with $T^{0.76}$ where T was the absolute temperature. For a Prandtl number of 0.733 he obtained the result

$$Nu_x = 0.388 \left(Gr_x \, Pr \right)^{\frac{1}{4}} \left(1 - 0.055 \frac{T_w - T_\infty}{T_\infty} \right) \qquad (2.37)$$

In a later paper Hara {59} solved the same problem by a more rigorous method, valid for values of $\left(\frac{T_w - T_\infty}{T_\infty} \right)$ up to four, and achieved the same result as equation (2.37).

Turbulent flow in natural convection on a vertical flat plate was first noticed by Griffiths & Davis {55} in the 1920's. The first theoretical approach was made by Colburn & Hougen {56}, who assumed that in the laminar sub-layer both the velocity and temperature varied linearly with the height above the plate, z, up to the sub-layer edge,

where $z = \delta_s$. The value of δ_s was found from experiments which determined the critical Reynolds number. If the area under laminar flow was small enough to be neglected the mean Nusselt number for air was found as

$$Nu_L = 0.108 \ Gr_L^{1/3} \tag{2.38}$$

Eckert & Jackson [57] obtained a more direct solution by using the integral equation method and assumed that the velocity and temperature profiles followed the equations

$$u = U \left(\frac{z}{\delta}\right)^{1/7}, \theta = \theta_w \left(1 - \frac{z}{\delta}^{1/7}\right) \tag{2.39}$$

These equations were found by examination of the experimental profiles of Griffith & Davis [55]. If the flow was assumed turbulent over most of the surface they derived the equation, for Pr = 0.733,

$$Nu_L = 0.0187 \ Gr_L^{2/5} \tag{2.40}$$

The small amount of experimental data on turbulent free convection correlates with both of the above results but has too much scatter to choose with any confidence between them.

FORCED CONVECTION

Isothermal Surface-Leading Edge Effects

Forced convection heat transfer from a flat plate has been well explained in the texts of Eckert & Gross [71] and Schlichting [74], among others. For the laminar region the former gave an analysis which assumed that the temperature profile followed the equation

$$\frac{\theta}{\theta_w} = \frac{3}{2} \frac{z}{\delta_{te}} - \frac{1}{2} \left(\frac{z}{\delta_{te}}\right)^3 \tag{2.41}$$

This was substituted in the heat flow equation, which was integrated to

give the heat transfer

$$Nu_L = 0.589 \sqrt{Re_L} \qquad (2.42)$$

Schlichting gave a comprehensive coverage of forced convection in his text. In his treatment of the thermal boundary layer in laminar parallel flow past a plate he reduces the Navier-Stokes continuity and energy equations to ordinary differential equations by substitution of the variables, a technique attributed to Blasius. These differential equations were solved to give the temperature profile and the heat transfer for all values of the Prandtl number.

for $0.6 < Pr < 10$

$$Nu_x = 0.332 \sqrt[3]{Pr} \sqrt{Re_x} \qquad (2.43)$$

an identical result to that of Eckert & Gross.

Schlichting quotes the turbulent flow heat transfer equations as

$$Nu_x = 0.296 \sqrt[3]{Pr} \; Re_x^{0.8} \qquad (2.44)$$

giving for the whole plate

$$Nu_L = 0.037 \sqrt[3]{Pr} \; Re_L^{0.8} \qquad (2.45)$$

As with free convection it is difficult to reproduce in experimental work the ideal conditions assumed for the theoretical analyses. The most troublesome factor appeared to be disturbances in the flow caused by the shape of the leading edge to the plate. It was found that an effective way to prevent this was to insert a long tapered nose onto the leading edge of the plate and locate the heated or cooled test section at some considerable distance downstream of the leading edge so that any disturbances had decayed when the test section was reached. However the measured heat transfer was not then directly applicable to a plate heated over its whole length as the thermal boundary layer had its origin at the start of the heated section, whereas the momentum boundary layer began at the leading edge. To bring the experimental data in line with the theoretical predictions a characteristic length was calculated

by Tribus & Klein {43} in 1953, which corrected the results for the unheated initial length of plate, for both laminar and turbulent flow. Their paper also embodied an extremely useful table summarising the analytical solutions deduced by earlier workers.

The results of experiments on humid air in turbulent flow over a plate containing an isolated cooled region were published in 1954 by Furber {44} . The mass and heat transfer were measured at a cooled test section. The characteristic length of the boundary layer was taken as that from the leading edge to the test section with a correction applied to allow for the uncooled starting length. This correction depended on the Reynolds number of the flow. The results followed the line

$$Nu_L = 0.034 \quad Re_L^{0.8} \tag{2.46}$$

Edwards & Furber {46} made a number of experiments to investigate the effects of free stream turbulence on the heat transfer from a flat plate in laminar, transition and turbulent flow in 1956. The heated test section was located a considerable distance back from the leading edge and two grids placed in the airstream altered the free stream turbulence. Experiments showed that this turbulence affected the point of transition, but did not effect the value of the fully laminar or fully turbulent heat transfer. When a square nose was fitted to the plate the flow was turbulent throughout the whole range of tests, following the same turbulent line as that obtained with the tapered nose. However, measurements of the velocity boundary layer revealed that it was three times thicker than that obtained with a tapered nose.

The experimental data followed the equations

laminar $$Nu_L = 0.39 \quad Re_L^{0.535} \tag{2.47}$$

turbulent $$Nu_L = 0.038 \; Re_L^{0.786} \tag{2.48}$$

In 1961 Tendeland, Nielson & Fohrman {52} conducted experiments to investigate the flow field over blunted flat plates and the effects on

turbulent boundary layer growth and heat transfer at a Mach number of 4.7. Although the velocity of the airstream is much higher than used in the present work, their findings are relevant to present results. They found, by velocity profile measurements, that for natural transition the characteristic length of the turbulent boundary layer was less than that from the leading edge but for artificially induced transition, the length was not readily determined. The presence of a boundary layer trip caused thickening of the layer which could not be correlated with the geometric length of run of the layer. The effective length could only be determined by empirical methods, by measuring the local skin friction coefficient and calculating the length of run for a fully turbulent layer to reach this skin friction coefficient.

It was found that with a plate of 6.4mm front edge radius the heat transfer was higher than predicted for a sharp nosed plate at a distance from the leading edge of up to 10 leading edge diameters, but decreased to only 80% of the sharp nosed plate values at a considerable distance from the leading edge.

Ede & Saunders {48} published in 1957 the details of experimental work done in 1938. Measurements were made of the heat transfer from a flat plate in a stream of water. The plate had an unheated zone upstream of the heated test section, and the effect of the length of the unheated zone was investigated by placing the heated section in a series of positions along the plate. Initial experiments with a wedge shaped nose gave a generally higher, but erratic, heat transfer than found when a tapered and sharply pointed nose was used. With undisturbed flow the results indicated that there was laminar, transition and turbulent flow over the plate depending on velocity and distance from the leading edge. When the flow was disturbed artificially the heat transfer results indicated turbulent flow throughout. In the laminar region, the combination of a large number of previous theoretical solutions

allowing for an unheated region and uncertainty of whether the flow at points of measurement was truly laminar over the whole heated section or not prevented a firm conclusion being made and the need for further, more precise, experimental work was observed. In the turbulent region the theoretical analysis of Rubesin was in best agreement with experiment, giving the heat transfer as

$$Nu_x = 0.036 \frac{\left(1 - y^{\frac{39}{40}}\right)^{\frac{32}{39}}}{1 - y} Re_x^{0.8} Pr^{1/3} \qquad (2.49)$$

where $y < x$, x being the distance from the leading edge and y the distance from the leading edge to where the heated section commences.

In 1961 Hanna & Myers {51} gave a theoretical prediction of the turbulent heat transfer from a flat plate by using an analogy between heat and momentum transfer. As a simple relationship between the temperature and velocity fields does not exist because of the dependence of the velocity field on the kinematic viscosity the analysis was based on finding an appropriate, but fictitious, velocity distribution related to the actual temperature profile. Assuming that the velocity profile followed a $\frac{1}{n}$ th power law profile they derived the equation

$$St\, Pr^{\left(\frac{n+1}{5n+1}\right)} = \frac{f}{2} \qquad (2.50)$$

where f is the friction factor.

An experimental investigation of the boundary layer flow on a rotating flat plate was made by Persh & Sherwood { 47 } in 1956. The radius of the plate was large compared to its width so the plate behaved more like a flat plate in an airstream than a rotating disc. The plate extended both sides of the centre of rotation so that each plate travelled in the wake of the other. The boundary layer velocity profiles, measured with survey rakes fixed to the plate, indicated that a rather thick separated region occurred near the leading edge with reattachment downstream and turbulent flow throughout. The separation was eliminated by fitting extensions to smooth the flow at the leading and trailing edges of the plate, but laminar flow could not be achieved,

from which it appeared that a laminar flow could not be established on a surface which advanced into a wake or region of velocity deficiency.

Non-Isothermal Surface

In 1950 Lighthill {42} made a theoretical examination of the heat transfer through a laminar boundary layer, for an arbitrary distribution of main stream velocity and of wall temperature, for all values of the Prandtl number and up to large values of Mach number. He analysed viscous heating of the surface as well as dissipation from a heated wall.

Davies & Bourne {45} calculated the heat and mass transfer in laminar and turbulent boundary layers on a flat plate with arbitrary variation of surface temperature and mainstream velocity distribution. In the laminar region this method represented an improvement on that of Lighthill, which was based on a linear approximation to the exact velocity profile, whereas Davies & Bourne assumed a power law representation of the velocity profile of the form $u = C\, x^m$. The solution for the surface temperature was presented as a series in x, the distance from the leading edge of the momentum boundary layer. The heat and mass transfer in the turbulent boundary layer was analysed using the same methods. This paper made no contribution to the theoretical prediction of the heat transfer from a flat plate as an exact solution already existed, evaluated by Chapman & Rubesin, but was presented as proof of the validity of a new method of solution.

SUMMARY

An exact solution of the boundary layer equations for free convection heat transfer with laminar flow was made by Ostrach, giving for air

$$Nu_x = 0.388\ (Gr_x Pr)^{\frac{1}{4}}$$

The difference between this solution and an approximate one by Schmidt & Beckmann, with Pohlhausen, was very small, the constant of the equation being changed to 0.39. The experimental results correlated well with this expression, being only slightly higher due to extraneous air currents.

For turbulent flow, the experimental data, although considerably scattered, supported the theoretically derived expressions of Colburn & Hougen and Eckert & Jackson, which are respectively:-

$$Nu_L = 0.108\ Gr_L^{1/3}$$

$$Nu_L = 0.0187\ Gr_L^{2/5}$$

The derivation of these results was semi-empirical; for the first the experimental value of the critical Reynolds number was needed and for the second, the velocity and temperature profiles were based on experimental findings.

Hara studied the effects of the usual assumption that fluid properties did not vary within the boundary layer, and he found that this gave an inaccurate prediction when the temperature difference between the surface and fluid stream was high. The equation for the heat transfer, modified for variable fluid properties was given as

$$Nu_x = 0.388\ (Gr_x\ Pr)^{\frac{1}{4}} \left(1 - 0.055\ \frac{T_w - T_\infty}{T_\infty}\right)$$

so for a 1% change in the predicted heat transfer a surface temperature difference of 53°C is needed with an ambient temperature of 20°C.

The theoretical predictions of the forced convection heat transfer by Eckert & Gross and Schlichting correlated well with experimental data from Furber and Edwards & Furber when allowance was made for the unheated initial length of the plate. The effect of this unheated portion gave rise to considerable discrepancies during early experiments but it has now been thoroughly investigated, a theoretical analysis being given by Tribus & Klein.

A number of experiments have been made to investigate the effects of leading edge shape and freestream turbulence. A blunt leading edge caused turbulent flow over the whole plate whilst the heat transfer had the same turbulent values as found after natural transition on a sharp edged plate with a long tapered nose; the latter caused the least disturbance to the flow. However all heat transfer measurements were made well downstream of the leading edge, whilst velocity measurements immediately beyond the nose showed a separated region of flow with a thick boundary layer following it, so it is likely that heat transfer measurements taken there would have given results vastly different from usual turbulent flow ones.

Freestream turbulence again advanced the onset of transition to turbulent flow but did not affect the values of the heat transfer coefficients compared to those found with natural transition to turbulent flow.

For many applications (aircraft, vehicles, etc.) it has been desirable to produce a leading edge shape which caused a minimum of disturbance to the airflow. For heat transfer applications (i.e. heat exchangers) however, it is more often the aim to achieve maximum efficiency of transfer and an increase in the resistance to airflow may be of secondary consideration, therefore it is surprising that such a small amount of work has been found on leading edge effects, whilst the indications are that a large increase in the heat transfer coefficient may be available.

Chapter 3

APPARATUS AND PROCEDURE

3.1 INTRODUCTION

The conventional steady state technique was used to measure the heat transfer coefficient. This method was used in preference to the more recently developed mass transfer techniques and to cooling curve methods. The apparatus was based on that of Cobb & Saunders [32], with some modifications in the light of their results. It consisted of an electrically heated disc which was rotated both in still air in a curtained enclosure, and in an air crossflow in a wind tunnel.

The heat transfer coefficients were calculated from measurements taken when steady state was achieved, of the heat input to the disc, the disc surface and ambient temperatures and the area of convective heat transfer. Allowances were made for the heat losses to the rim of the disc, to the shaft, and by radiation, all of which were minimised by initial design and subsequent modifications to the rig.

Due to the iterative nature of the calculations of the mean heat transfer coefficients, a computer programme was developed to process the results.

The accuracy of the experimental data, as deduced from the accuracy of the component measurements, was $\pm$ 5%.

3.2 ALTERNATIVE EXPERIMENTAL METHODS

Experiments to measure the heat transfer from a rotating disc could be performed in a number of ways, as indicated by the methods described

in previous papers. Kreith, Taylor & Chong {34} eliminated the problem associated with measuring temperatures of, and supplying heat to, a rotating body by using a mass transfer technique. This was successful for the disc in an open environment but when used to find the effect of nearby stationary planes inaccuracies arose because the system was unable to allow for recirculation of hot air. Direct measurement of the heat transfer by Richardson & Saunders {35} showed that this recirculation had a considerable effect on the heat transfer (see figure 2.12). As experiments were to be made with sectors of material adjacent to the disc surface, which could cause recirculation of the flow, the mass transfer technique was rejected.

The heat transfer coefficient could also be found by measuring the cooling curve of a disc brake when mounted on a vehicle or dynamometer, but it is difficult to separate with any accuracy the heat losses due to convection, conduction and radiation. In addition the equipment needed is costly and the environment difficult to control. For these reasons the heat transfer was found by direct measurement with a steady state system, using a rig to simulate the conditions of operation.

Having decided upon the experimental technique, the general principles of the apparatus were next to be considered. The heat could be supplied to the disc in a variety of ways, by friction through a disc brake, by radiation transfer from a hot body located adjacent to the surface, by induction heating, or by an electrical heater mounted inside the disc, the heat being conducted to the surface. Friction heating could not be effectively controlled due to temperature effects on the brake linings, and a close hot body or induction heating apparatus would disturb the airflow in the vicinity of the disc, so these could not be used. Internal electrical heating can be closely controlled, the only problem being to pass current to the rotating disc, using slip rings, with their inherent losses. These, however, can be reduced to a very small level by careful design. It was, therefore, decided to use an

internal electric heater to supply the heat flux to the disc surface.

Surface temperatures were to be limited to 100°C so as to minimise distortion of the disc and allow freedom in the selection of materials. In addition, it was desirable to keep temperature differences small to prevent large changes in the fluid properties within the boundary layer. For this temperature range and for ease of use thermocouples were the obvious choice for measurement of the disc surface temperature. The thermocouples were mounted flush with the disc surface to measure the temperatures directly, whereas previous workers have mounted them below the surface and applied a correction to the readings to obtain the required temperature. The former method is more desirable provided the thermocouples are mounted so as not to alter the characteristics of the surface.

3.3 APPARATUS

GENERAL CONSTRUCTION

A number of requirements had to be considered in the construction of the rig. Vibration at the disc needed to be negligible to prevent interference with the natural point of transition. The electrical supply to the heaters, being A.C., must be kept as distant as possible from the thermocouple circuitry to prevent interference with the thermocouple signals. The disc material needed to have a smooth surface finish like a brake disc and a high thermal conductivity to maintain a uniform surface temperature with a varying heat transfer coefficient. These features will now be discussed in turn, as the construction of the apparatus is described.

A scale drawing of the rig is given in figure 3.01, and a general photograph in figure 3.02. Appendix 4 lists the manufacturers of the component parts of the rig.

FIGURE 3.01

DRAWING OF EXPERIMENTAL RIG

SCALE 1/10 FULL SIZE

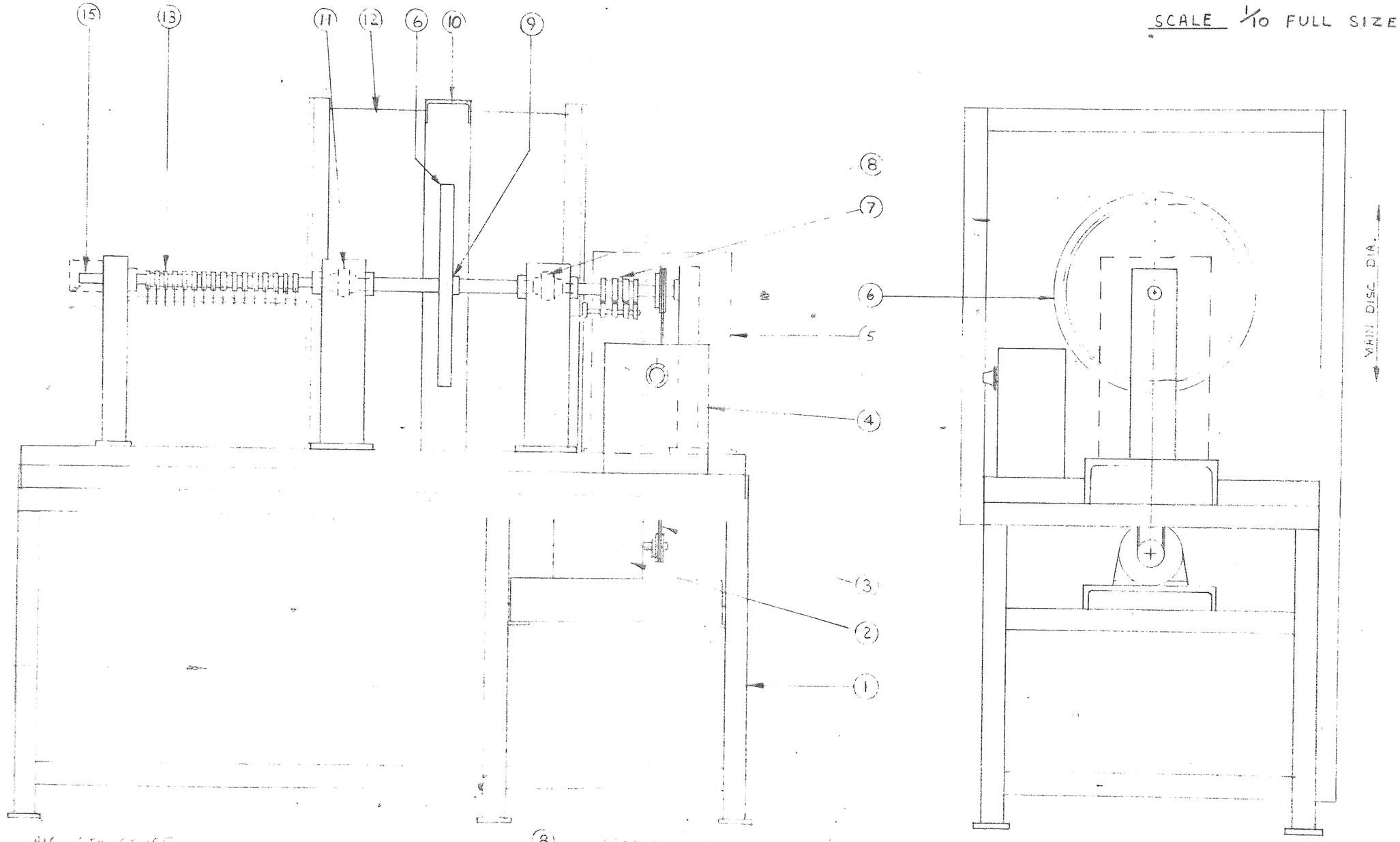

(1) RIG STRUCTURE
(2) VARIABLE SPEED D.C. MOTOR
(3) VEE BELT DRIVE
(4) VARIABLE SPEED CONTROL UNIT
(5) BELT & POWER SLIP RING GUARD
(6) DISC
(7) SLIP RINGS CARRYING POWER TO HEATERS
(8) FLEXIBLE COUPLING
(9) DISC MOUNTING FLANGE
(10) DISC GUARD
(11) FLEXIBLE COUPLING
(12) CURTAIN ENCLOSURE
(13) SLIP RINGS FOR THERMOCOUPLE E.M.F.'S
(14) CUPBOARD
(15) THERMOCOUPLE CONSTANT TEMPERATURE JUNCTIONS.

FIGURE 3.02

RIG USED FOR EXPERIMENTS IN STILL AIR

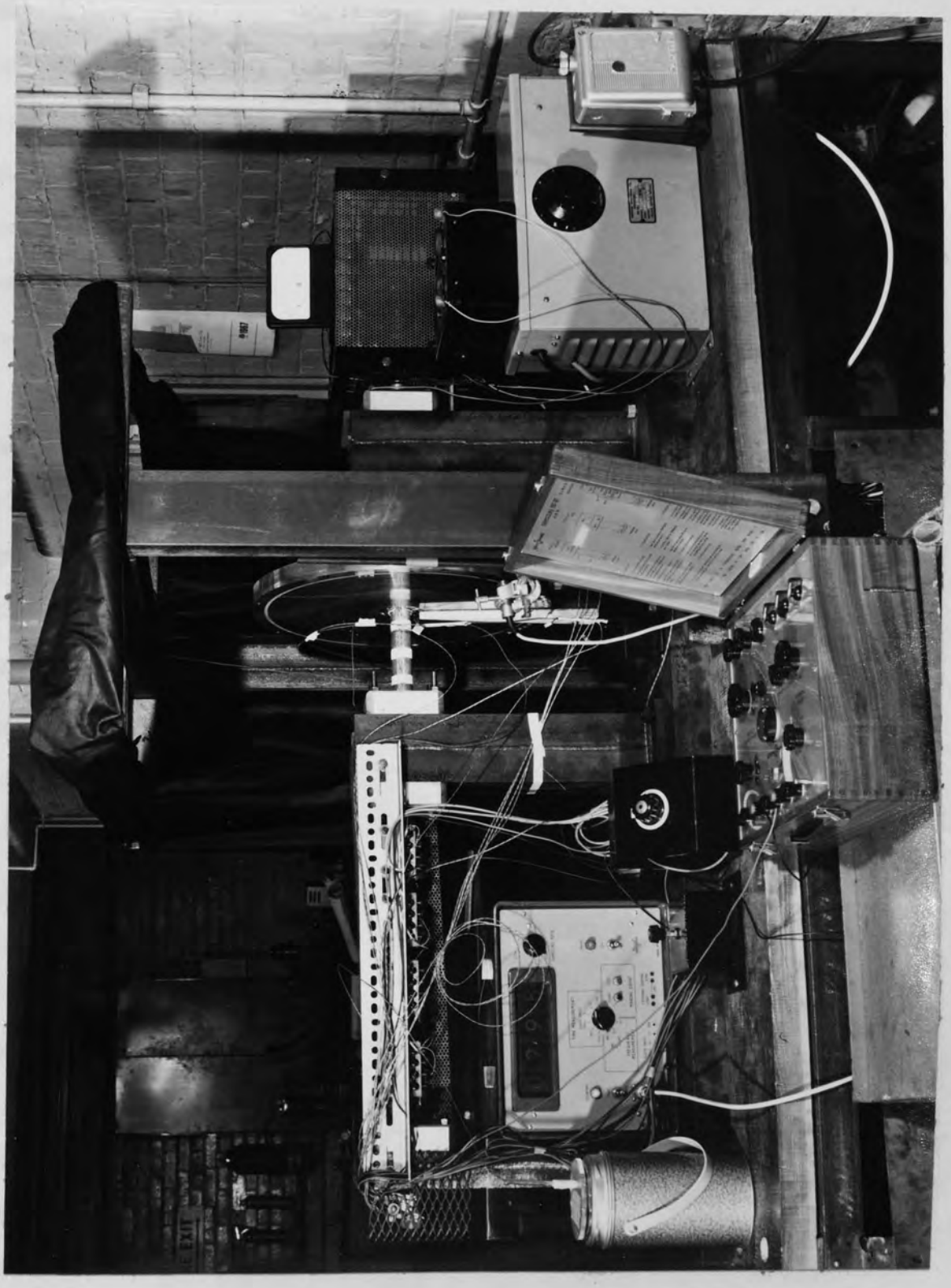

In order to prevent vibration the rig was constructed to be rigid and the possible sources of vibration were isolated. Four bearing pedestals, made from channel section mild steel, were bolted to a 1.7m length of heavy 0.3m wide channel, which was supported by a table constructed from angle iron. The shaft was split into three parts, connected by rubber flexible drives, to stop transmission of vibrations from one shaft to the next, necessitating six self-aligning bearings. One shaft carried the driven vee belt pulley and heater power slip rings, with a cage around them for safety, the next carried the disc, and the third the thermocouple slip ring units. The electric motor was mounted, through rubber feet, onto a separate table below the main shaft and the drive was transmitted with a vee belt and pulleys.

An enclosure was needed around the disc to shield it from air movements in the room. The size of this enclosure was determined from the measurements of Richardson & Saunders [35] on the effects of a nearby stationary plane on the heat transfer from a rotating disc (figure 2.12). This revealed that with a reasonable enclosure size of 0.6m square, and a main disc diameter of 0.4m (disc diameter to gap width = 1.3) the heat transfer would be reduced to 98% of the isolated disc value. The top of the enclosures was left open to prevent a large recirculation of hot air which would occur if the disc were fully enclosed. This would lead to a lengthening of the time needed to reach steady state and would also give problems in the measurement of the ambient temperature. Cobb & Saunders [32] had a ratio of disc diameter to distance from the disc to the bearing support of 8.1, which could have had an appreciable effect on the airflow near the disc, and so for the present apparatus this ratio was reduced to 2.4. As this lengthened the disc shaft it entailed a slight increase in the disc shaft diameter to keep the whirling speed above top operational speed, taking it from 25mm to 32mm.

Appendix 3 shows the calculation of the disc shaft whirling speed, which was found to be 8870 r.p.m. for the disc and shaft balanced to an accuracy of 3600g.mm. well above the top speed of 3000 r.p.m. It was not expected that the disc shaft would appreciably affect the airflow on the disc surface as the shaft diameter was only 32mm, as compared to the main disc diameter of 400mm, and would therefore impart a much lower velocity to the air.

DISC CONSTRUCTION

A scale section drawing of the disc is shown in figure 3.03. The disc was formed of two outer aluminium plates, clamped over the main electric heater. A ring of three countersunk screws held the plates to a Tufnol mounting flange, which was in turn taper doweled to the shaft. The outer parts of the plates were secured by an insulating ring, which was held by the split guard heater ring, held in turn by a ring of eight countersunk screws.

The surface of the aluminium disc was finished to 0.2μm by metal polishing and, when mounted on the shaft, ran true to 0.33mm axially and at the rim was eccentric by 0.015mm.

The main heater consisted of 0.64mm diameter "Wiggin Brightray Alloy C" nickel-chromium wire (max. current 5 amp at 500°C straight wire free air temperature) wound in a constant pitch spiral on a sindanyo former. Another sindanyo sheet of the same thickness was placed over the former to give full electrical insulation to the heater. The heater was wound to give a uniform heat flux, and as for most tests the heat transfer coefficient varied little over the surface of the disc, and the aluminium sheets transferred heat in the lateral direction very quickly, this was sufficient to give a predominantly uniform surface temperature. The outside surfaces of the sindanyo case were pressed into close contact with the aluminium plates to ensure even heat flow.

FIGURE 3.03

CONSTRUCTION OF DISC

Scale $\frac{1}{2}$ full size

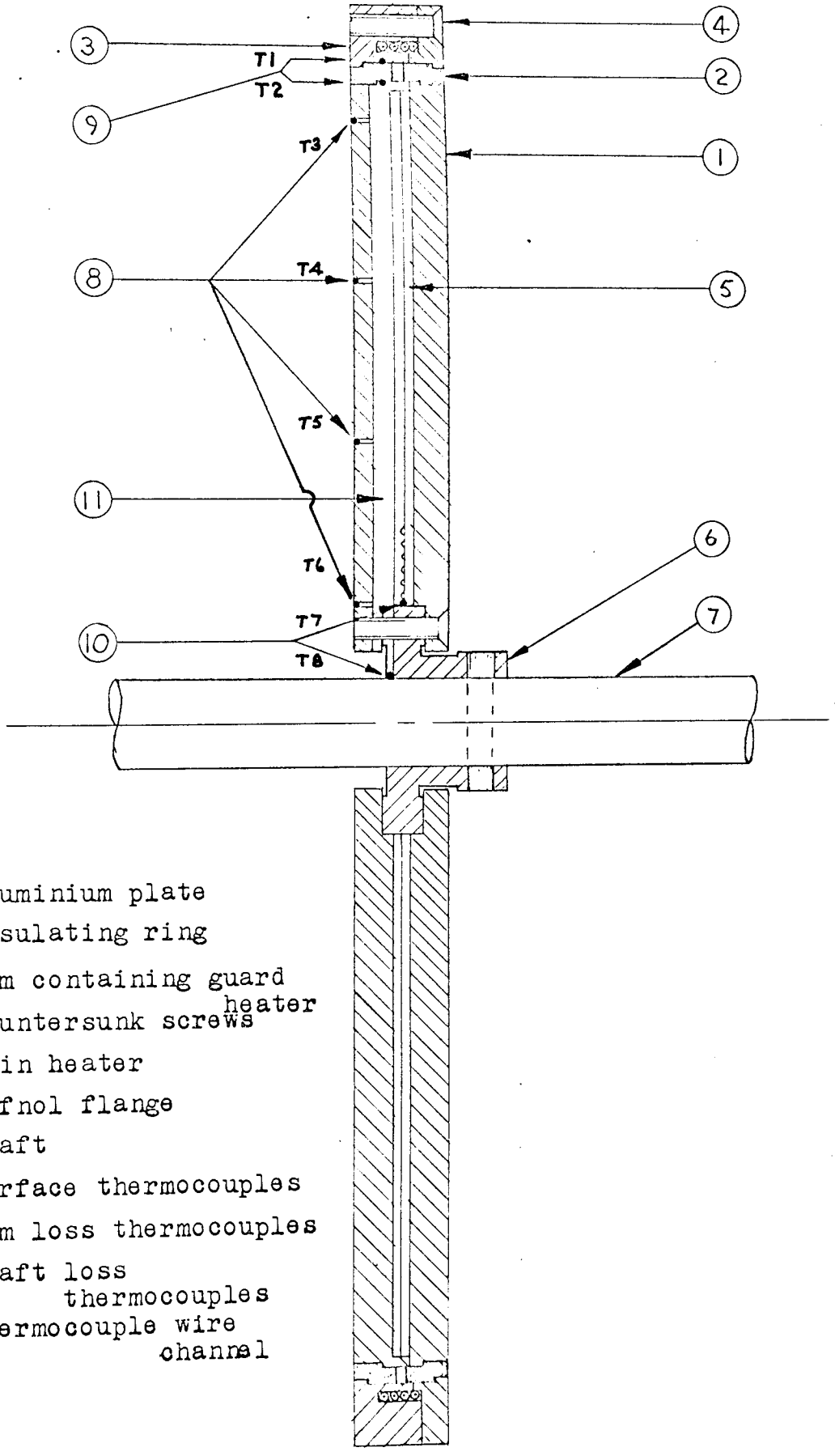

(1) aluminium plate
(2) insulating ring
(3) rim containing guard heater
(4) countersunk screws
(5) main heater
(6) Tufnol flange
(7) shaft
(8) surface thermocouples
(9) rim loss thermocouples
(10) shaft loss thermocouples
(11) thermocouple wire channel

The resistance of the main heater was 120 ohm at 20°C.

The guard heater was needed because the rim of a thin rotating disc convects away a considerable amount of heat, due to its large surface area and high heat transfer coefficient, compared to the disc surfaces. Therefore, either a thick insulating ring or a separate guard heater must be fitted to the outside of the disc. A thick insulating member would considerably increase the settling time of the system due to its slow rate of heat absorption and the calculation of heat losses would be difficult as the ring would convect at both side surfaces and at the rim. In addition, a heat flow to the rim would set up a temperature variation with radius on the surface of the disc, which is required to be as near isothermal as possible. A separate guard heater was therefore attached to the outside of the main heater. The power supply to this was varied to bring the temperature difference between the two heaters virtually to zero and prevent a loss of heat from the main disc to the rim.

The guard heater was formed of two aluminium rings, with the same heater wire as used in the main heater threaded into a glass fibre insulating sleeve and wound in to a groove. The resistance of the guard heater was 23 ohm at 20°C. Cobb & Saunders did not use an insulating ring between the main and guard heaters, but machined the adjoining faces to give a small area of contact. However, evaluation of their heater balance graph (figure 3.04) shows that the temperature difference across the gap between the disc and guard ring had to be kept to 0.3% of the disc to ambient temperature difference to achieve an experimental accuracy of ± 3%. For a minimum temperature difference of 10°C this corresponds to ± 0.03°C, whilst for a maximum of 80°C this difference was still only ± 0.24°C, or approximately ± 10.9 μV potential from a thermocouple. This was very small to be accurately measured with the Pye thermocouple test set as the galvanometer needle can only

FIGURE 3.04

Sensitivity of balance of guard heater to main heater

—x— tests at 500 rpm, allowance made for heat flow

—+— tests at 500 rpm, no allowance made for heat flow

—⊙— experimental data from Cobb & Saunders [32] at 460 rpm

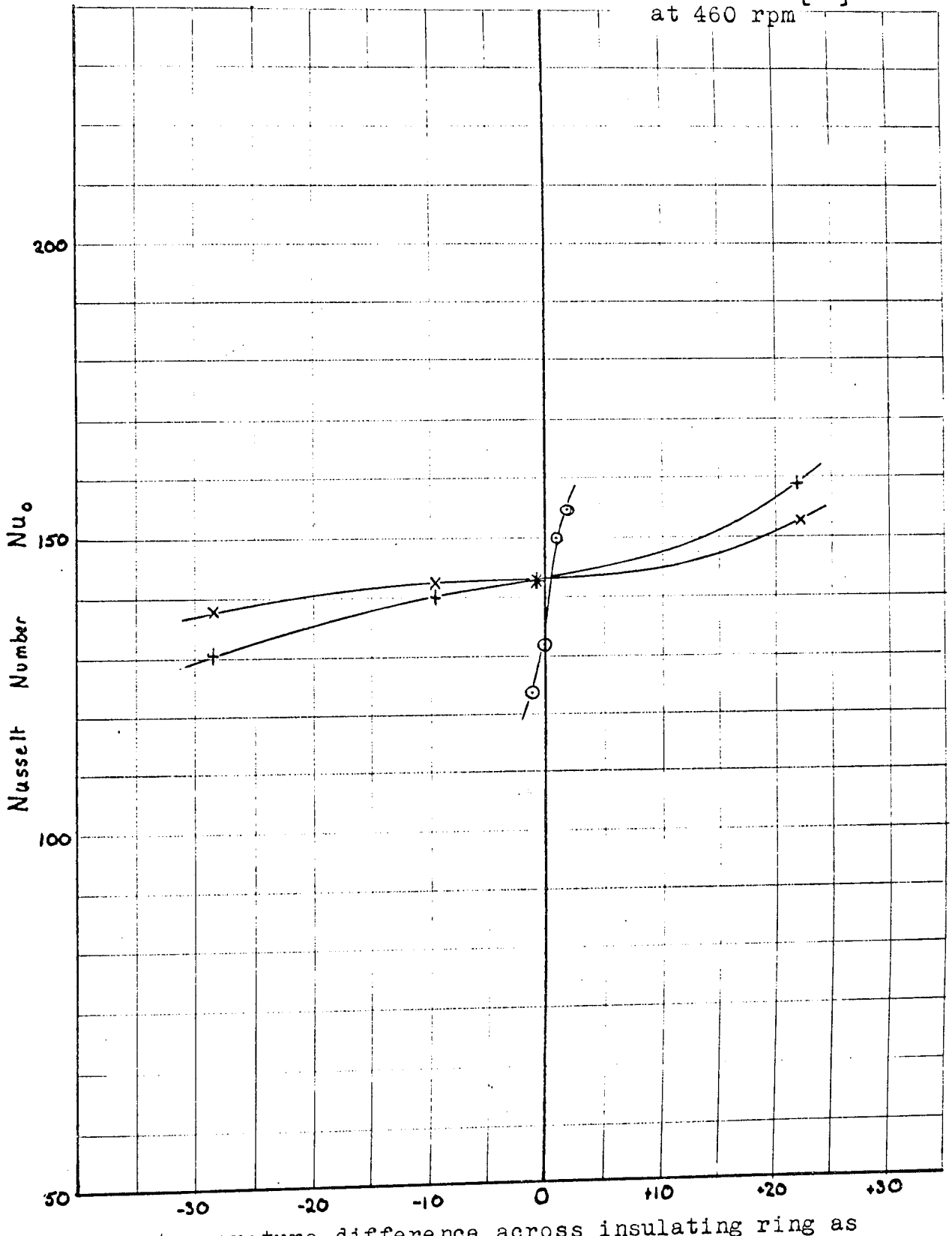

be set to an accuracy of ± 2.5 μV, equivalent to 25% of the maximum allowable error.

Initial tests were made without an insulating ring between the main disc and guard ring, and the heat transfer results verified that a balance could not be accurately maintained, calculations showed that for a reasonable temperature difference of 1.0°C, a heat flow of 760 watt was created, equivalent to the maximum main disc power. By inserting two plywood insulating rings with an air gap at the centre, as shown in figure 3.03, this heat flow was reduced to only 2 watt. Experiments with this arrangement produced the heater balance graph shown in figure 3.04. For a ratio of temperature difference across insulator to disc temperature above ambient of ± 5% an experimental accuracy of ± 2.1% was reached. This was further reduced by calculation of the heat loss across the insulator to ± 0.7%, as explained in the section on "Calculations".

THERMOCOUPLES

Eight thermocouples were mounted on the disc assembly, two to measure the temperature difference across the Tufnol mounting flange, two to measure the temperature difference across the rim, and the remaining four mounted flush with the disc surface at different radii on one side only. They were mounted all on one side to measure as closely as possible the temperature variation with radius. Other tests, to be described later, were made to see if both sides of the disc were operating at the same temperature.

The two rim thermocouples were mounted on opposite sides of the plywood insulating ring, on the same radius, inside the disc. The two thermocouples which measured the heat loss to the shaft were placed one on the Tufnol mounting and the other on the shaft as shown in figure 3.03. It was assumed that the shaft, having a much higher

thermal conductivity than the Tufnol, would be of constant temperature in the vicinity of the flange, and so the thermocouple was fixed to the shaft surface at the side of the flange.

The four surface thermocouples were placed at radii of 95%, 70%, 45% and 20% of the main disc outer radius. They were fitted in grooves flush with the surface, and cemented in position with Araldite. As Araldite is a good insulator the thermocouple junctions were fixed in position to protrude slightly above the surface and were then ground down to be perfectly flush. With a junction diameter of 0.76mm the temperature rise from the surface to the junction centre position was calculated as 0.15°C for 100°C disc surface temperature. Araldite was not allowed to cover the thermocouple as this would lead to a much higher error, for example, an Araldite thickness of only 0.03mm above the thermocouple would give a junction temperature 1°C above the surface temperature when the latter was 100°C. The thermocouple leads ran level with the surface for 100 wire diameters, to minimise lead conduction, and were then channeled into the interior of the disc.

The leads from all the thermocouples ran in a channel inside the disc on one side, came out at the base and then travelled along a channel in the shaft. The heater supply wires travelled along a channel on the opposite side of the disc.

ROTATION

A continuously variable speed from 30 to 3000 r.p.m. was decided upon, corresponding to a rotational Reynolds number from 8000 to 800,000. This gave a rotational speed slow enough to observe natural convection heat transfer effects, shown by Young {31} to be effective up to a Reynolds number of 40,000, and at the maximum speed 70% of the disc would be covered by turbulent flow, assuming a transitional Reynolds number of 240,000.

The power required to rotate the disc against frictional resistance was found from the equation for the moment coefficient by Theordorsen & Regier {10} .

$$Cm = 0.146\ Re_o^{-0.2} \quad \text{for turbulent flow} \qquad (3.01)$$

At 3000 r.p.m. $Re_o = 10^6$

giving $Cm = 0.009$

using $$Cm = \frac{T_q}{\frac{1}{2}\omega^2 R_o^5 \rho} \qquad (3.02)$$

we have $T_q = 0.335$ N.m.

This requires a power of 106 watt at 3000 r.p.m. (0.142 hp). In addition the losses in the bearings, belt drive and slip rings have to be overcome.

A 373 watt (0.5hp) variable speed D.C. motor with a Variac and rectifier control gave a speed range of 70 to 3000 r.p.m. at full load and was used with a Fenner vee belt drive of two ratios, 1:1 and 1:2.26. A single pulley of 0.15m (6 in) was fixed to the pulley/slip ring shaft, whilst two pulleys of 0.15m and 0.07m (2.65 in) could be interchanged on the motor. Two belts were needed, the one not in use being stored around the pulley/slip ring shaft, and the height of the motor table was adjustable to give the correct tension to the belt.

Subsequent tests proved this motor to be overloaded when tests were made with sectors on the disc, which occasionally rubbed the disc and considerably increased the friction drag. The motor continued to function, but required frequent renewal of the carbon brushes. To check for overloading an ammeter and voltmeter were connected to the motor supply. It was found that mains variation only occasionally caused speed changes greater than $\pm$ 3%, and when this occurred the test was repeated, so an electrical damping circuit was not required in the motor supply.

The rotational speed was measured with a Hasler hand tachometer, located in a centre at the end of the pulley/slip ring shaft. This tachometer had graduations of 2 r.p.m. It was calibrated with an electronic pulse counter focussed on the eight bolts at the periphery of the disc, giving eight pulses per revolution. A discrepancy of 2 r.p.m. was found throughout the speed range, which was ignored. Below approximately 60 r.p.m. the speed was measured by counting the revolutions in a minute.

ELECTRIC HEATERS

The construction of the heaters has been described and the method of power control will now be shown. The supply was taken from 240v AC mains and reduced to the required voltage with a series of resistance circuits, or alternatively increased with a Variac connected in the over-voltage position. The electrical circuits are shown in figure 3.05.

The required main heater power was calculated from the rate of convective heat transfer found by Richardson & Saunders and the maximum required surface temperature of 100°C. The guard heater power was estimated from the guard ring surface and rim rate of convective heat transfer, as shown in Appendix 5. These calculations gave a requirement of 470 watt for the main heater and 235 watt for the guard heater, a ratio of 2:1. However, when tests commenced it was found that more power was needed for the guard heater, as the dissipation from the rim was much higher than expected, lowering the ratio to 1.275:1. The power of the guard heater was therefore increased to 360 watt by reducing the resistance of the control rheostats. When the tests were run in the wind tunnel the main heater power was increased due to the high heat transfer coefficients found with air crossflow. An over-voltage connected Variac was used giving up to 750 watt for the main heater.

FIGURE 3.05

HEATER CIRCUITS

Note Quoted currents are rated values of wire

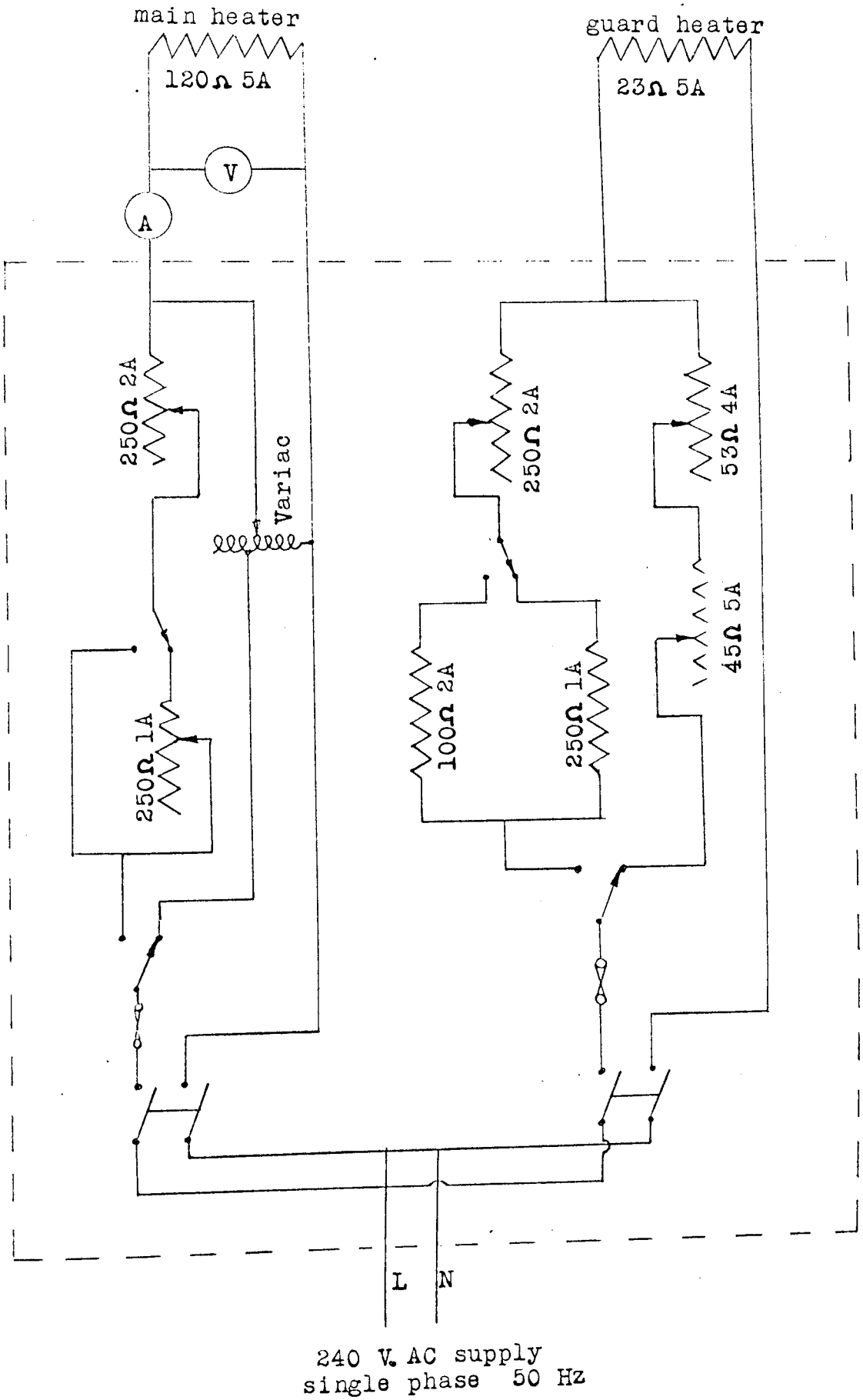

Figure 3.06 shows the box of slidewire resistors used to control the heater power.

The power to the main heater was measured with a 0-3A ammeter and 0-300v voltmeter connected into the circuit. The voltmeter could also be switched into the guard heater circuit to measure the voltage there. A voltage reading was sufficient as an accurate measurement of the guard heater power was not needed. These gauges were calibrated with a Cambridge AC dynamometer wattmeter, of accuracy to BSS 89, Pr grade. The resultant calibration curve is shown in figure 3.07 and this was incorporated into the computer programmes which processes the results. The maximum error was 2.5% at 50 watt, and above 140 watt the error settled to an average of -1.1%.

The power was transmitted to the heaters through four gun-metal slip rings, with low metal grade graphite brushes, supplied by Star Electro Carbons Ltd. Preliminary tests were carried out on these rings to determine the power loss. Two rings were connected in series and resistance readings taken at rotational speeds up to 3000 r.p.m. For both pairs of rings the resistance was less than 0.01 ohm at all speeds, both with the rings dirty and cleaned with fine emery. A photograph of the slip rings is shown in figure 3.08.

TEMPERATURE MEASUREMENT

The location of the thermocouples in the disc assembly were described in a previous section. Eight other thermocouples were positioned in the enclosure around the disc to measure the ambient temperature.

Nichrome-Constantan thermocouples were used for their high e.m.f. per temperature difference value and the low thermal conductivity of both of the constituent wire materials, hence increasing the accuracy of temperature measurement and reducing the lead conduction. The junctions were formed by resistance welding, using a capacitor

FIGURE 3.06

SLIDEWIRE RESISTOR BOX IN
HEATER CONTROL CIRCUIT

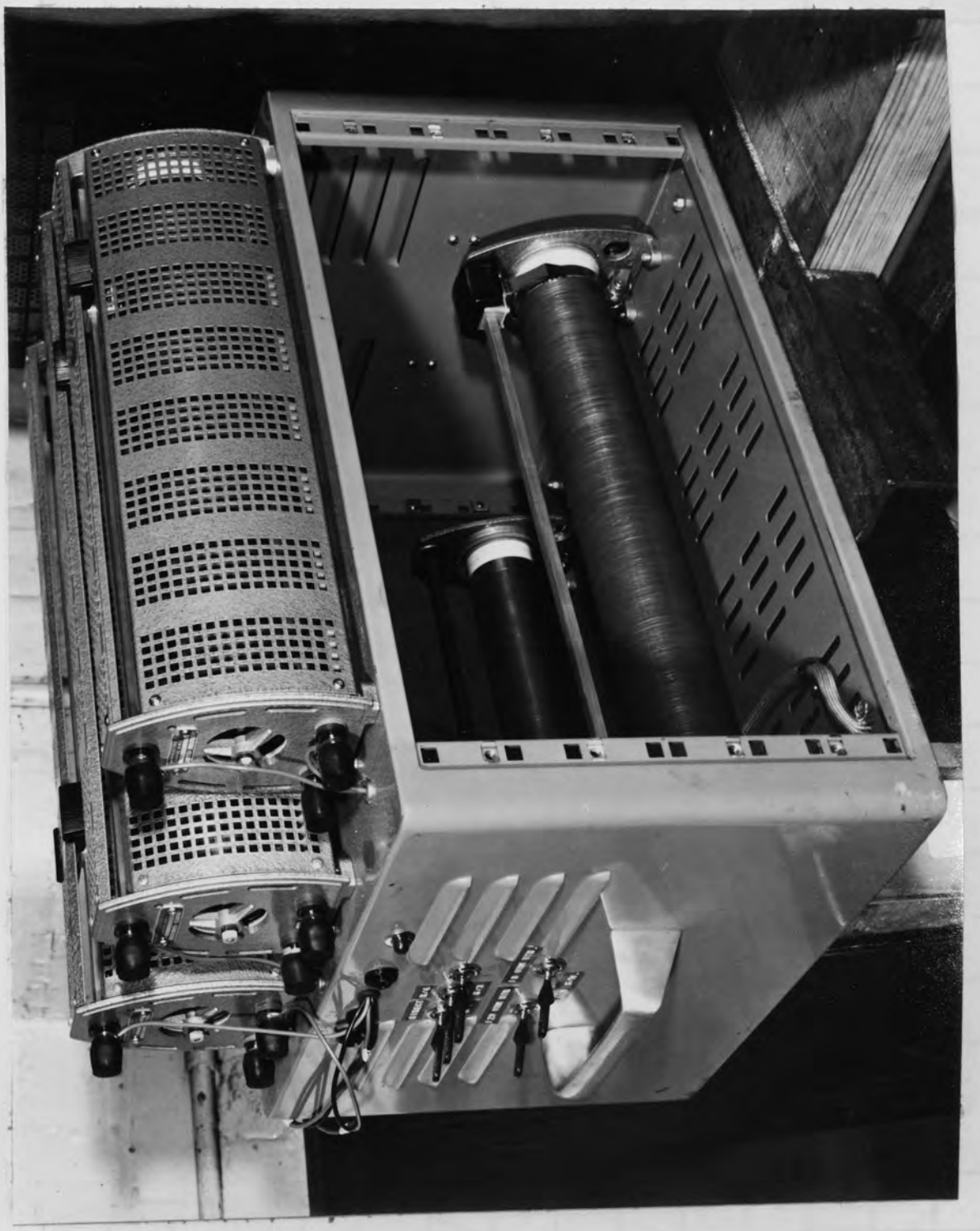

FIGURE 3.07

Calibration of Ammeter and Voltmeter

× measured error

——— mean line used to correct experimental results

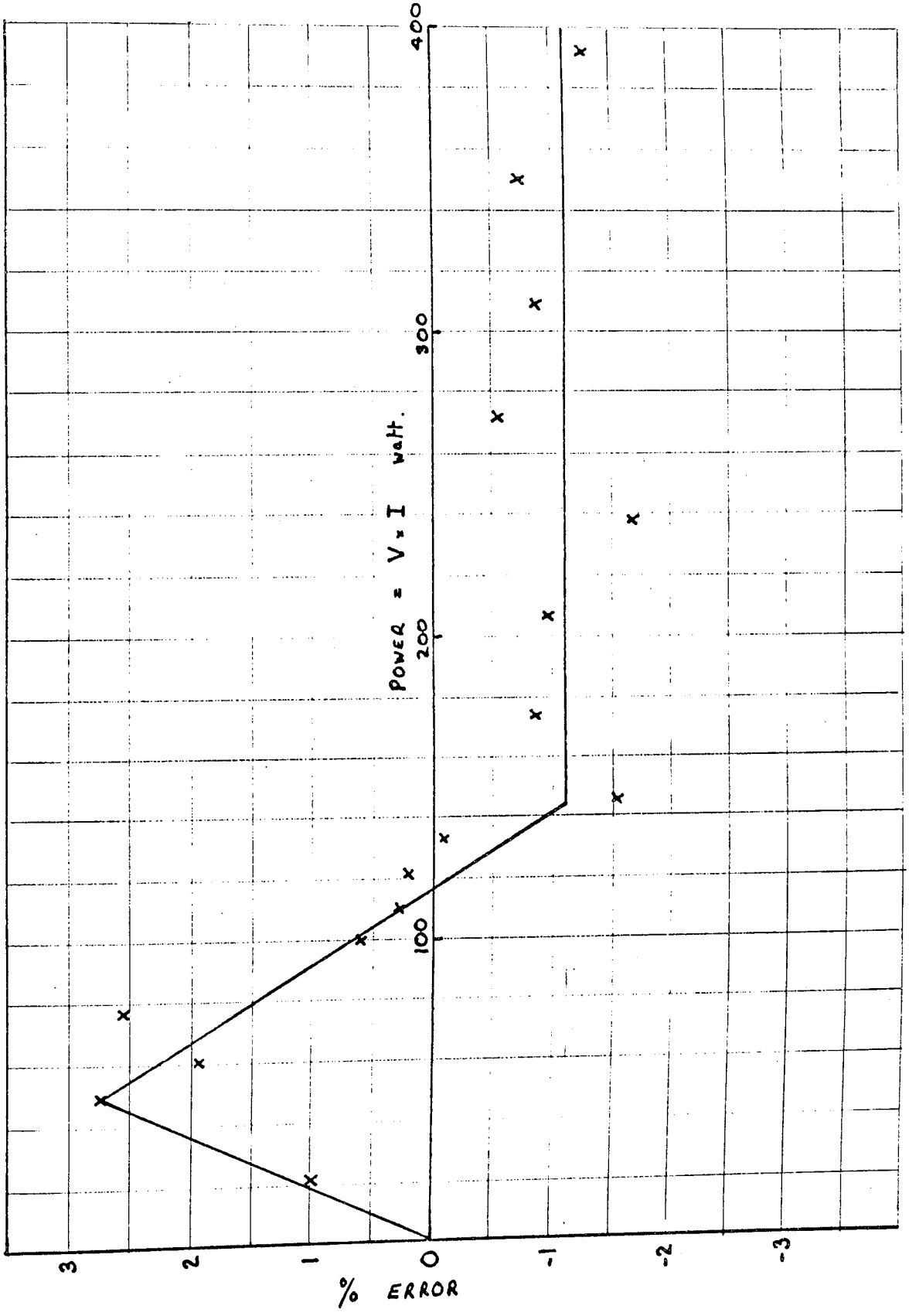

FIGURE 3.08

HEATER SUPPLY SLIP RINGS, METERS

AND VEE BELT DRIVE

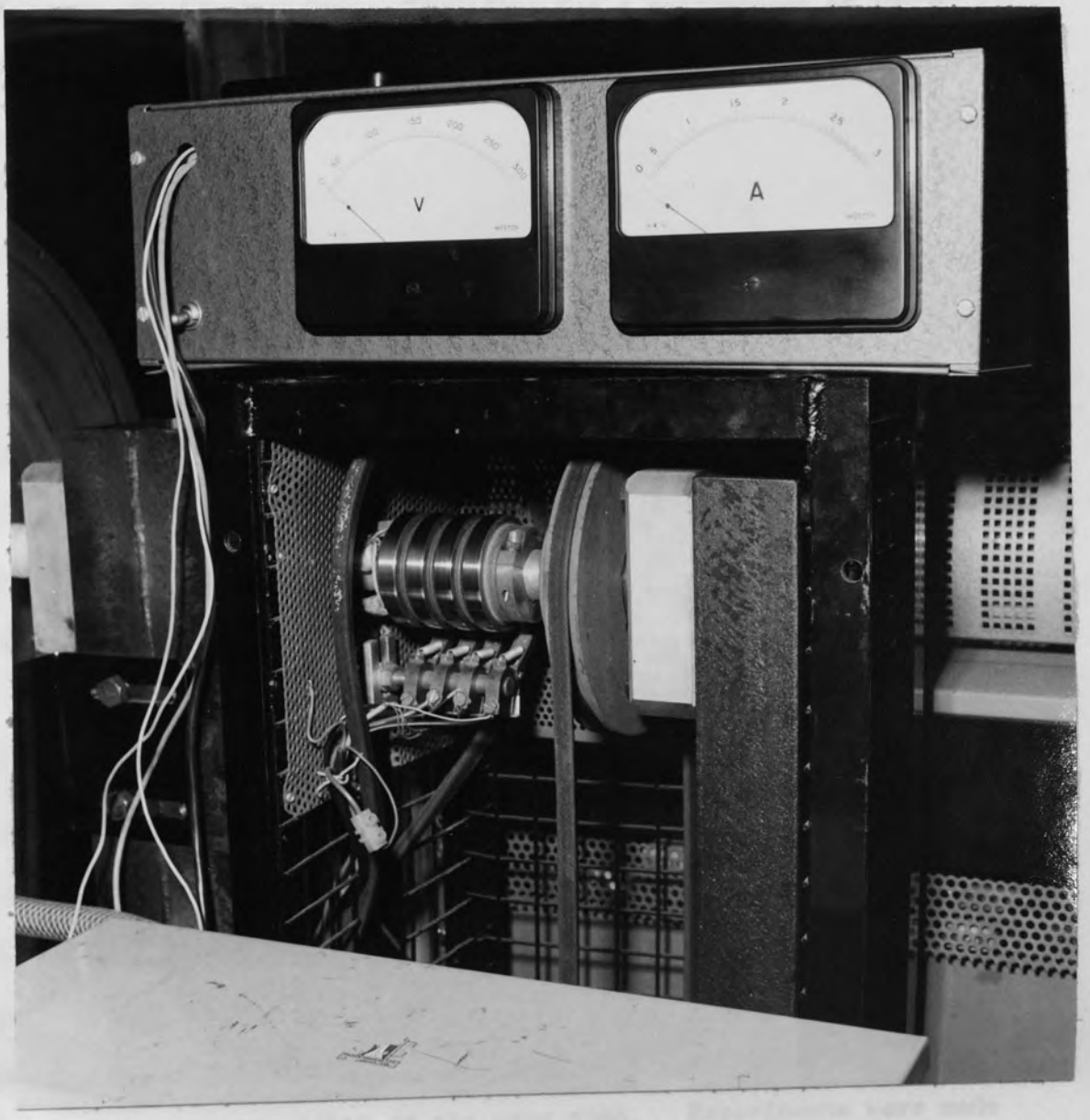

discharge machine, which gave junctions of approximately 0.75mm diameter. The thermocouples were calibrated from 0 to 100°C, prior to installation onto the rig, against a N.P.L.-calibrated mercury-in-glass thermometer. All the thermocouples agreed to within 0.6%, and the average potential over this range was 45.3 μV/°C. Both calibration and rig tests used an ice/water cold junction and a Pye thermocouple test set to measure the potential. The potentiometer needle of the test set could be zeroed to ± 2.5 μV (0.06°C), whilst the set was calibrated to ± 0.1% or ± 5 μV, whichever was the smaller. Therefore for a measurement of 100°C (4700 μV) the accuracy was ± 4.7 μV. A fifth order polynomial equation was fitted to the thermocouple calibration curve to facilitate computer calculation of the temperature from the potential reading. This polynomial

was $$T = 0.08814 + 24.66\ Em - 2.169\ Em^2 + 0.8452\ Em^3 - 0.1823\ Em^4 + 0.01473\ Em^5\ ^0C \qquad (3.03)$$

with Em in mV. This showed a zero error of -0.088°C and a deviation of + 0.196, - 0.102°C from the experimental results. After installation the thermocouples were checked at ambient temperature and the readings were all within 0.3°C at 20°C.

Richardson & Saunders discovered recirculation currents inside the enclosure of their rig which required more than one thermocouple to determine the mean ambient temperature. With the present apparatus it was found that four thermocouples placed in the axial inflow stream of air on each side of the disc were sufficient to find the ambient temperature. There was a noticeable difference between ambient temperatures taken on either side of the disc, but very little variation between measurements taken on the same side. Experiments were made with shields on the ambient thermocouples to stop radiation heat transfer from the disc, but the increased surface area of the shield increased

the recorded temperature instead of decreasing it. An unshielded thermocouple increased from 27.3°C to 27.4°C for a disc temperature of 84°C, whilst with a shield it increased to 27.7°C. Recirculation within the enclosure at 700 r.p.m. increased the ambient temperature to 32.9°C for no shield, and 33.3°C with a shield. These tests verified that the recirculation error must be measured but the radiation effect from the disc to an unshielded thermocouple can be neglected.

The thermocouple circuits are shown in figure 3.09. The nichrome and constantan wires are brought from the disc, through channels in the shafts to the extreme end of the thermocouple slip ring shaft where they are left to protrude beyond the last bearing. Here they are soldered to copper wires which return to one slip ring each. From the slip ring brush copper wires go to a multi-position switch which connects one pair in turn to the measuring circuit. Copper wires travel from the multi-switch to a point very close to the rotating soldered joints at the end of the shaft, to give as near equal temperature to them as possible. They are then soldered to nichrome and constantan wires again, which in turn have their junction in an ice/water mixture in a wide mouth thermos flask to form the cold junction. This circuit fulfills a number of requirements. The connections from thermocouple wire to copper wire are all within a small area, as near a constant temperature enclosure as possible, shown in the photograph of figure 3.10. The rotational movement of the shaft prevents hot-spots in this region by ensuring a continuous movement of air. Only one cold junction is needed, as this is in the measuring circuit and so if a variation in the temperature of the ice/water mixture occurs it affects all thermocouple readings alike and minimises the error. The ambient thermocouple wires are brought to the constant temperature enclosure, where they join the same circuit as the disc ones.

FIGURE 3.09

THERMOCOUPLE CIRCUITS

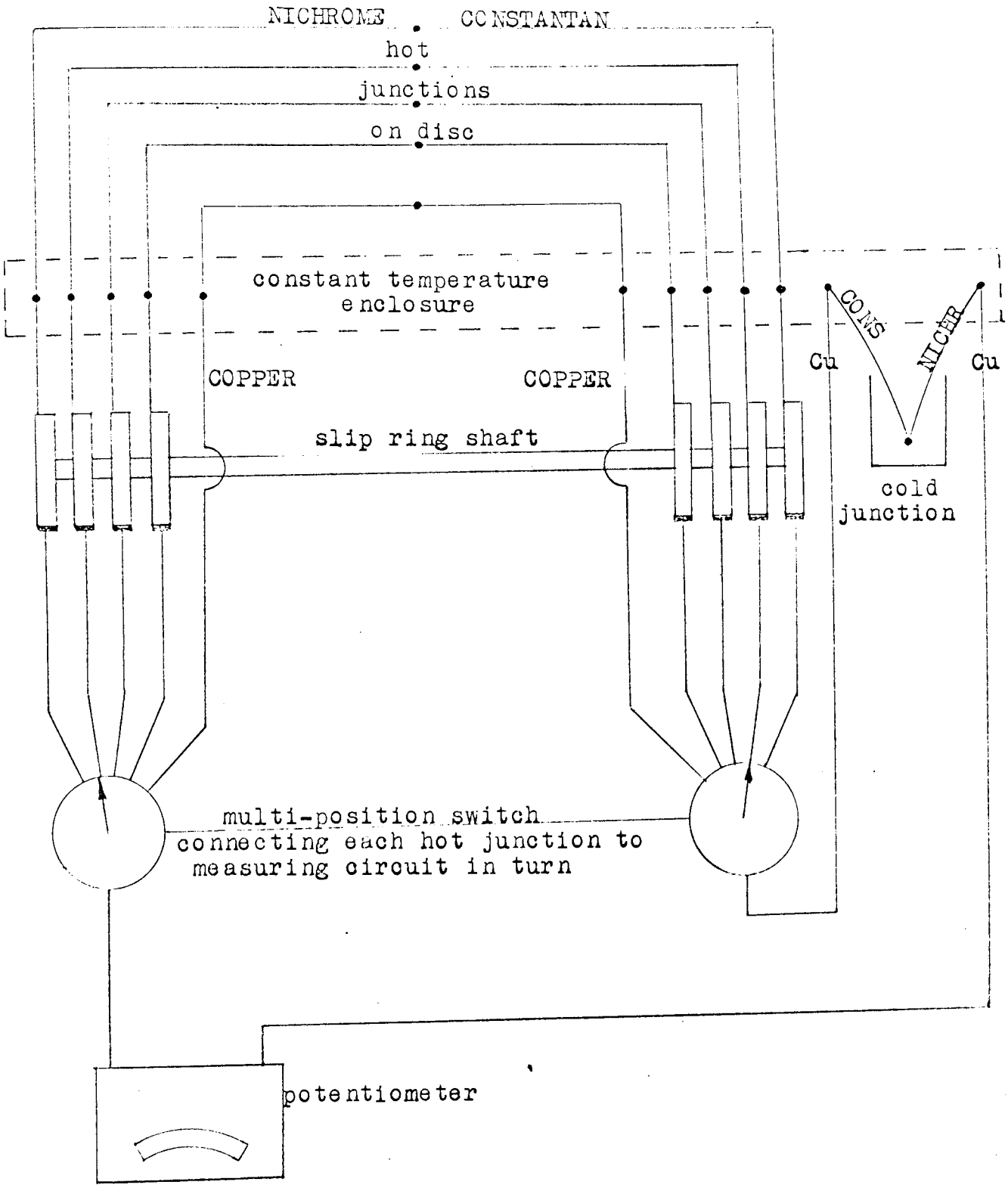

FIGURE 3.10

SLIP RINGS CARRYING THERMOCOUPLE SIGNALS

AND CONSTANT TEMPERATURE JUNCTIONS

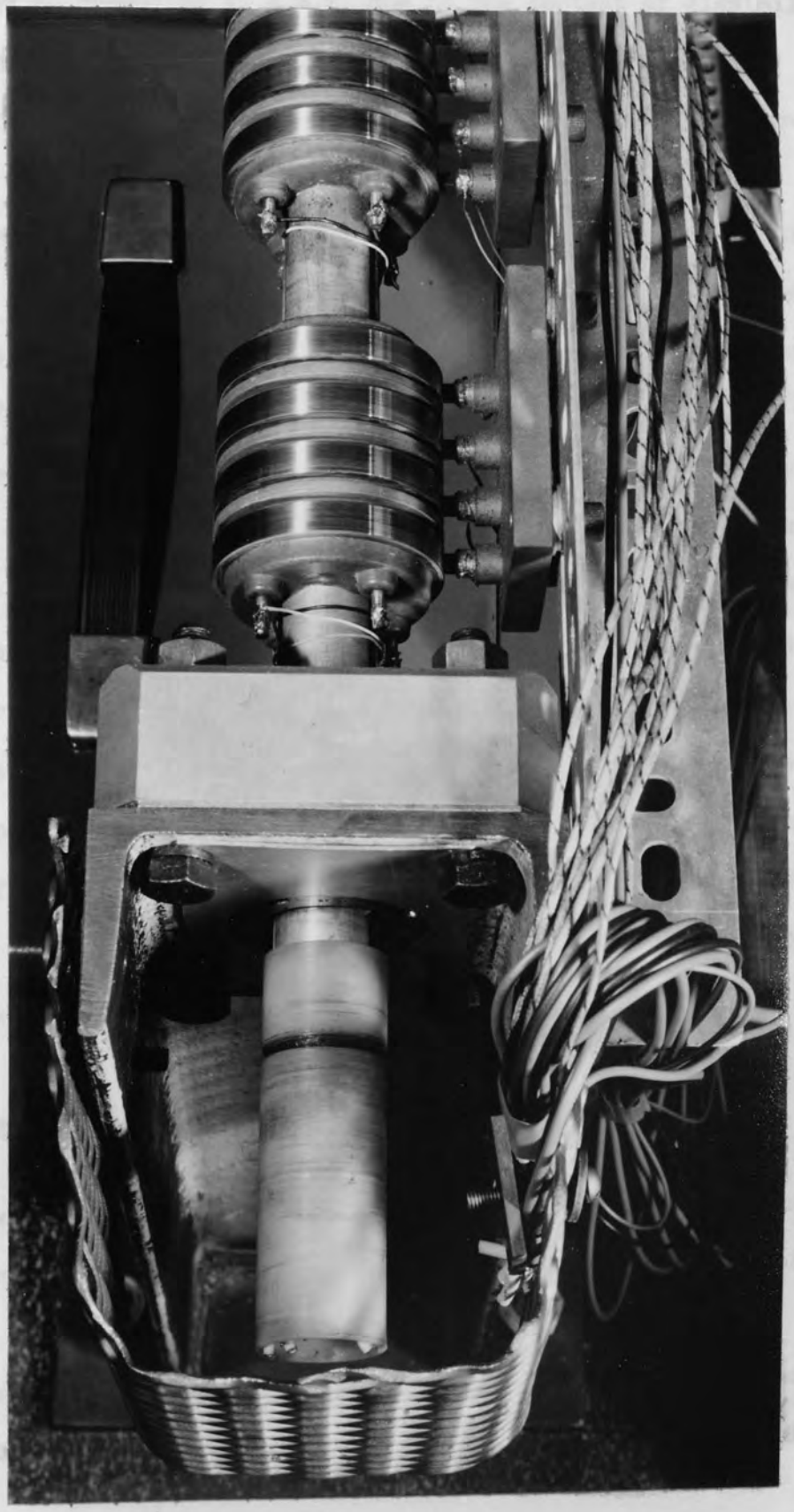

The slip rings are made of gun-metal (88% Cu, 10% Sn, 2% Zn) using high metallic copper-carbon brushes. These brushes are small compared to the ring, and work under a very lightly loaded spring. They make reliable transmitters of thermocouple e.m.f.s for two reasons, the rings and brushes both contain a high percentage of copper, reducing the chances of producing an e.m.f. due to the contact of dissimilar metals, and the low spring load and high ring mass keep running temperatures low, again reducing any potential created at the brush-ring interface.

The rings were tested to find the effect of speed and running time on e.m.f. transmitted. The rings were cleaned with very fine emery before tests commenced. Speed had no effect on the readings, and during a run of $7\frac{1}{4}$ hours the reading rose by only $0.375^{\circ}C$ at around $25^{\circ}C$. The rings were not re-cleaned during this time but it was subsequently found that they oxidised whilst they were stationary, rather than accumulated a film of carbon during a run, so they were cleaned prior to each daily run of tests. However, dirty rings were noticed immediately as they gave an erratic reading, not a constant inaccurate one.

Two thermocouple multi-switches were used to feed all sixteen thermocouples to the measuring circuit in turn. These had silver plated contacts for a long wear life and low electrical resistance. Frequent switching over a period of a few minutes was occasionally made during the tests, with no effect on the thermocouple readings.

WIND TUNNEL

The wind tunnel was a blower type with a closed working section and open return. The air was supplied by a centrifugal fan driven by a 20 hp motor. From the fan the air entered a large expansion and contraction chamber with flow diffusers, which gave a more uniform velocity distribution and reduced the level of turbulence intensity.

With the original test section of 0.46m square the level of turbulence intensity was guaranteed less than $\frac{1}{2}\%$ of the mean velocity. A new test section was designed to fit around the disc and between the bearing supports of the rig resulting in a duct of 0.7m by 0.25m. The new duct changed from the original size to the new one in a length of 0.46m and then ran for 0.56m before reaching the test section containing the disc. A photograph of the rig in position with the tunnel and showing the new ducting is given in figure 3.11. The tunnel was manufactured by Plint & Partners Ltd.

Calculations of the friction in the original duct at 30m/s entrance velocity gave a loss of 1.5m of air (5.4m/s) and with the new duct the friction loss was 3.7m (8.5m/s), but the reduction in area gave an increase of 9m/s. Therefore the air velocity in the new test section was calculated to be 30.5m/s for the same setting that gave 30m/s originally. In fact, measurements of the duct effect were only made at the maximum speed, where the original speed was 36.5m/s whilst the new one was 34.5m/s, indicating that the frictional resistance was slightly higher than expected.

The details of the entrance velocity variation and temperature measurements, blockage area and wall constraint effects are given in chapter 4, part 3.

VELOCITY MEASUREMENT IN THE BOUNDARY LAYER

To measure the velocity in a boundary layer a very small bore pitot tube is needed due to the rapid change of velocity with distance. In addition a large range of velocity has to be measured with close accuracy to obtain a good representation of the profile. To achieve these a pitot tube was made from a hypodermic needle. The end of the needle was modified to a rectangular shape 0.12mm x 0.76mm, and the long side

FIGURE 3.11

RIG WITH WIND TUNNEL FOR

EXPERIMENTS IN AIRSTREAM

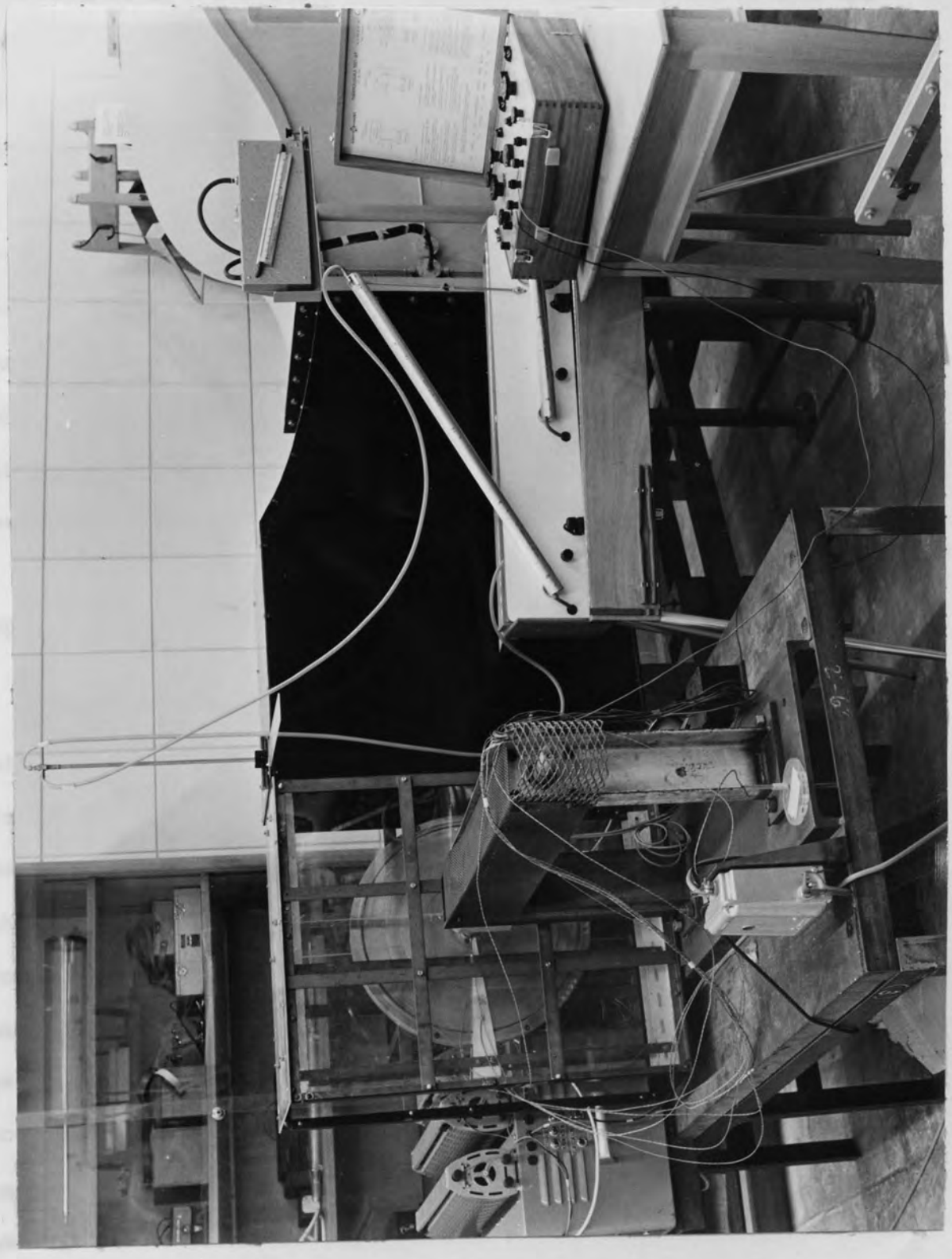

mounted parallel to the disc surface in order to measure across as small an axial width as possible. The total pressure was transmitted through a plastic tube to a Hilger & Watt type MDC electrical micromanometer. This is a transducer which converts pressure to an electrical signal which is then read directly on a gauge. By using three transducer heads (500-0-500, 50-0-50, 5-0-5 N/m^2) pressure heads from 0.2 to 1000 N/m^2 were measured, giving air velocities from 0.58 to 40.6 m/s at 20°C. Each head had a guaranteed accuracy of 1%. The static head was taken as atmospheric pressure outside the boundary layer.

To measure the angle of yaw the pitot was mounted onto an arm which rotated against an angular scale, of accuracy $\pm$ 0.5°, such that the end of the pitot tube moved around a point. The pitot was then rotated until maximum velocity was recorded on the micromanometer, and then that angle was the angle of yaw at that point. The yawmeter is illustrated in a photograph in figure 3.12. The axial position of the pitot was set with a depth micrometer, reading to 0.025mm (0.001 in).

FLOW VISUALIZATION

Flow visualization was achieved by releasing a visible gas into the airstream. Two gases were used, titanium tetrachloride, which smokes in contact with air, and paraffin smoke. The former was kept in a wash bottle and air was blown through it, forming smoke, which was carried to the required release point through a rubber tube. This arrangement was portable but had to be used with care due to the corrosive action of the smoke. Paraffin smoke was made with a smoke generator. This was safer, although just as unpleasant in heavy concentration. The machine took a few minutes to warm up and was cumbersome, needing a long tube to carry the smoke to the release point. The rate of release of either smoke could be easily varied.

FIGURE 3.12

PITOT TUBE ON TRAVERSING YAWMETER

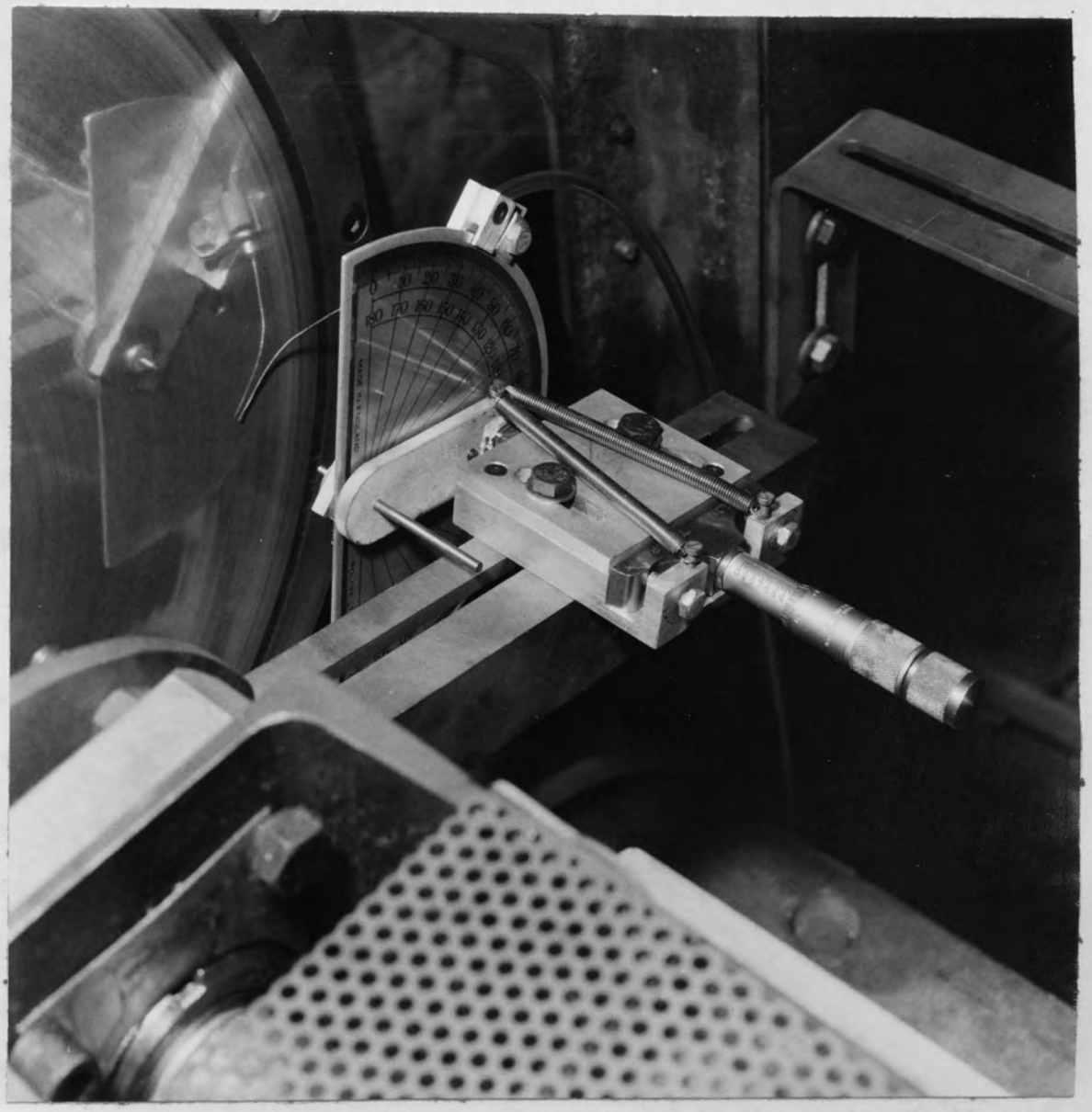

EXPERIMENTAL CHECKS

During construction of the disc the main heater was clamped firmly against the inside faces of the aluminium plates and each side of the disc was made and treated identically. This meant that each side of the disc should conduct the same amount of heat from the middle and both surfaces should be of the same temperature. All the thermocouples were mounted on one side of the disc to obtain a good coverage of the surface for an accurate picture of the variation of surface temperature with radius. Therefore the temperature of each side of the disc could not be checked with the disc rotating. Since a high rate of convective heat transfer was needed to show up any discrepancies tests were made with the disc stationary in the wind tunnel with an air crossflow of 15m/s. Thermocouples were taped to each side of the disc in identical positions and they gave the readings shown in figure 3.13, where they indicate that the heat flow to each side of the disc was not identical but followed the average ratio

$$\frac{Q \text{ couple}}{\frac{1}{2} Q \text{ total}} = \frac{2\ \theta \text{ couple}}{\theta \text{ couple} + \theta \text{ no-couple}} = 1.148^{+\ 0.003}_{-\ 0.007} \qquad (3.04)$$

Tests were also made with the disc stationary in still air but the results were too easily affected by stray air currents and were considerably scattered. The above ratio indicates that there was 15% extra heat flow to the side of the disc with the thermocouples mounted on it. As the disc was not dismantled whilst all the other tests were made it was reasonable to assume that this ratio remained constant; it could only depend on the internal resistance to heat flow of the disc.

When the ambient temperature was measured in the enclosure it was found that those thermocouples on the hotter side of the disc consistently indicated higher temperatures, due to recirculation from this hotter surface. Therefore the heat transfer calculations were made for one side of the disc only, as the surface whose temperature was

FIGURE 3.13

Measurements of heat flow to each side of the experimental disc

crossflow velocity 14·6 m/s, disc stationary

power input watt	temperature of thermocouples placed in identical positions on opposite sides of the disc above ambient °C		correction factor $\frac{2\,\theta_{couple}}{\theta_{couple}\ \theta_{non\text{-}couple}}$
	θ_{couple}	$\theta_{non\text{-}couple}$	
716	35·5	25·1	1·170
	38·2	29·3	1·130
	36·8	27·6	1·142
		average	1·148
524	25·1	17·9	1·169
	27·8	20·8	1·144
	26·0	19·7	1·139
		average	1·151
334	16·4	11·7	1·169
	18·0	13·5	1·142
	16·8	12·7	1·139
		average	1·150
324	17·7	12·1	1·189
	17·8	13·0	1·156
	17·2	14·3	1·091
		average	1·145
509	27·4	18·6	1·190
	27·7	20·3	1·152
	27·8	21·9	1·119
		average	1·154
754	39·4	28·7	1·156
	41·3	30·3	1·152
	41·4	32·8	1·116
		average	1·141

average correction factor from all the above readings $= 1{\cdot}148\ ^{+0{\cdot}003}_{-0{\cdot}007}$

continually measured could draw an ambient supply from that side of the enclosure only. The heat flow to that side of the disc was easily calculated from the total heat input multiplied by the ratio of heat flow to that side (equation 3.04).

Previous work has shown that the heat transfer coefficient is independent of radius for laminar flow and varies with radius to the index 0.6 for turbulent flow, hence for a uniform heat flux the surface temperature should not deviate greatly from constant. In addition the high thermal conductivity of the aluminium relative to the low thermal convection from the surface should further help to produce a uniform surface temperature. Experiments showed that the surface was uniform to within $\pm$ 8% of the disc to air temperature difference for the worst case of a stationary disc in still air (natural convection) and to $\pm$ 4% for all the other cases.

The heat transfer from a rotating disc in still air was measured at a rotational Reynolds number of 120,000 with the disc in a curtained enclosure, in a test section of a wind tunnel and with the curtains removed, leaving the enclosure as a large room. The same results were found for each case, indicating that the enclosures did not affect the heat transfer, with the proviso that in the curtained enclosure and the wind tunnel the ambient temperature was measured with care to ensure that any recirculation of hot air was allowed for. Natural convection was negligible at that Reynolds number.

The overall accuracy of the results, as deduced from the accuracy of each component measurement was $\pm$ 5%. The scatter of results for the disc rotating in still air and in an air crossflow was $\pm$ 4% but a larger scatter was created by friction effects when sectors were placed on the disc.

3.4 PROCEDURE

In this section the method of taking the measurements will be described along with the checks that were needed. Certain assumptions had to be made in the calculation of the experimental data, and these will be described along with their justification and the effect of their being in error, and finally the processing of the results will be explained.

Preliminary tests were made to discover the length of time needed for the system to reach steady state. The longest time was with the lowest rate of convective heat transfer, which was natural convection from a stationary disc in still air, taking four hours to reach steady state. The shortest was with an air crossflow on the disc, taking about thirty minutes to reach steady state. The rotational speed took forty-five minutes to one hour to stabilize at the start of a day as the bearings warmed up slowly, allowing a gradual increase in speed.

The first test of the day would commence as follows. The guard and main heaters were set at approximately the powers required, the average ratio was found to be approximately

$$\frac{\text{main heater power}}{\text{guard heater power}} = 1.275 \qquad (3.05)$$

The speed was set just below that required and then while the system was settling down the ice/water cold junction flask was prepared, and the thermocouple slip rings cleaned and checked. Surface temperature readings were taken at intervals until they remained constant, indicating that steady state had been reached. The temperatures on each side of the insulating ring between the guard and main heaters were taken and the guard heater power adjusted to bring their difference to within $\pm$ 5% of the disc to ambient temperature difference. The guard heater was designed to have a much quicker response than the main heater and

therefore settled to a new temperature much quicker.

When the system had settled to a steady surface temperature the heater power inputs and the rotational speed were measured, then the disc and ambient thermocouple potentials. The power inputs and the rotational speed were then measured again and if they deviated from the first readings by more than $\pm$ 3% (due to mains variation) the test was repeated. It was found that only at certain times of the day, corresponding to dinner-time and evening shut down in the factory, did the mains fluctuate more than this.

The measurements that were taken with auxiliary equipment, the wind tunnel and the air jet, are described in the relevant section in chapter 4.

3.5 ASSUMPTIONS

The majority of the assumptions are concerned with the calculation of the heat losses to the rim, to the shaft and due to radiation.

To calculate the heat loss to the rim it was assumed that heat was conducted unidirectionally through the insulating ring, with no loss to the edge and no heat loss through the central air gap. The thermal conductivity of the wood was taken as 0.125 J/m s ^{o}K. The accuracy of the allowance for rim loss has already been shown to limit the error of the heat transfer coefficient to only $\pm$ 0.7%.

The heat loss from the disc to the shaft through the Tufnol mounting was treated as a unidirectional flow through three thick cylinders. The two outer ones had an outside edge temperature identical to the disc surface temperature. The inner cylinder had an outside temperature as measured by the thermocouple fixed to it. All three cylinders had an inside temperature identical to the shaft. The thermal conductivity of the Tufnol was given as 0.356 J/m s ^{o}K by the manufacturers.

The emissivity of a polished aluminium surface was given as 0.039 to 0.057 by Kaye & Laby {70} , and a mean value of 0.048 was used in the calculations. The maximum heat loss by radiation was 4% of the total heat input so the range of 19% in the emissivity only gives a possible error of 0.8% in the heat transfer coefficient.

The fluid properties were taken at the mean of the disc and ambient temperatures. Values of the viscosity and thermal conductivity for air were taken from tables of measurements by K. Sigwart, reproduced in the text of Eckert & Gross {71} . The relevant section of these tables is given below, converted to S.I. units; values at intermediate temperatures were found by linear interpolation.

Temperature	Viscosity	Thermal Cond.	Prandtl No.
T ^{o}C	ν m^2/s	k W/m ^{o}K	Pr
-23.3	9.51×10^{-6}	0.02223	0.722
26.6	15.7×10^{-6}	0.0262	0.708
76.6	20.8×10^{-6}	0.03	0.697

It is worthy of note that for all the experiments the Prandtl number was within the range from 0.699 to 0.708.

3.6 CALCULATIONS

The processing of each set of measurements would have been extremely tedious and time consuming and as the calculations were of an iterative nature a computer programme was developed to do them (Programme no. CVAE 21).

The computer programme is shown in figure 3.14 and a print-out shown in figure 3.15

All measurements were recorded in laboratory books, with each item dated. The date was also recorded on the computer print-out and the processed results were assembled into a loose-leaf folder,

FIGURE 3.14

```
CVAE21;
"BEGIN" "REAL" W,P,AMP,V,TAV,TC,VIS,K,PR,RED,LS,LR,LRAD,Q,H,NU,
R,R1,U,RET,PA,TA,F,F1,E,N;
"INTEGER" A,KK;
"ARRAY" T[3:12];
"INTEGER" "ARRAY" C[1:5];
"SWITCH" SS:=J;
"READ" N;
J:
KK:=1;
INSTRING(C,KK);
"READ" W,P,AMP,V;
"FOR" A:=3 "STEP" 1 "UNTIL" 12 "DO"
"BEGIN" "READ" T[A];
T[A]:=32+9/5*(-.08814+24.66*T[A]-2.169*T[A]↑2+.8452*T[A]↑3-.1823
*T[A]↑4+.01473*T[A]↑5);
"END";
"READ" PA,TA;
TAV:=(T[6]+T[7]+T[8]+T[9])/4;
TC:=(TAV+T[12])/2;
"IF" TC < 80 "THEN"
"BEGIN" VIS:=10.22+(TC+10)/90*6.66;
K:=.01287+(TC+10)/90*.00229;
PR:=.722-(TC+10)/90*.014;
"END" "ELSE"
"BEGIN" VIS:=16.88+(TC-80)/90*5.5;
K:=.01516+(TC-80)/90*.00219;
PR:=.708-(TC-80)/90*.011;
"END";
R:=7.9375;
R1:=.875;
RED:=3.14159*W*R↑2*1₀5/(30*VIS*144);
LS:=(T[10]-T[11])*2*3.14159*.4375*8.5₀-4*4.1868*2.54*5/(9*LN(1.375
/.625))+(T[9]-T[11])*2*3.14159*.4375*8.5₀-4*4.1868*2.54*5/(9*
LN(.875/.625));
LR:=(T[4]-T[3])*1.25₀-3*2*3.14159*8.09375*2.4*5/(.1875*9);
LRAD:=.048*.1714*(((460+TAV)/100)↑4-((460+T[12])/100)↑4)*2*3.14159
*(R↑2-R1↑2)/144*.29307;
Q:=AMP*V;
"IF" Q<48 "THEN" E:=Q/48*2.7 "ELSE"
"IF" Q<142 "THEN" E:=-.0405*Q + 4.74 "ELSE" E:=-1.1;
Q:=Q*(1+E/100);
Q:=Q-(LS+LR+LRAD);
Q:=N*Q/2;
H:=144*Q/(3.14159*(R↑2-R1↑2)*(TAV-T[12])*.29307);
NU:=H*R/(K*12);
F:=.99820-.00116*(TA-20)/5;
F1:=.07678*520*PA/((TA*9/5+492)*762);
U:=SQRT(64.4*P*F*62.43/12/F1);
U:=256*U/236;
RET:=U*17.813*1₀5/(VIS*12);
TAV:=TAV-T[12];
KK:=1;
"PRINT" ''L5'';
OUTSTRING(C,KK);
"PRINT"
''L2'EXPERIMENTAL RESULTS FOR ROTATING DISC IN AIR CROSSFLOW

NETT HEAT INPUT',SAMELINE,ALIGNED(3,1),Q,
''S'WATT'S5' TEMPERATURE DIFFERENCE',TAV,
''S'F'L'LOSSES',ALIGNED(2,1),LS,
''S'',LR,''S'',LRAD,''S5'PR',ALIGNED(1,3),PR,
'L'HEAT TRANSFER COEFFICIENT',ALIGNED(2,3),H,
''S'B.TH.U./FT2.H.F.'L'AIR CROSSFLOW VELOCITY',ALIGNED(3,1),U,
''S'FT/SEC'S4'DISC R.P.M.',ALIGNED(4,0),W,''L'RE DISC',
''S'FT/SEC'S4'DISC R.P.M.',ALIGNED(4,0),W,''L'RE DISC',
ALIGNED(6,0),RED,''L'RE CROSSFLOW',RET,
```

FIGURE 3.15

Data input and Print out from computer programme CVAE 21 used to process experimental results

Data input

```
1.148
'7-8-68'
518  2.35  2.27  278  2.136  2.061  2.061  1.942  1.959  2.009
1.96  2.532  1.341  1.136  750  25

 CVAE21
```

Computer print out

```
7-8-68

EXPERIMENTAL RESULTS FOR ROTATING DISC IN AIR CROSSFLOW

NETT HEAT INPUT 357.1 WATT      TEMPERATURE DIFFERENCE  32.6 F
LOSSES  1.8  -1.3  1.5      PR 0.706
HEAT TRANSFER COEFFICIENT 27.570 B.TH.U./FT2.H.F.
AIR CROSSFLOW VELOCITY 112.4 FT/SEC     DISC R.P.M.  518
RE DISC 133251
RE CROSSFLOW 936352
NU 1174.2
```

with the data input. Any test could then be traced from the computer print-out, to the data input and to the laboratory book, by following the date. A maximum of five tests were conducted in any one day, so it was comparatively easy to locate any individual test should the results give cause for further study of the experimental measurements.

Each of the calculations in the programme will now be described. These are in English units as the programme was written at the beginning of the project before the S.I. system was introduced.

GENERAL HEAT BALANCE

The general heat balance equation for the experimental disc is

$$Q_{couple} = h_m A_o (T_w - T_\infty) \qquad (3.06)$$

In these experiments the total heat input to the disc, Q, and $(T_w - T_\infty)$ the temperature difference between the surface and the enclosure on the thermocouple side of the disc, were measured.

Q_{couple} was calculated from

$$Q_{couple} = \frac{Q \times 1.148}{2} \qquad (3.07)$$

and A_o was found from

$$A_o = \pi (R_o^2 - R_i^2) \qquad (3.08)$$

The total heat input, Q, was found by

$$Q = \text{amp} \times \text{volt} \times \text{calibration factor} - (\text{rim loss} + \text{shaft loss} + \text{radiation loss}) \qquad (3.09)$$

LOSSES

The heat losses from the disc in $\underline{B.Th.U}_s$ are calculated as follows

$$\text{rim loss across insulating ring} = k_{in} A_{in} \frac{dQ}{dl_{in}} = \frac{1.25 \times 10^{-3} \times 2\pi 8.09375 \times 2.4 \times 5(T2-T1)}{0.1875 \times 9} \qquad (3.10)\ *$$

* Note. The number following T refers to the thermocouple position indicated in figure 3.03, page 62.

shaft loss $= \frac{k_s \, 2\pi \, l (T_{so} - T_{si})}{\log_e (R_{so}/R_{si})}$ where R_{so} and R_{si} are the inner and outer mounting radii (3.11)

across tufnol mounting $= \frac{(T7-T8) 2\pi \, 0.4375 \times 8.5 \times 10^{-4} \times 4.1868 \times 2.54 \times 5}{9 \log_e (1.375/0.625)}$

$$+ \frac{(T6-T8) 2\pi \, 0.4375 \times 8.5 \times 10^{-4} \times 4.1868 \times 2.54 \times 5}{9 \log_e (0.875/0.625)}$$

radiation loss $= \varepsilon \sigma \, (T_w^4 - T_\infty^4) \, Ao$ (3.12)

$$= 0.048 \times 0.1714 \left[\left(\frac{460 + T_w}{100} \right)^4 - \left(\frac{460 + T_\infty}{100} \right)^4 \right]$$

$$\times \frac{2\pi (Ro^2 - Ri^2)}{144} \times 0.29307$$

DIMENSIONLESS PARAMETERS

The Nusselt number, Nu, and Reynolds number of rotation, Re_o were found as below

$$Nu = \frac{h_m R_o}{k} \qquad Re_o = \frac{N R_o^2 \, 2\pi}{\nu \, 60} \tag{3.13}$$

The Reynolds number of crossflow, Re_t, was found from the wind tunnel air velocity, U, and the characteristic length, taken as the main disc diameter, giving

$$Re_t = \frac{U \quad 2R_o}{\nu} \tag{3.14}$$

Chapter 4

PRESENT WORK

The experimental work was divided into six sections. The first consisted essentially of a repetition of some investigations into the flow and heat transfer from a rotating disc in still air which had been carried out by earlier workers. The remaining sections were concerned with the study of the heat transfer from a rotating disc in situations which had not previously been examined. The effects of superimposing a crossflow of air, and masking certain sectors of the disc, were considered both separately and together. Finally the effects of disturbing the boundary layer with trip wires and scrapers, and of directing a jet of air at the disc, were studied.

The experiments were idealized representations of a disc brake fitted to a vehicle. Masking the disc simulated the brake caliper; the crossflow over the disc simulated that normally induced by the movement of the vehicle. The experiments with boundary layer disturbing devices and air jets were concerned with possible methods of increasing the heat transfer from disc brakes.

Where possible, an attempt has been made to provide a theoretical analysis of the effect of the variable under study, and in all cases the experimental data are presented in a non-dimensional form.

The basic experimental procedure that applies to all sections of this chapter has been described in Chapter three. However, the procedure and checks that apply to a particular investigation only will be outlined in the section concerned with that investigation.

4.1 ROTATING DISC IN STILL AIR

A number of researchers have measured and predicted the heat transfer from a rotating disc in still air, and their results have already been discussed in Chapter two. There is some disagreement in their findings and hence it was thought worthwhile to repeat some of their work in an attempt to clarify the situation. A further object of these tests was to prove the equipment by taking results, under conditions already investigated, and comparing them with previous ones.

When a disc rotates in still air it causes the air to be drawn in an axial direction to the disc surface, where the rotation imparts to the air tangential and outward radial components of velocity which cause it to flow in a spiral path over the surface, eventually to leave at the rim. The airflow comes into the category of forced convection as it is induced by the motion of the disc and not by its temperature. At low Reynolds numbers the airflow over the disc surface is laminar, and as the Reynolds number increases the flow goes through a transitional region to turbulent flow. Therefore, at any rotational speed, on a disc of sufficiently large radius, one would find an inner laminar region, then a region of transition and an outer region of turbulent flow. At very low rotational speeds vertical natural convection currents are set up over the disc surface due to the buoyancy effects of the hot air layer close to the surface.

Measurements have been made of the heat transfer with laminar, transition and turbulent flow, and with natural convection. Flow profiles have been measured and flow visualization techniques used.

NATURAL CONVECTION

At low rotational speeds, with Reynolds number below 2×10^4, natural convection has an appreciable effect on the heat transfer

coefficient. Richardson & Saunders {35} gave the following result for the heat transfer in the region of laminar and natural convection flow, in terms of the Nusselt, Grashof and Reynolds numbers.

$$Nu_o = 0.4\ (Gr_o + Re_o^2)^{\frac{1}{4}} \qquad (4.01)$$

This result was supported by measurement down to $(Gr + Re^2)^{\frac{1}{2}} = 10^4$.

In the present investigation it was found that random air movements in the room had a significant effect on the heat transfer at low rotational speeds although the disc was isolated by a curtained enclosure, open only at the top. Further experiments were made when the room was empty of other people which resulted in a lower heat transfer every time. Figure 4.01 shows that the experimental data follows that of Richardson & Saunders down to $(Gr + Re^2)^{\frac{1}{2}} = 1.3 \times 10^4$ but then the results taken with the disc stationary deviate from equation (4.01) and give a higher heat transfer.

The average heat transfer coefficient for a disc, treated as a stationary vertical flat plate, can be calculated from the equation for natural convection heat transfer evaluated by Ostrach {54}, which has been shown to correlate well with earlier experiments. This is described in detail in Appendix 1, where the following result is obtained

$$Nu_o = 0.38\ (Gr_o)^{\frac{1}{4}} \qquad (4.02)$$

which is not far removed from the result of Richardson & Saunders for a stationary disc. The combination of Richardson & Saunders' results and the calculation of the heat transfer coefficient at zero speed make it seem unlikely that the heat transfer coefficient should deviate from the line of equation (4.01).

It is significant that only the present results taken with the disc stationary deviate from that line. In this condition the surface temperature is only uniform to within 15% of the disc to air temperature

FIGURE 4.01

Heat Transfer from a Disc rotating in Still Air

Showing the Influence of Natural Convection

× experimental data, with extraneous air disturbances

⊙ data taken at times of little air disturbance

S. data taken with disc stationary

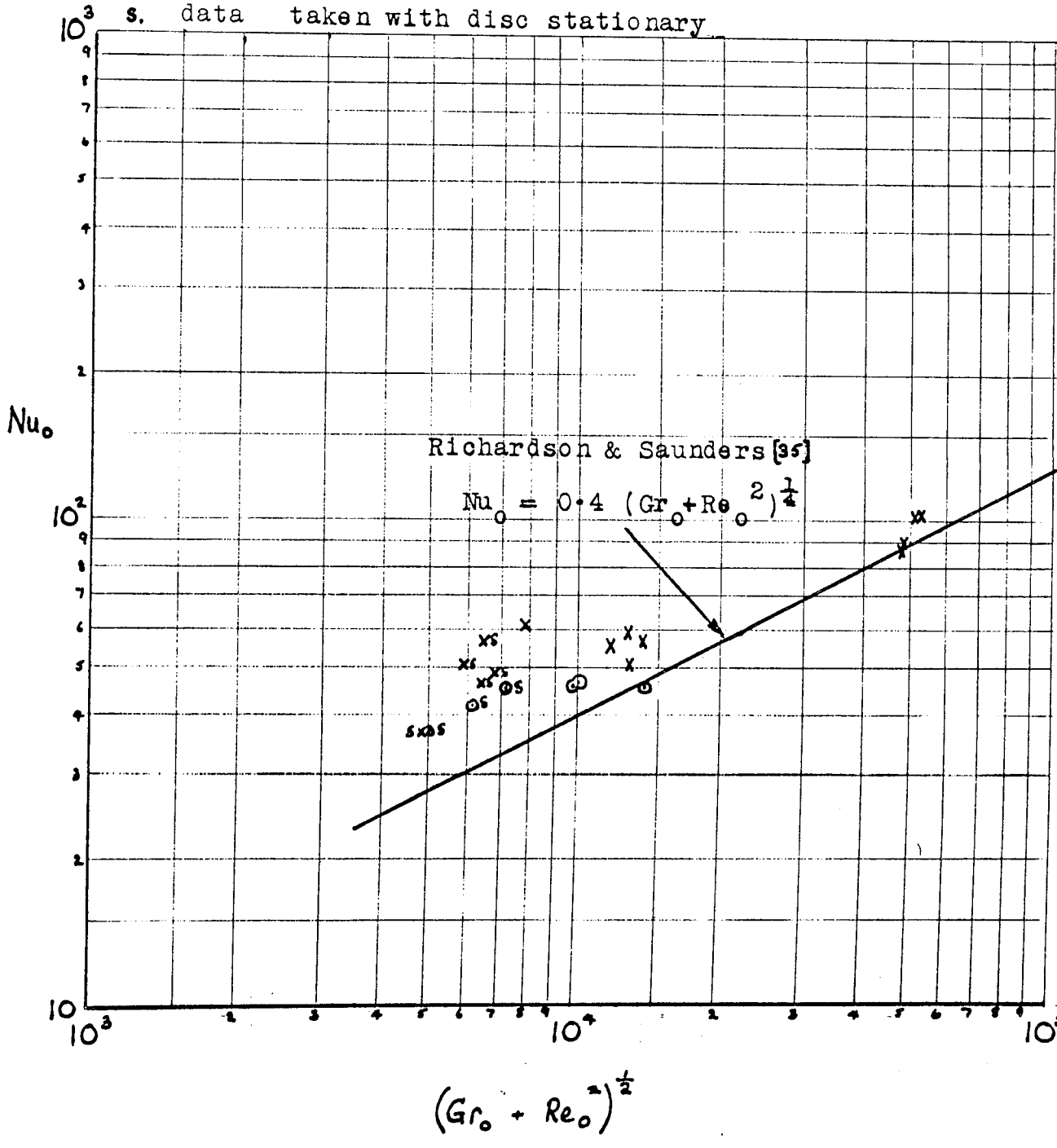

difference whereas the slowly rotating disc was uniform to within 1%. Therefore it is assumed that the heat transfer from the stationary disc was increased due to a non-uniform surface temperature.

LAMINAR REGION.

The experimental results in the laminar region are given in figure 4.02, where they are shown to be in close agreement with those of Richardson & Saunders, following the equation

$$Nu_o = 0.4\ Re_o^{\frac{1}{2}} \qquad (4.03)$$

giving $$h_m = 0.4\ k \left(\frac{\omega}{\nu} \right)^{\frac{1}{2}} \qquad (4.04)$$

This illustrates the interesting phenomenon, predicted by Karman { 3 } in 1921, that the heat transfer coefficient is independent of disc radius for laminar flow, and so if all of the disc surface is under laminar flow then the local and mean heat transfer coefficients are identical.

Later in this chapter some experiments will be described with the disc rotating in a crossflow of air in the test section of a wind tunnel. At the same time some measurements of the heat transfer were made with the disc in the tunnel duct but rotating in still air. These are compared with measurements taken whilst the disc was rotating in the curtained enclosure in figure 4.02. As they do not differ it is reasonable to assume that neither enclosure was having any effect on the heat transfer from the disc. When the rig was designed the size of the enclosure was determined on the basis of work by Richardson & Saunders on the effect of stationary planes close to the disc, to ensure that the enclosure did not effect the airflow induced by the disc rotation.

Particular attention was paid to the measurement of the ambient temperature in the enclosure, as described earlier in Chapter three, pp 74 , as Richardson & Saunders found that Cobb & Saunders { 32 }

FIGURE 4.02

Heat Transfer from a Rotating Disc in Still Air

Laminar and Turbulent flow regions

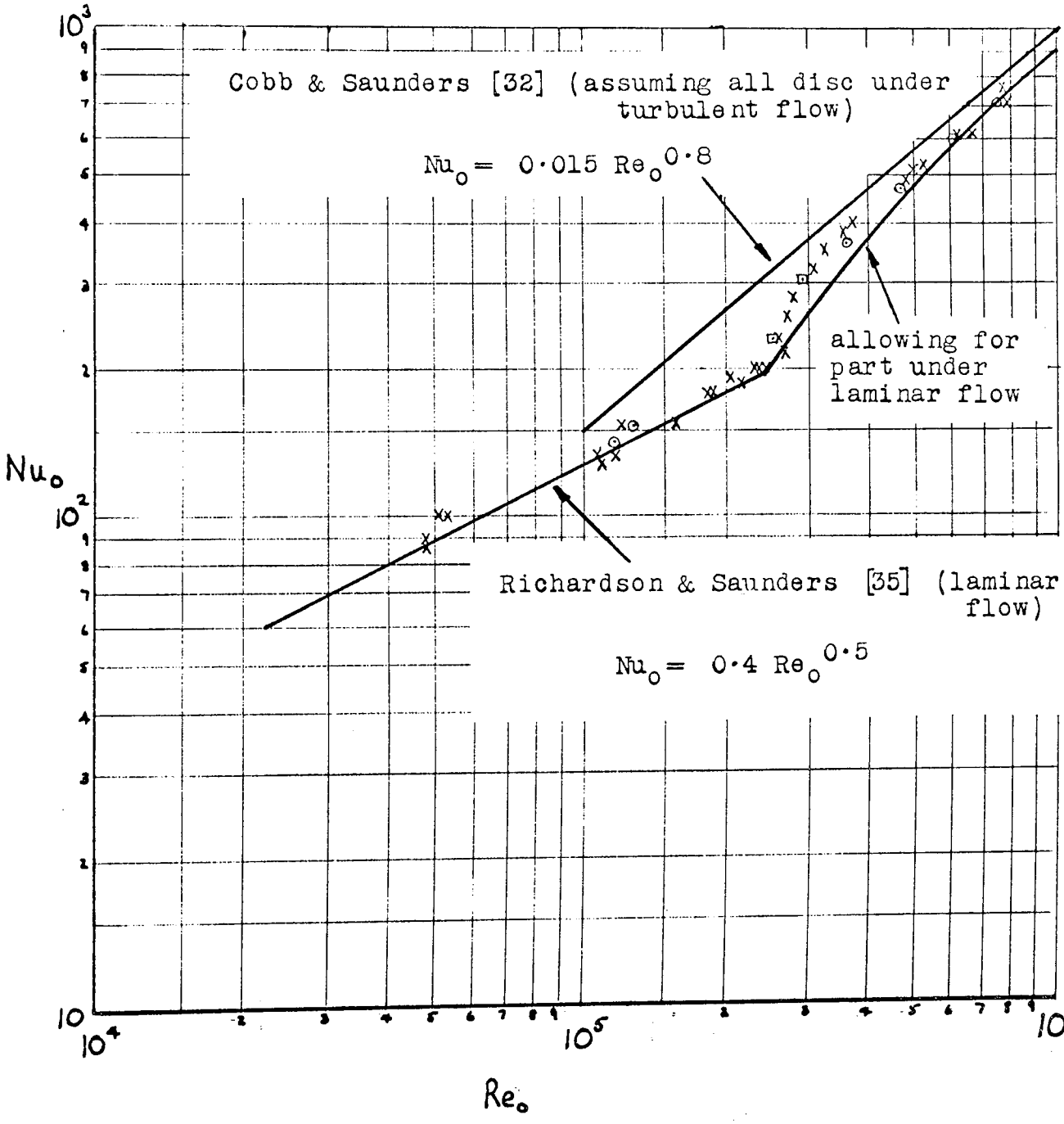

had incorrectly measured this parameter, which had produced a 10% error in their results.

Some laminar flow profiles were measured with a 0.12 x 0.76mm pitot tube connected to an electrical micromanometer. The static pressure was taken outside the boundary layer. The tangential profile, plotted non-dimensionally in figure 4.03, is the same for all Reynolds numbers, as shown earlier for the heat transfer, and agrees with the prediction of Cochran {4} , and the measurements of Gregory, Stuart & Walker {11} . The radial profile proved too small to be measured with any consistency. The angles of yaw of the flow were found by determining the angle of maximum velocity when rotating the pitot against an angular scale. The rectangular shape of the pitot was chosen to get velocity readings close to the disc and gave good results for the tangential component of the velocity but this shape made the pitot insensitive to direction of flow and not a good tool for measuring angle of yaw. It can be seen from figure 4.04 that the measurements taken were scattered around the results of Gregory, Stuart & Walker. As the previous measurements of flow profiles, by different people, agreed well the achievement of a general correlation was considered sufficient and no attempt was made to improve the results.

TRANSITION REGION

Gregory, Stuart & Walker {11} reported that above a fixed Reynolds number instability appeared in the form of stationary vortices in the boundary layer. They found that an acoustic stethoscope made from a length of plastic tube could be used to determine the onset of instability and turbulence. By listening to one end while the other was held in the boundary layer, the critical radii could be detected, as there was silence in the laminar region, a note offairly definite pitch as vortices were formed and a roar in the turbulent region. The vortices

FIGURE 4.03

Tangential Velocity Profile on a Rotating Disc

Laminar Flow Region

experimental data:-

×	53 rad/s	14 cm radius	Re_o = 69400
△	115 rad/s	14 cm radius	Re_o = 150000
□	158 rad/s	14 cm radius	Re_o = 206000

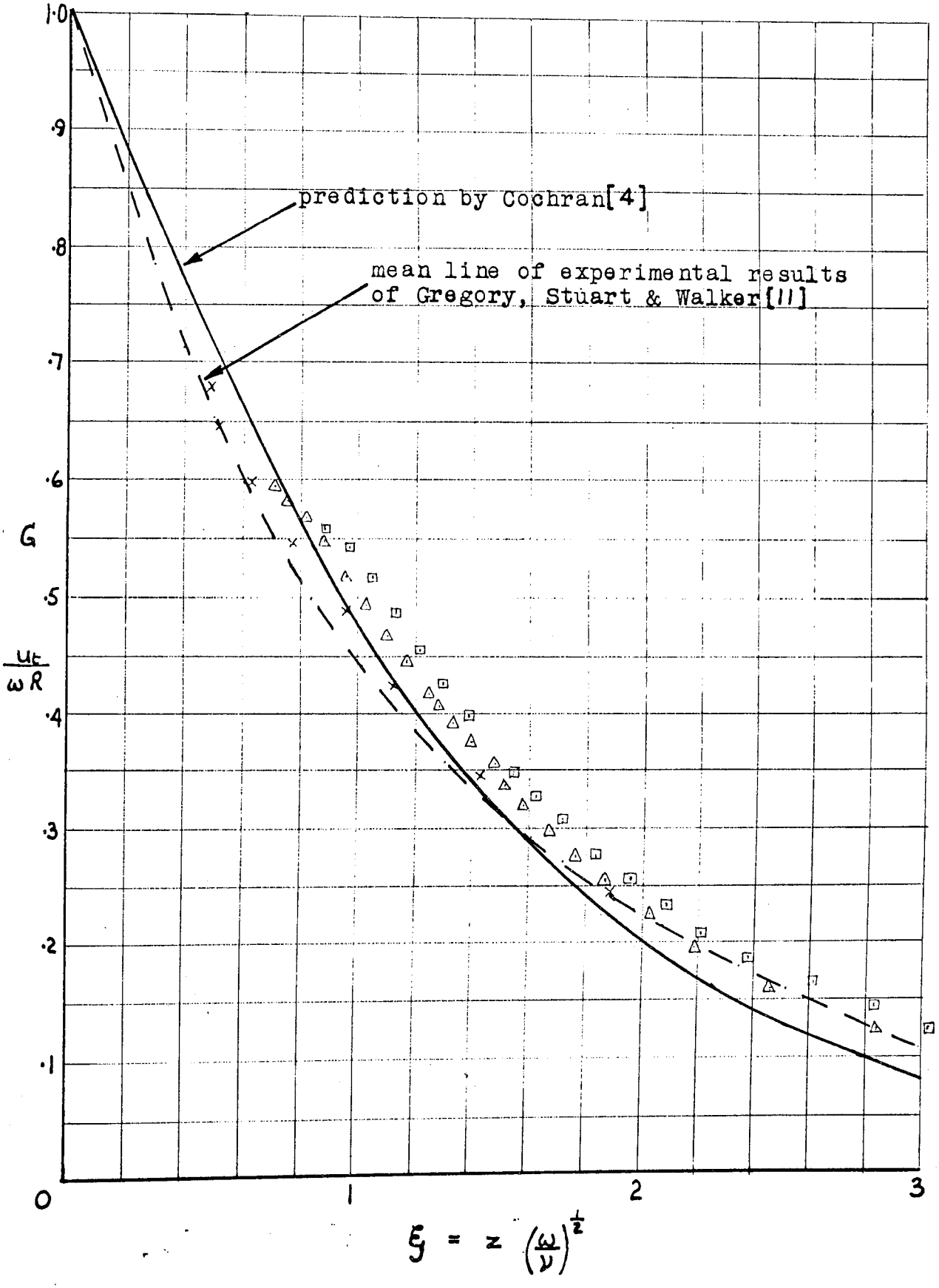

FIGURE 4.04

Angle of Yaw of Airflow on a Rotating Disc

Laminar flow region

× experimental data at 158 rad/s, 14cm radius

$Re_o = 206000$

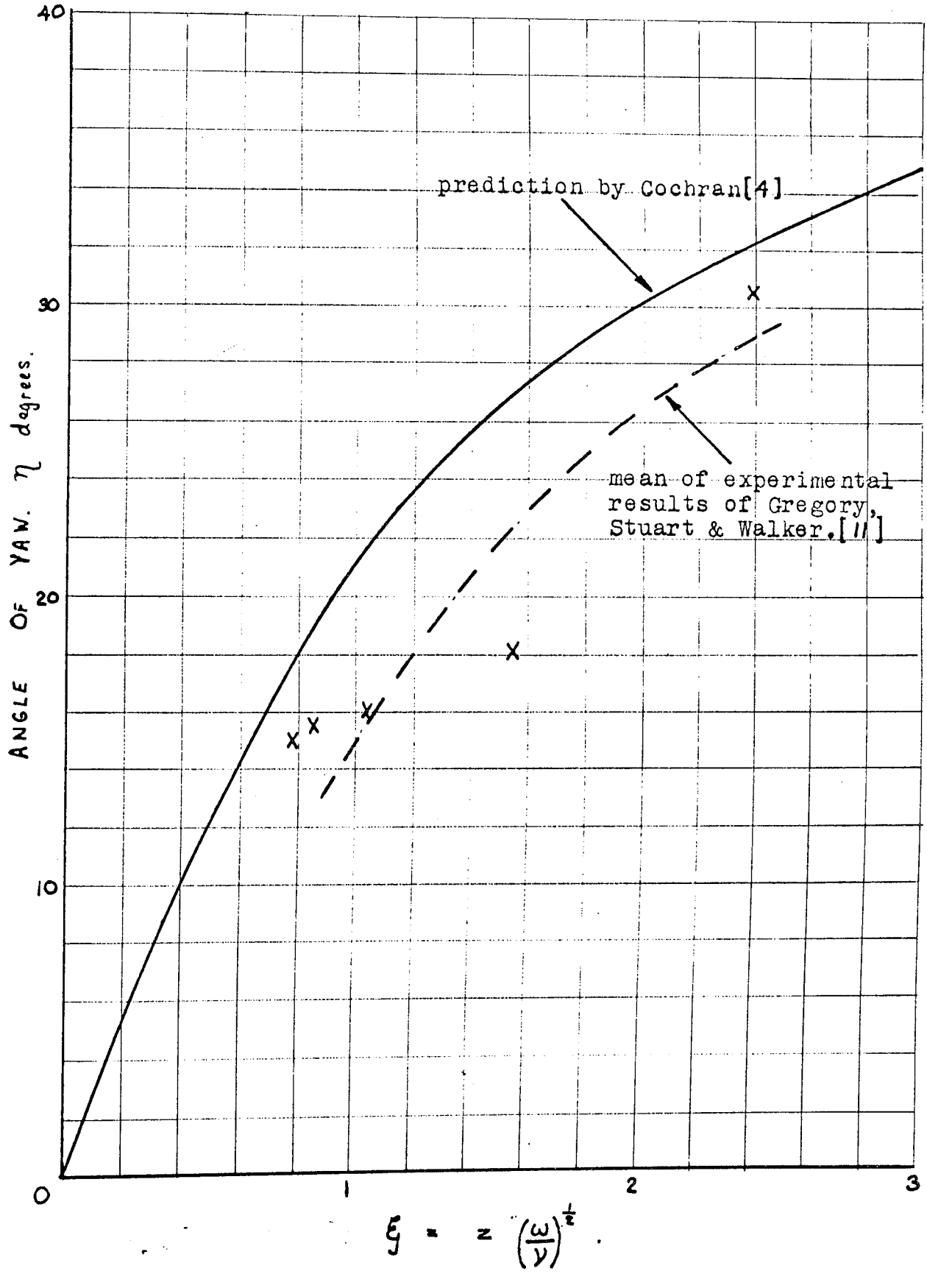

existed only over a short range of Reynolds numbers beyond which full turbulent flow developed.

The author repeated the experiments with a stethoscope and found the results shown in figure 4.05, the average values being:-

$$\text{Instability began at } Re_R = 1.27 \times 10^5$$
$$\text{Turbulence began at } Re_R = 2.3 \times 10^5 \qquad (4.05)$$

The onset of instability and turbulence came at lower Reynolds numbers than found by Gregory, Stuart & Walker, but the point of transition on the graph of heat transfer, figure 4.02, agreed with that of Richardson & Saunders and with the present stethoscope measurements. The most likely explanation for the high readings of Gregory, Stuart & Walker is that they probably had an extremely smooth and flat disc, and no disturbances in the vicinity of their rig, both of which would serve to delay the onset of instability.

TURBULENT REGION

As the disc speed increases, the radius at which transition occurs is reduced, so that the mean heat transfer coefficient increases rapidly at first due to the combination of the higher local coefficients caused by turbulent flow and the fact that they operate on a large radius and therefore a large area. With further increases in speed the rate of growth of the mean heat transfer coefficient is reduced because the turbulent flow affects a progressively smaller extra area. Correspondingly, in figure 4.02, a line through the experimental data rises steeply from the onset of transition but flattens off to become asymptotic to a line representing the whole of the disc under turbulent flow.

At the maximum speed turbulent flow covered only 70% of the disc surface, but the results indicated that turbulent flow over the whole

FIGURE 4.05

Table of Acoustic Measurements of Onset of Instability and Transition on a Rotating Disc

Author's Measurements

disc speed	onset of instability		onset of transition	
r.p.m.	radius cm.	$Re_o \times 10^{-5}$	radius cm.	$Re_o \times 10^{-5}$
2830	7·39	1·08	10·22	2·08
2220	8·96	1·26	12·76	2·55
1730	9·91	1·25	14·52	1·96
1292	12·78	1·49	16·90	2·62
mean		1·27		2·30

Gregory, Stuart & Walker Measurements [11]

3200	8·9	1·82	11·04	2·82
2900	9·4	1·85	11·50	2·77
2585	9·82	1·80	12·50	2·91
2200	10·68	1·81	13·20	2·77
1950	12·26	2·12	14·58	2·99
1700	12·02	1·78	15·22	2·85
1370	13·71	1·86	17·13	2·90
1250	15·22	2·10	17·78	2·85
600	21·5	2·00	25·00	2·70
mean		1·904		2·84

surface would give the mean turbulent Nusselt number

$$Nu_o = 0.015\, Re_o^{0.8} \qquad (4.06)$$

This is identical to the findings of Cobb & Saunders {32}, who have also shown that the mean heat transfer coefficient can be predicted in the transition region by allowing for part of the disc under laminar flow and the remainder under turbulent flow. This was repeated for the present results, as follows:-

assuming that the local turbulent heat transfer is given by

$$Nu_r = C\, Re_r^{0.8} \qquad (4.07)$$

and the laminar heat transfer is taken from equation 4.03

$$Nu_r = 0.4\, Re_r^{0.5}$$

Each local heat transfer coefficient acts over an area of $2\pi R\, dR$ giving the average heat transfer coefficient as

$$h_m \pi R_o^2 = \int_0^{R_{cr}} h_r(\text{laminar}) 2\pi R\, dR + \int_{R_{cr}}^{R_o} h_r(\text{turbulent}) 2\pi R\, dR \qquad (4.08)$$

$$= \int_0^{R_{cr}} 0.4k \left(\frac{\omega}{\nu}\right)^{0.5} 2\pi R\, dR + \int_{R_{cr}}^{R_o} Ck \left(\frac{\omega R^2}{\nu}\right)^{0.8} 2\pi R\, dR$$

$$\therefore \quad h_m R_o^2 = \left[0.8k \left(\frac{\omega}{\nu}\right)^{0.5} \frac{R^2}{2}\right]_0^{R_{cr}} + \left[C\, 2k \left(\frac{\omega}{\nu}\right)^{0.8} \frac{R^{2.6}}{2.6}\right]_{R_{cr}}^{R_o}$$

$$\frac{h_m R_o}{k} = Nu_o = \left[0.4 \left(\frac{\omega R_{cr}^2}{\nu}\right)^{0.5} \frac{R_{cr}}{R_o}\right] - \left[\frac{C}{1.3} \left(\frac{\omega R_{cr}^2}{\nu}\right)^{0.8} \frac{R_{cr}}{R_o}\right] + \left[\frac{C}{1.3} \left(\frac{\omega R_o^2}{\nu}\right)^{0.8}\right]$$

Now $$\frac{Re_{cr}}{Re_o} = \frac{R_{cr}^2}{R_o^2}$$

So $$Nu_o = 0.4 \frac{Re_{cr}}{Re_o^{0.5}} + \frac{C}{1.3} \left[Re_o^{0.8} - \frac{Re_{cr}^{1.3}}{Re_o^{0.5}}\right] \qquad (4.09)$$

For turbulent flow over the disc, $Re_{cr} = 0$, equation 4.09 gives

$$Nu_o = \frac{C}{1.3} Re_o^{0.8}$$

so that from equation 4.06 we have $C = 0.0195$.

Using this value in equation 4.09, Nu_o was calculated for a range of Re_o, with $Re_{cr} = 2.3 \times 10^5$, to give the curve plotted in figure 4.02. This curve deviates from experiment by a maximum of 15%, during the early part of the transition region, but is in agreement above a Reynolds number of 650,000. It was thought that this might have been caused by recirculation of turbulent disturbances within the enclosure but when experiments were made with the curtains removed from the rig the same results were found. No other reason for the deviation could be found; however, analysis of behaviour in a region of transition has always been difficult and many characteristics of the flow have yet to be explained.

The measurement of the turbulent tangential profile, shown in figure 4.06, is close to that of Gregory, Stuart & Walker. In this graph the distance from the disc, z, is made non-dimensional by comparing it with the boundary layer momentum thickness δ^{**}

$$\text{where} \quad \frac{\delta^*}{\delta^{**}} = \frac{\text{displacement thickness}}{\text{momentum thickness}} = 1.4 \qquad (4.11)$$

$$\text{and} \quad \delta^* = 0.0656 R \left(\frac{\nu}{R^2 \omega}\right) \qquad (4.12)$$

The radial component of velocity and angle of yaw were not explored due to the insensitivity of the pitot, as explained in the section on laminar flow.

SUMMARY

The heat transfer from a rotating disc in still air has been measured for laminar, transition and turbulent flow over the disc, with the following results:-

FIGURE 4.06

Tangential Velocity Profile on a Rotating Disc

Turbulent Flow Region

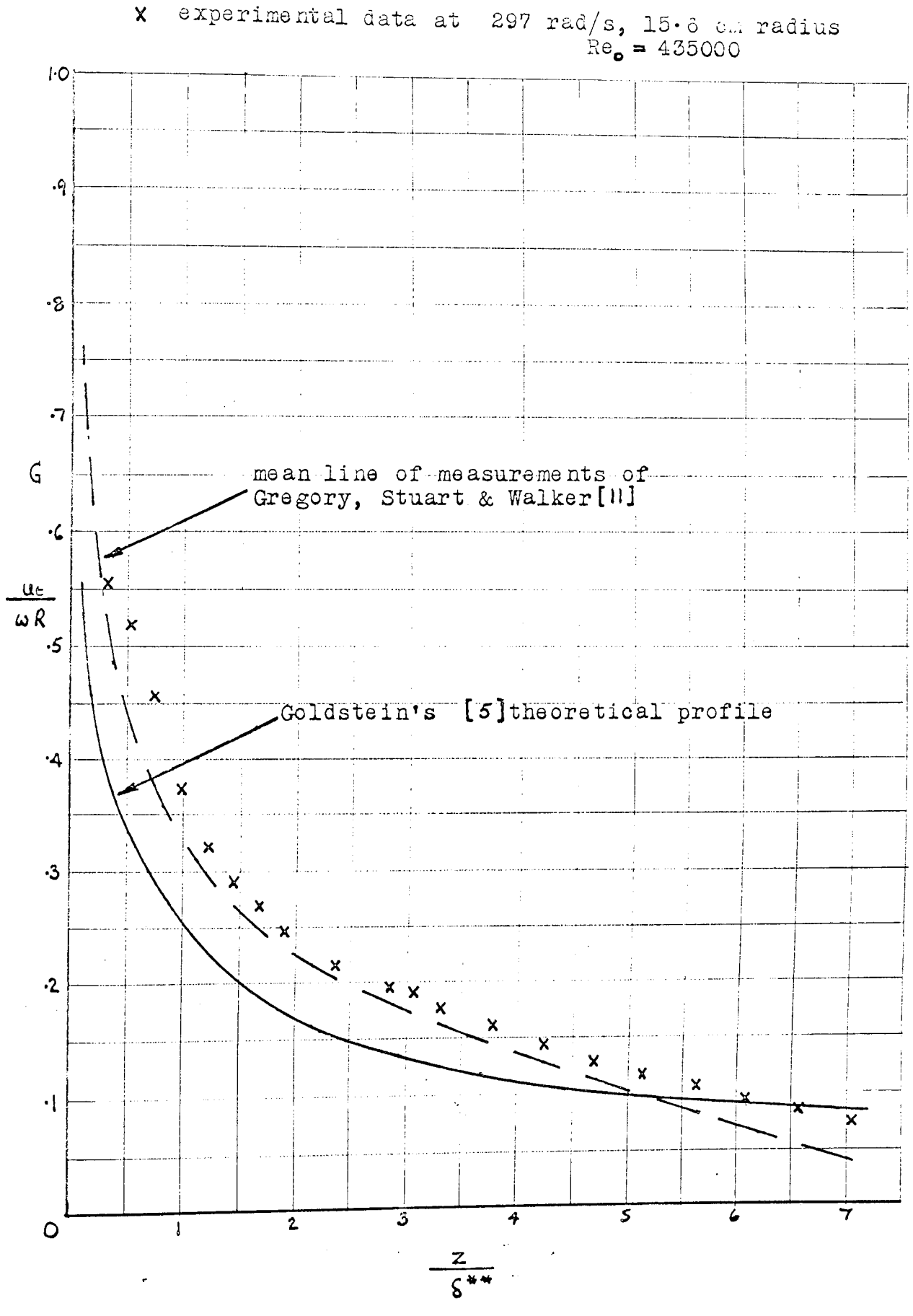

1. For laminar and natural convection flows, the results agreed with those of Richardson & Saunders {35} down to $(Re_o^2 + Gr_o)^{0.5} = 1.3 \times 10^4$.

viz $$Nu_o = 0.4 \ (Re_o^2 + Gr_o)^{0.25}$$

below this, the discrepancy was attributed to non-uniformity of the disc surface temperature.

2. Transition began at a Reynolds number of 240,000, in agreement with the findings of Cobb & Saunders {32} .

3. The heat transfer for all the disc under turbulent flow was found, by extrapolation of the results, to be given by

$$Nu_o = 0.015 \ Re_o^{0.8}$$

identical to the results of Cobb & Saunders {32} . By allowing for the outer part of the disc under turbulent flow, and the inner under laminar, reasonable agreement was reached with the measurements in the transition region.

The tangential profiles measured in the laminar and turbulent regions were close to the results of Gregory, Stuart & Walker {11} but the pitot tube was not sufficiently sensitive to be of use in the measurement of the radial profile or the angle of yaw.

An important aim of this set of tests was to check the apparatus and the consistency of results from it. These showed that the apparatus was behaving as expected and further experimental work could then proceed with confidence.

4.2 ROTATING DISC IN STILL AIR WITH A SECTOR MASKED OFF

A caliper provides the means of applying the torque to a disc and hence is an essential part of a disc brake, which by its presence blanks off a sector of the disc surface and destroys the rotational symmetry of a free disc. The caliper reduces the area available for convective heat transfer and also disturbs the airflow induced by rotation over the

remainder of the disc surface. The effect of this on the flow and average heat transfer coefficient of a rotating disc was therefore investigated.

It was assumed that any obstacle thicker than the boundary layer would have the same effect on the flow and so the caliper was simulated by two sectors of wood 13mm thick, one mounted each side of the disc. The accuracy of this assumption was verified by tests with sectors of different thickness. To obtain a complete analysis the sector angle was varied from 0 to 360 degrees. A zero degree sector was formed from a piece of thin wood, 40mm wide, tipped with baize and resting on the disc surface. This interrupted the airflow on the surface without significantly reducing the convective area. The other sectors were faced with baize to allow for the slightly uneven disc surface, so that close contact could be maintained without high levels of friction heating. The 10 degree sector is shown in position in the photograph of figure 4.07.

PRELIMINARY EXPERIMENTS

The procedure particular to this set of tests will now be discussed along with the experimental checks.

To determine the amount of heat caused by friction between sector and disc a number of heat transfer tests were made on the same run, with different heat inputs, whilst keeping the disc speed and sector angle constant. The net heat input, after allowing for rim, shaft and radiation losses, was plotted against the surface to ambient temperature difference. An example of this is given in figure 4.08. For no friction heating the line should go through the origin, but if it reads a negative value of heat input for zero temperature difference an allowance has to be made for friction heating. This negative value of heat input is subtracted from the net heat input for each test, to bring

FIGURE 4.07

SECTOR OF 10° ANGLE IN POSITION ON DISC

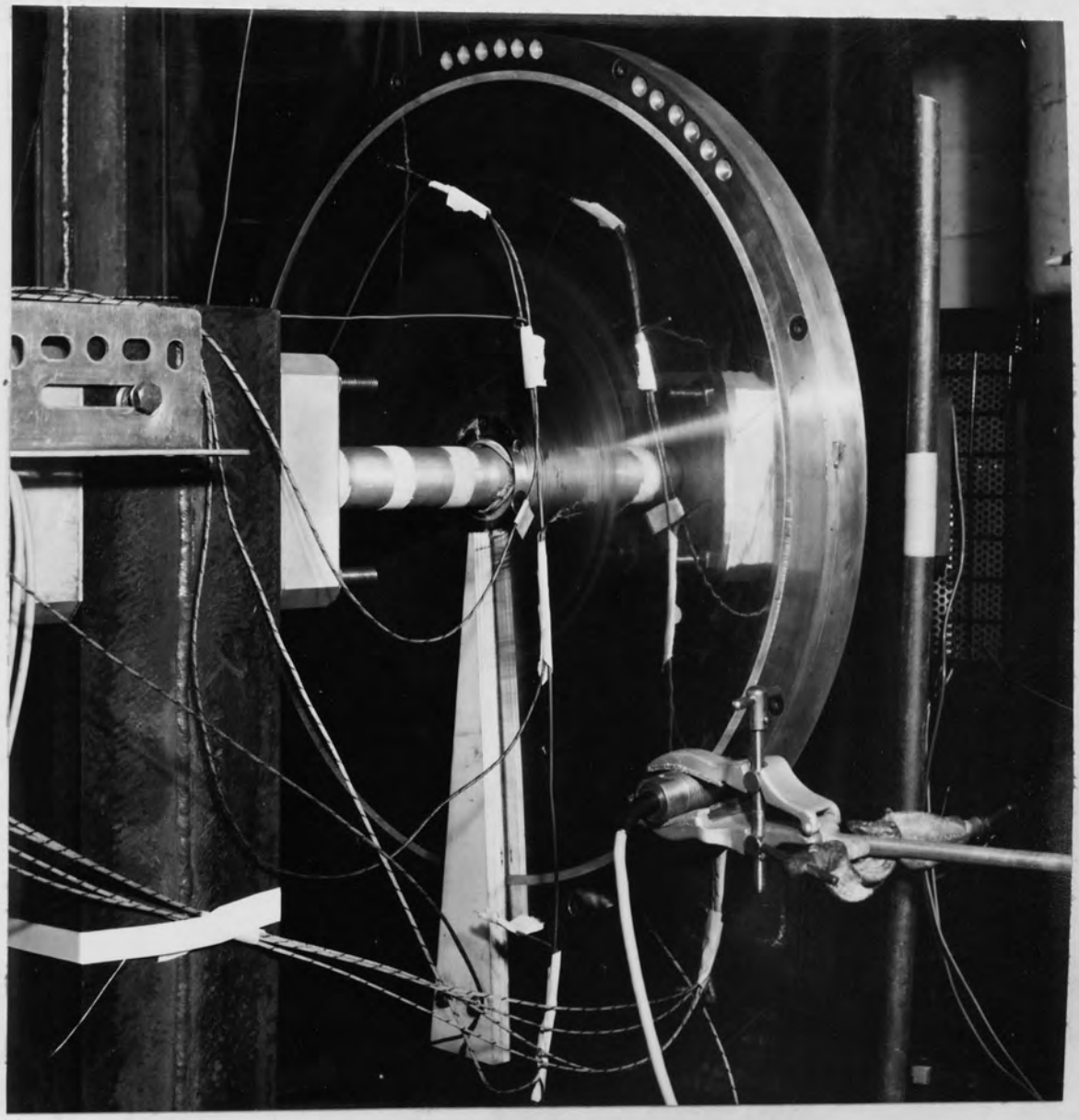

FIGURE 4.08

Example of Measurement of Friction Heating on 180° Sector

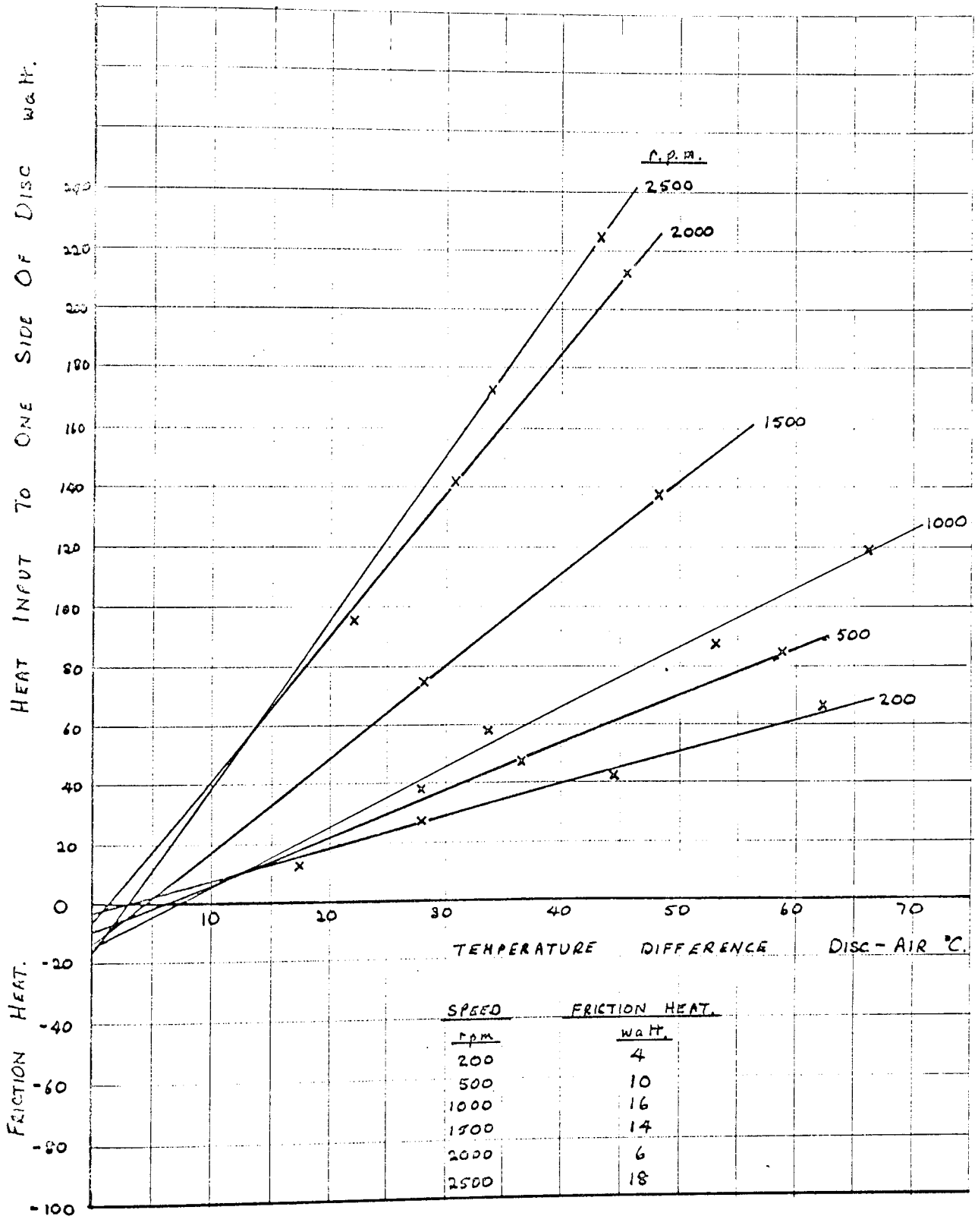

SPEED rpm	FRICTION HEAT watt
200	4
500	10
1000	16
1500	14
2000	6
2500	18

the line back through the origin. This facility is included in the computer programme CVAE 22, which processed the experimental results.

The heat loss through the sector was calculated by measurement of the thermal conductivity of the sector and the temperature on each side of it. The heat losses through the edges of the sector were neglected as the edge area is small compared to the face area of the sector, except for small angles, where the total loss is small compared to the heat input to the disc anyway. The thermal conductivity of the wood and baize sectors was found by measuring the heat loss through the 360 degree sector with the disc stationary. The outside surface temperature of the sector was measured with thermocouples taped to the surface whilst the inside surface was assumed to be the same as the disc surface temperature. The rim and shaft losses were allowed for in the usual way, leaving the thermal conductivity of the sector as the only unknown. Figure 4.09 shows the plot of temperature difference across the sector against heat flow through it, which gave

$$\frac{\theta}{Q} = 0.834 \quad \frac{^{o}K}{W}$$

$$\text{therefore} \quad k = 0.1208 \quad \frac{W}{m\ ^{o}K}$$

This compared well with a value for wood from Kaye & Laby { 70 } of

$$k = 0.15 \quad \frac{W}{m\ ^{o}K}$$

During the heat transfer tests with the disc rotating it was again assumed that the temperature of the inside sector surface was identical to the disc surface temperature and the outside temperature was measured by taping thermocouples to it.

The ambient temperature was taken from thermocouples placed in the airstream travelling to the uncovered disc surface, the temperatures recorded by thermocouples facing a sector were noticeably higher due to the greater rate of radiation from the wood surface than from the polished aluminium surface of the disc, and these readings were therefore ignored.

FIGURE 4.09

Heat Flow through 360° Sector on one side of the Disc to determine Thermal Conductivity of the Sector

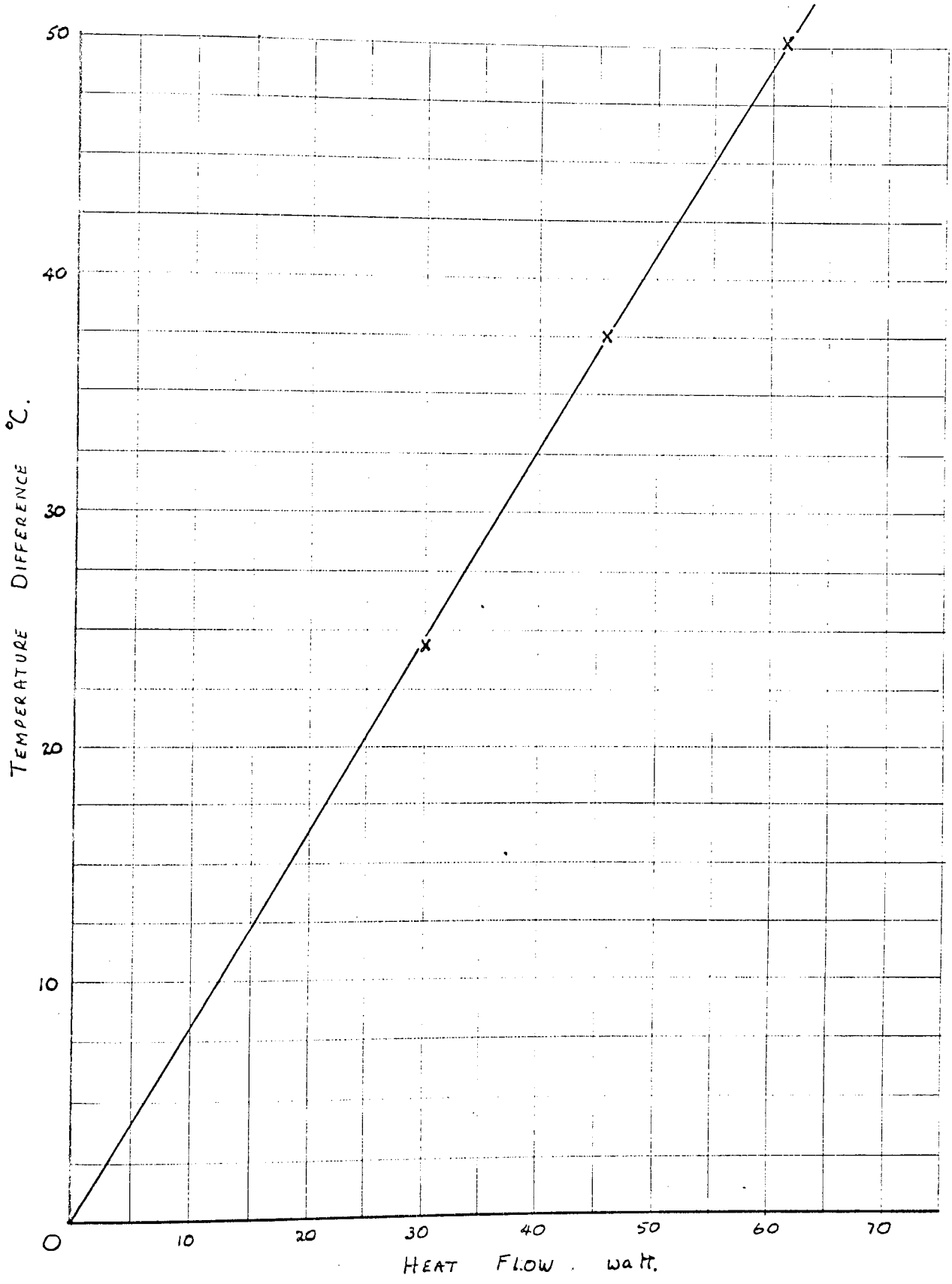

Experiments were made to check the assumption that the thickness of the sectors did not affect the heat transfer and therefore that they accurately simulated the much thicker calipers. As it was not desirable to alter the whole sector thickness, and hence its heat absorption rate, the effect was achieved by fixing false cardboard edges to the sector, this being the only region that could affect the airflow. Figure 4.12 shows that with a 90 degree sector of 13, 25, and 51mm effective thicknesses, at a Reynolds number of 120,000, there was no difference between the measured heat transfer coefficients and hence no change in the airflow.

HEAT TRANSFER EXPERIMENTS

The mean heat transfer coefficient was measured at various sector angles over the full range of disc speeds. Two sets of graphs were plotted, one with fixed angles and varying speed and the other with fixed speeds and a varying sector angle. The sector angle was not continuously variable but was limited to steps of 30°.

The results were plotted in dimensionless form, for sector angles of 0°, 10°, 90°, 180°, 270°, in figures 4.10, 11, 12, 13 and 14, respectively, compared in each case to the heat transfer from a rotating disc with no sectors. Figure 4.15 reproduces the mean lines through the experimental data for ease of comparison. Figures 4.16 and 4.17 show the effect of sector angle at two rotational Reynolds numbers, one each in the laminar and turbulent regions.

The rather complicated effects of the scraper and sectors on the heat transfer were due to a combination of the following disturbances to the flow, revealed by flow visualization experiments made with titanium tetrachloride smoke released into the airstream.

At low rotational speeds the boundary layer of air was deflected back across the disc surface by the front edge of the scraper or sector,

FIGURE 4.10

Heat Transfer from a Rotating Disc in Still Air with one Scraper on each side of the Disc

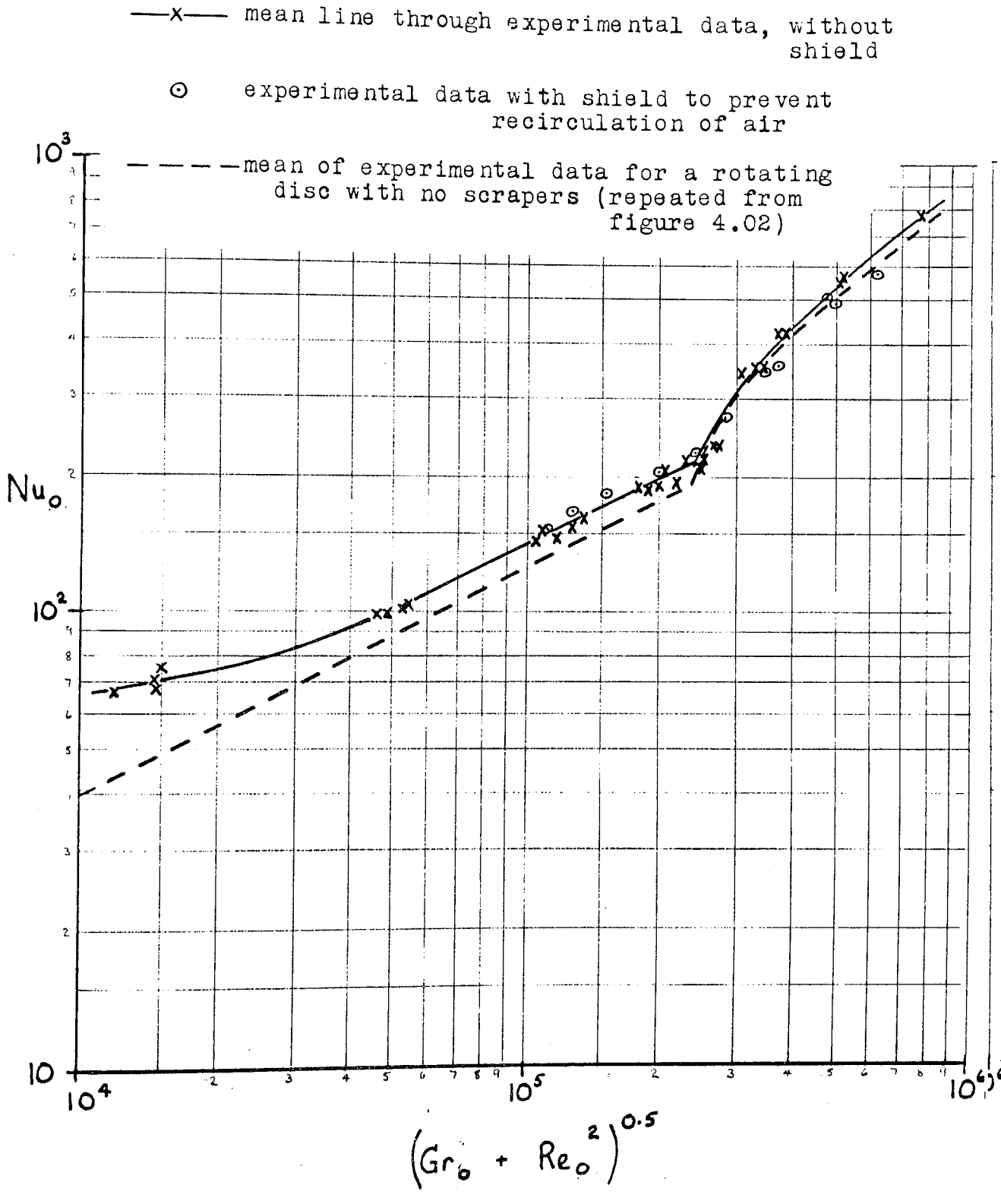

FIGURE 4.11

Heat Transfer from a Rotating Disc in Still Air with a 10° Sector on each side of the Disc

12·7 mm thick sector

——x—— experimental data, no shield on sector

⊙ " " , shield across from sector to bearing stand

----□--- " " , shield extended to floor, completely preventing recirculation

— — — — " " , disc with no sectors, repeated from figure 4.02

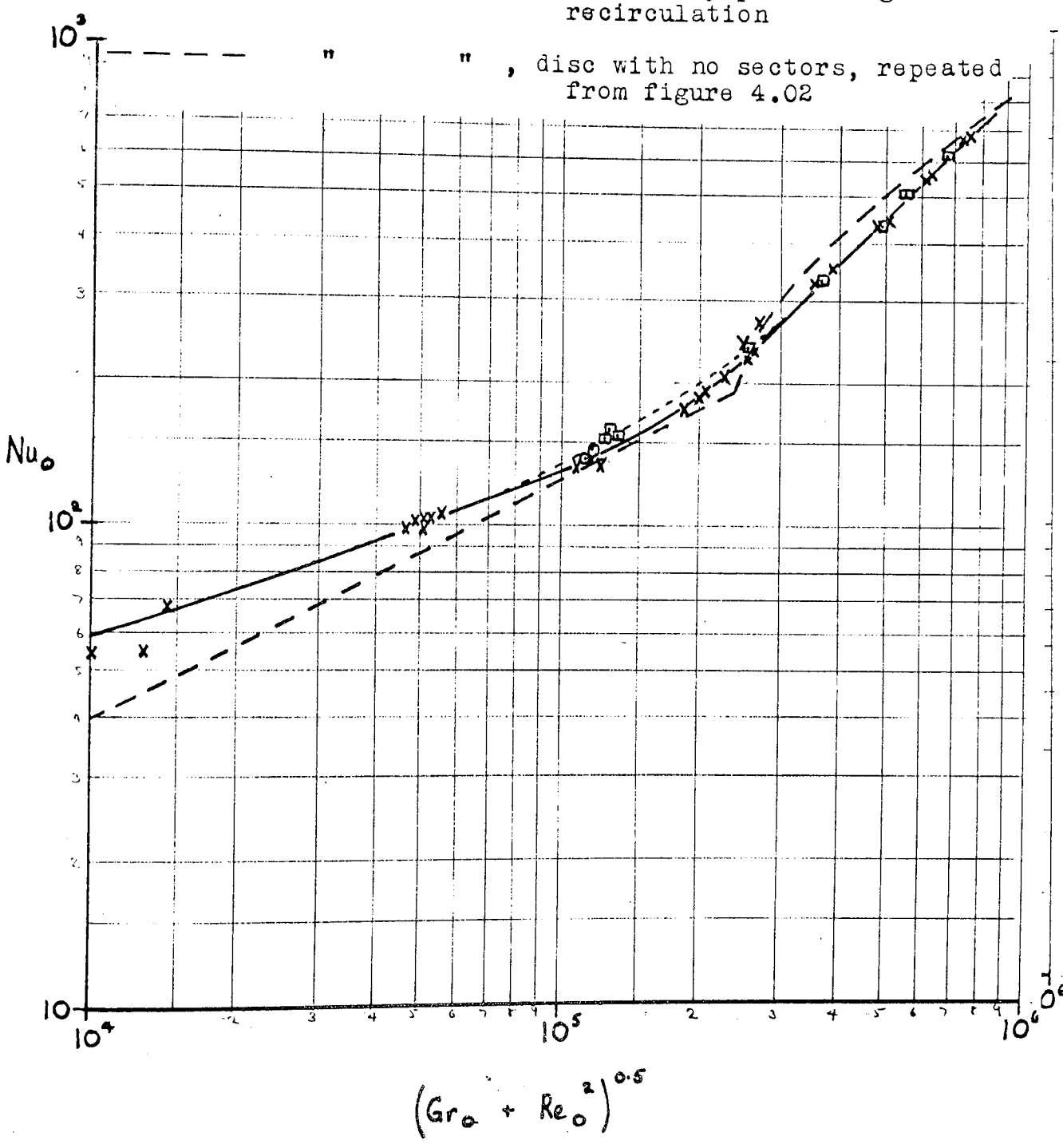

FIGURE 4.12

Heat Transfer from a Rotating Disc in Still Air

90^{o} Sector on each side of the Disc

—X— experimental data , 12·7mm thick sector

⊙ " " , 25·4mm " "

⊡ " " , 50·8mm " "

— — — disc with no sectors, (figure 4.02)

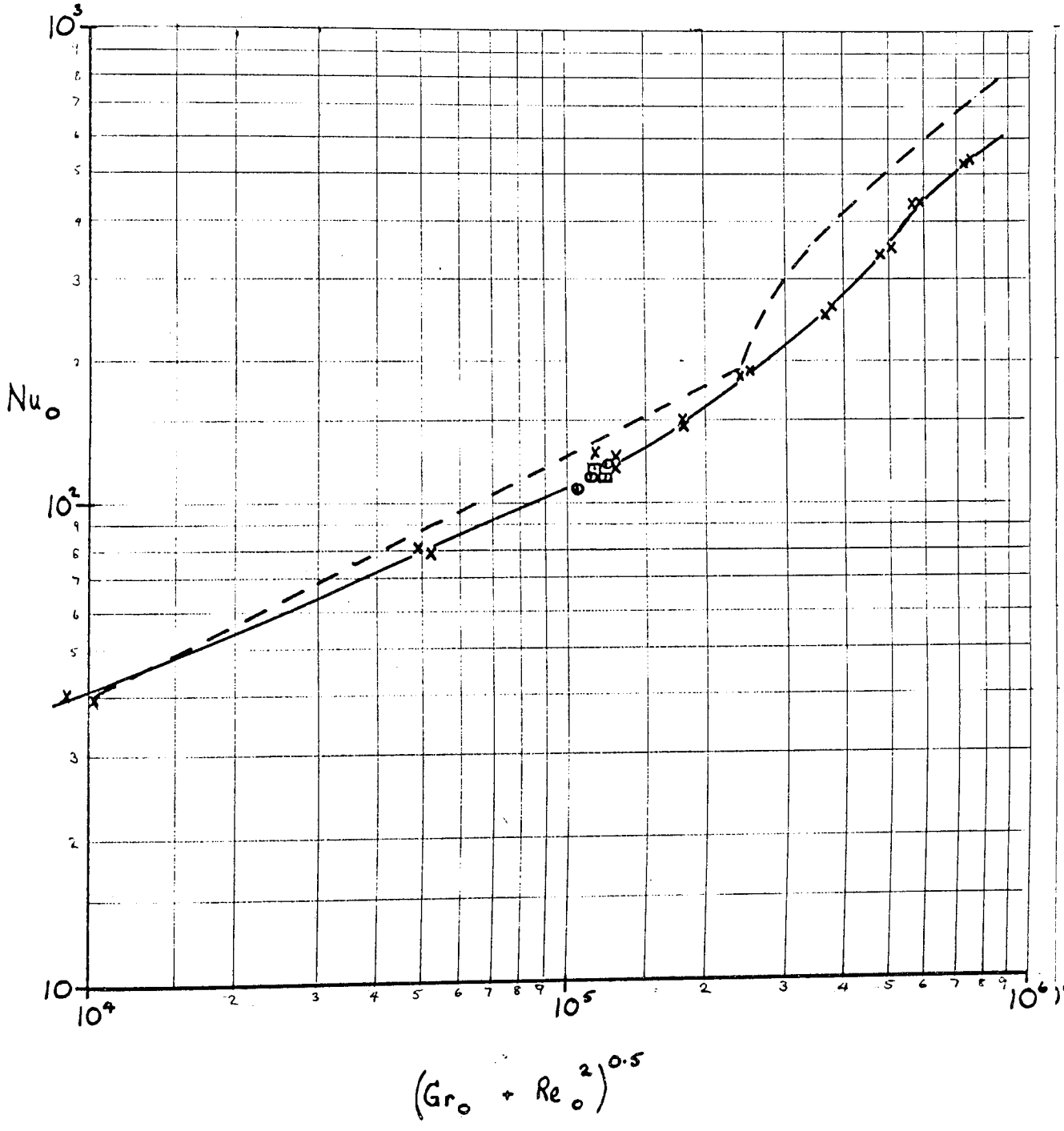

FIGURE 4.13

Heat Transfer from a Rotating Disc in Still Air

180° Sector on each side of the Disc

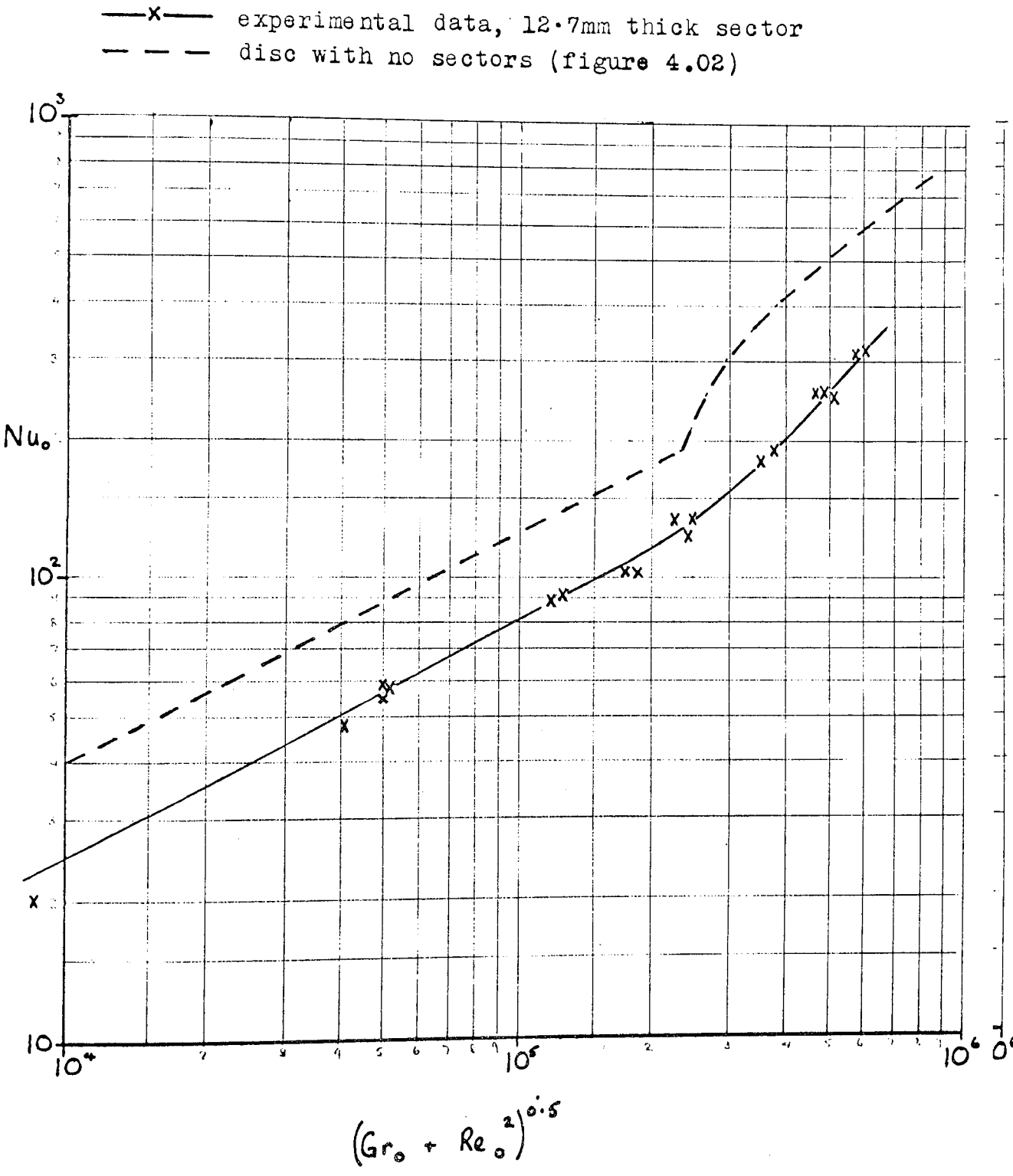

FIGURE 4.14

Heat Transfer from a Rotating Disc in Still Air

270° Sector on each side of the Disc

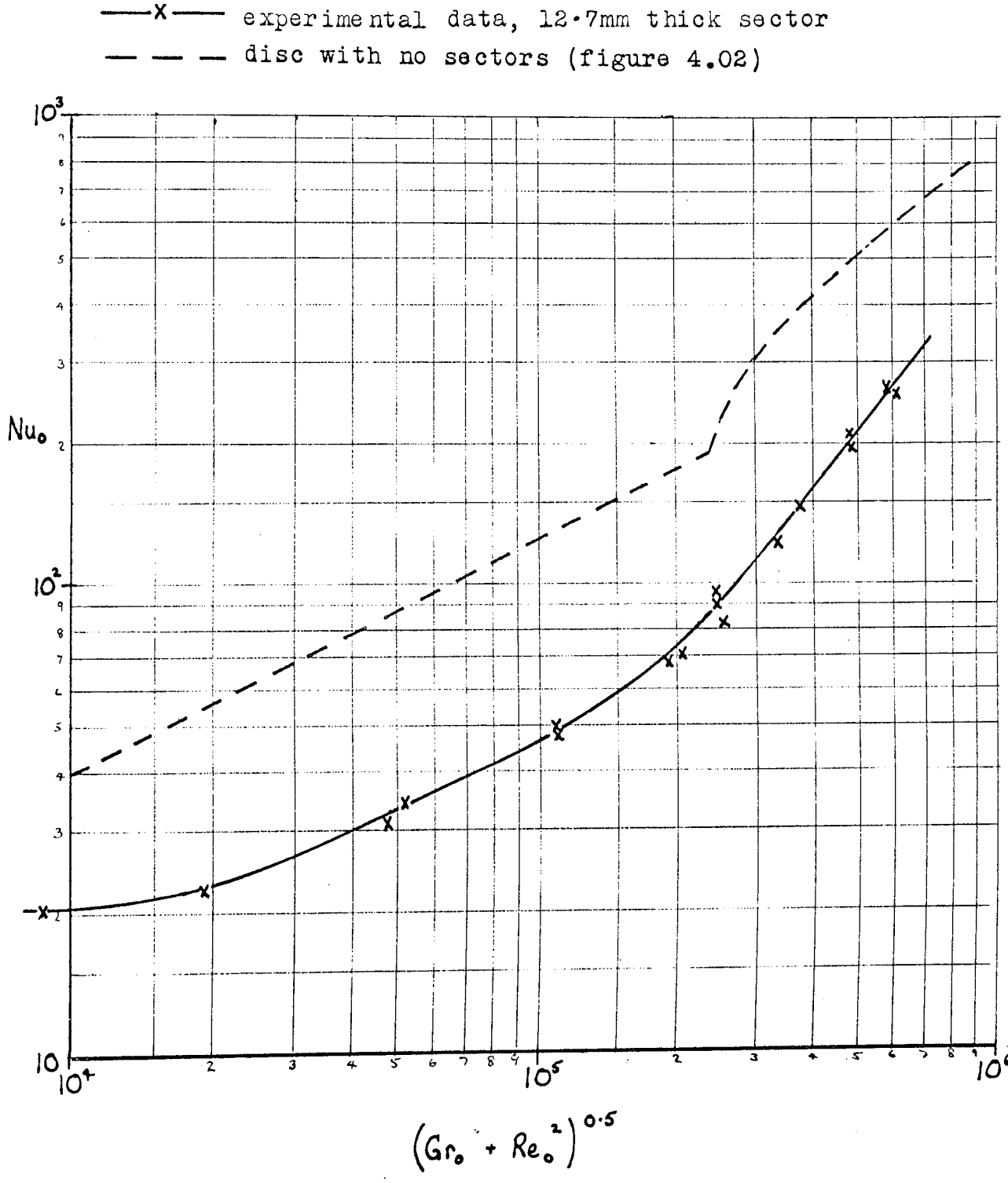

FIGURE 4.15

Comparison of Experimental Data for the Heat Transfer from a Disc rotating in Still Air with various Sectors of the Disc Masked Off

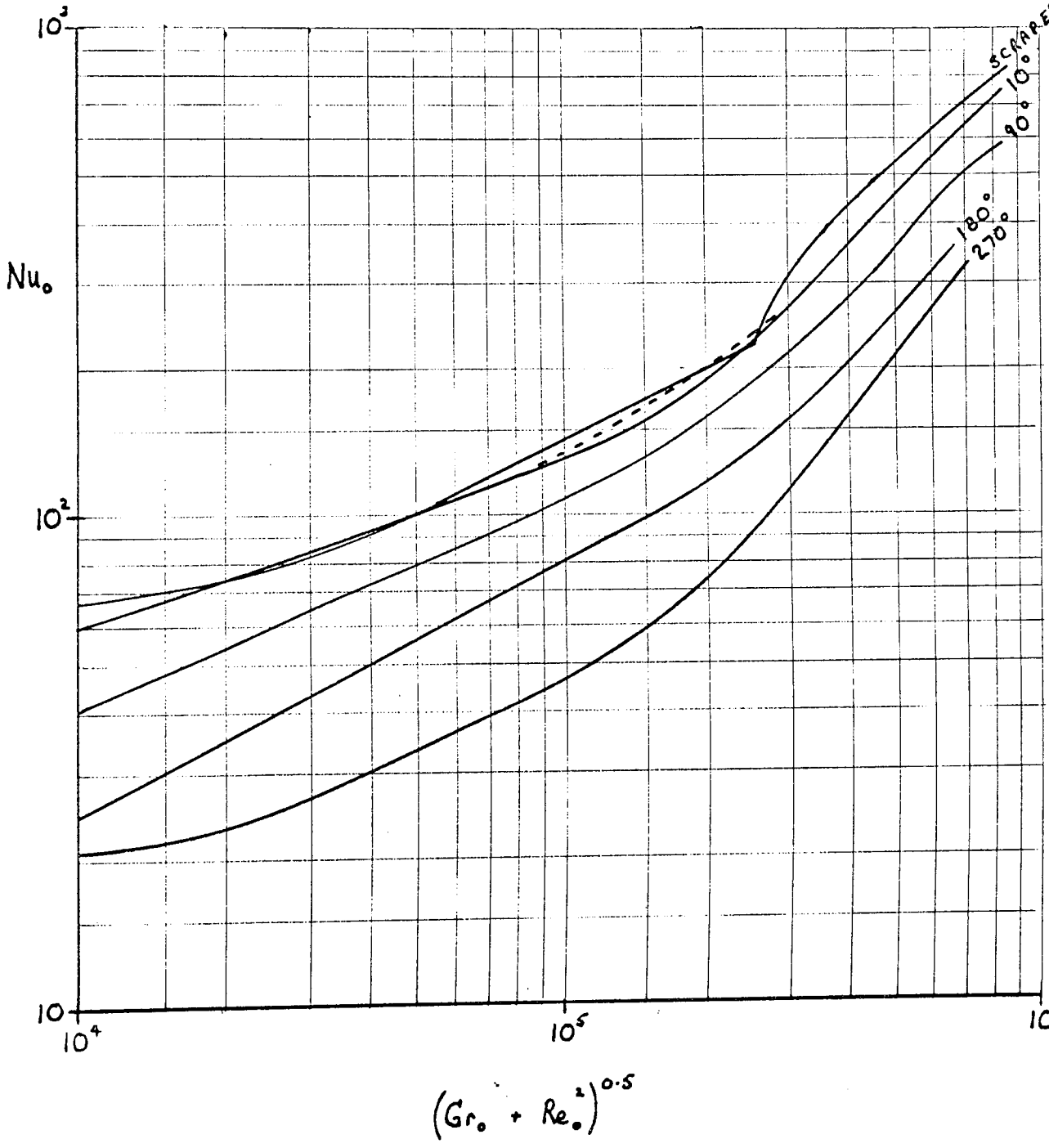

FIGURE 4.16

Effect of varying the sector of Disc masked off on the Heat Transfer from a Disc rotating in Still Air at a Reynolds number of 120,000

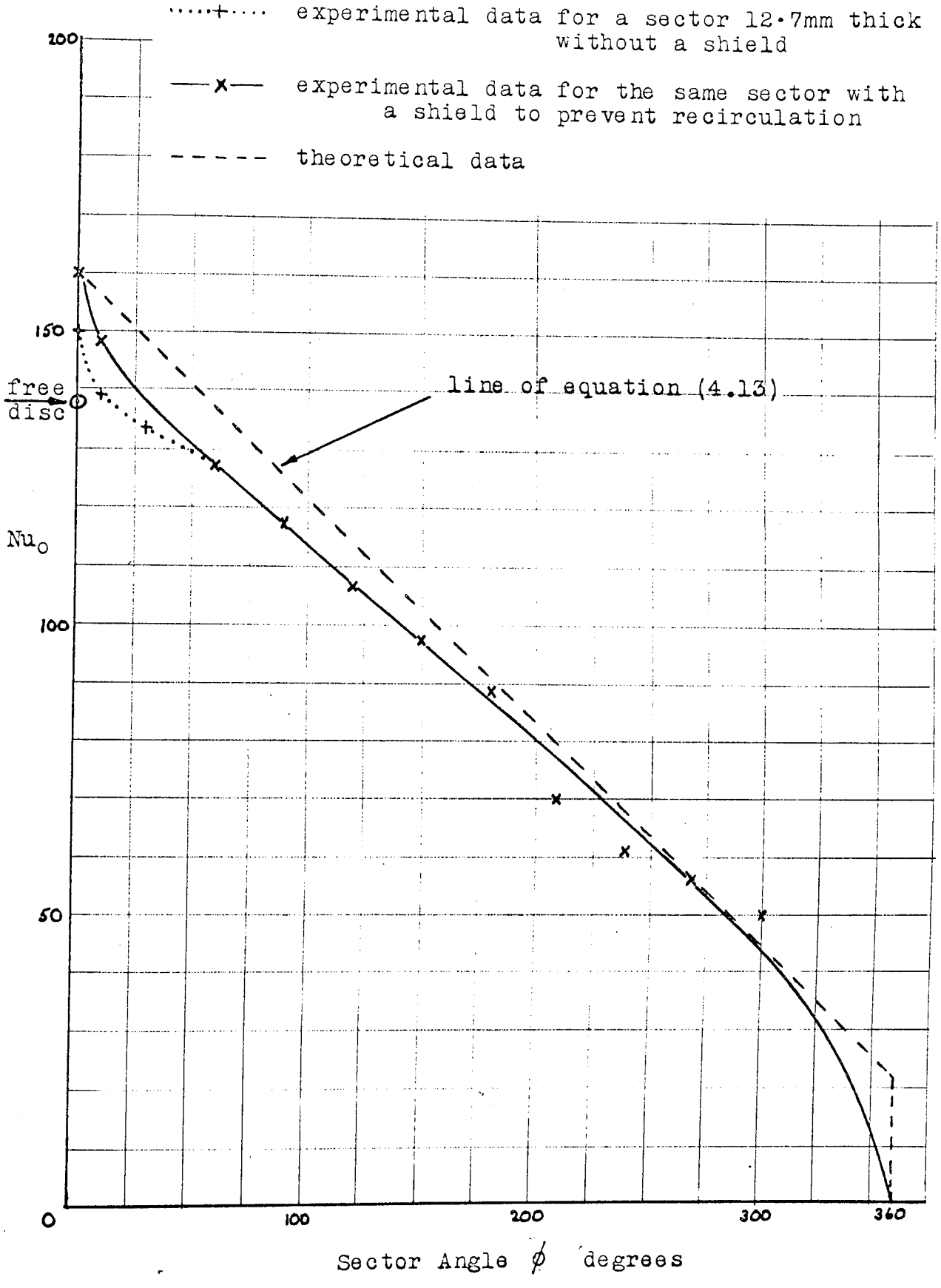

FIGURE 4.17

Effect of varying the sector of Disc masked off on the Heat Transfer from a Disc rotating in Still Air at a Reynolds number of 500,000

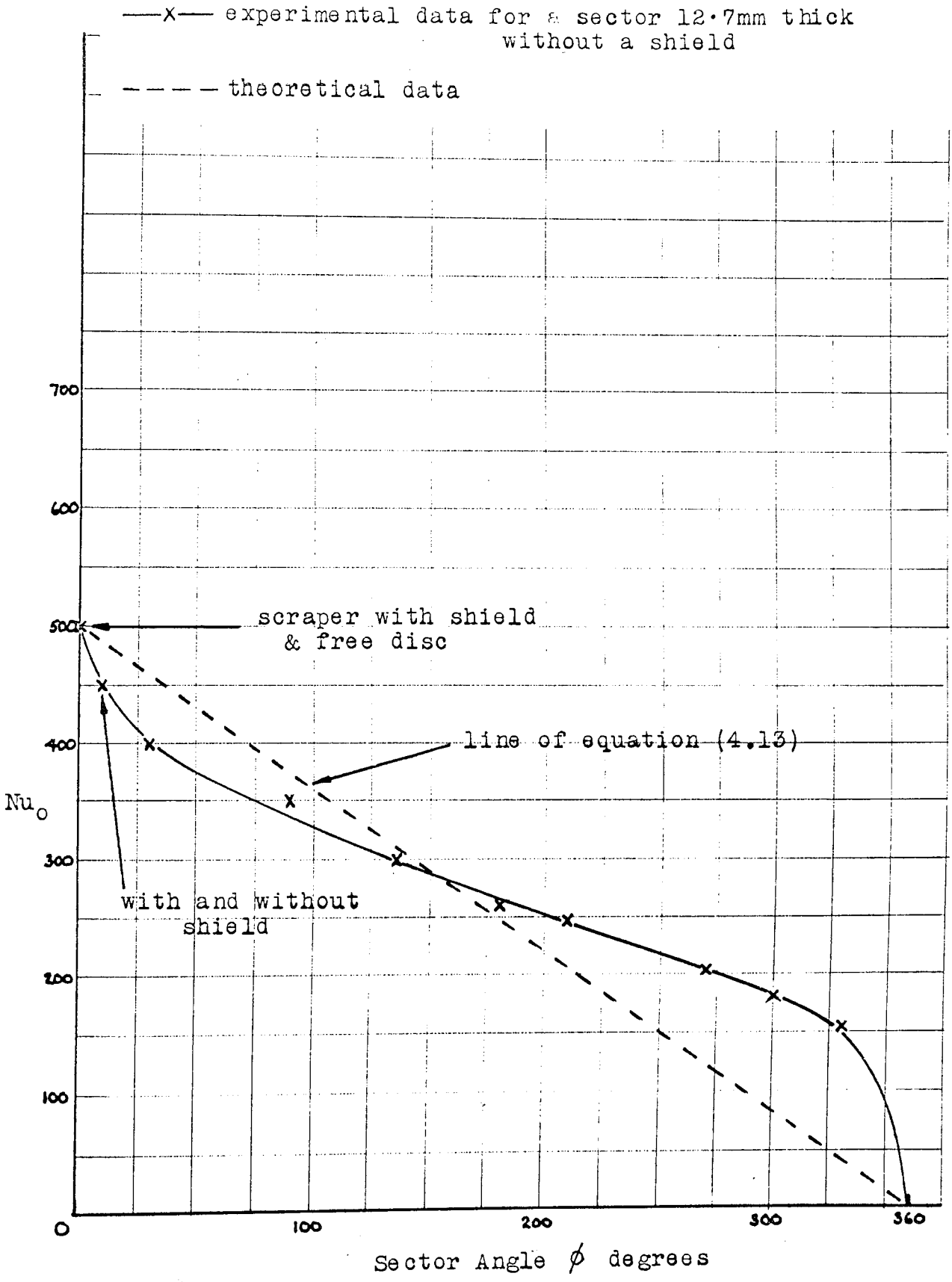

as shown in figure 4.18

At higher speeds, in both the laminar and turbulent regions, the leading edge of the scraper or sector created a swirl of air which travelled across the surface in front of the leading edge, again shown in figure 4.18. With a scraper or sectors of small angle some air also travelled over the scraper or sector and returned to the disc surface. When a cardboard shield was fitted from the top of the scraper or sector to the adjoining bearing stand flow visualization showed that this recirculation was prevented.

In the turbulent region, on a free disc, transition to turbulent flow began when the boundary layer had travelled a certain distance from the disc centre, therefore it always occurred at a radius the length of which depended on the speed. However, with a sector on the disc and no recirculation of flow a new boundary layer must be formed behind the sector. This had to travel beyond the free disc radius of transition before it changed to turbulent flow, and hence a larger area of the disc surface was under laminar flow than occurred at that speed with a free disc.

The effect on the heat transfer of fitting a scraper to each side of the disc was shown in figure 4.10. For one set of tests a shield was attached to each scraper to prevent recirculation of air. At low Reynolds numbers, around 1.4×10^4, the heat transfer was 50% above that for a free disc due to the scraper deflecting the boundary layer of air back across the disc surface. In the remainder of the laminar region the scraper with the shield continued to have a heat transfer 17% above that for a free disc due to the swirl of air over the surface in front of the scraper. Without the shield the heat transfer was reduced slightly due to recirculation of air of above ambient temperature to the disc surface on the other side of the scraper. In the turbulent region with a shield, the heat transfer was identical to that of a free disc as

FIGURE 4.18

Visualization of Flow over Scraper on a Rotating Disc in Still Air

$Re_o = 1{\cdot}5 \times 10^4$

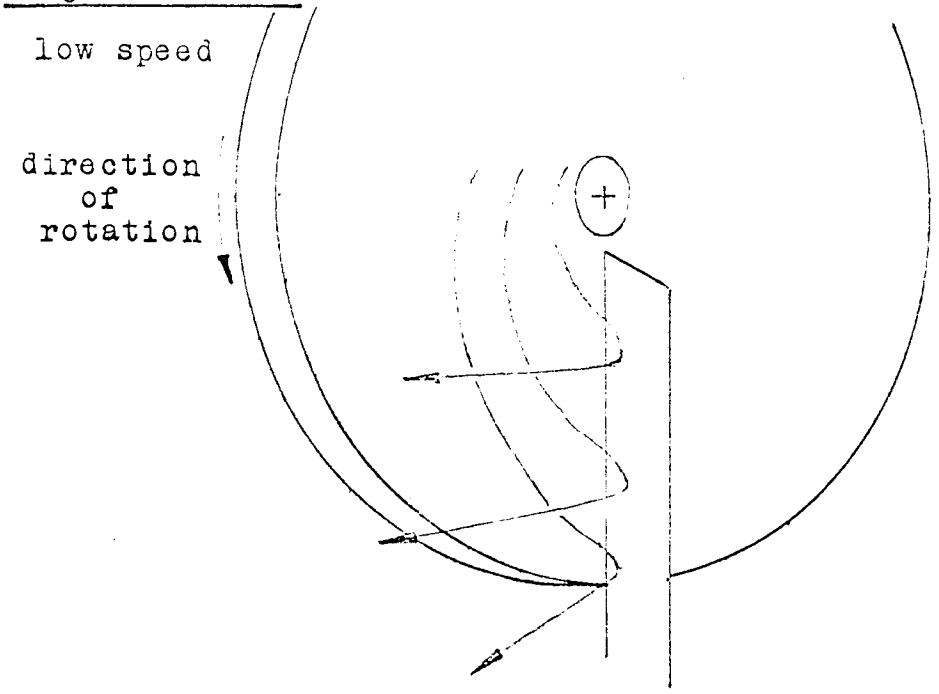

Note: no shield to prevent recirculation of flow

$Re_o = 10^5$ to 10^6

laminar and turbulent regions of flow

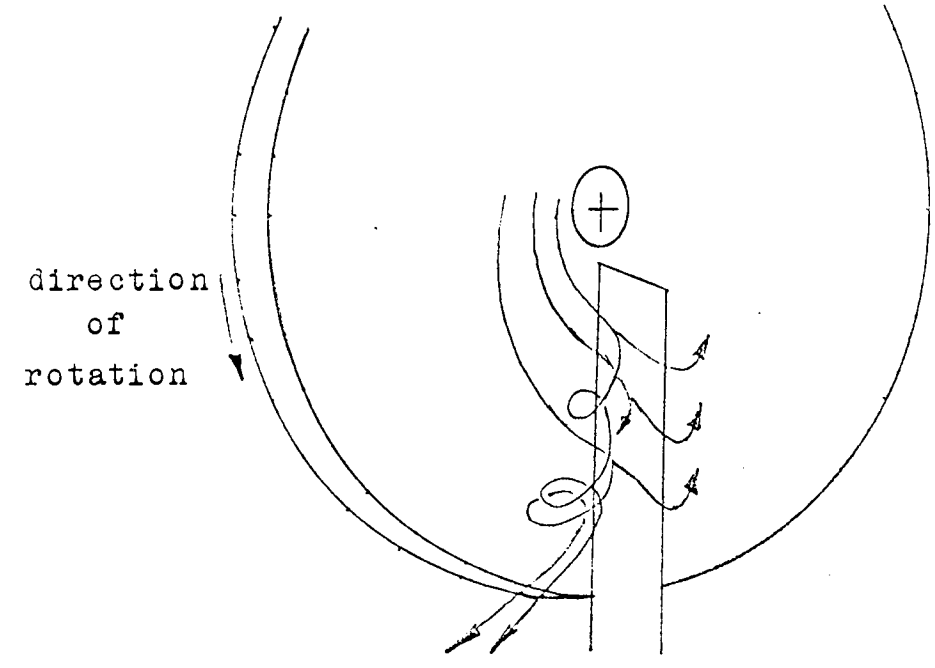

the improvement in the heat transfer due to the slight swirl ahead of the scraper was counteracted by an increase in the area under laminar flow behind the scraper. Without the shield some flow recirculated over the scraper and turbulent flow continued as with a free disc, producing a higher overall heat transfer due to the swirl ahead of the scraper.

The heat transfer curves for a disc with sectors of 10°, 90°, 180° and 270°, shown in figures 4.11 to 14, all followed a similar pattern. The heat transfer at low Reynolds numbers was considerably higher than with a free disc due to deflection of the boundary layer back across the disc surface by the front edge of the sector. In the remainder of the laminar region the Nusselt number varied approximately with $Re_o^{0.5}$ in the usual way. The heat transfer did not change sharply at the onset of turbulent flow, as with a free disc, but gave a considerably extended transition region which changed gradually from laminar to turbulent heat transfer. This was caused by the increased laminar area behind the sector and the general disturbances caused to the flow. Near the maximum end of the range of Reynolds numbers tested the heat transfer approached the usual turbulent type; Nusselt number varying with $Re_o^{0.8}$.

It was expected that with a shield fitted to the sectors to prevent recirculation the heat transfer coefficient would follow the line

$$h = \frac{(360 - \phi)}{360} h_{free} + (h_{scraper} - h_{free}) \qquad (4.13)$$

where $(h_{scraper} - h_{free})$ represents the increase in the heat transfer due to the disturbance of the air at the leading edge of the sector. Tests carried out on a 90° sector showed that, beyond 13mm, the thickness had no effect on the heat transfer, so that $(h_{scraper} - h_{free})$ should be the same for the scraper and all the other sectors. By plotting equation (4.13) in figures 4.16 and 4.17 the results become somewhat easier to explain.

In the laminar region at $Re_o = 120{,}000$ (figure 4.16) with the 10° sector and a shield to prevent recirculation, the heat transfer dropped

to 5% below the expected value. Flow visualization indicated no change in the swirl over the disc surface ahead of the sector, shown in figure 4.19, and this was supported by experiments with the 90° sector whose thickness was varied from that of the sector to beyond that of the scraper with no effect on the heat transfer. No other reason was found for this deviation from the expected result. With no shield, the heat transfer was reduced further due to recirculation of air to the other side of the sector. Figure 4.16 shows that recirculation occurred up to a sector angle of 60° at a Reynolds number of 120,000, so no shield was needed beyond this. At higher angles of sector, in the laminar range, the heat transfer gradually came back to the line of expected heat transfer, from which it had deviated by a maximum of 5.5%.

In the region of turbulent flow, Re_o = 500,000 (figure 4.17) with the 10° sector, the heat transfer dropped below the expected line due to the increased area of laminar flow behind the sector. The shield had no effect on the heat transfer as the increased velocity of the air prevented it from being recirculated back to the disc.

At higher angles of sector the effect of the increased laminar area was gradually lessened until at an angle of 160° the heat transfer came back to the expected line. Beyond this the heat transfer gradually increased due to the swirl over the surface of the disc in front of the leading edge of the sector, which affected a progressively larger percentage of the uncovered area of disc.

The full range of sector angles has been covered, and it is unlikely that information will be required beyond a Reynolds number of 800,000, so an adequate range of tests have been made. Should values be required at Reynolds numbers above this, extrapolation of the measured lines should be sufficiently accurate, as with the flow predominantly turbulent it is unlikely that further changes in the pattern of the airflow will occur.

FIGURE 4.19

Visualization of Flow over 10^{o} Sector on a Rotating Disc in Still Air

$Re_o = 1.5 \times 10^4$

low speed

direction of rotation

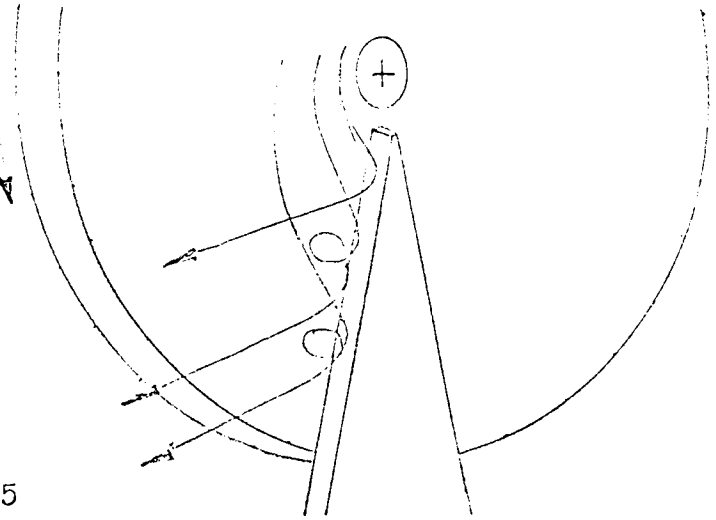

$Re_o = 2 \times 10^5$

laminar region

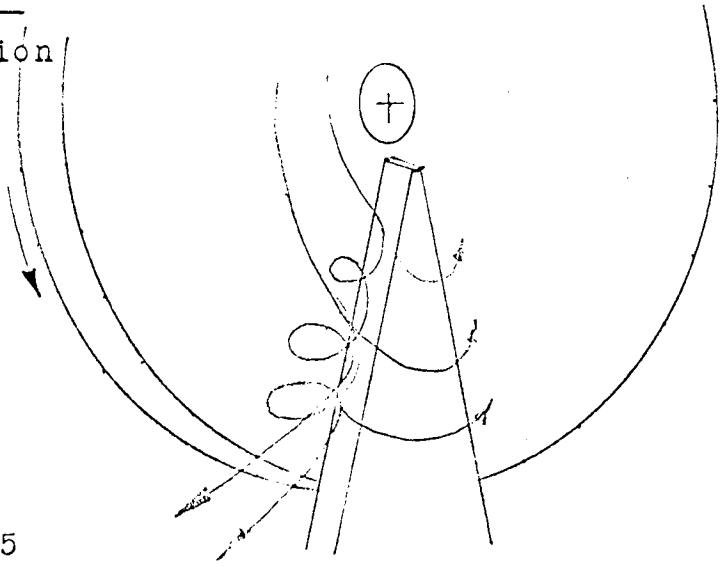

$Re_o = 7 \times 10^5$

turbulent region

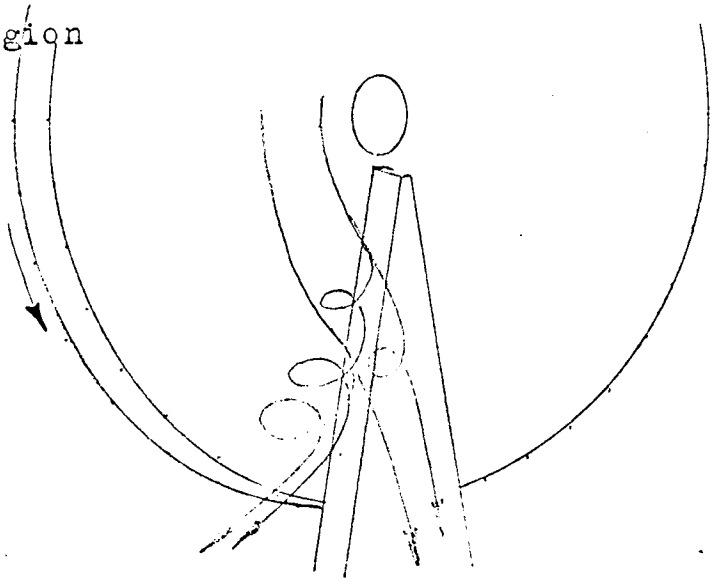

Note: no shield to prevent recirculation of flow

SUMMARY

A scraper with a shield to prevent recirculation increased the laminar heat transfer to 17% above that from a free disc. But in the turbulent region, recirculation must be allowed to continue to get an increase of 12% above that of a free disc.

For sectors covering from 0° to 360° of the disc surface a complex pattern of airflowwas created which prevented the heat transfer from varying directly with the area of disc left uncovered. The increase in heat transfer due to the disturbance of the flow varied with rotational speed in such a way that it proved too difficult to fit an equation to the effect of sector angle on the heat transfer.

A brake extends approximately 70mm above the disc surface, and such a high obstruction coupled with the fact that the angle subtended by a caliper will not be less than 40° makes it extremely unlikely that any recirculation of air will occur over the caliper. Therefore it can be assumed that for disc brake applications the effects of recirculation can be ignored.

Interpolation and cross-plotting between the curves in figure 4.15 will give the Nusselt number for any caliper from 0° to 360° and any rotational Reynolds number from 10^{4} to 10^{6}.

4.3 ROTATING DISC IN AN AIR CROSSFLOW

Disc brakes are usually fitted to vehicles and hence operate in an airstream which flows across and parallel to the disc surface. The heat transfer coefficient of a rotating disc in an air crossflow is therefore an important parameter in the calculation of disc brake operating temperatures.

An air crossflow was obtained by mounting the disc in a wind tunnel with a test section of 0.7m x 0.25m which produced an airflow of from 5

to 32 m/s velocity. The heat transfer coefficient was measured for a range of rotational and crossflow speeds.

The theoretical treatments of the heat transfer from a rotating disc and from forced convection over a flat plate are very different and an exact solution of the superposition of the two systems could not be found. An approximate analysis has been evolved which agrees well with the experimental results and may prove to be useful with other systems.

PRELIMINARY EXPERIMENTS

A survey of the airflow in the entrance to the test section was made, following the procedure of British Standard 848, Part 1, 1963. This is described in Appendix 2 , where it is shown that the mean velocity differed from that measured with a pitot tube at the centre point of the entrance by 1.6%. Therefore, during tests, the velocity was measured at the centre point as this was much quicker than taking a survey of the airflow and was more accurate than measurements from the tunnel static pressure manometer. Heat transfer tests taken with the pitot tube left in the centre position did not differ from those taken with it moved to one side, indicating that the pitot did not affect the airflow in the test section.

As the cross sectional area of the disc varied with distance down the test section the height of a plate of equal area and length to the disc was used to calculate the disc blockage area. The effective plate height was found to be three-quarters disc diameter. The disc blocked 6% of the test section, which was within the recommended maximum of 8%. The measured airspeed was increased by this percentage. Flow visualization showed that distortion of the airflow caused by the disc did not reach the tunnel wall, so there were no wall constraint effects.

The temperature of the air was measured with a thermocouple positioned upstream of the disc. This was initially traversed across the entrance to the test section and showed no variation in stream temperature.

The main disc diameter R_o was used as the effective plate length for the calculation of the crossflow Reynolds number $Re_t = \frac{U\ R_o}{\nu}$. The Reynolds number due to rotation and the Nusselt number remained the same as used in 4.1.

$$Re_o = \frac{\omega R_o^2}{\nu} \qquad Nu_o = \frac{h_m R_o}{k}$$

HEAT TRANSFER EXPERIMENTS

Measurements of the heat transfer coefficient taken at various crossflow and rotational speeds are presented as a plot of Nusselt number against crossflow Reynolds number for a series of rotational Reynolds numbers in figure 4.20. It is helpful to the discussion and analysis of these results if they are re-plotted with the same data and the axes interchanged as shown in figures 4.21 and 4.22. In figure 4.20, at high crossflow Reynolds numbers, the lines tend to come together, indicating that the rotational flow has only a small effect on the heat transfer, and the crossflow Reynolds number predominates. A similar pattern can be seen in figure 4.21, but in this case the rotational flow does not dominate the heat transfer so much at high rotational Reynolds numbers, the crossflow still influencing the heat transfer to some extent. Figure 4.22 presents the experimental results in yet another way, plotting the crossflow against the rotational Reynolds numbers for a series of values of the Nusselt number. This shows still more clearly how the heat transfer tends to be dominated by each flow at opposite extremes of the range of tests.

FIGURE 4.20

Experimental data for the Heat Transfer from a Rotating disc in an Air Crossflow

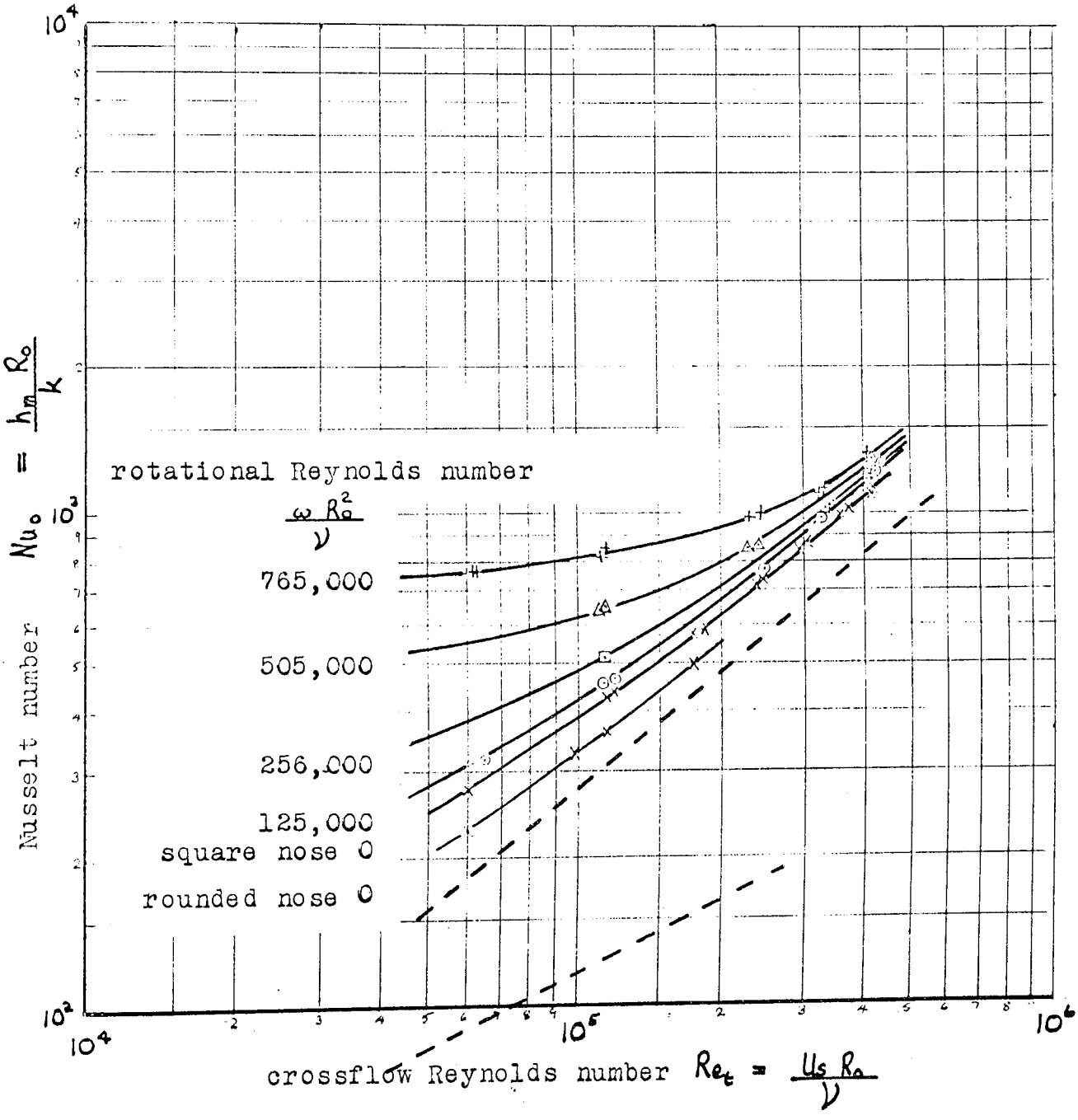

FIGURE 4.21

Experimental Data for the Heat Transfer from a Rotating Disc in an Air Crossflow

Data repeated from figures 4.20 and 4.02

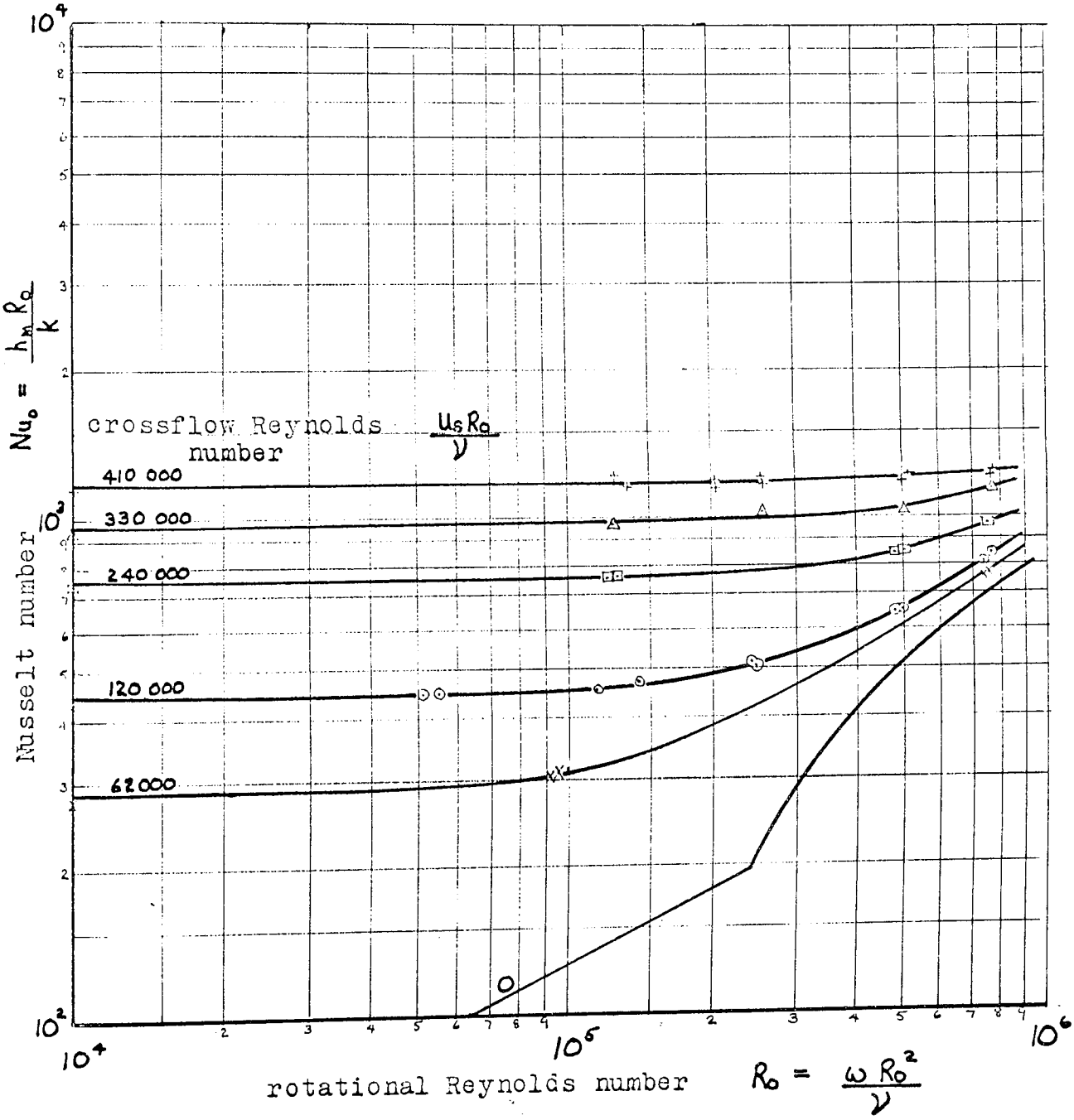

FIGURE 4.22

Experimental Data for the Heat Transfer from a Rotating Disc in an Air Crossflow

Data repeated from figure 4.20

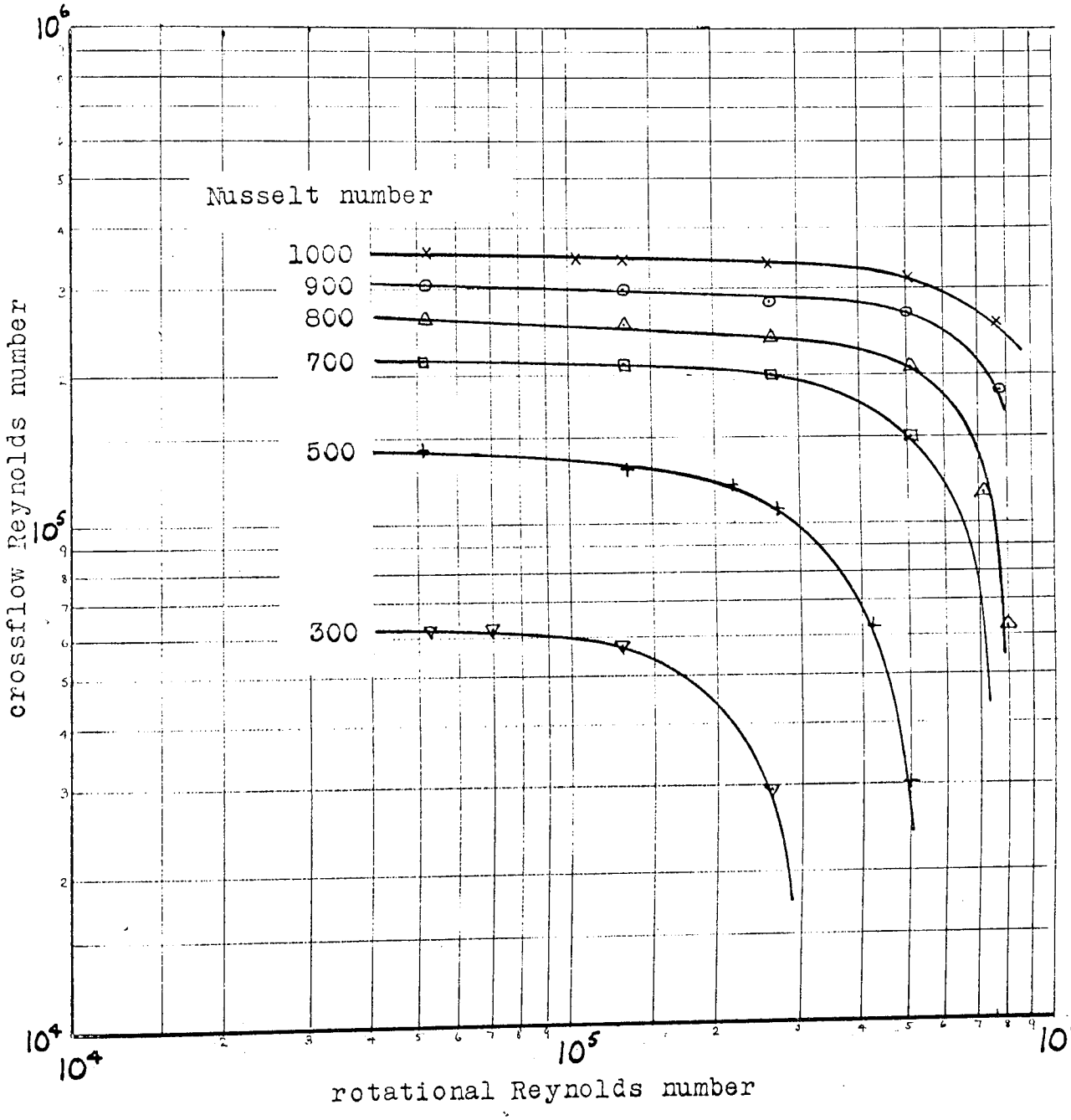

Most of the tests were taken with the leading edge of the disc havings its normal square shape with sharp corners, but some tests were made on a stationary disc with the leading edge built up with plasticene to a more streamlined shape, as shown in figure 4.23.

In figure 4.20 the curves at zero rotational speed for the different edge shapes both have a slope of 0.8 over most their length; the usual slope of a turbulent heat transfer line, with the square-nosed line running 14% above the rounded-nose line. Edwards & Furber [46] studied the effects of freestream turbulence and leading edge shape on the heat transfer from a flat plate and their measurements showed that the square nose produced turbulent flow at Reynolds numbers well below that where the flow over a rounded-nose plate reverted to laminar flow. However, as the line of heat transfer of the rounded-nose disc also had a slope of 0.8 in figure 4.20 it seems reasonable to assume that this must have been caused by the other condition which maintains turbulent flow; high freestream turbulence. This would not be unexpected as the wind tunnel had a short settling length prior to the test section. This could not be lengthened due to the dimensional limits imposed by the installation. To further investigate this point, flow visualization experiments were made with paraffin smoke in a stream of 5 m/s. This revealed the airflow around the disc as shown in figure 4.24. Separation occurred at the leading edge of the square nosed disc, indicated by a reversal of flow over a short initial length of the surface, followed by reattachment further downstream and turbulent flow thereafter. The rounded-nose eliminated the separation but the flow still appeared to be turbulent along the whole of the surface. It was noted that when the wind tunnel fan was switched off and smoke visualization continued, the flow eventually became laminar over the rounded-nose disc at a very low airspeed, corresponding to the findings of Edwards & Furber. The extremely disturbed airflow over the initial

FIGURE 4.23

Shapes of Leading Edges of Disc and Plate

Square leading edge of experimental disc

Rounded leading edge of experimental disc

Leading edge of plate used by Ede & Saunders [48]

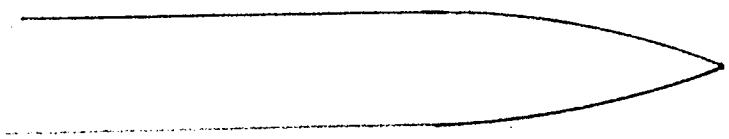

FIGURE 4.24

Flow Visualization on a Disc in an Air Crossflow with a Square and Rounded Leading Edge

Square leading edge

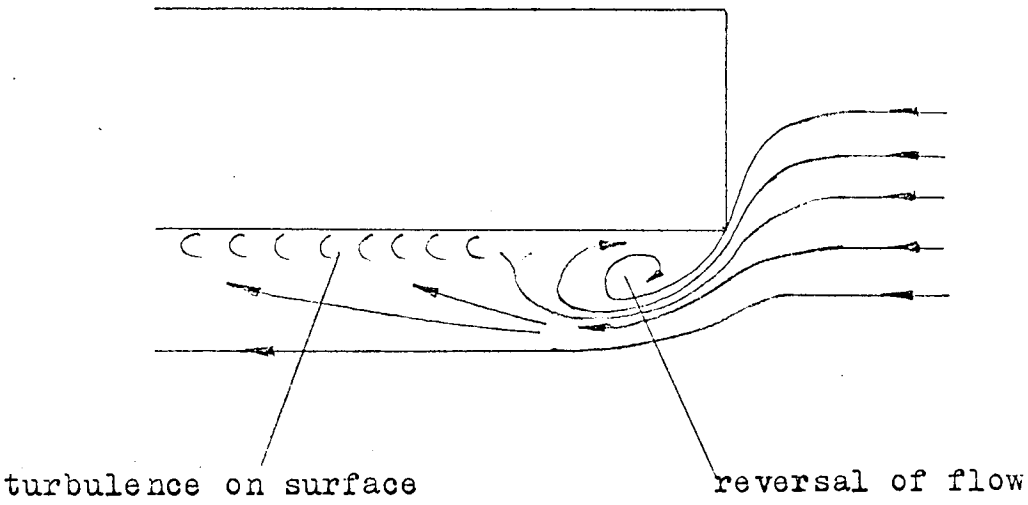

Rounded leading edge

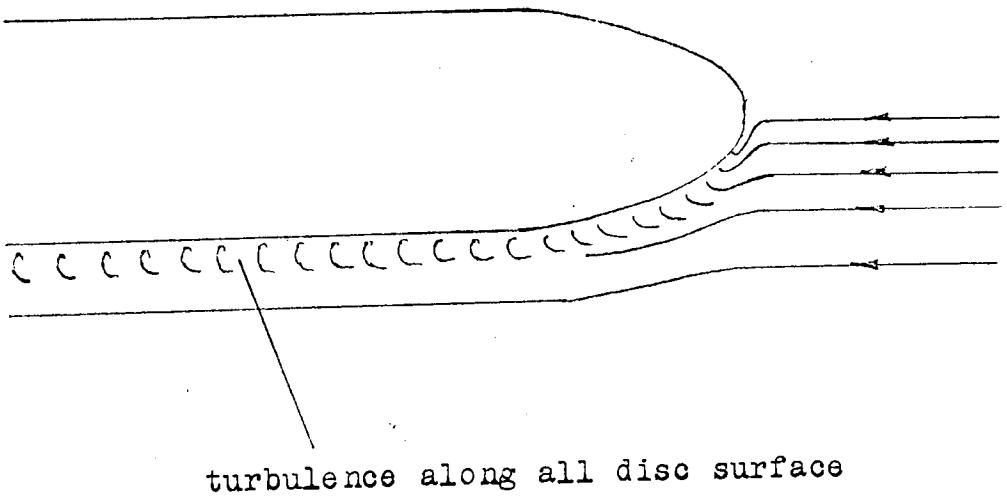

part of the disc surface (approximately 15% of the disc area) might well have given the higher heat transfer shown in figure 4.21 for the square-nosed disc. Edwards & Furber were working well downstream of the square leading edge on their plate, when the separation effects would have disappeared, explaining why they found no increase in the heat transfer. Supporting this, Ede & Saunders {48} noted an increase in the heat transfer from a flat plate when it had a wedge shaped nose with measurements taken in a water stream, but the results were erratic and no quantitive measurements were reported.

It is expected that the disc or plate thickness would have an effect on the turbulence and separation induced by a blunt nose. The disc diameter would also affect the heat transfer coefficient as the larger the disc, the smaller percentage of area covered by the separated region of flow. The usual brake discs have a thickness to diameter ratio of 3% to 8%, the experimental disc being 6.3%, so it would not be unreasonable to assume that over this short range the increase in heat transfer due to separation would be similar for all existing vehicle disc designs.

From figure 4.20 the Nusselt number for a square-edged disc at zero rotational speed varied with the crossflow Reynolds number to the index 0.8 over most of the range of crossflow velocities that were tested but at the lowest speeds it began to deviate from that slope, indicating that it was becoming more dependent on some other variable. At the lowest crossflow velocity of 5 m/s and with the low surface temperatures involved it is extremely doubtful if natural convection were causing this deviation so it could only be attributed to the effects of separation. Therefore at low airspeeds it is possible that different sized discs would produce a greater or lesser deviation from the experimental data.

The majority of present applications fall within the range of the experimental results, but in order to allow extrapolation with confidence

a theoretical analysis of the heat transfer was attempted.

THEORETICAL ANALYSIS

Obviously, the experimental measurement of the heat transfer from a rotating disc in an air crossflow involved rotating the disc and forcing air over it in a direction parallel to the face of the disc. It was therefore natural to consider the theoretical analysis of the heat transfer from the system as that of the two following separate systems superimposed.

1. Heat transfer from a circular flat plate parallel to an airstream.
2. Heat transfer from a rotating disc in still air.

It has been shown in Chapter two that both of these systems have been the subject of a number of papers, both theoretical and experimental, so it is not difficult to compare the theoretical predictions of previous workers with experimental results before attempting to use them in the present analysis.

Circular Flat Plate

The heat transfer measurements and predictions for a rectangular, as opposed to a circular, flat plate are tabulated and plotted in figure 4.25. These are extracted from work by Schlichting {74}, Edwards & Furber {46}, Pohlhausen and Karman (the last two cited in {46}). It can be seen that they lie close together, predictions agreeing well with measurements. The predictions of Schlichting will be used for further evaluations of heat transfer from a circular flat plate, in both laminar and turbulent flow.

The theoretical prediction of Schlichting was converted from that for a rectangular flat plate in an air crossflow to a circular flat plate with a heated rim in an air crossflow. This was achieved by using the local heat transfer coefficient as predicted by Schlichting,

FIGURE 4.25

Heat Transfer from a Rectangular Flat Plate

No	Author	expt or theory	LAMINAR	TURBULENT
1	Schlichting	theory	$Nu=0.592Re^{0.5}$	$Nu=0.033Re^{0.8}$
2	Edwards & Furber	expt	$Nu=0.39Re^{0.535}$	$Nu=0.038Re^{0.786}$
3	Pohlhausen	theory	$Nu=0.52Re^{0.5}$	
4	Karman	theory		$Nu=0.04Re^{0.781}$

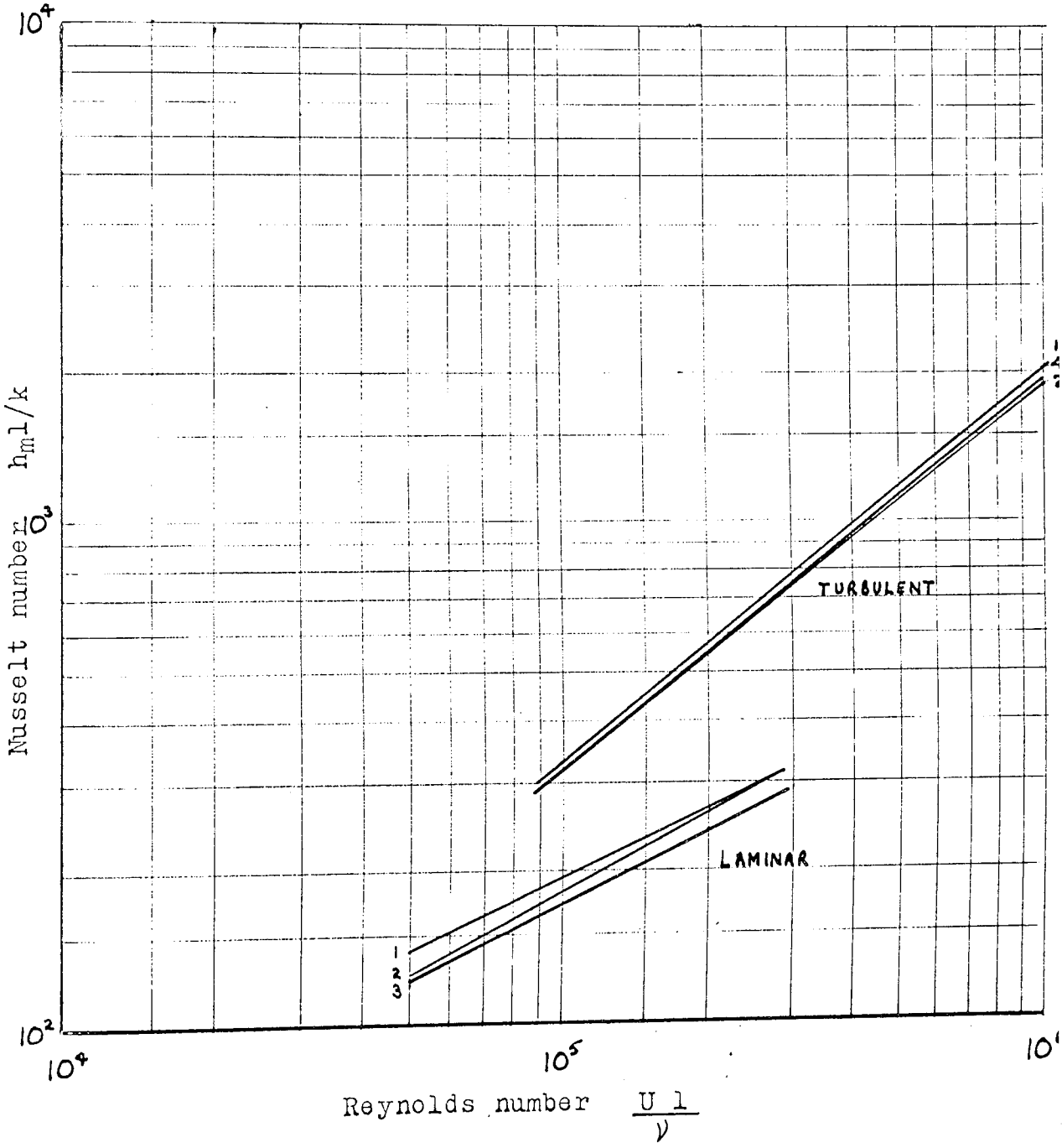

which is dependent on the distance of the point being considered from the leading edge of the plate. In fact $h_{local} \propto \frac{1}{x^{0.2}}$ for turbulent flow over the plate. The value of $\sum \frac{1}{x^{0.2}}$ was evaluated for the author's experimental disc in the same way as $\sum \frac{1}{x^{0.25}}$ was found in Appendix 6, giving the result

$$\frac{1}{A} \sum_{x=0}^{x=2R} \frac{A}{xo.2} = 0.355 \qquad \frac{1}{mm^{0.2}} \qquad (4.14)$$

Now Schlichting gave, for turbulent flow

$$h_x = 0.0296 \frac{k}{x} \sqrt[3]{Pr} \; Re_x^{0.8} \qquad (4.15)$$

For a Prandtl number of 0.7

$$h_x = 0.0296 \times 0.887 \; k \left(\frac{U}{\nu}\right)^{0.8} \frac{1}{x^{0.2}} \qquad (4.16)$$

$$= 0.0263 \; k \left(\frac{U}{\nu}\right)^{0.8} \frac{1}{x^{0.2}} \qquad (4.17)$$

Integrating this over the plate gives

$$h_m = 0.0263 \; k \left(\frac{U}{\nu}\right)^{0.8} \frac{1}{A} \sum_{x=0}^{x=2R} \frac{A}{x^{0.2}} \qquad (4.18)$$

Using 4.14 in 4.18

$$h_m = 0.00935 \; k \left(\frac{U}{\nu}\right)^{0.8} \frac{1}{mm^{0.2}} \qquad (4.19)$$

For the experimental disc Ro = 201.6mm.

and $Nu_o = \frac{h_m \; Ro}{k}$

$\therefore$ $Nu_o = 0.00935 \left(\frac{U}{\nu}\right)^{0.8} Ro^{0.8} \; 201.6^{0.2}$ (4.20)

$= 0.027 \left(\frac{U \; Ro}{\nu}\right)^{0.8}$ (4.21)

Now $Re_t = \frac{U \; Ro}{\nu}$

Therefore $$Nu_o = 0.027 \, Re_t^{0.8} \qquad (4.22)$$

A similar procedure for laminar flow leads to

$$Nu_o = 0.364 \, Re_t^{0.5} \qquad (4.23)$$

These are the predicted equations for the heat transfer from the disc used for these experiments, when stationary in an air crossflow.

Figure 4.20 showed the measurements of heat transfer from the disc, when stationary in an air crossflow, and compared them with the theoretical predictions outlined above (equations 4.22 and 23). The theoretical heat transfer line was 20% lower than that found from the disc with a rounded nose. It is most likely that the nose shape still caused some disturbance of the flow, hence increasing the heat transfer, as Ede & Saunders used the nose shape shown in figure 4.23 before laminar flow was achieved in water. It was thought that the circular shape of the disc might distort the airflow but flow visualization showed that the flow across the disc remained parallel to the axis of the tunnel as assumed when calculating $\frac{1}{A} \sum \frac{A}{x^{0.2}}$ for the experimental disc.

As no qualitative evidence has been found on which to base a prediction of the heat transfer over a square nosed disc, including the effects of separation, the experimental work must be used as a basis for the prediction of the heat transfer from a rotating disc in an air crossflow. A law of the form $Nu = C \, Re^n$ can be approximated to the experimental data for the stationary disc with a square nose in an air crossflow. The law was found to be

$$Nu_o = 0.036 \, Re_t^{0.8} \qquad (4.24)$$

which represented an increase of 33% on that predicted from stationary surface theories. By reversal of the procedure from equation (4.22) to (4.17) we obtain the local heat transfer equation

$$Nu_x = 0.0358 \, Re_x^{0.8} \qquad (4.25)$$

Rotating Disc in Still Air

The heat transfer from a rotating disc in still air has been extensively investigated and the results were discussed in detail in Chapter two. The present measurements of the heat transfer from this system were described in Part 1 of this chapter.

As the air crossflow induced a turbulent boundary layer over the whole of the disc surface it is assumed that this disturbed the rotational flow and caused it to be turbulent also, even at speeds when it would normally have been laminar.

In Section 4.1 it was shown that the experimental results, extrapolated for the condition of turbulent flow over the whole disc, could be represented by the equation

$$Nu_o = 0.0152\ Re_o^{0.8} \qquad (4.26)$$

This agreed with predictions by Dorfman {1} and Cobb & Saunders {32} . From the same section is obtained the equation for the local turbulent Nusselt number

$$Nu_R = 0.0195\ Re_R^{0.8} \qquad (4.27)$$

Superposition of the Two Systems

The complicated flow pattern around a rotating disc in an air crossflow results from a combination of the two flow patterns previously referred to, and therefore the heat transfer will be regarded in a similar manner.

According to Reynolds analogy, under suitable circumstances, the heat transfer coefficient, the shear stress at the surface, and the freestream velocity are related:-

$$h = \frac{\tau_s\ C_p}{u}$$

As an empirical device, the heat transfer coefficient can be regarded as a vector quantity instead of a scalar one, and given the

freestream direction (which is the same as the shear stress direction). A local heat transfer coefficient at any point on a surface resulting from the superposition of two streams can then be formally calculated as the vector sum of the two heat transfer coefficients that would exist at that point if both streams were acting separately. The mean heat transfer coefficient is then found from a numerical integration of the resultant local coefficients over the surface.

To assess this method it was first used to predict the mean heat transfer from square and circular plates with two different crossflows existing simultaneously. For such systems the heat transfer can, of course, be found directly by calculating the resultant flow and the mean heat transfer coefficient due to that flow. The differences between the two sets of results were:- for the square plate 6.6% and for the circular plate 7.7%. As this seemed a reasonable agreement, the heat transfer from a rotating disc in an air crossflow was evaluated in the same way. The equations (4.25) and (4.27) presented in the previous sections were used for the calculation of the local heat transfer coefficients.

The crossflow heat transfer coefficient was given the same direction as that of the crossflow, which must be parallel to the direction in which the distance from the leading edge, x, is taken. It was more difficult to decide which direction to give to the rotational heat transfer coefficient as the only flow at the surface is tangential, but it is the radial component of the flow in the boundary layer which carries heat away from the disc. However, examination of the method reveals that the same mean heat transfer coefficient results whether the radial or the tangential direction is used, though local coefficients would, of course, be different. It is assumed, for these calculations, that the disc is stationary with a rotational airstream imposed on it. In reality, as the disc rotates, each point on the surface would change its heat transfer coefficient continuously in one revolution, so truly local

coefficients only exist at one instant in time.

A computer programme was developed (see figure 4.26) which calculated the local values of the heat transfer coefficients for given values of rotational and crossflow speeds from the equations for the local coefficients for given values of rotational and crossflow speeds from the equations for the local coefficients and added them vectorially, for a grid of finite areas over the disc surface. It was found that when the grid was increased beyond 90 areas there was no increase in the accuracy of the answer.

The values of the mean heat transfer coefficient calculated in this way are plotted in figure 4.27, along with the experimental data. With the disc stationary the predicted values deviate from experiment by up to 10%, due to the separation effects having a greater influence on the heat transfer at low airspeeds. In the range of crossflow and rotation existing simultaneously the maximum deviation is 5.3%, with a mean of 2.3%. As the experimental results ranged from dominance of one Reynolds number on the heat transfer, through a region where the Nusselt number depended on both systems to a condition where the other Reynolds number was predominant, then the theoretical analysis has been proved acceptable over an adequate range of conditions.

Prediction of the Heat Transfer from a Brake Disc

Brake discs do not have a guard heater rim, which was a necessary part of the experimental equipment, and so the heat transfer for these was predicted by modifying the theoretical analysis just outlined.

The same local equations for rotation and crossflow convection heat transfer are used

viz. crossflow $Nu_x = 0.0358\ Re_x^{0.8}$

rotation $Nu_r = 0.0198\ Re_r^{0.8}$

FIGURE 4.26

Algol Computer Programme to predict the Heat Transfer from a Rotating Disc in an Air Crossflow

```
CVAE27;
"BEGIN" "REAL" C1,C2,AS,RS,R1,R2,US,W,H,A,B,X,TP,TD,HP,HD,
 AREA,NU,VIS,RE
"SWITCH" SS:=J;
"READ" AS,RS,C1,C2;
AS:=AS*3.1416/180;
R1:=8.906;   R2:=7.938;
J:    "READ" US,W;
H:=0;    W:=3.1416*W/30;
"FOR" A:=AS/2 "STEP" AS "UNTIL" 6.2832 "DO"
"FOR" B:=RS/2 "STEP" RS "UNTIL"   R2   "DO"
"BEGIN"
     X:=SQRT(R1*R1-(B*COS(A))↑2) - B*SIN(A);
     TP:=C1*US↑1.8/X↑0.2*12↑1.8;
     TD:=C2*W↑1.8*B↑1.6;
     HP:=TP/US;
     HD:=12*TD/(W*B);
     AREA:=AS*RS*B;
     H:=SQRT(HP*HP+HD*HD-2*HP*HD*COS(A))*AREA+H;
"END";
VIS:=19.5₁₀-5;
NU:=H/(3.1416*R2*VIS↑0.8*12↑2.6);
RE:=US*R2/(VIS*12);
"PRINT" ''L3'ROTATING DISC WITH CROSSFLOW, BOTH TURBULENT
CROSSFLOW', SAMELINE,ALIGNED(4,0),US,'FT/SEC      DISC SPEED',
W*30/3.1416,'RPM'L'NU ='',ALIGNED(4,1),NU,'
RE ='',ALIGNED(7,0),RE;
"GOTO" J;
"END";
```

FIGURE 4.27

Comparison of Experimental and Theoretical Data for a Rotating Disc in an Air Crossflow

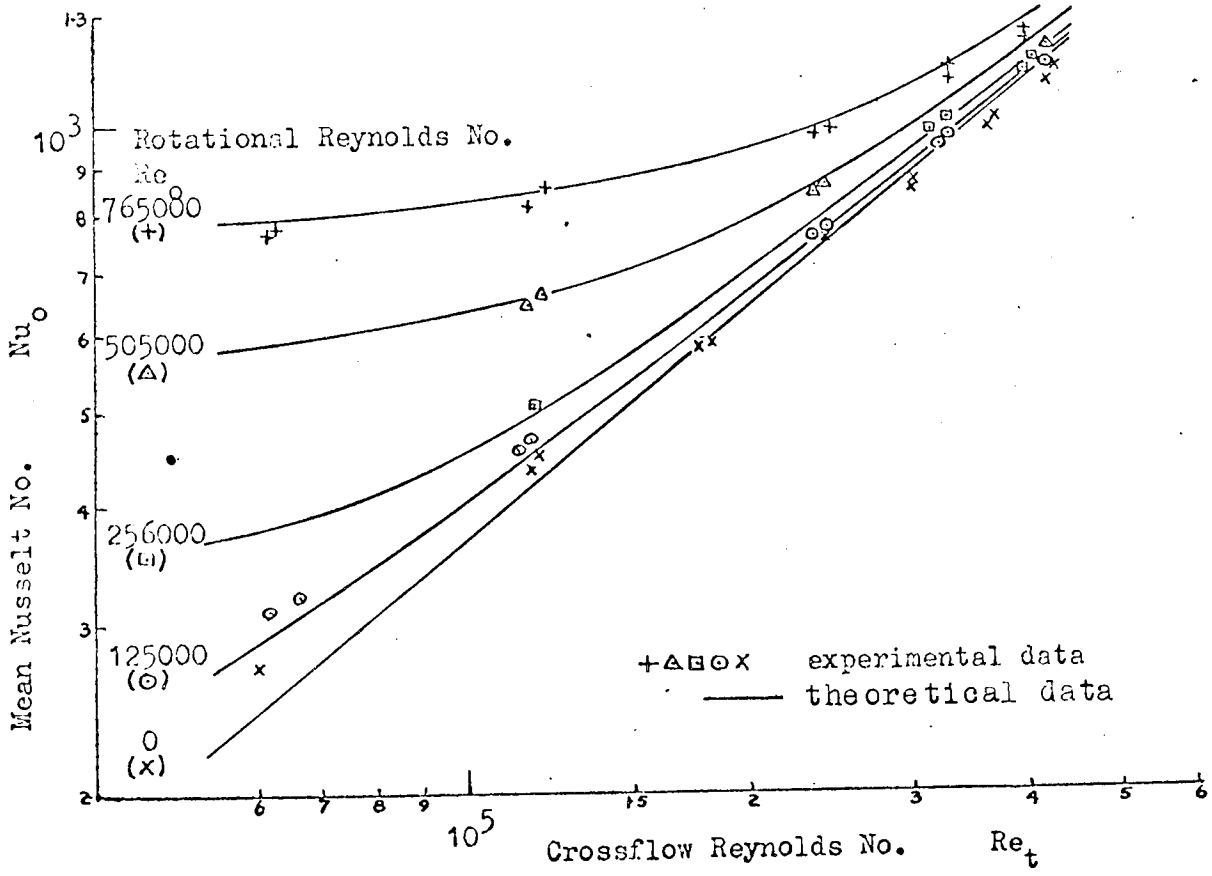

The two systems are superimposed in the manner just explained but the length x is calculated from the main disc edge instead of from the guard rim edge. The results are presented in non-dimensional form in figure 4.28, which will be used as a data sheet for the prediction of disc brake operating temperatures.

SUMMARY

Measurements have been made of the heat transfer from a rotating disc in an air crossflow and a method of analysis has been presented which agrees with these results to within 10%, the mean deviation being 2.3%.

An increase in the heat transfer of 33% above that predicted from stationary surface theories was caused by separation of the boundary layer at the disc leading edge. This increase was assumed to be unchanged for other sizes of disc so that experimental data for a rotating disc in still air and a stationary disc in a crossflow could be used to predict the heat transfer from a brake disc (without a guard rim) for a wide range of rotational and crossflow speeds and a data sheet constructed (see figure 4.28).

The method of prediction may be useful with other superimposed systems which do not lend themselves to a complete theoretical analysis but whose component parts have been thoroughly investigated.

4.4 ROTATING DISC IN AN AIR CROSSFLOW WITH A SECTOR MASKED OFF

When a disc brake is fitted to a vehicle not only is a crossflow of air imposed on it, as studied in Section 3, but a caliper is also on the disc, as described in Section 2. This section studies the combined effects of blanking off sectors of the disc when it rotates in an air crossflow.

FIGURE 4.28

Data Sheet for the Heat Transfer from Brake Discs when Rotating in an Air Crossflow

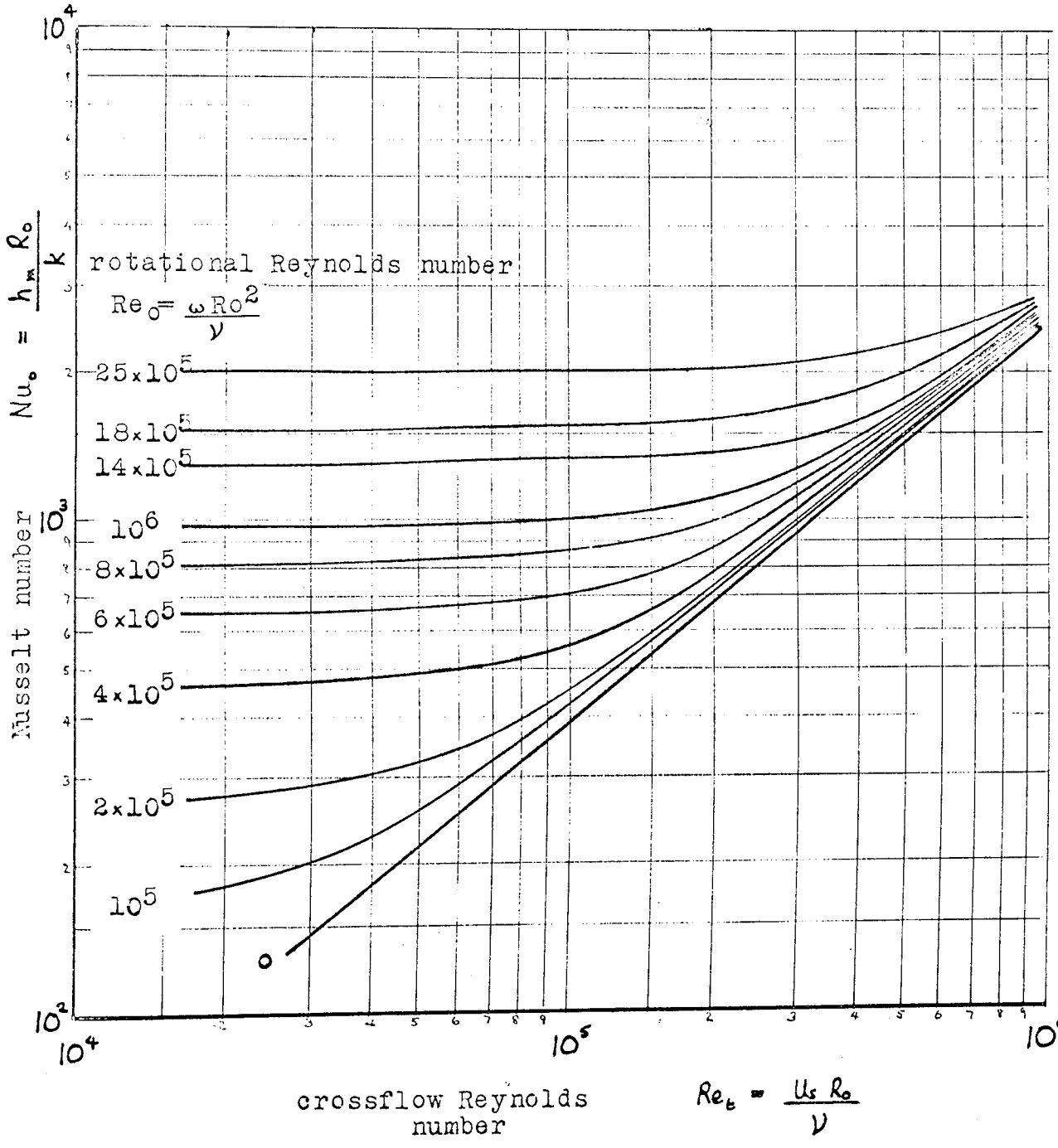

No further preliminary experimental work was needed beyond that already described in previous sections.

HEAT TRANSFER EXPERIMENTS

The effect of sector position relative to the direction of air crossflow on the heat transfer was first investigated by installing the 90° sector in three positions, as shown in figure 4.29. The table of results in figure 4.29 show that the maximum difference was 10% between the leading and trailing positions, which occurred at the highest crossflow velocity. This was reasonable, as the position of the sector would have no effect on the rotational heat transfer, but would affect the crossflow heat transfer. Blanking off the trailing 90° gave the highest heat transfer as the area with the lowest local heat transfer coefficients was covered.

The brake caliper is usually fitted to the trailing sector of the brake disc on a vehicle and so the remainder of the investigations were conducted with the sectors in that position.

Some tests were made with the disc stationary and a crossflow of 15 m/s, equivalent to a crossflow Reynolds number of 180,000. These are presented as a plot of Nusselt number against sector angle in figure 4.30. The heat transfer reduced slowly at first and then more rapidly as the sector angle approached 360°. This was due to two reasons; the sector was fitted in the trailing position and hence first covered the area of lowest local heat transfer coefficients (the heat transfer coefficients are highest at the leading edge of a flat plate in a stream and then reduce with distance from the leading edge) and then, with increase in angle, progressively covered the areas of higher heat transfer. Also , the area at the front edge of the disc has extremely high local coefficients due to the separation of flow there, and this area is the last to be covered. Secondly, the surface thermocouples were placed in

FIGURE 4.29

Table Showing the Effect of Position of the 90° Sector on the Heat Transfer from a Rotating Disc in an Air Crossflow

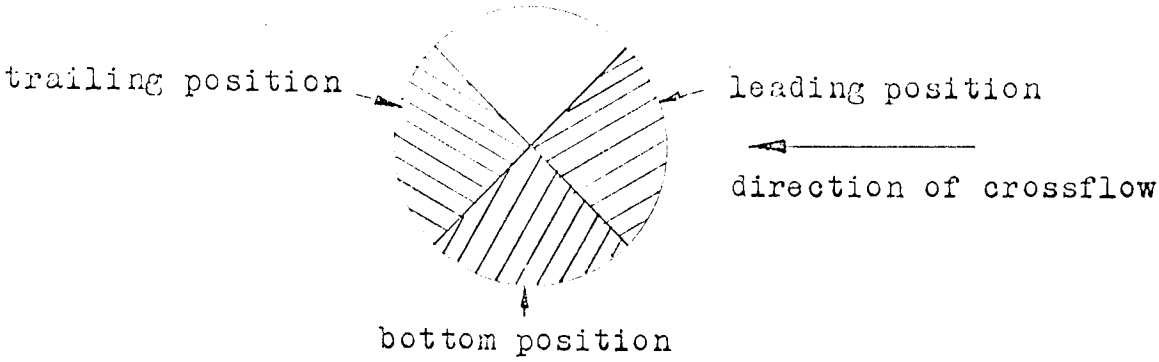

Speeds		Measured Nusselt Number			Variation
rpm	m/s	trailing	bottom	leading	%
1497	10	442	446·5	425·6	4
1494	31·9	826·9	885·5	909·9	10
1498	14·6	544	538·3	543·2	1
192	14·9	460·8	485·2	495·3	7

FIGURE 4.30

Heat Transfer from a Stationary Disc in an Air Crossflow with Sectors of Various Angles Masking the Surface

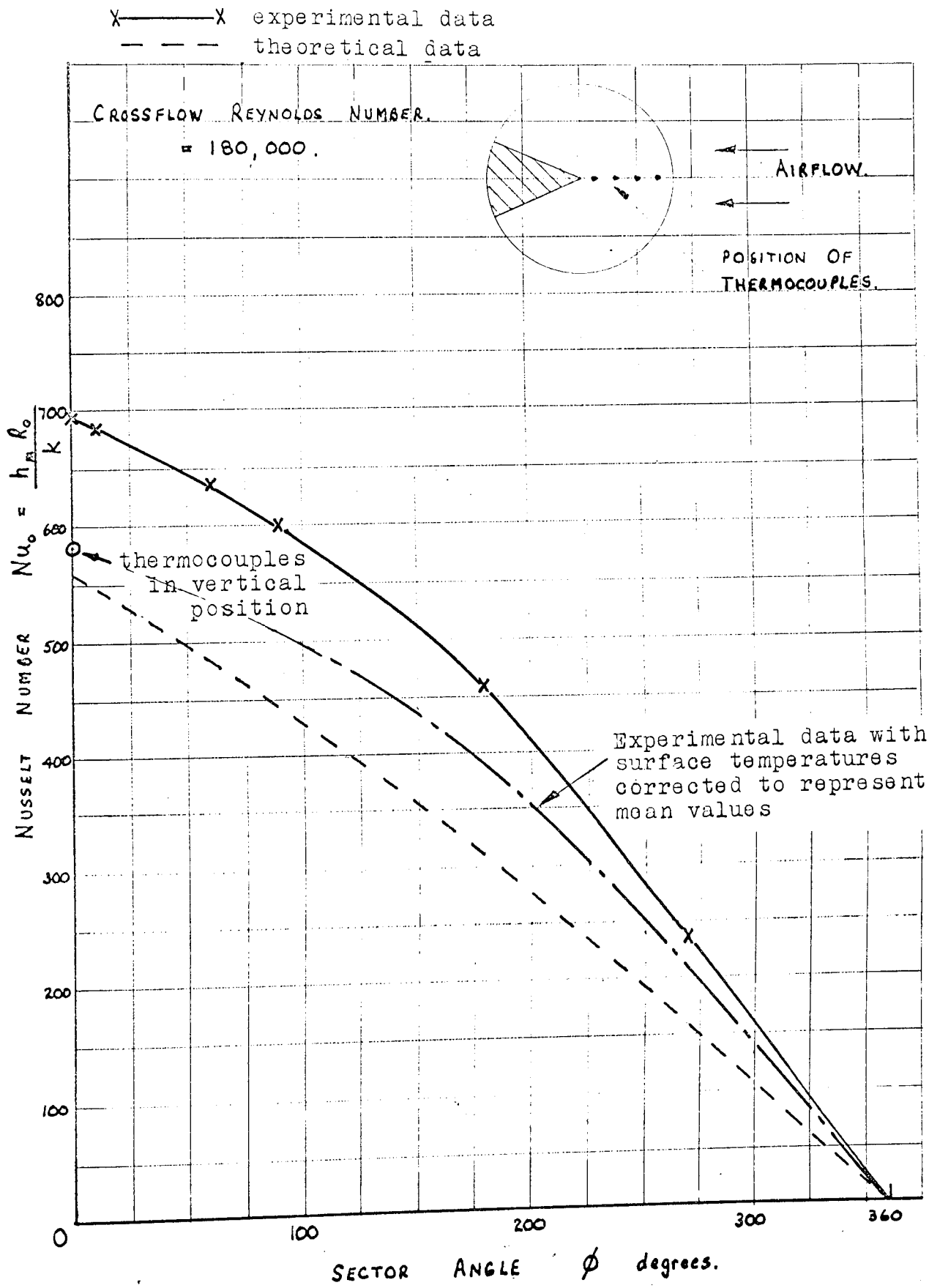

the leading horizontal position, as shown in figure 4.30 and with the surface temperature uniform to only 8% the thermocouples did not indicate accurately the mean surface temperature until the sector angle approached 360°. For small angles they indicated a lower temperature than the true mean, which resulted in the calculation of a higher heat transfer coefficient than actually existed. This is shown up by the position of the no-sector measurement of the mean heat transfer coefficient with the thermocouples vertical, which differed by 15% from the result of horizontal temperature measurements. An approximate correction was applied by reducing the difference directly with angle, which is also shown in figure 4.30.

Further experiments were made at various crossflow and rotational speeds, giving the results plotted in figure 4.31. For these experiments the disc was rotating, so the thermocouples mounted on the surface were subjected to the full range of the local heat transfer coefficients in every revolution. Therefore the temperatures indicated by these thermocouples were mean ones and could be used to make a reliable calculation of the mean heat transfer coefficient, unlike the situation with the disc stationary, where the reliability of the thermocouples to give the mean surface temperature depended both on their position and the ability of the aluminium disc, with its high thermal conductivity, to maintain a uniform surface temperature.

The sector of 0° was the scraper. For each pair of rotational and crossflow speeds there was little difference between the Nusselt number found with no sectors on the disc and that found with the scraper on the disc. This is because the scraper covered a negligible area of the surface and had little effect on the air crossflow as it was mounted parallel to it.

For a data sheet it was desirable to construct a graph to give the effect of caliper angle on the heat transfer at all crossflow and

FIGURE 4.31

Heat Transfer from a Disc Rotating in an Air Crossflow with Sectors of Various Angles Masking the Surface

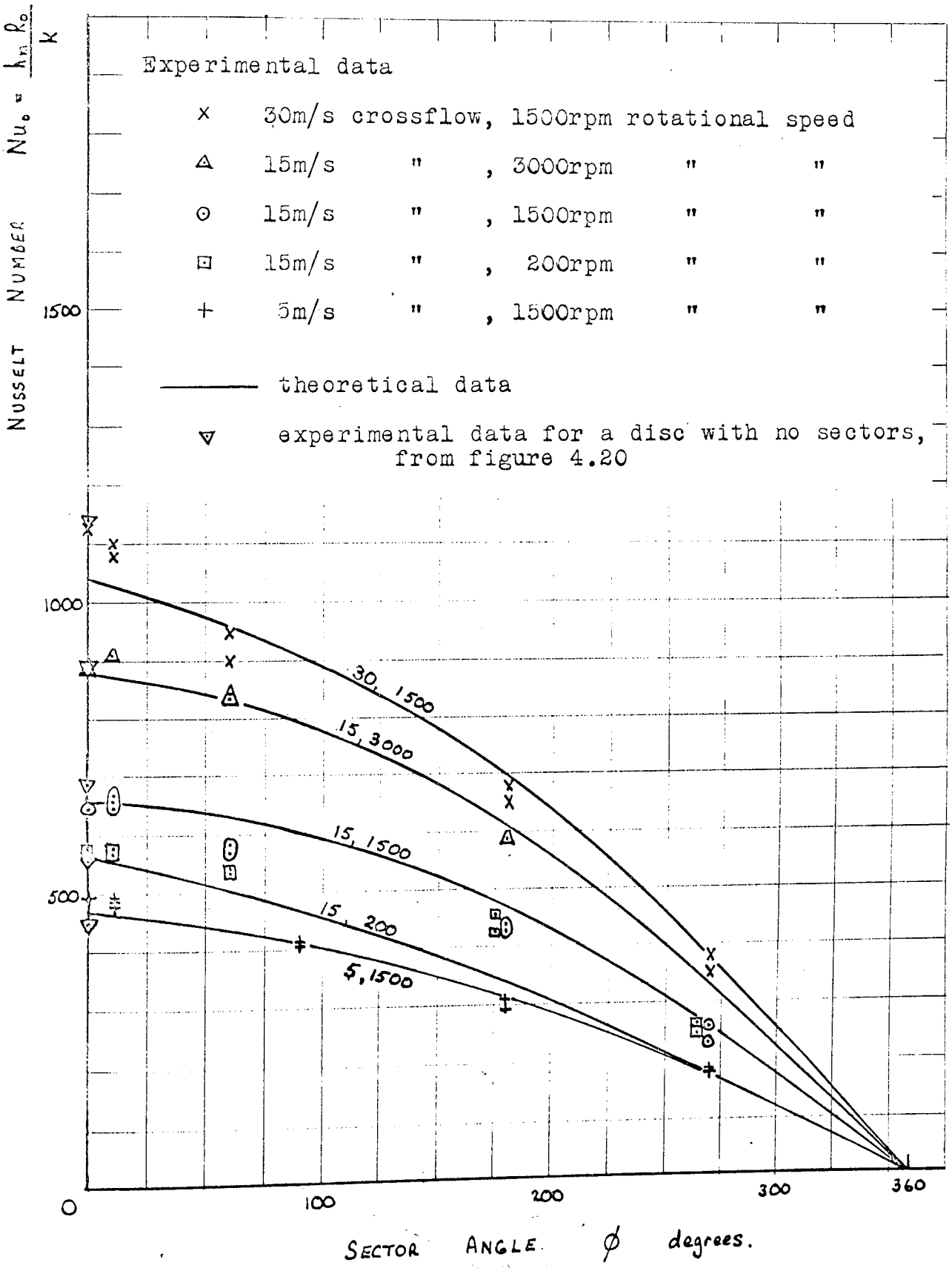

rotational speeds within the range of the tests. The average percentage drop in the heat transfer from that for a free disc was calculated for each of the experiments (values of Nu_o for a free disc taken from figure 4.20) and plotted in figure 4.32. The variation of Nusselt number with rotational and crossflow speeds for a fixed sector angle was never greater than 13%, so that a mean line through these points was accurate to $\pm$6.5%, for the range of crossflow Reynolds number from 60,000 to 420,000 and rotational Reynolds number from 50,000 to 800,000.

This section of work, coupled with the measurements described in Section 2, has given the effect of caliper angle for an adequate range of crossflow and rotational speeds, encompassing all applications of a disc brake on a vehicle or dynamometer.

THEORETICAL ANALYSIS

A theoretical correlation was based on the method of prediction used in Section 3. The local heat transfer coefficients were calculated by vector addition of the two coefficients that would exist at that point if the crossflow and rotational flow existed separately. The resultant local coefficients were then averaged, not over the whole surface as in Section 3, but over the area of disc left uncovered by the sector under consideration. The mean heat transfer coefficient was calculated thus for the value of rotational and crossflow speeds used in the experiments. The theoretical predictions are compared with experimental data in figures 4.30 and 4.31. This method of prediction allowed for the fact that the sector covered areas of low heat transfer for small angles and moved progressively into the areas of higher heat transfer but did not make any allowance for the existence of much higher local heat transfer coefficients just behind the leading edge due to the effects of separation.

FIGURE 4.32

Average Effect of Sector Angle on the Heat Transfer from a Rotating Disc in an Air Crossflow

Re_o = 50,000 to 800,000

Re_t = 125,000 to 765,000

Based on experimental data with the sector in the trailing position

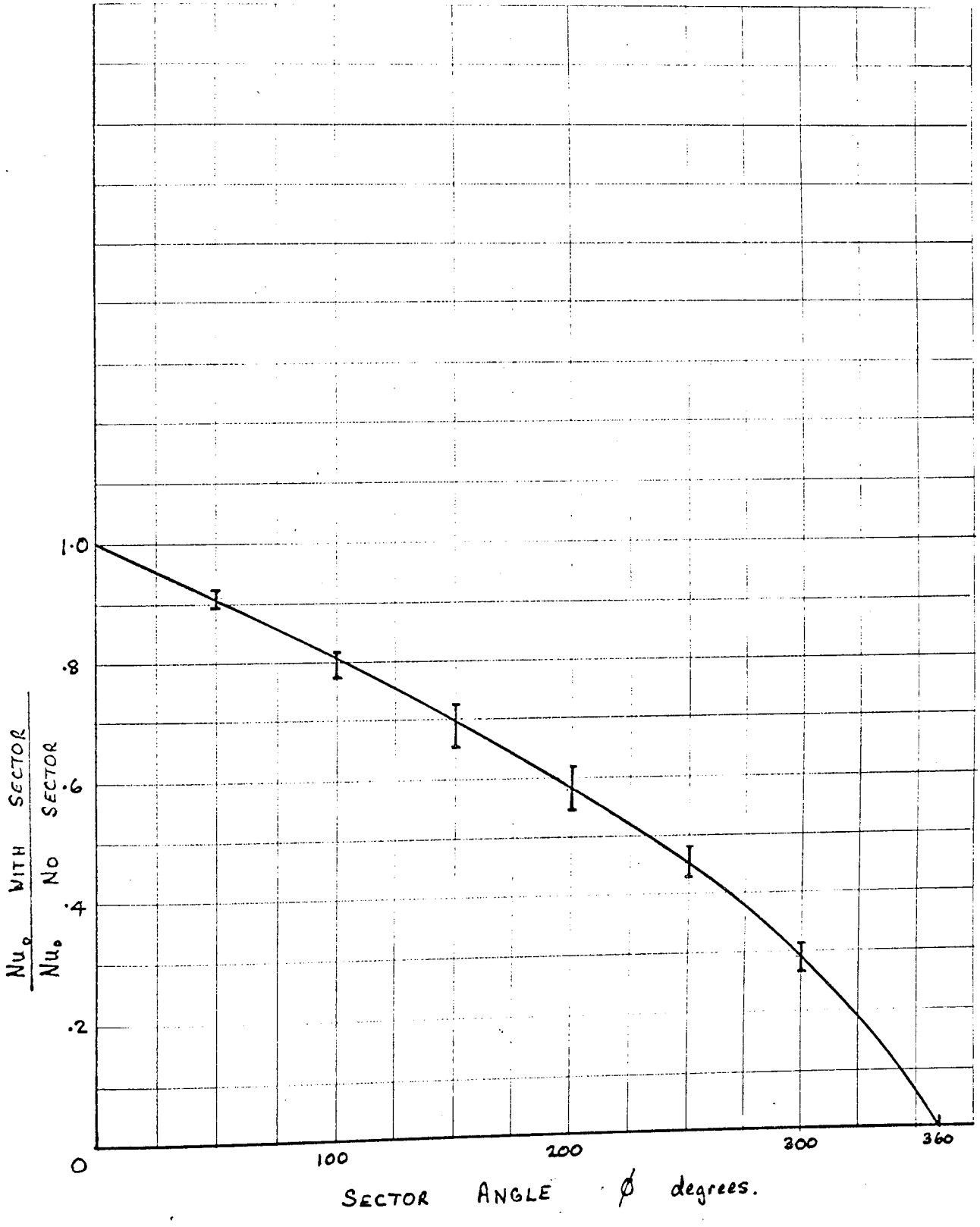

In figure 4.30 the experimental curve, even when corrected for the thermocouples not reading the mean surface temperature, gives results above the theoretical data. This deviation was probably due to separation of the flow at the leading edge, causing a non-uniform surface temperature, which was more marked with the disc stationary than when rotating, and was not allowed for in the analysis.

Correlation between experiment and theory is more successful in figure 4.31, where crossflow and rotation existed simultaneously, except for the result at 15 m/s and 200 r.p.m. It was shown in Section 3 that the effects of separation were more noticeable at low crossflow speeds, indicated by the deviation of the experimental data from variation with $Re_t^{0.8}$ in figure 4.20. This effect of separation at low airspeeds was almost certainly the cause of the discrepancy between experiment and theory at 15 m/s and 200 r.p.m. At the rotational speeds of 1500 and 3000 r.p.m. the effects of separation were negligible compared to the rotational heat transfer and so a much closer agreement was achieved by the theory.

SUMMARY

The effect of sector angle at various crossflow and rotational speeds was investigated. By allowing for the areas of the disc blanked off, the theory presented in Part 3 gave results close to the measured ones, except at low rotational speeds when separation of flow at the leading edge had a considerable effect on the heat transfer.

A curve of the average effect of sector angle on the heat transfer, for the range of rotational Reynolds number of 50,000 to 800,000 and crossflow Reynolds number of 60,000 to 420,000, was prepared from the experimental data, and revealed a maximum scatter of only 13%.

4.5 EXPERIMENTS TO TRIP THE BOUNDARY LAYER ON A DISC ROTATING IN STILL AIR

During the experiments in Section 2, the effect of disturbing the boundary layer with a scraper was found, but the resultant increase in heat transfer was found to be due to swirling of the air upon deflection by the scraper; the flow beyond the scraper was not triggered from laminar to turbulent type. Further tests are described in this section to find the effect of another type of boundary layer disturbing device, the Prandtl trip wire. The phenomenon of artificially tripping a laminar boundary layer, by placing a wire in it, in order to produce transition to turbulent flow at a lower Reynolds number than natural transition, was discovered by Prandtl, and named after him.

Firstly, experiments were made with the wires stationary, mounted on a radius, both close to the surface and at one half the boundary layer thickness away. Then one, two and three wires respectively were attached to the disc surface, on equiangular radii, and rotated with the disc. Finally, a circle of wire was attached to the disc surface. For all these tests both sides of the disc were treated identically in order to ensure an even heat flow to each side.

The results of these experiments are shown in figure 4.33, compared to the heat transfer from a free disc.

STATIONARY WIRES

Experiments were made at rotational Reynolds numbers from 40,000 to 800,000 with a 1.84mm diameter wire situated on a radius and mounted as close as possible to the disc surface. The results showed that the heat transfer increased by approximately 10% in the laminar range, with no increase in the turbulent range. This was the expected effect of disturbing the laminar boundary layer and causing premature transition

FIGURE 4.33

Experiments to Trip the Boundary Layer on a Disc Rotating in Still Air

× 1·84mm dia. wire touching surface
⊛ 1·84mm dia. wire 0·76mm from surface
⊙ 0·64mm dia. 1 wire on surface
⊡ 2 wires on surface
+ 3 wires on surface
▽ circular mounted wire

——— free disc (figure 4.02)
– – – line for all turb. flow $Nu_o = 0{\cdot}015\ Re_o^{0{\cdot}8}$

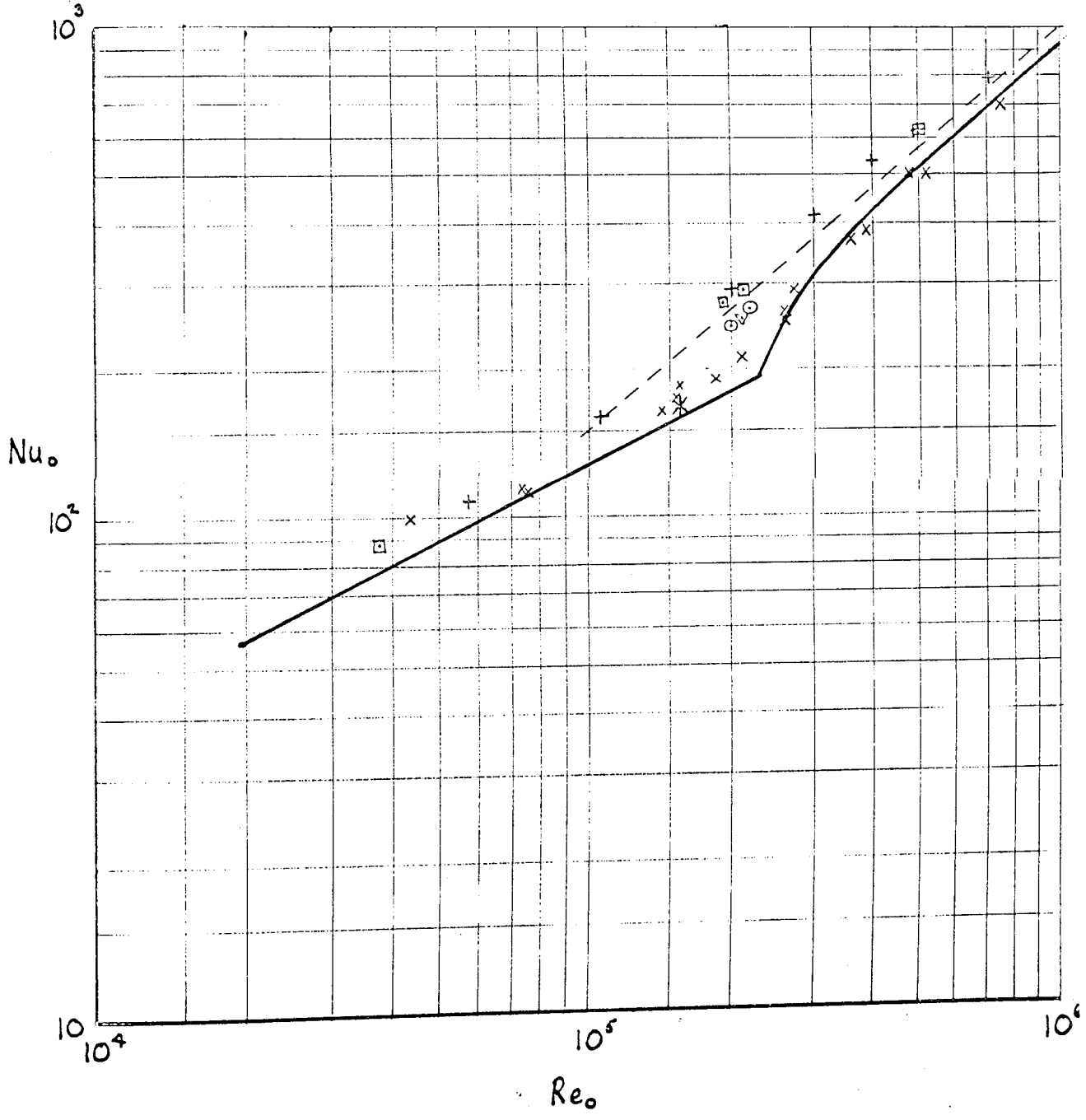

to turbulent flow. However, the wire would not disturb the flow on the whole surface as the flow on the disc follows an equiangular spiral path; the diagram below indicates the approximate area that would be affected.

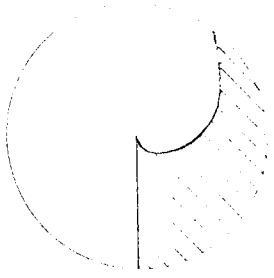

As the angle of the spiral (angle of yaw) varied according to the axial distance from the disc surface in the boundary layer it is not possible to predict the increase in the heat transfer as there is no way of calculating the area affected by turbulent flow.

One test was made with the trip wire at 0.76mm distance from the disc surface, or approximately one half boundary layer thickness at the test conditions. This increased the heat transfer by 5% only, emphasising that it is the flow close to the disc surface which predominantly affects the heat transfer.

WIRES FIXED TO THE DISC SURFACE

Experiments were made with one, two and three wires of 0.64mm diameter, sellotaped in turn to the disc surface on equispaced radii. The results are again shown in figure 4.33. The tests with one wire showed a large increase in the heat transfer, but this was not a realistic result for the mean heat transfer as the surface thermocouples were positioned just behind the wire, in the disturbed region, and hence they were reading local temperatures which were lower than the average surface temperature.

The tests with one and two wires were conducted mostly at a rotational Reynolds number of 2×10^5, which is just prior to the point of natural onset of transition. Tests were made at this point as any

premature change to turbulent flow would give the greatest change in the heat transfer because the laminar and turbulent lines of heat transfer were furthest apart there.

As the number of wires was increased to two and then three the temperature measurement came nearer the average one. Both a stationary wire and one fixed to the disc should have the same effect on the heat transfer as they both disturbed the flow over an equal surface area. This can be checked from the tests with three wires on the disc surface. At a Reynolds number of 2×10^5

$$3 \times (Nu_{(\text{stationary wire})} - Nu_{(\text{free})}) + Nu_{(\text{free})}$$

$$= 3\,(210-176) + 176$$

$$= 278$$

whereas the measured value of Nu for three rotating wires was 290 giving a discrepancy of only 5%.

It is interesting to note that the heat transfer with three wires is higher than the line for all the disc under turbulent flow, whereas if it were only triggering turbulent flow it could not go above this line. This was probably caused by separation of flow behind the wires, which has previously been found to drastically increase the local rate of heat transfer.

As the flow follows a spiral path across the surface a wire fixed to the surface in a circle should disturb the flow over the whole disc area beyond the circle. An experiment was made with wire fixed to the surface on a circle of radius 70mm, which should result in 11% of the disc having laminar flow and the remainder turbulent. The measured Nusselt number, when compared to that for a free disc and to the value of the Nusselt number if all the disc were under turbulent flow, indicated that 25% of the disc was under laminar flow. There exists an axial inflow of air to the whole of the disc surface and it is

possible that this damps the turbulent disturbance and eventually causes the boundary layer to revert to laminar form. This would explain why the measured laminar area was higher than expected.

SUMMARY

Prandtl trip wires were found to increase the heat transfer due to their effect of triggering the flow from laminar to turbulent.

The unusual spiral path of the flow over a disc means that radially mounted trip wires only affect a part of the flow, but a wire mounted in a circle produced turbulent flow over a larger area of the disc. There is an indication that the flow reverts to a laminar type some distance after being artificially triggered to turbulent flow due to the axial inflow of air stabilizing the boundary layer.

For disc brake applications it would only be possible to use the stationary wires as the disc surfaces must be flat to contact the friction pads. The small increase in heat transfer would be unlikely to merit their use as it would make negligible difference to disc temperatures.

4.6 ROTATING DISC IN STILL AIR WITH FORCED CONVECTION FROM AN AIR JET

A disc brake on a vehicle is often shrouded by the surrounding body and wheel parts or by a dirt shield, preventing the majority of the air crossflow induced by the vehicle motion from reaching it. The resultant mean heat transfer coefficient is low compared to that with the disc in a full crossflow, and in order to prevent overheating of the disc it may need to be cooled by other methods.

A possible method would be to provide a forced convection airflow across the disc surface from a nozzle with high pressure air supplied

by a pump on the engine of the vehicle. For power and weight reasons it would be desirable to derive the optimum combination of maximum increase in heat transfer for a minimum mass flow of air. The air flow would have maximum effect if it were directed onto the disc surface, so as to combine with the rotational flow boundary layer, much as the air crossflow did in Part 3.

The work described in this section was to investigate the effect of nozzle exit width, angle of jet to the disc, distance from the disc, and air jet speed, on the heat transfer. General trends were evaluated to allow further and more detailed investigation of this method of cooling should it be shown to provide a useful increase in the heat transfer for an economical supply of air.

EQUIPMENT

Figure 4.34 shows diagrams of the nozzles, supply circuit and their positioning relative to the disc and figure 4.35 gives a photograph of the nozzle.

The nozzles were mounted one on each side on a radius of the disc so that the whole of the disc continually passed under them, and to fit there, they were made the same width as the main disc radius. The nozzles were designed to give as near uniform airspeed across the exit as possible, and subsequent measurements gave the velocity profiles shown in figure 4.36, which were adequately straight.

The exit width of the nozzles could be varied from zero to 1.5mm by means of two adjusting screws, and they were set by inserting the appropriate feeler gauge into the slot.

The air velocity was measured with a small pitot tube held in the mouth of the nozzle, and connected to a water manometer. The static pressure was assumed to be ambient, due to the difficulty of measuring it in such a narrow stream of air.

FIGURE 4.34

Diagrams of Nozzle, Air Supply Circuit and Nozzle Positioning

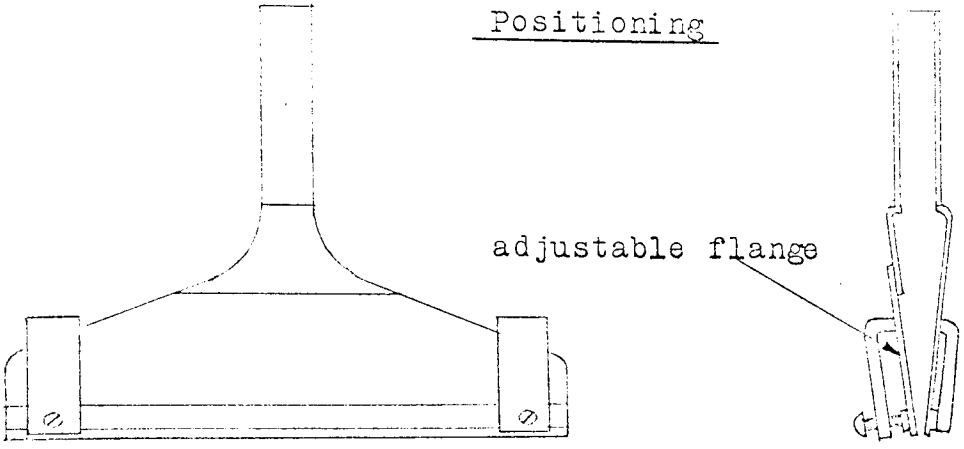

Scale drawing of Nozzle, 0·4xfull size

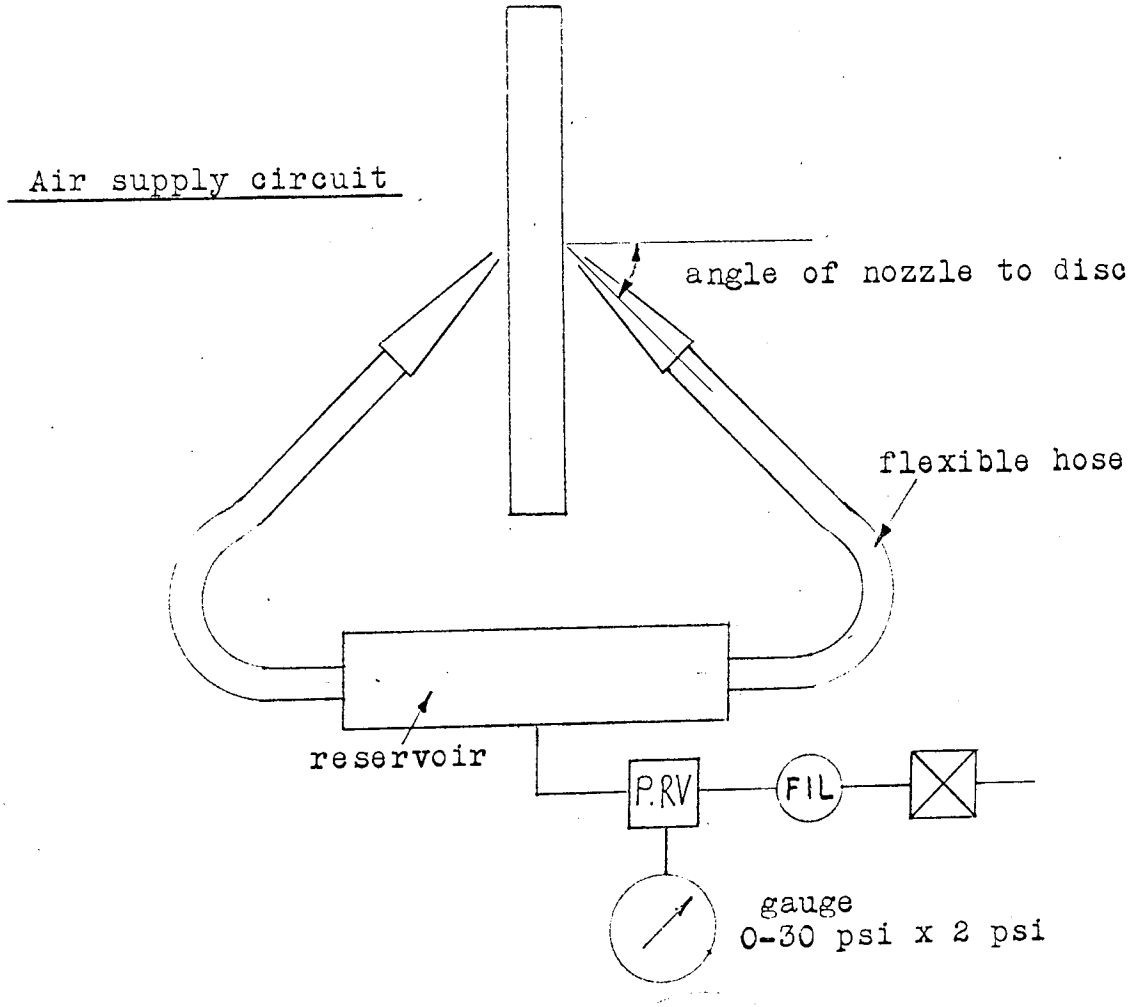

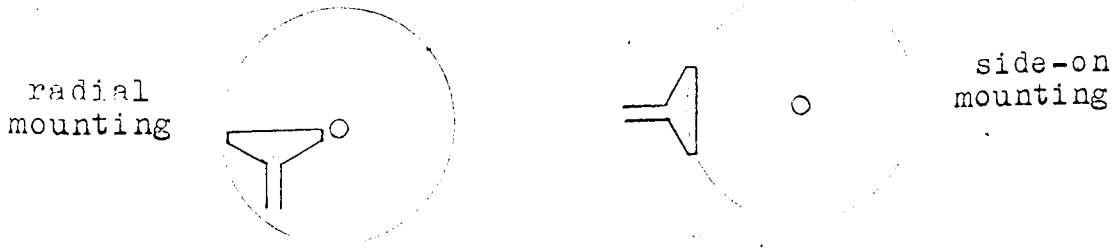

Nozzle positioning on Disc

FIGURE 4.35

NOZZLE IN RADIALLY MOUNTED POSITION ON DISC

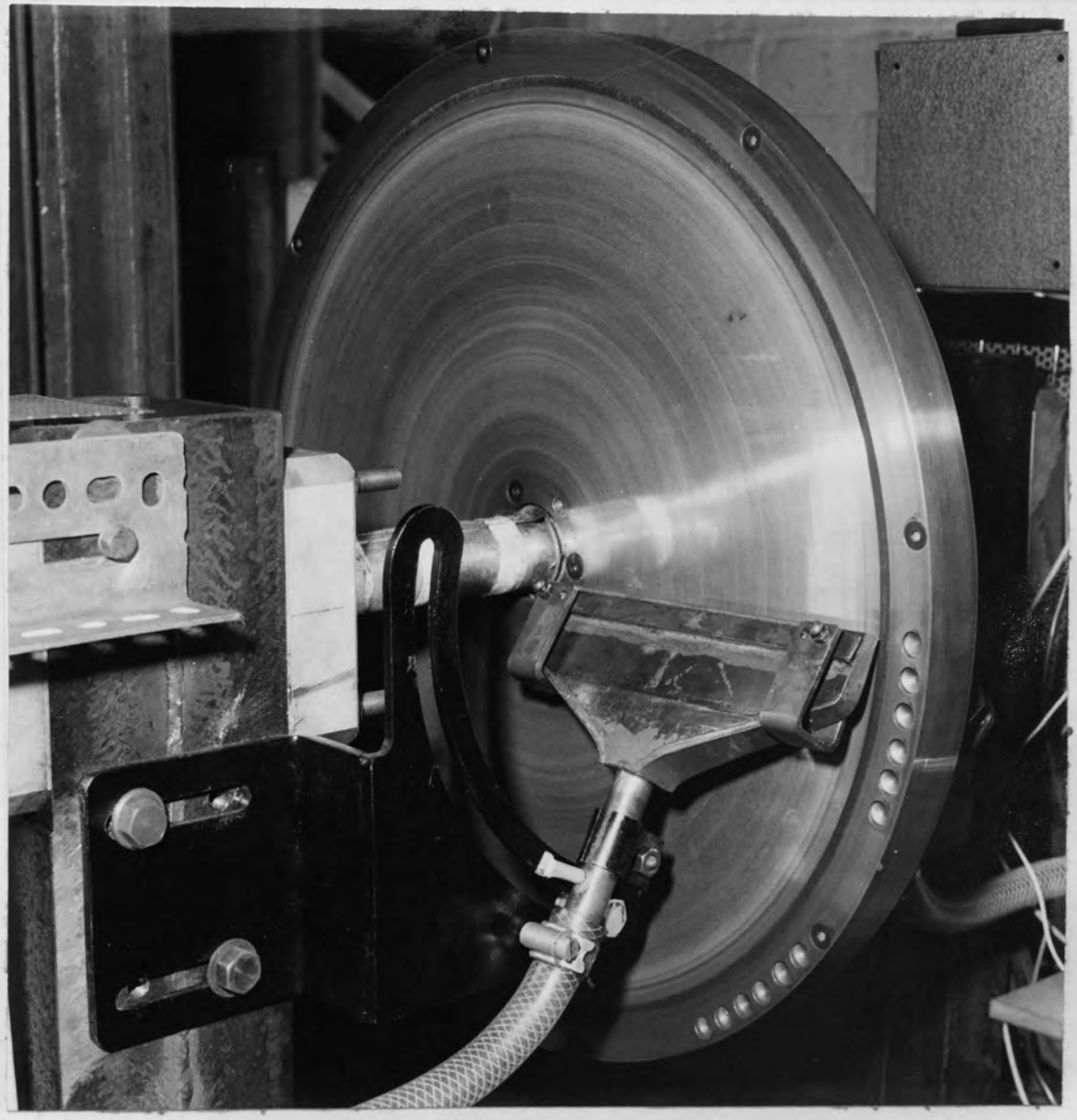

FIGURE 4.36

Velocity Profile across Nozzle Exit

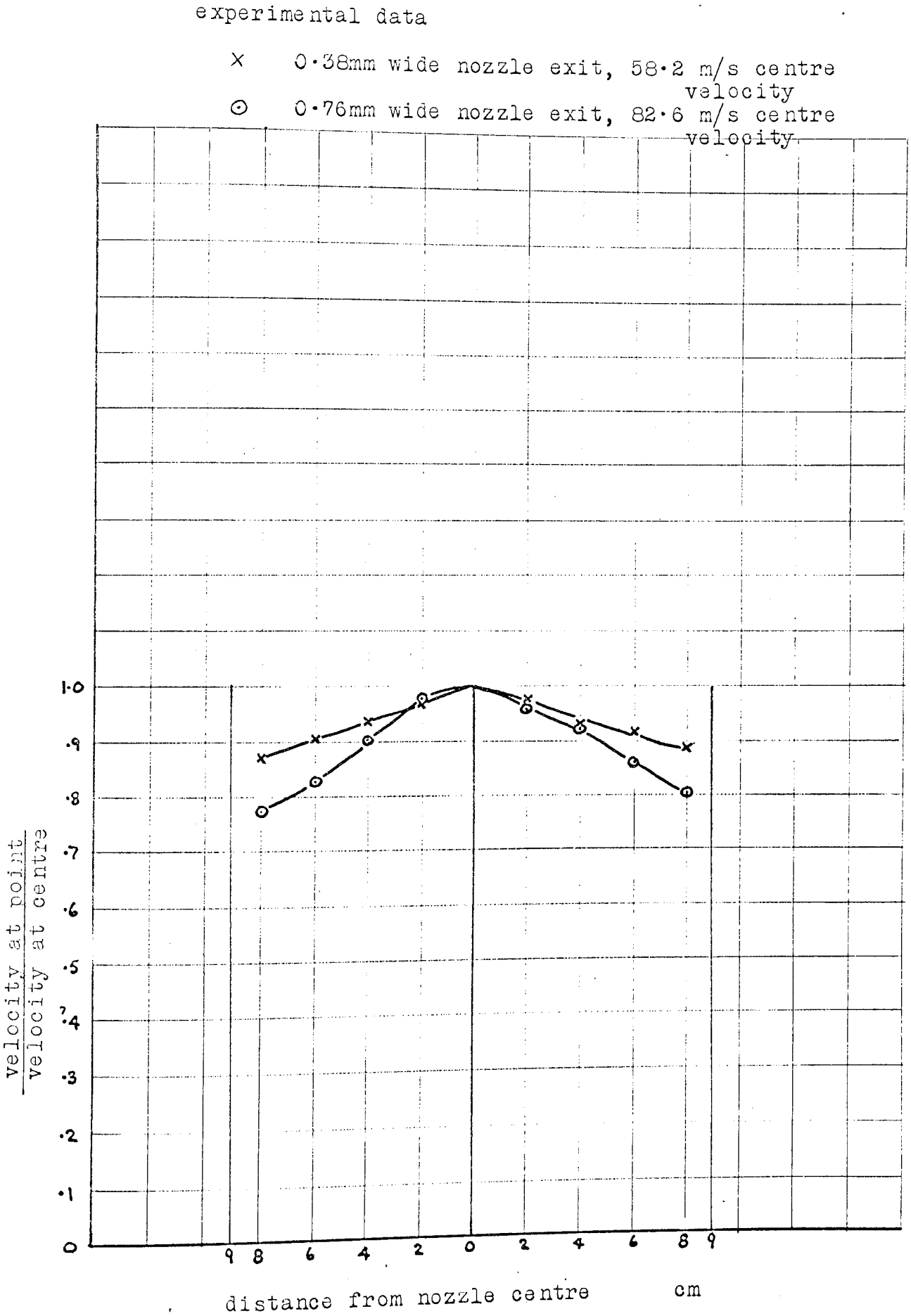

During tests the air velocity was measured indirectly by reading a static pressure gauge placed in the supply line immediately after the pressure control valve. For each nozzle opening the gauge was calibrated against the exit velocity, giving the calibration curves shown in figure 4.37.

HEAT TRANSFER EXPERIMENTS

Figure 4.38 shows the effect of the angle of inclination of the nozzle to the disc surface. The 90° position occurred when the nozzle was normal to the surface. The tests were conducted with the nozzle exit at 0.38mm and at three different airspeeds. In each case the optimum angle was between 70° and 90°, blowing against the direction of rotation. When the airjet blew in this direction it supplemented the rotationally induced airflow (which travels relative to the surface in the opposite direction to the rotation), hence tending to increase the heat transfer. However, the area affected by the flow from the air jet had a greater effect on the heat transfer than the direction of flow and flow visualization showed (figure 4.39) that at the 90° position the air jet split into two parts on hitting the disc, one half flowing each way over the disc. As the angle of inclination was reduced so the jet tended to flow in one direction only over the disc, halving the affected surface area. For these reasons the optimum angle was only slightly away from the 90° position to the side with the air jet blowing against rotation. On a vehicle installation the ideal mounting position of the air jet would be normal to the disc, as the same effect would result with the disc rotating in either direction, and as this position was only marginally below the optimum one it was used for the remaining tests.

The effect of distance from the nozzle exit to the disc was investigated with the nozzles set to 0.76mm with 37.5 m/s airspeed.

FIGURE 4.37

Calibration of Exit Velocity from Nozzles to Line Gauge Pressure

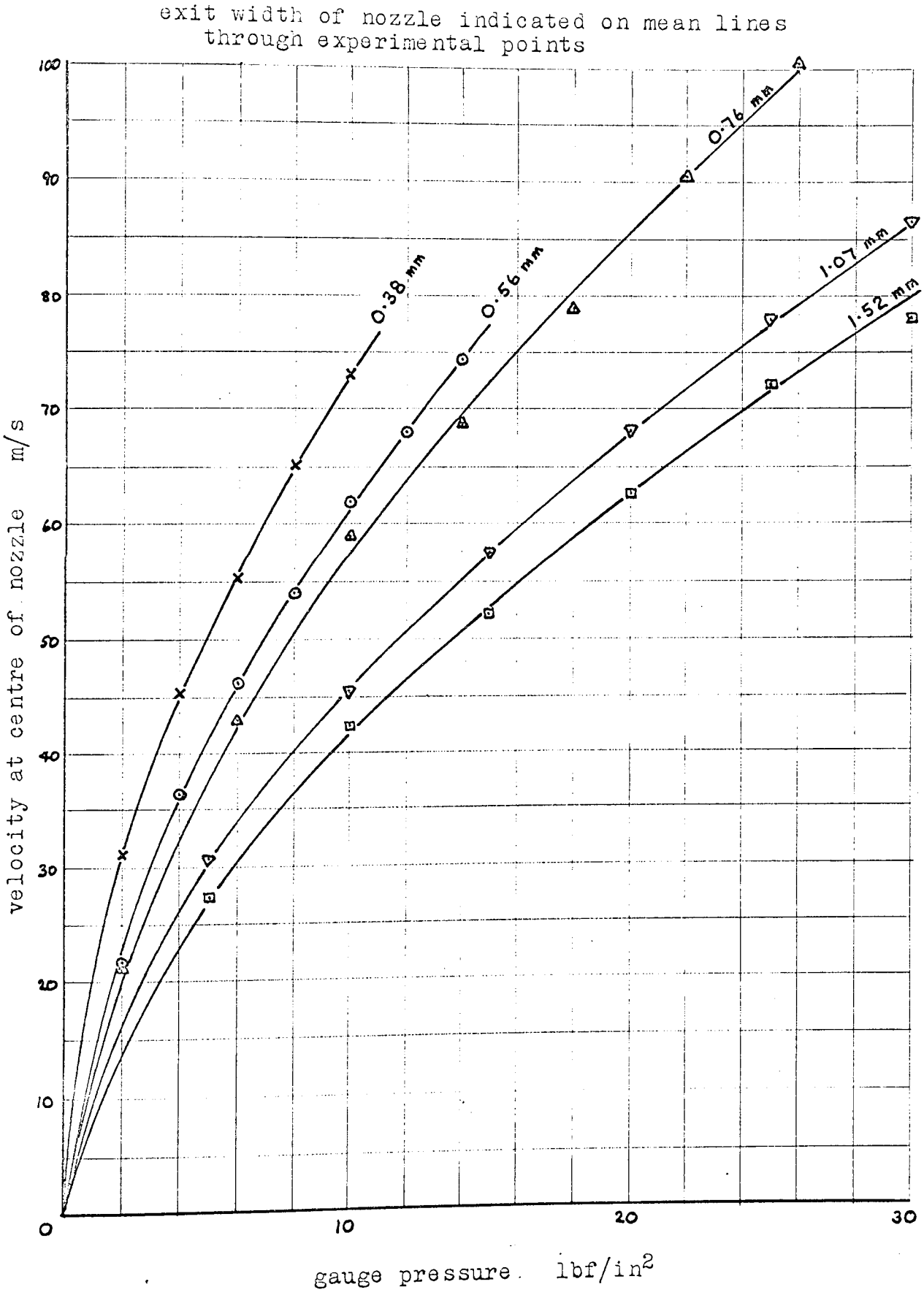

FIGURE 4.38

Effect of the Angle between Nozzle and Disc on the Heat Transfer, Nozzle mounted in Radial Position

experimental data

0·38mm wide nozzle exit, 12·7mm from nozzle exit to disc

$Re_o = 200,000$

air velocity at centre of nozzle

⊙ 35 m/s

× 38 m/s

\+ 51 m/s

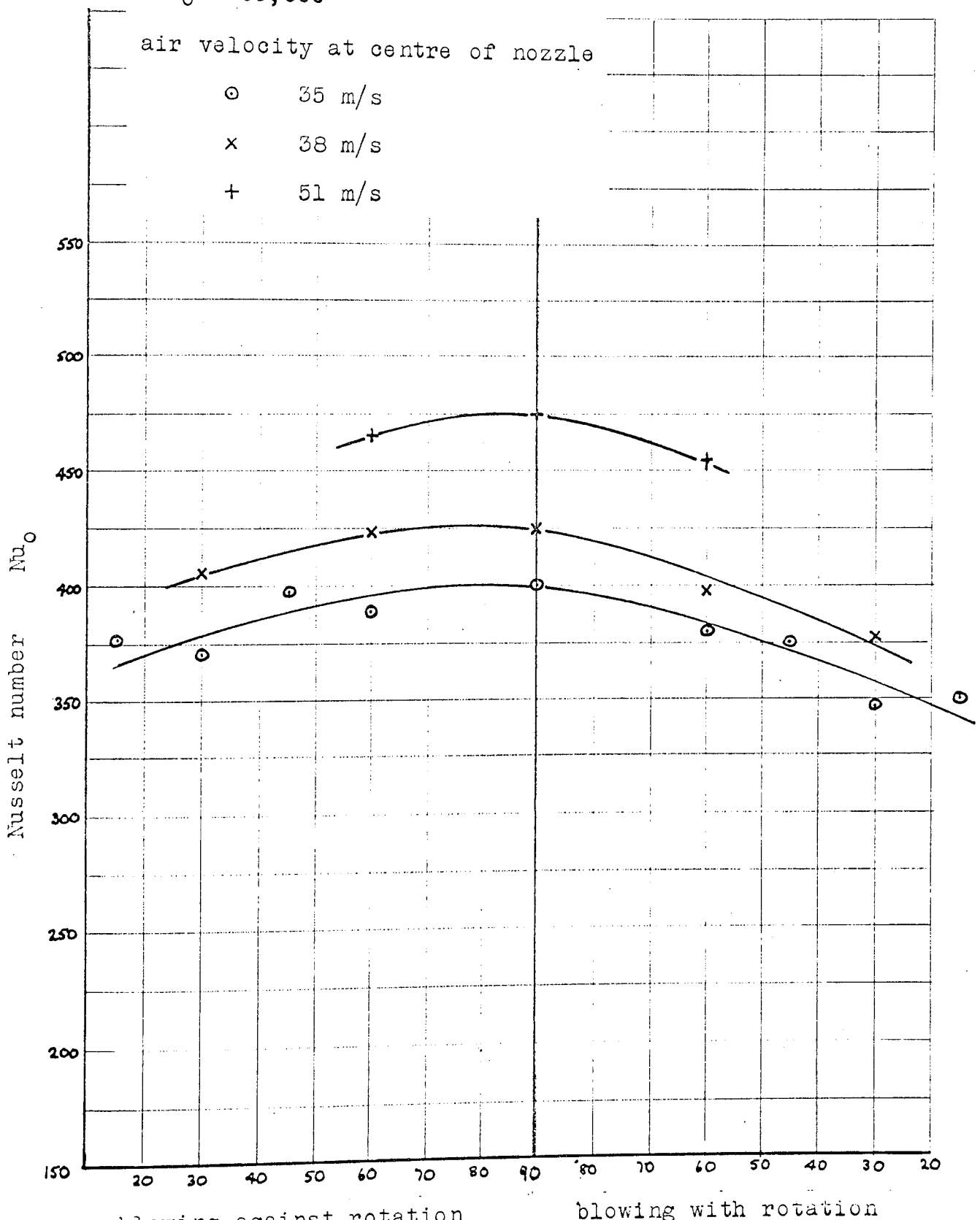

FIGURE 4.39

Visualization of Flow with Nozzle mounted Radial to Rotating Disc

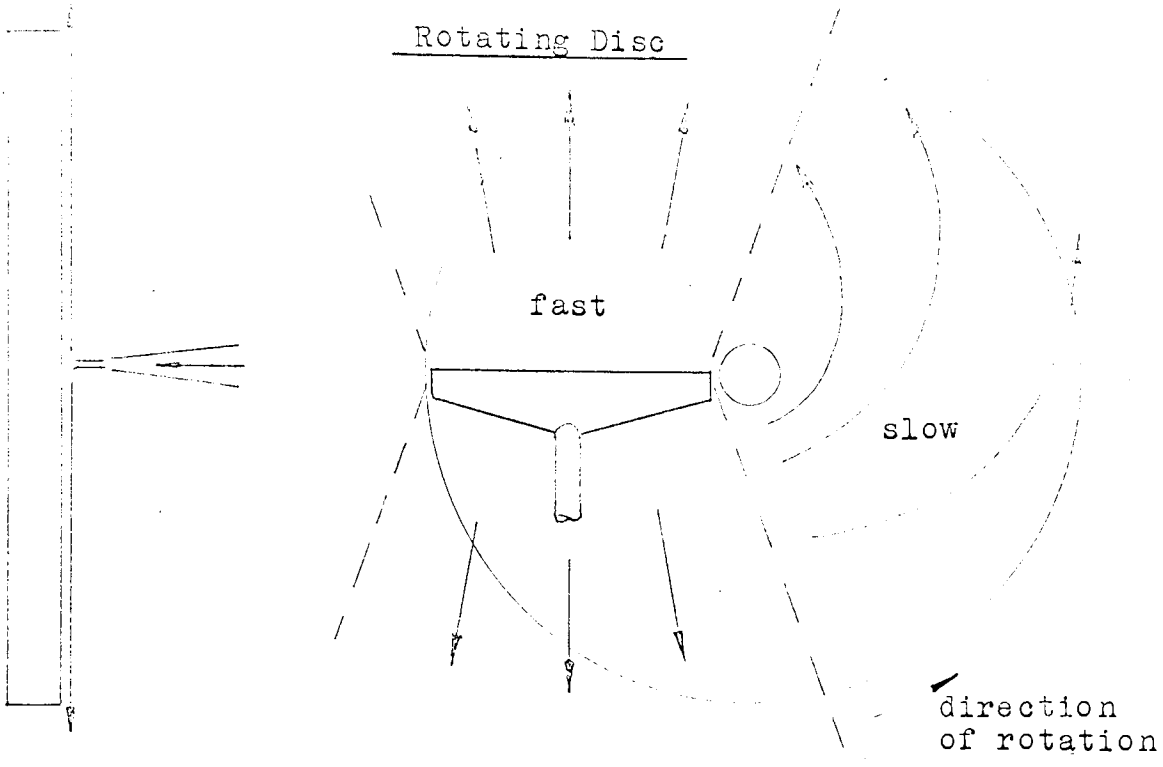

high nozzle jet velocity, low rotational speed

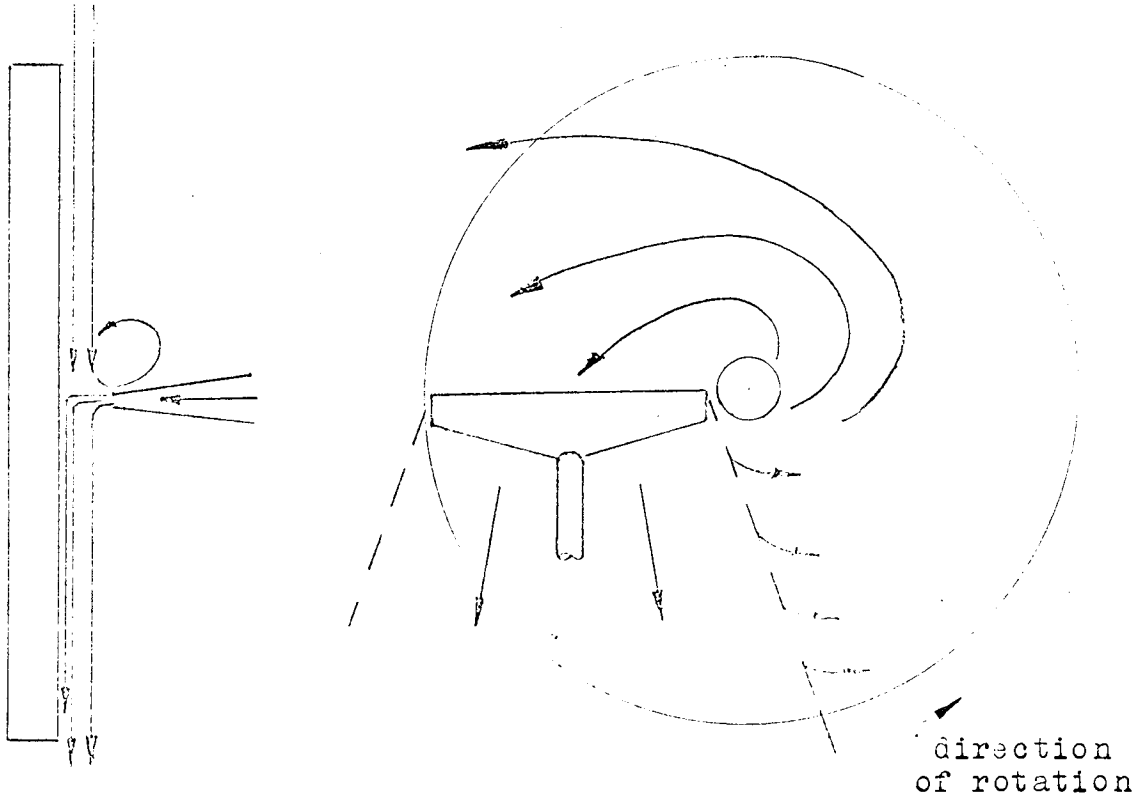

low nozzle jet velocity, high rotational speed

Figure 4.40 shows that considerable scatter was obtained with these tests, such that a line could not be drawn through the experimental data with any confidence. However, the general trend indicated that the heat transfer increased as the distance was reduced, but the effect up to a distance of 60mm was very gradual. Obviously, when a distance is reached such that the air jet has considerably slowed before hitting the disc then the heat transfer would be considerably reduced, but this position appears to be well outside the range of distances tested.

Figure 4.41 shows that the air jet velocity affects the heat transfer in the usual forced convection manner. At low airspeeds the relationship between the Nusselt number and the velocity is the laminar one - plate length and viscosity are nearly constant so the jet velocity would vary with the jet Reynolds number

$$Nu_o = K_1(V)^{0.5}$$

and at higher velocities it changes to the turbulent relationship

$$Nu_o = K_2(V)^{0.8}$$

With the nozzle in the radial position the heat transfer did not vary greatly with change in exit width; from 0.38mm to 1.52mm there was an increase of only 30% in the Nusselt number. Some change was expected as the velocity of a thicker air jet would not decay as fast as that for a thin one due to its higher momentum.

Experiments were made with the nozzle mounted sideways-on to the edge of the disc as shown in figure 4.34. This increased the area of the disc covered by the airstream and hence the Nusselt number was expected to be higher than that with the jet in the radial position but figure 4.41 shows that it had the opposite effect, the heat transfer was lower than that found with the same nozzle in the radial position. The probable explanation was that the radial air jet combined more effectively with the rotational flow than the side-on jet, hence giving a higher resultant velocity across the disc and a higher heat transfer.

FIGURE 4.40

Effect of Distance from Nozzle Exit to Disc Surface on the Heat Transfer

× experimental data

0·76mm nozzle exit velocity, 37·5m/s jet velocity
nozzle mounted at 90° to disc surface, Re_o = 200,000

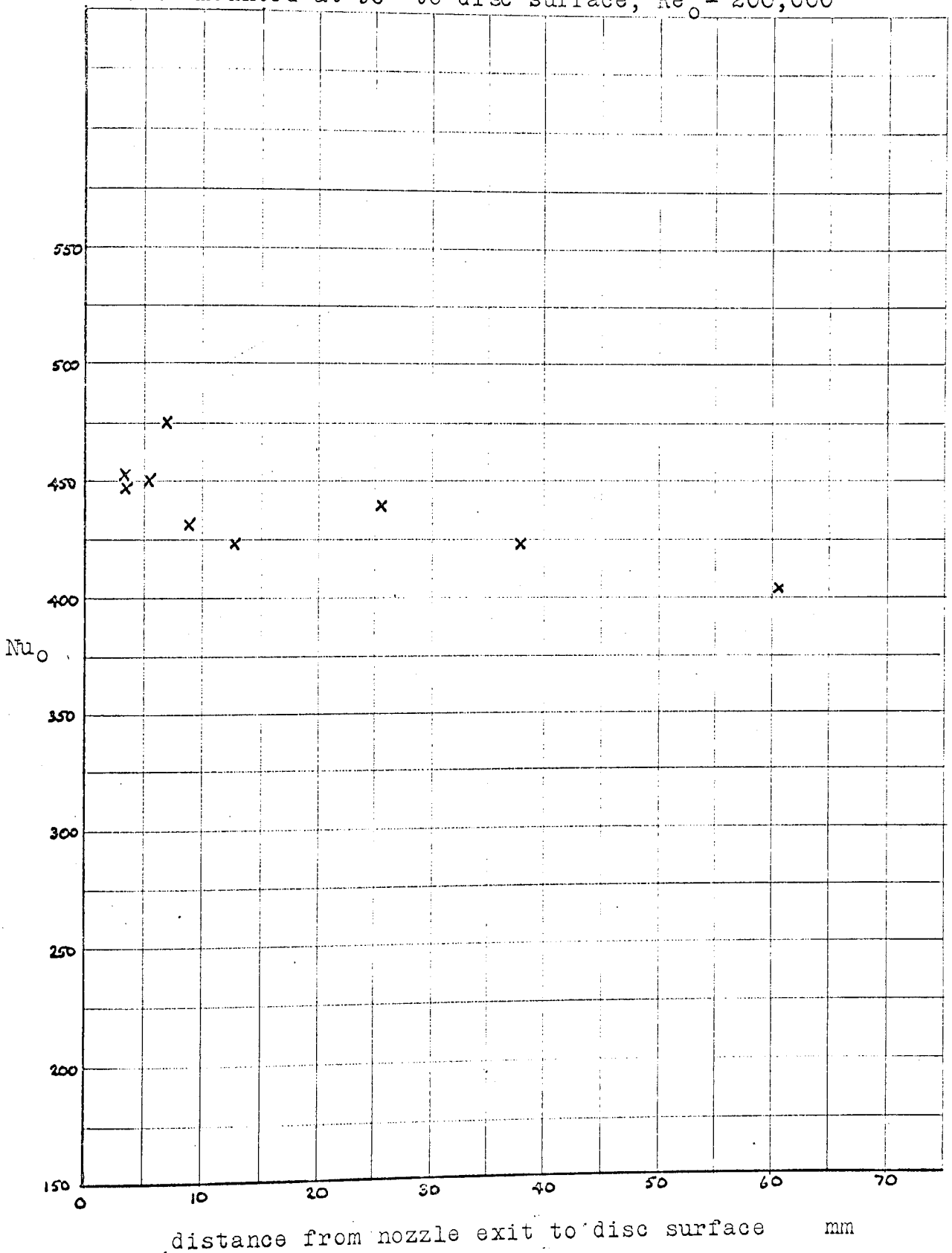

FIGURE 4.41

Effect of Air Velocity from Nozzle Exit on the Heat Transfer, at a Rotational Reynolds number of 200,000

experimental data

+	0·76mm wide exit,	nozzle	mounted	side-on	to	disc		
×	0·38mm wide exit,	nozzle	mounted	radial	to	disc		
⊙	0·56mm	"	"	,	"	"	"	"	"
△	0·76mm	"	"	,	"	"	"	"	"
▽	1·07mm	"	"	,	"	"	"	"	"
⊡	1·52mm	"	"	,	"	"	"	"	"

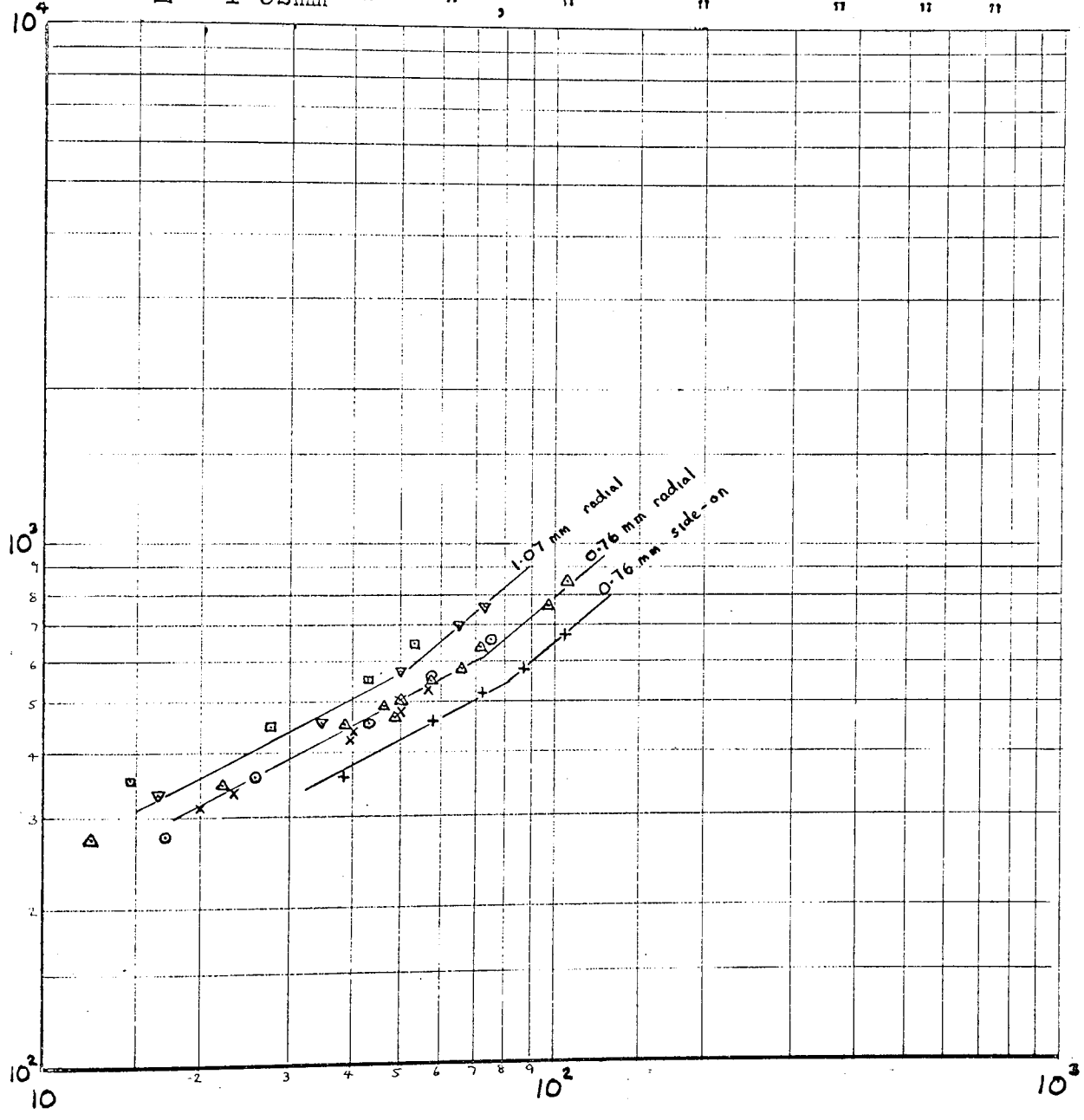

Nu_o

velocity of air jet m/s

Figure 4.42 is a plot of the Nusselt number against the volume airflow, showing that the smallest opening of the nozzle is the most effective in increasing the heat transfer, in terms of the mass of air needed. This is most important, as on a vehicle the air must be supplied from a pump driven by the engine and the size of this pump is strictly limited. From figure 4.02 at Re_o = 200000, for a disc in still air, the Nusselt number was 175. A reasonable sized pump for fitting to a commercial vehicle delivers 0.025 kg/s of air or 1.3 m^3/min at atmospheric pressure. The nozzles used in this experiment are approximately twice as wide as those needed on a vehicle, due to the smaller disc rotor width, and there are four brakes per vehicle, so the equivalent air supply to one brake on figure 4.42 is 0.66 m^3/ min. This gives a Nusselt number of 350 for the 0.38mm nozzle, double that for the disc rotating in still air.

Results were taken with varying rotational Reynolds numbers for fixed nozzle velocities to give the results plotted in figure 4.43. This shows the same trend as found with the air crossflow in Part 3. At low rotational Reynolds numbers the nozzle air jet tends to dominate the heat transfer, whilst at higher values of rotational Reynolds numbers the rotational flow has a greater influence.

Finally, figure 4.44 shows the effect of angle for the side-on positioned nozzle, showing that the smaller the angle of inclination, the higher was the heat transfer. This is because the nozzle was aimed at the edge of the disc and any air spilt behind the disc had no effect on the heat transfer as it did not contact the disc surface. The higher the angle of inclination, the more air was lost off the edge of the disc and so less air was left to travel across the disc surface.

FIGURE 4.42

Effect of Volume Airflow from the Nozzle on the Heat Transfer

rotational Reynolds number $Re_o = 200,000$

experimental data

+ 0·76mm wide exit, nozzle mounted side-on to disc
× 0·38mm wide exit, nozzle mounted radial to disc
⊙ 0·56mm " " " " " " "
△ 0·76mm " " " " " " "
▽ 1·07mm " " " " " " "
⊡ 1·52mm " " " " " " "

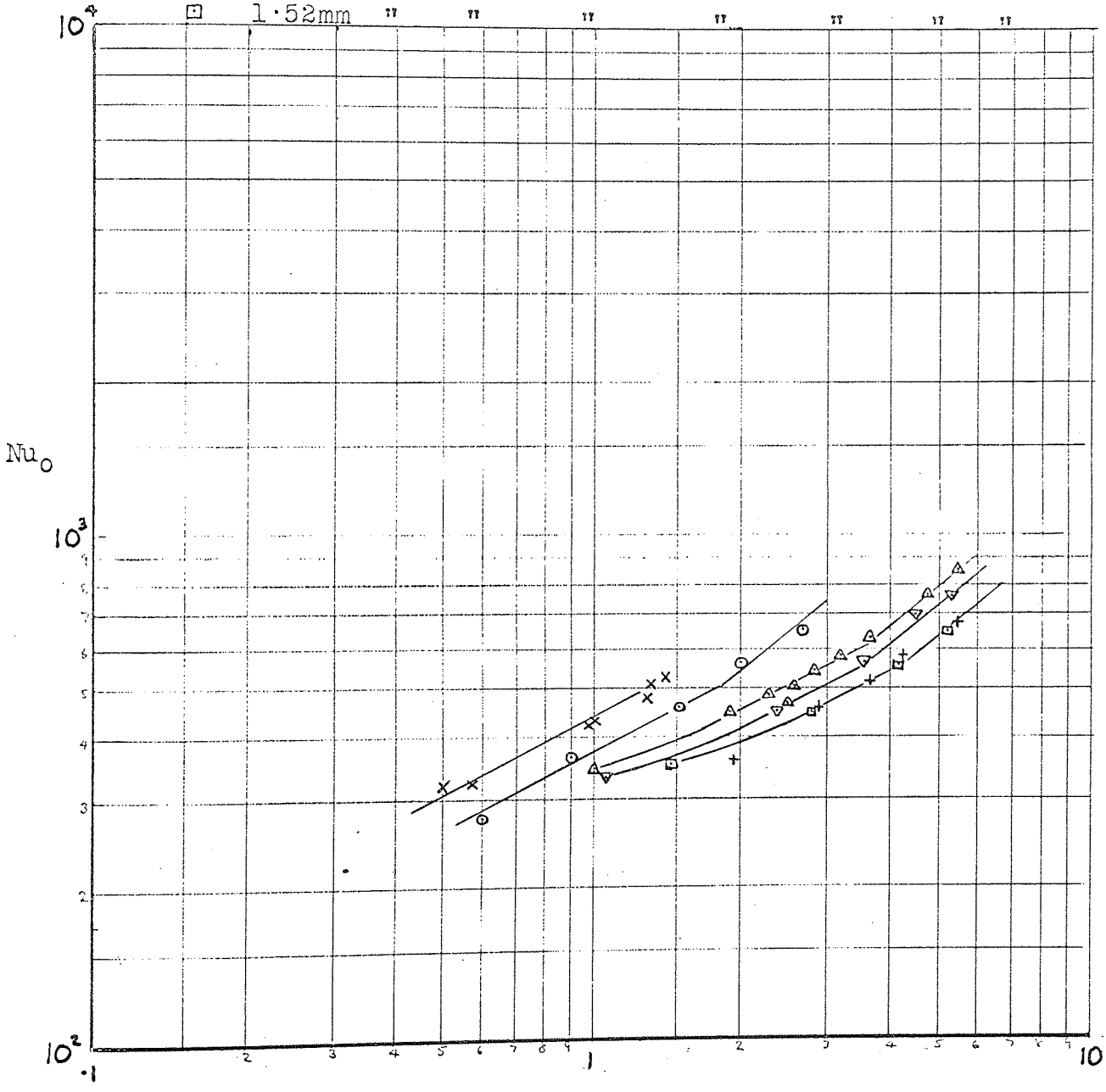

volume airflow m^3/min

FIGURE 4.43

Plot of Nusselt number against Rotational Reynolds number for Various Air Jet Velocities from Nozzle

nozzle mounted radial to disc, at 90° to surface and exit at 1·27 cm from it

experimental data
—×— 0·38mm exit width, 40m/s jet velocity
—⊙— 0·38mm " " , 60m/s " "
—+— 0·76mm " " , 71m/s " "
—△— 0·76mm " " ,109m/s " "
——— disc with no nozzle cooling (figure 4.02)

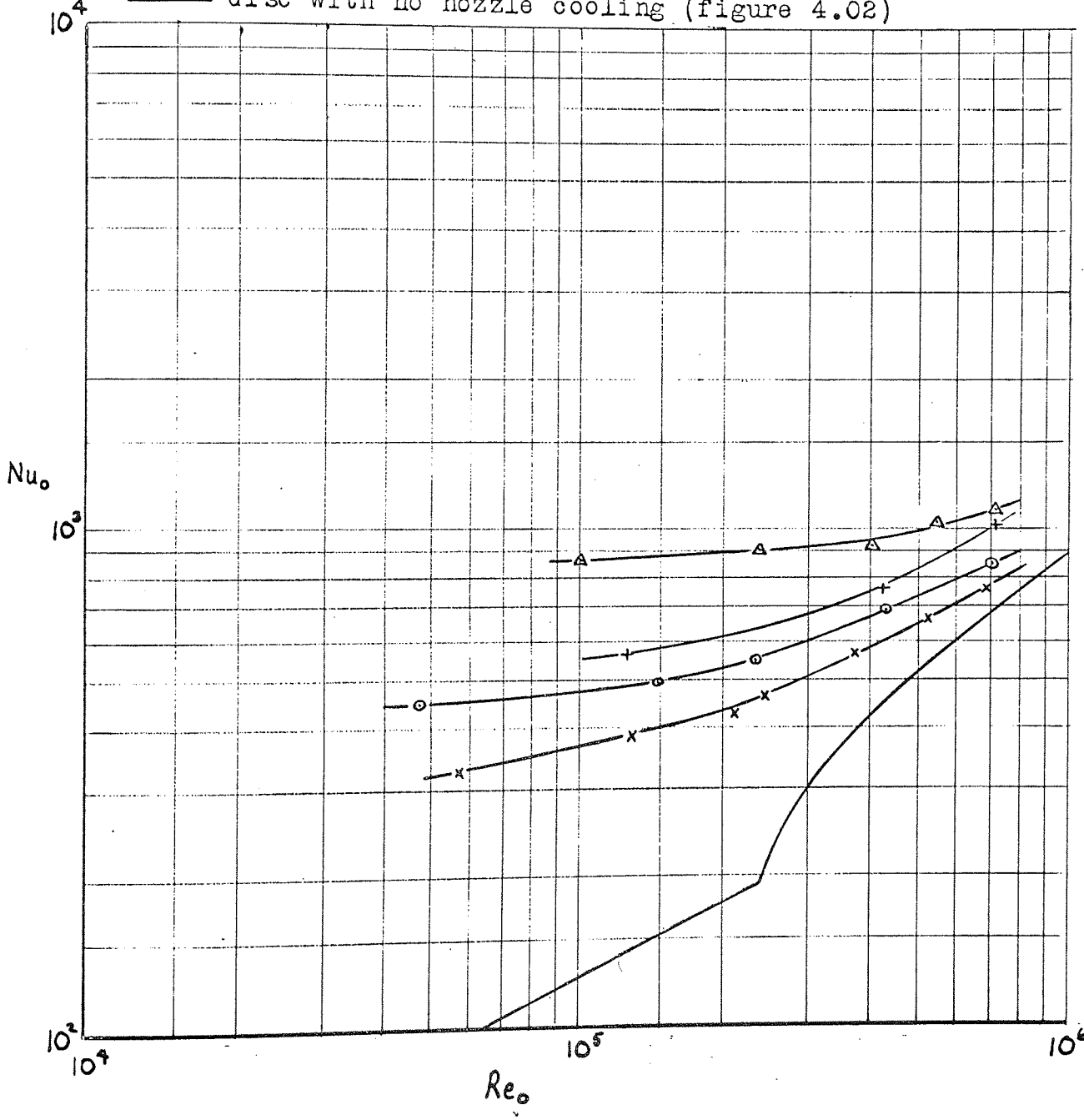

FIGURE 4.44

Effect of Angle of Inclination of Nozzle to Disc when Mounted in Side-on Position at $Re_o = 200,000$

0·76mm exit width, nozzle 1·27 cm from disc surface

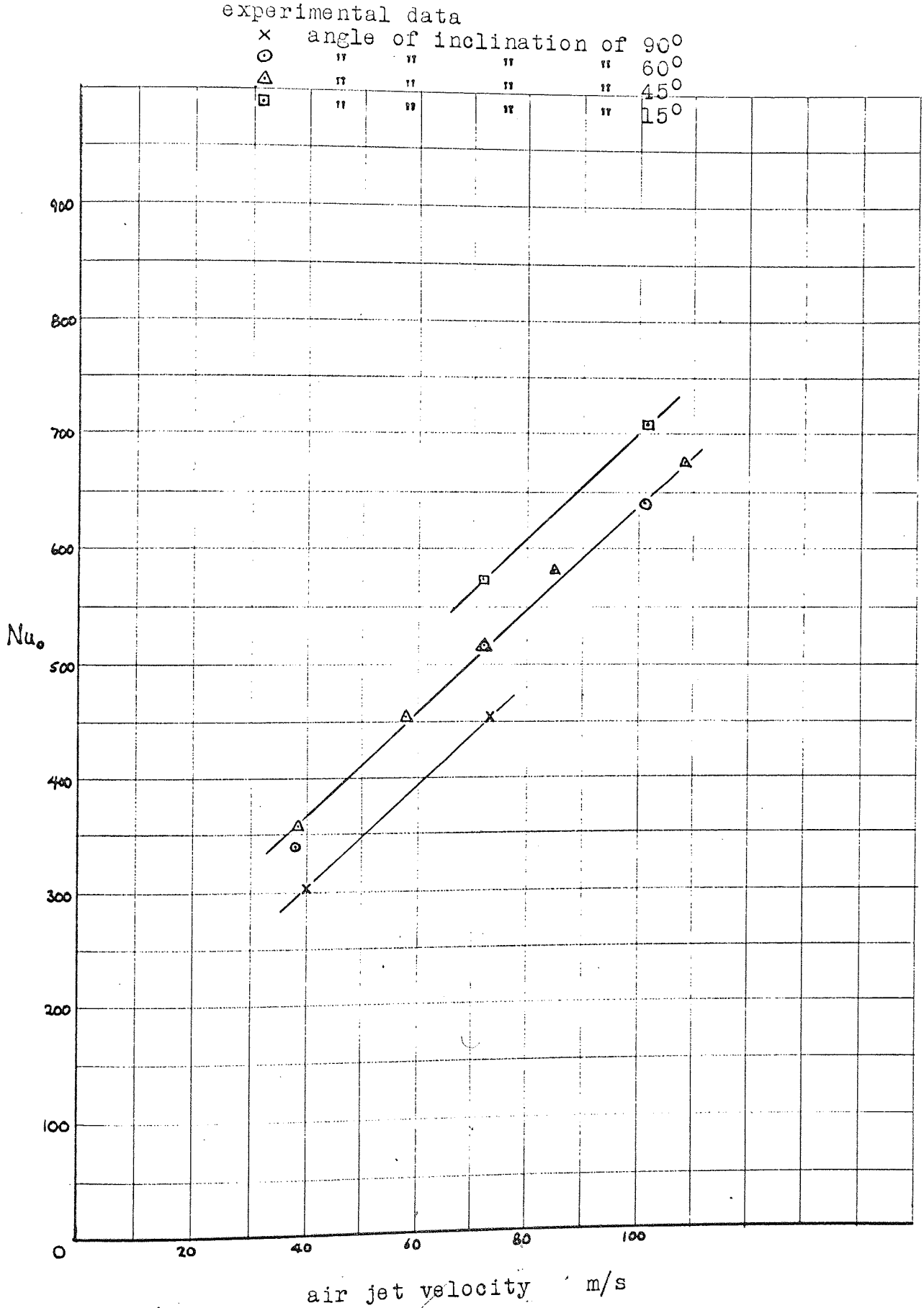

The maximum increase in the heat transfer for minimum mass flow of air was achieved with the smallest nozzle exit width, with the nozzle mounted at 90^{o} to the disc surface. For a mass flow of air of 0.025 kg/s to two brakes the Nusselt number would be double that for a disc in still air at a rotational Reynolds number of 200000. The distance between nozzle and disc had little effect up to a distance of 60mm.

A variety of graphs indicating the effects of air jet velocity, rotational speed, nozzle angle and distance from the disc were constructed from the experimental data. These would enable a number of alternatives in the arrangement of air jet cooling nozzles to be examined.

4.7 COMPARISON OF RESULTS

At the beginning of the chapter it was explained how the conditions of duty of a disc brake were to be simulated for the experiments. This involved dividing the environmental conditions into component parts and imposing each one in turn onto a disc so as to isolate their effects on the heat transfer and obtain a fuller understanding of them than could be obtained if they were applied together. It now remains to compare the data from these tests to assess the influence that each condition exerts upon the heat transfer.

Air crossflow (due to vehicle motion) was found to have the most marked effect on the heat transfer; figure 4.28 shows thatfor a typical vehicle installation, at 65 km/h (40 mph) with a 0.4 m (15.5 in) diameter disc and 0.5 m (20 in) rolling radius, giving $Re_{it} = 87000$ and $Re_{o} = 225000$, $Nu_{o} = 440$. From figure 4.02 the same disc rotating with no crossflow gave $Nu_{o} = 190$, so an increase of 130% was found in the convective heat transfer.

Slightly different effects were found with a sector of the disc masked off (simulation of a caliper) depending on whether the disc was immersed in a crossflow or not. Without a crossflow the heat transfer was improved from that of a free disc at low caliper angles, but this effect was considerably diminished with the addition of the more effective crossflow. Masking a sector of the disc did not reduce the heat transfer as much as might have been expected from the convective area covered, due to the resultant disturbance of the flow and variation of the local heat transfer coefficients across the surface. Hence, for a caliper of 40^{o} subtended angle, covering 11% of the disc area, the heat transfer was altered to between 89% and 106% of that for a free disc, depending on the environment.

Boundary layer trip wires had a small effect on the heat transfer coefficient as they only changed the flow from laminar to turbulent over a small area of the surface. Due to the direction followed by the rotational airflow, a considerable number of wires would be needed to promote turbulent flow over the whole surface.

A considerable increase in the heat transfer from a disc rotating in still air was obtained by directing a jet of air at the disc, but in reality the amount of air available would depend on the size of pump that could be economically fitted to a vehicle. This improvement may be useful as the airflow induced by vehicle movement in some installations can be completely excluded by the surrounding body parts and/or a dirt shield, so some form of additional cooling may be necessary in these cases, and in installations on slow moving vehicles.

Chapter 5

APPLICATION OF RESULTS

5.1 INTRODUCTION

The experimental and theoretical data described in Chapter four provided the information which was needed to make an analysis of the temperature of discs during a braking operation, as well as giving an understanding and allowing comparison of the effects of the environment on the heat transfer from a disc. The results may also be useful in other applications involving rotating machinery, such as motors or turbines.

In this chapter an approximate analysis is presented which predicts disc brake operating temperatures both during a braking period and after it. A considerable amount of work has been done by Newcomb {67} to predict the temperatures of disc brakes installed on a vehicle or dynamometer but he assumes that the disc only acts as a heat sink during the braking period, and cools when the brakes are released. This relies upon the usual small braking period relative to overall running time and hence is of sufficient accuracy for medium and heavy duty stops, above 0.1g, but introduces a significant error for low duty stops or constant speed drag braking.

General computer programmes for use on an Elliot 903 have been produced to make the calculations for the prediction and comparisons are made with experimental results.

5.2 PREDICTION OF DISC BRAKE TEMPERATURES

Heat is supplied to a disc by friction between the brake pads and disc surface and is then dissipated from it by conduction, convection and radiation. During long stops or constant speed braking the cooling of a disc has a considerable effect on the disc temperature, but for short stops it has no effect as all the heat is absorbed by the inherent heat sink of the disc. The heat loss by conduction and radiation can be calculated with existing data, and the present work has given the data necessary for the calculation of the heat transfer by convection.

For any thermal system a heat balance can be constructed which may be independent of time, a steady state heat balance, or may vary with time, a transient heat balance. However, if an allowance is made in a steady state heat balance for the heat absorbed by a heat sink then it may be applied to each increment of time in a transient system. Only when the time increment is given a finite size does the equation become inaccurate as it must then use mean values of the variables. The resulting series of approximate equations are ideally suited to solution on a computer by an iterative procedure.

The thermal system of a disc brake is rarely allowed to reach steady state as the heat input is constantly changing, and so the method described above is used to solve the transient heat balance for the disc temperatures. This is equivalent to setting up a differential equation for the disc temperatures and solving it by a numerical method.

The following sections will describe the construction and solution of the transient heat balance for a disc brake. Two conditions have been investigated, constant speed drag braking and uniform deceleration stops, from which it is possible to build up any pattern of brake duty and find the resultant disc temperature variation. The method can be applied to any size spot-type disc brake.

Figure 5.01 is a diagram of a typical spot-type disc brake, showing all the dimensions needed for data in the programmes.

HEAT BALANCE

As previously described, a steady state heat balance is constructed and a term for the heat absorption by the disc is included, giving

heat in by friction = heat stored in disc
+ heat conducted to caliper and disc mounting
+ convection from disc surface and rim
+ radiation from disc surfaces.

Each one of these components will now be developed.

HEAT INPUT

Two types of energy input to the brake will be considered, constant energy and uniform deceleration; for the latter, energy varies with speed.

A uniform rate of energy input occurs when the brake is used as the load on a dynamometer or with a constant speed drag application on a vehicle. The data needed for the computer programme is the power absorption, P, and the time increment, t.

$$E = P \times t \tag{5.01}$$

The more usual vehicle stop is treated as uniform deceleration. If the vehicle weight per brake is L and the vehicle speed at the beginning of a time increment is U_1 and at the end U_2 then we have

$$E = \frac{1}{2} L \left(U_1^2 - U_2^2 \right) \tag{5.02}$$

The disc angular velocity ω is related to the vehicle speed by the rolling radius RR.

$$\omega = \frac{U}{RR} \; 100 \tag{5.03}$$

FIGURE 5.01

Drawing of Spot-Type Disc Brake showing relevant dimensions

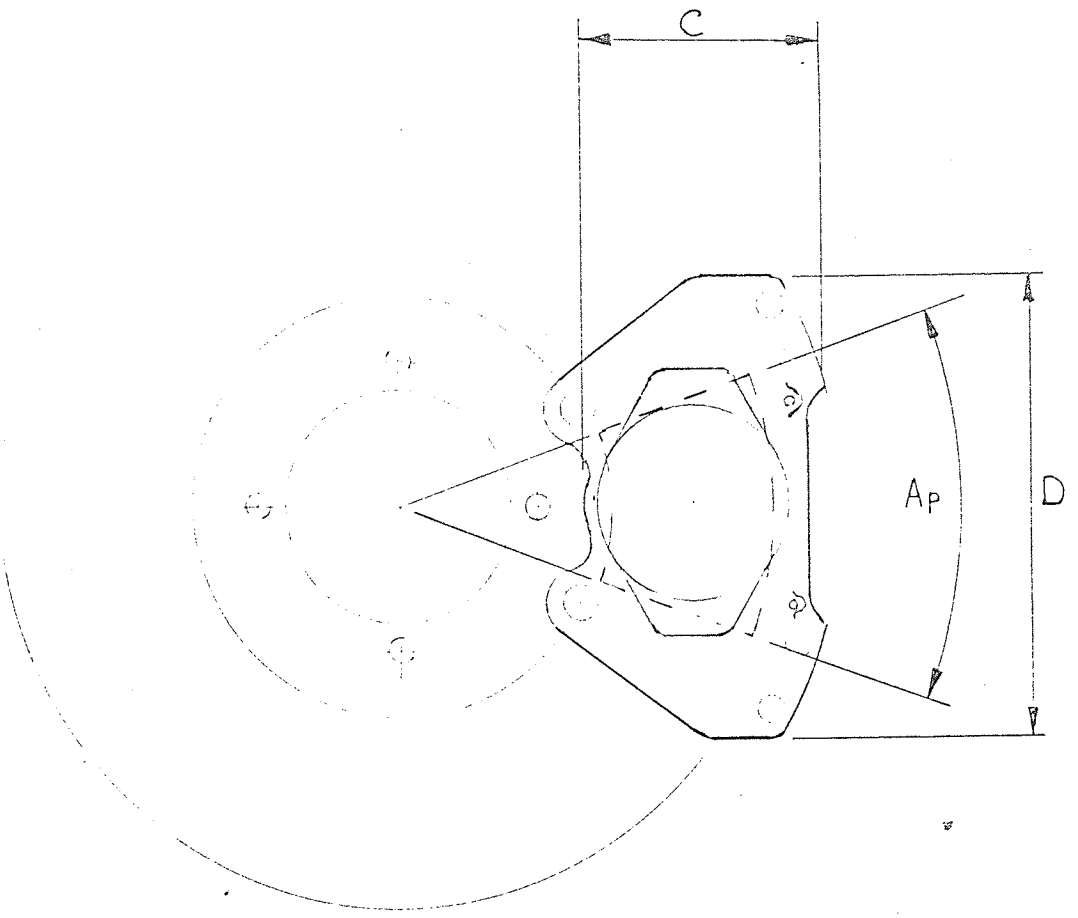

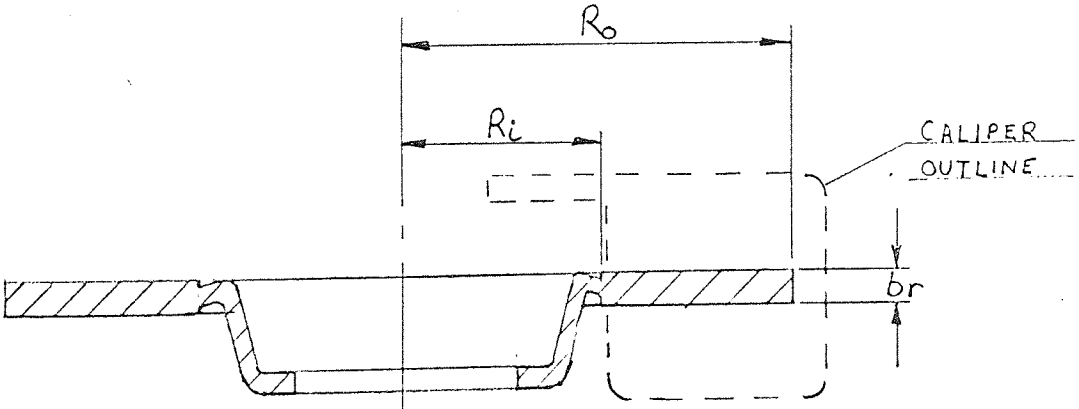

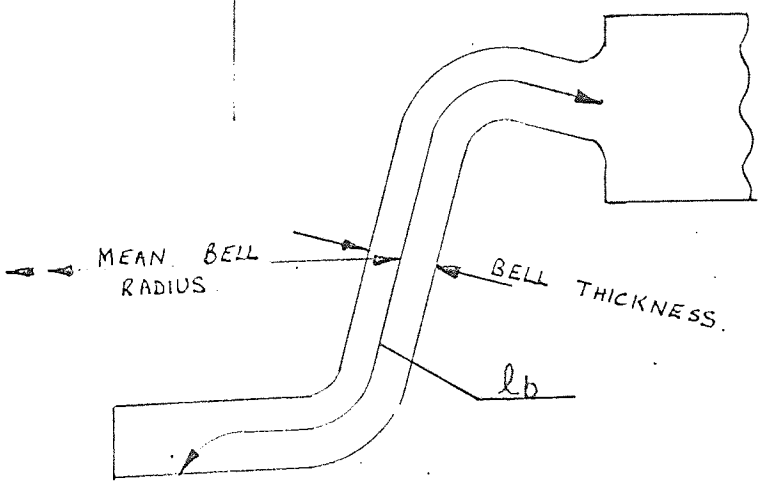

ENLARGED VIEW OF BELL

This gives the energy input as

$$E = \frac{1}{2} L (\omega_1^2 - \omega_2^2) \left(\frac{RR}{100}\right)^2 \quad (5.04)$$

HEAT ABSORBED BY DISC

It is assumed that the rotor stores heat uniformly throughout its mass, however the surface temperature must be higher than the bulk temperature to allow heat to flow in.

As this method of prediction is only of advantage for low energy input rates, then the temperature gradient across the disc will not be far removed from linear, and so it is assumed linear for these calculations.

The following constants are assumed for cast iron (Kaye & Laby{ 70 })

density $\rho = 7.26 \times 10^6 g/m^3$ (5.05)

coefficient of specific heat $Cp = .13$ (5.06)

thermal conductivity $k = 50.1 W/m\ ^oK$ (5.07)

If br is the rotor width and R_o and R_i the outer and inner radii respectively we get the equation for the rotor mass

$$m = 0.0228\ br\ (R_o^2 - R_i^2) \quad (5.08)$$

and the thermal energy to the rotor is

$$E_d = 544\ m\ (T_{b2} - T_{b1}) \quad (5.09)$$

where T_{b1} and T_{b2} are the disc bulk temperatures at the beginning and end of any time increment.

The equation for the conductive heat flow into the centre of the disc is given by

$$E_d = \frac{k\ 2\pi}{br/2}(R_o^2 - R_i^2)\ (T_{s2} - T_{b2})t \quad (5.10)$$

$$= 6.3\ \frac{t}{br}(R_o^2 - R_i^2)\ (T_{s2} - T_{b2}) \quad (5.11)$$

Equating 5.09 and 5.11 we get the relationship for the surface temperature

T_{s2}

$$T_{s2} = 1.97 \frac{br^2}{t} (T_{b2} - T_{b1}) + T_{b2} \qquad (5.12)$$

CONDUCTIVE LOSS TO DISC MOUNTING

The disc loses heat through the bell to the disc mounting. The volume of metal at the mounting is large compared to the bell and therefore may be assumed to be an infinite heat sink. The heat path area is given by

A_{be} = 2π mean bell radius x bell thickness (see fig. 5.02)

and the path length, l_{be} is the bell length from the rotor, at disc bulk temperature, T_b, to the mounting, at ambient temperature T_a. The convective loss from the bell is ignored as it is usually shrounded by the vehicle axle casing and bearing housing. The mounting joint resistance is assumed to be zero. The equation for the conductive loss is then

$$E_{mo} = k_{be} \frac{A_{be}}{l_{be}} t \left(\frac{T_{b1} + T_{b2}}{2} - T_a \right) \qquad (5.13)$$

$$= 0.501 \frac{A_{be}}{l_{be}} t \left(\frac{T_{b1} + T_{b2}}{2} - T_a \right) \qquad (5.14)$$

CONDUCTIVE LOSS TO CALIPER

The friction heat is generated at the interface between the lining and disc and hence some heat is conducted through the lining pad to the caliper. It is important to allow for this to obtain an indication of the brake fluid temperature in the caliper bore as under certain conditions it is possible the fluid may vaporize before the disc overheats.

Due to the low thermal conductivity of the pad it is the dominant factor on the conduction of heat to the caliper. If, on a typical

caliper, only the pad is considered in the calculation of heat flow, then an error of 7% arises from the neglect of the pad backplate and caliper flow path. Due to the complexity of these calculations and the variation from caliper to caliper, this error is acceptable.

The equation for the conduction to the caliper is then

$$E_{cal} = k_{lin} \frac{A_{lin}}{l_{lin}} \left(\frac{T_{s1} + T_{s2}}{2} - T_{cl} \right) \qquad (5.15)$$

The thermal conductivity of the lining material is taken as

$$k_{lin} = 0.836 \ \text{W/ m } ^{o}\text{K} \qquad (5.16)$$

A_{lin} is the total lining area contacting the disc and l_{lin} is the mean lining thickness (half worn).

The caliper temperature will increase as heat is fed into it, and this can be calculated with the heat balance;

heat conducted to caliper = heat stored + heat lost by convection.

The heat losses by radiation and conduction are neglected due to the low caliper surface temperature and the long conduction path to the mounting. The convection losses are due to natural and forced convection. To calculate these the caliper is approximated to two flat plates, which have sides of length C x D, as shown in figure 5.01.

The equation for the heat transfer by natural convection from a vertical flat plate, as taken from Schlichting {74} is:-

$$Nu = 0.491 \ Gr^{\frac{1}{4}} \qquad (5.17)$$

which gives, using the properties of air at a temperature of 27°C from Eckert {71} and omitting some lengthy arithmetic,

$$h_{nat} = \frac{13.2}{D^{\frac{1}{4}}} \qquad (5.18)$$

The heat transfer coefficient produced by forced flow over a flat plate is again given by Schlichting

$$h = 0.0296 \ \frac{k}{C} \ \sqrt[3]{Pr} \ Re^{0.8} \qquad (5.19)$$

giving

$$h_{forced} = 181 \frac{U^{0.8}}{C^{0.2}} \qquad (5.20)$$

If interaction effects are neglected the total heat transfer coefficient for the caliper is

$$h_{cal} = h_{nat} + h_{forced} \qquad (5.21)$$

The heat balance for the caliper is then

$$0.00836 \frac{A_{lin}}{l_{lin}} t \left(\frac{T_{s1} + T_{s2}}{2} - T_{c1} \right) = h_{cal} \frac{2 D x C (T_{c1} - T_a) t}{10^4} + W_{cal} 0.13 (T_{c2} - T_{c1}) 4.186 \times 10^3 \qquad (5.22)$$

Transposing

$$T_{c2} - T_{c1} = \frac{0.00836 \frac{A_{lin}}{l_{lin}} t \left(\frac{T_{s1} + T_{s2}}{2} - T_{c1} \right) - h_{cal} \frac{2 D x C (T_{c1} - T_a) t}{10^4}}{W_{cal} 544} \qquad (5.23)$$

CONVECTION LOSSES

The disc loses heat to the atmosphere by natural and forced convection, the latter due to rotation and air crossflow induced by the vehicle motion. It has been found that the natural convection heat transfer is negligible, even on a stationary disc, when compared to the conduction losses, and therefore it is ignored.

A number of experiments were described in the previous chapter, which measured the heat transfer coefficient throughout a wide range of rotational and crossflow speeds and caliper angles. Data sheets were constructed from these results and presented in figures 4.28 and 4.32. For rotation without crossflow figure 4.15 gives the effect of caliper angle.

For the condition of constant speed which gives uniform energy absorption, only one value of the heat transfer coefficient applies, for the particular speed of rotation, airflow and caliper angle, read as a value for Nu from one of the above figures.

This is used in the equations:-

$$h_d = \frac{Nu\ k\ 100}{R_o} \qquad (5.24)$$

to give

$$E_d = \frac{h_d\ 2\ A_d\ t}{10^4} \left(\frac{T_{s1} + T_{s2}}{2} - T_a \right) \qquad (5.25)$$

If a constant deceleration stop is considered the heat transfer coefficient will vary with time due to the continuous change of disc and vehicle velocities. The wheel and vehicle speeds will be related for any particular vehicle by the rolling radius according to the equation (5.03). This enables a series of points to be drawn on figure 4.28 for the Nusselt number at the intersection of rotational and crossflow Reynolds numbers, which will approximate to a straight line on the logarithmic plot and hence obey the law:-

$$Nu_o = Cl\ (Re_o)^{C2} \qquad (5.26)$$

The values of Cl and C2 are fed into the computer, along with the ratio

$$\frac{\text{Nu with sector}}{\text{Nu without sector}}$$

from figure 4.32, or if there is no crossflow, from figure 4.15. The programme then calculates the heat transfer coefficient h_d from equation (5.24).

The convective heat transfer from the rim of the disc is calculated from work by Kays & Bjorkland {39}, who measured the heat transfer from a rotating cylinder in a crossflow. However, this only dealt with wide cylinders and it is not known how accurate this is for a narrow cylinder, where the flow on the rim will be affected by the flow from the disc surfaces. They give the equation

$$Nu_o = \frac{0.135}{2} \left[(0.5\{2Re_o\}^2 + \{2\ Re_t\}^2)\ Pr \right]^{1/3} \qquad (5.27)$$

neglecting free convection effects.

i.e.
$$h_{rim} = \frac{k}{R_o}\ 6\ (2\ Re_o^{\ 2} + 4\ Re_t^{\ 2})^{1/3} \qquad (5.28)$$

Then the equation for the convective heat loss from the rim is

$$H_{rim} = \frac{h_{rim}\ A_{rim}\ t}{10^4} \left(\frac{T_{b1} + T_{b2}}{2} - Ta \right) \qquad (5.29)$$

where

$$A_{rim} = 2\pi R_o b \qquad (5.30)$$

RADIATION LOSSES

Calculations made with the radiation heat transfer included have shown that it has only a small effect on the disc temperature when compared to the heat losses by convection and conduction, and it is therefore ignored.

SOLUTION OF THE HEAT BALANCE

The component equations may now be substituted into the heat balance given earlier.

For the condition of constant energy absorption this gives

$$P \times t = 544\ m\ (T_{b2}-T_{b1}) + 0.00836\ \frac{A_{lin}t}{l_{lin}}\left(\frac{T_{s1}+T_{s2}}{2} - T_c\right) + 0.501\ \frac{A_{be}t}{l_{be}}\left(\frac{T_{b1}+T_{b2}}{2} - T_a\right) + \frac{h_d\ 2A_d t}{10^4}\left(\frac{T_{s1}+T_{s2}}{2} - T_a\right) + \frac{h_{rim}\ A_{rim}\ t}{10^4}\left(\frac{T_{b1}+T_{b2}}{2} - T_a\right) \qquad (5.31)$$

where $m = 0.0228\ br(R_o^2 - R_i^2)$

and $T_{s2} = 1.97\ \frac{br^2}{t}\ (T_{b2} - T_{b1}) + T_{b2}$

$h_d = \frac{Nu_o\ k\ 100}{R_o}$

$A_d = \pi(R_o^2 - Ri^2)$

$h_{rim} = \frac{k}{R_o}\ 6(2\ Re_o^2 + 4\ Re_t^2)^{1/3}$

$A_{rim} = 2\pi\ R_o\ b.$

This is solved for T_{b2} to give

$$T_{b2} = \frac{E + \frac{T_{b1}}{2}(1088m + SK_2 - K_1 + SK_3) - \frac{T_{s1}}{2}(K_2+K_3) + T_{c1}K_2 + T_a(K_1+K_3)}{\frac{1}{2}(1088m + K_2\{S+1\} + K_1 + K_3\{S+1\})} \quad \text{.....(5.32)}$$

where

$$K_1 = 0.50 \frac{A_{be}\, t}{l_{be}} + \frac{h_{rim}\, A_{rim}\, t}{10^4} \quad (5.33)$$

$$K_2 = 0.00836 \frac{A_{lin}\, t}{l_{lin}} \quad (5.34)$$

$$K_3 = 2\times10^{-4}\, h_d\, A_d\, t \quad (5.35)$$

$$S = 1.97 \frac{br^2}{t} \quad (5.36)$$

$$E = P \times t \quad \text{for constant energy} \quad (5.37)$$

$$\text{or } \frac{L}{2\times10^4}(\omega_1^2 - \omega_2^2)(RR)^2 \quad \text{for constant deceleration} \quad (5.38)$$

During a stop the caliper temperature will rise, this is calculated with the heat balance shown in equation (5.23). Equation(5.23) is solved for T_{b2} over the time interval t with initial conditions set for T_{s1}, T_{b1}, T_a and T_{c1}. At the end of time t the values of T_{b2}, T_{s2}, and T_{c2} are substituted for T_{b1}, T_{s1} and T_{c1} and the process repeated.

The iterative process is done by computer; the flow diagram of the programme is shown in figure 5.02. A sample print out is shown in figure 5.03.

5.3 COMPARISON OF PREDICTION AND EXPERIMENT

This method of temperature prediction has only been compared with a small amount of experimental work to date (supplied by development department, Girling Ltd.), then as further comparisons are made the theoretical analysis will be developed. Two sets of results are compared here, one for constant deceleration stops and the other for constant energy absorption braking, both brakes are installed in still air, no comparison has yet been made with a crossflow on the disc.

FIGURE 5.02

COMPUTER PROGRAMME FLOW CHART

TEMPERATURE OF DISC BRAKE DURING CONSTANT DECELERATION STOP

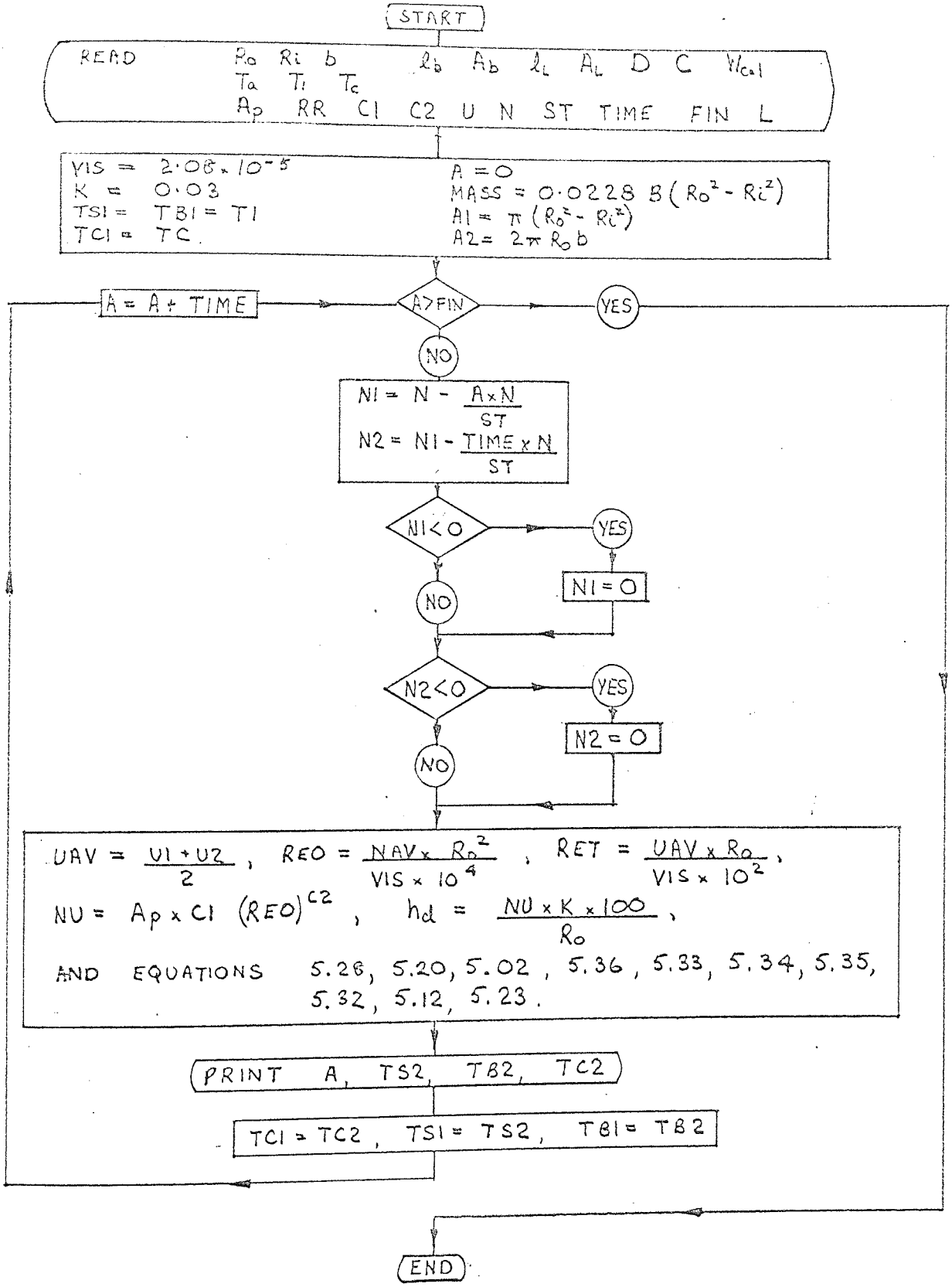

FIGURE 5.03

Sample of Results from Computer Programme to Calculate Disc Brake Temperatures

TS	surface temperature ^{o}C	N	disc speed rad/sec
TB	bulk temperature	U	crossflow velocity m/s.
TCAL	caliper temperature	STOP TIME	sec

16P CALIPER ON 11.06 DISC, NO CROSSFLOW

STOP TIME = 21.9 N = 75 U = 0

TIME	TS	TB	TCAL
0.0	30.00	30.00	20.00
1.0	107.68	48.59	20.02
2.0	122.13	66.20	20.06
3.0	135.84	82.87	20.10
4.0	148.63	98.61	20.15
5.0	160.52	113.43	20.21
6.0	171.50	127.33	20.27
7.0	181.59	140.32	20.33
8.0	190.77	152.40	20.40
9.0	199.06	163.57	20.47
10.0	206.46	173.83	20.55
11.0	212.97	183.20	20.63
12.0	218.60	191.67	20.71
13.0	223.35	199.26	20.79
14.0	227.22	205.95	20.87
15.0	230.22	211.76	20.96
16.0	232.36	216.69	21.04
17.0	233.63	220.75	21.13
18.0	234.04	223.93	21.21
19.0	233.59	226.24	21.30
20.0	232.30	227.69	21.39
21.0	230.17	228.28	21.47
22.0	227.23	228.03	21.56
23.0	225.63	227.46	21.64

Figures 5.04, 5 and 6 give the results for various constant deceleration stops. Previous experience has shown that although the disc temperature is measured with a thermocouple rubbing on the surface and should therefore indicate the surface temperature the response time of the thermocouple tends to reduce the indicated temperature to well below that of the surface and nearer to the bulk temperature. For this reason the temperature is compared to predictions of the bulk temperature. The assumption that above 0.1g all the energy goes into the heat sink of the disc is supported by these results. For the 0.106g stop the experimental result, the predicted one and the result calculated on the assumption that there is no cooling all lie within 7%. As the rate of deceleration is reduced the results deviate more, until for the 0.0202g stop the calculated temperature assuming no cooling is 80% above the measured values, and that predicted by this theory is 40% above the measured values. Therefore, in this area, the present method affords a considerable improvement over the previous method but still leaves a large discrepancy with experimental results.

Figures 5.07 and 8 compare results for three constant energy input conditions, or drag braking. Good agreement is achieved with the experimental results although the latter are not fully dependable as they were extracted third hand from tests made by another company many years ago, and the method of measurement is not now known. With this type of braking the disc will rapidly achieve a steady state condition, shown by the levelling out of the temperature, when the heat input due to friction is equal to the heat lost by the three modes of heat transfer.

5.4 LIMITATIONS OF PREDICTION

A serious limitation to extending this prediction to decelerations above 0.1g was found to be that under high rates of energy input the temperature gradient through the disc deviated from the assumed linear

FIGURE 5.04

Comparison of Experimental and Theoretical Results for 16P Caliper on 28·1 cm diameter disc with 1670 kg on wheel

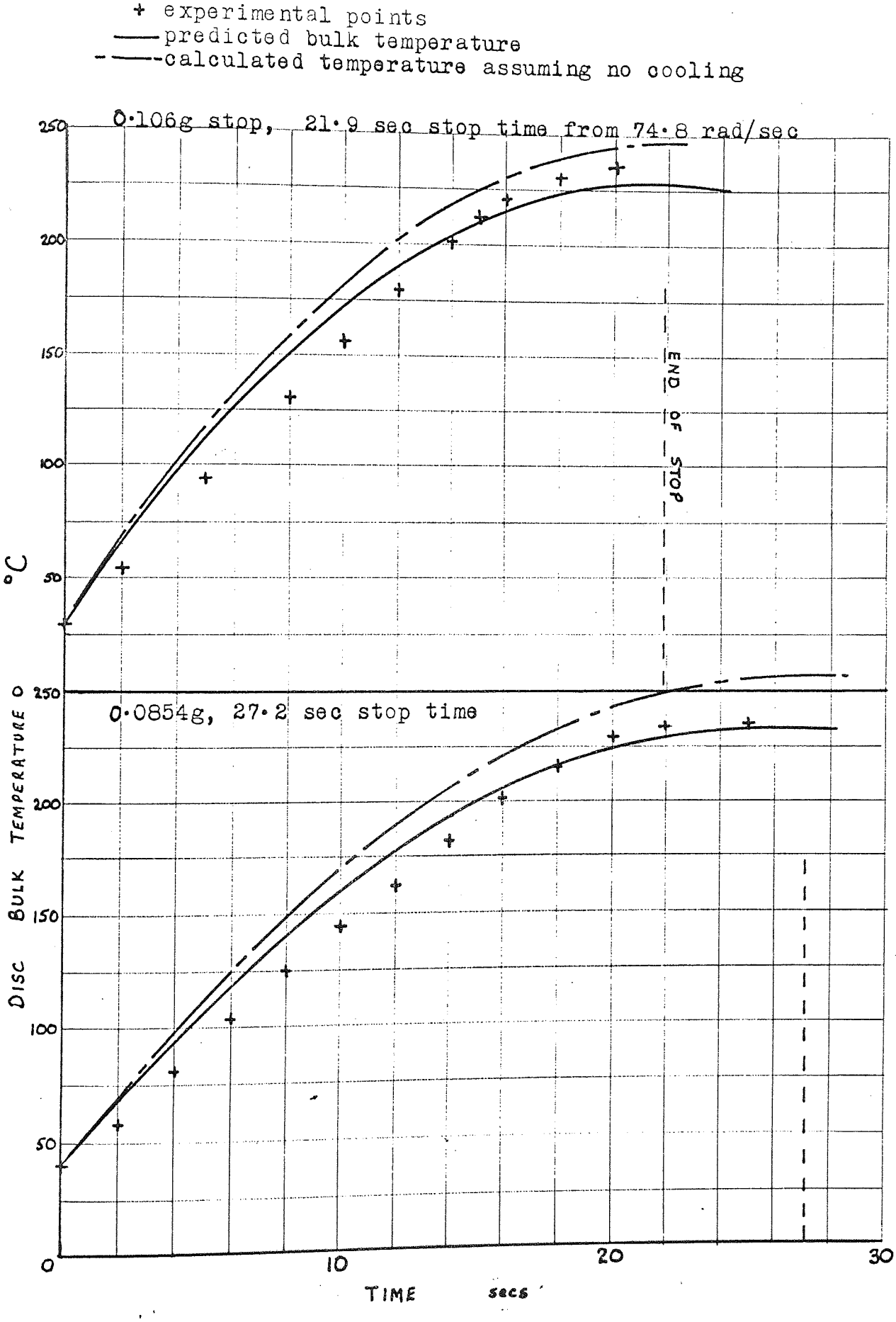

FIGURE 5.05

Comparison of Experimental and Theoretical Results for 16P Caliper on 28·1 cm diameter disc with 1670 kg on wheel

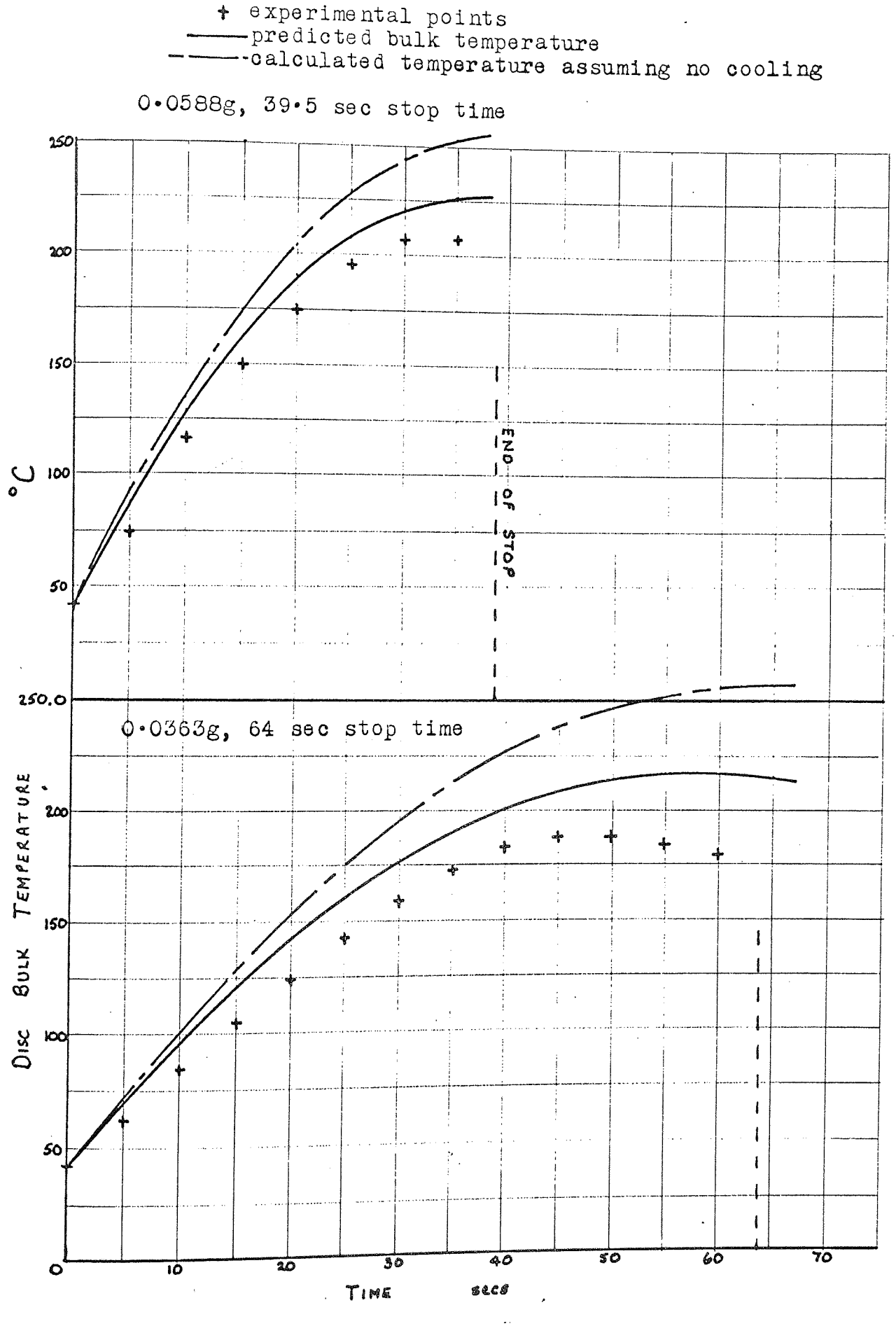

FIGURE 5.06

Comparison of Experimental and Theoretical Results for 16P Caliper on 28·1 cm diameter disc with 1670 kg on wheel

+ experimental points
—— predicted bulk temperature
- - - - calculated temperature assuming no cooling

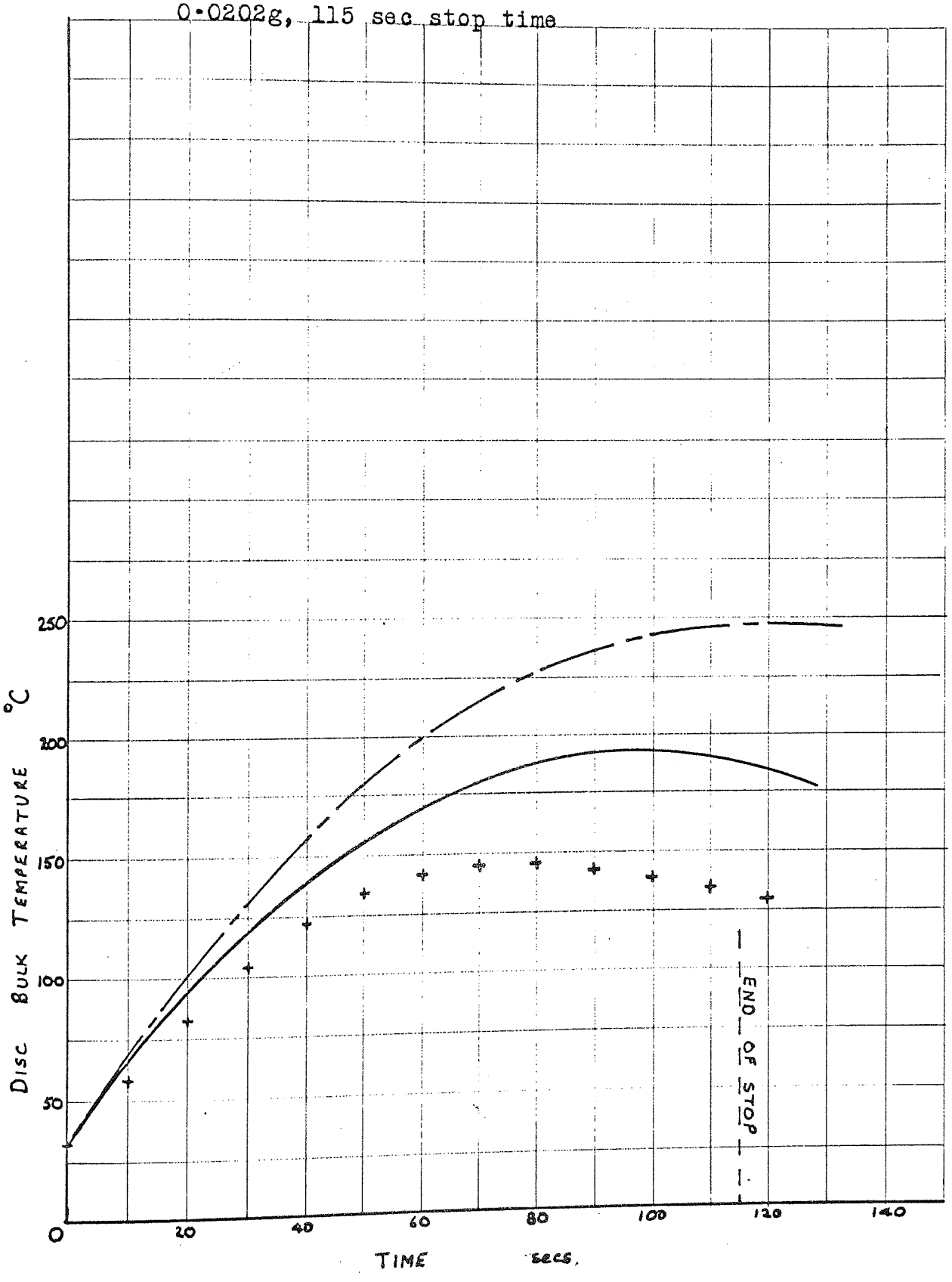

FIGURE 5.07

Comparison of Experimental and Theoretical Results for 16P Caliper on 28·1 cm diameter disc with constant energy input

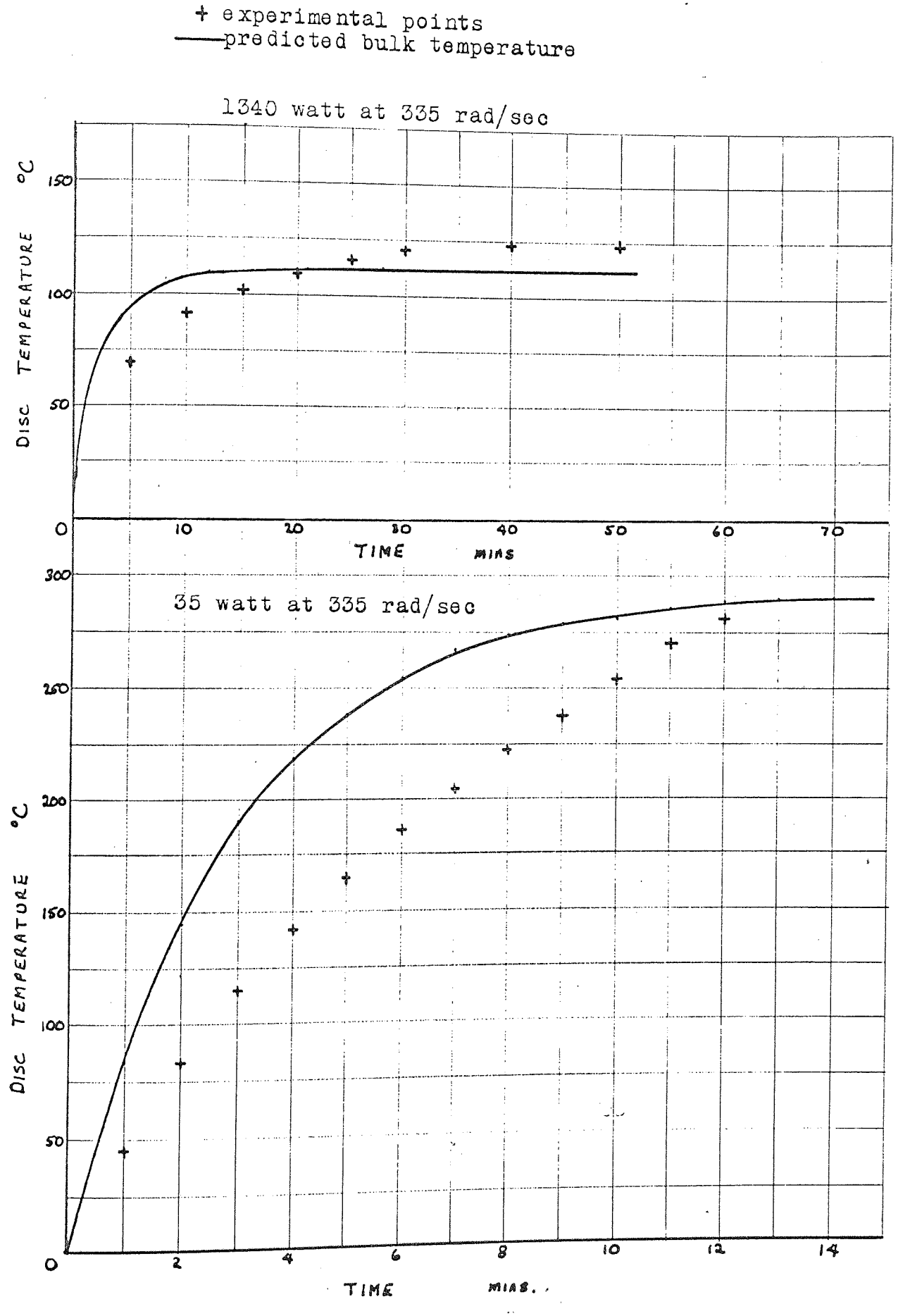

FIGURE 5.08

Comparison of Experimental and Theoretical Results for 16P Caliper on 28·1 cm diameter disc with constant energy input

+ experimental points
—— predicted bulk temperature

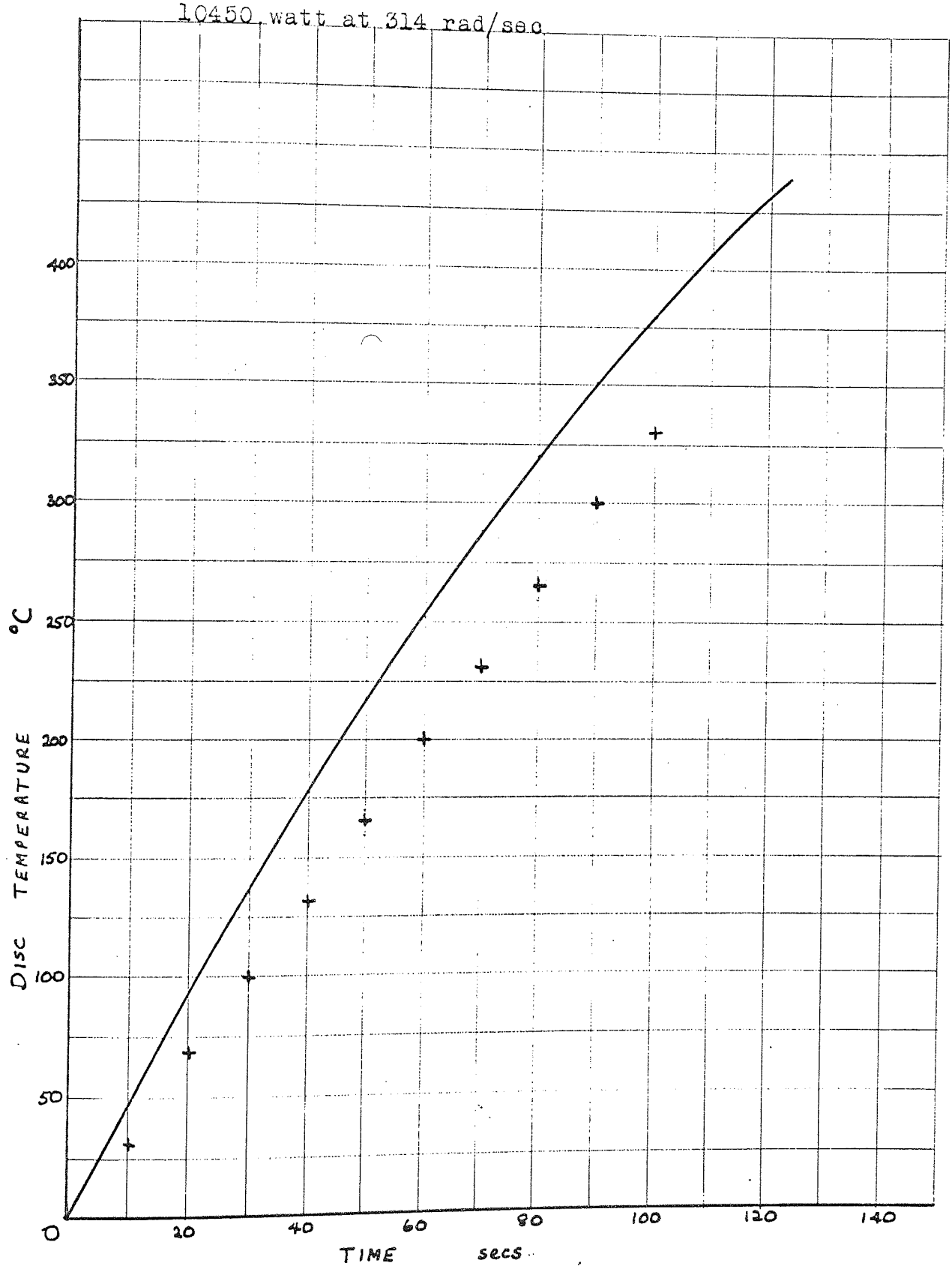

one to take the form shown below.

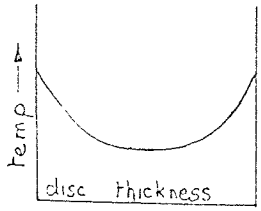

The effective disc width is then smaller than the actual one which causes the programme to calculate T_s much higher than experiment shows. However, with this rate of energy input, the cooling is insignificant so the method of Newcomb {57} to calculate the surface temperature is quite acceptable. It was found that around 0.1g the surface temperature predicted by Newcomb, that found by the present method and experimental data all agreed, but for higher rates of energy input the present method yielded surface temperatures higher than those of Newcomb. At energy input levels below 0.1g the prediction of Newcomb gave temperatures above the present predictions due to the disregard of cooling in the method of Newcomb.

No information is available at present to assess at what level of constant energy input the surface temperature prediction becomes inaccurate, and further experimental measurements at high input rates will be needed to check this.

5.5 FURTHER WORK

It is obvious from comparison with experimental work that the method needs to be checked over a much wider range of disc sizes and operating conditions before its validity can be proved.

In the short term the programme can be modified to allow for the variation of the fluid properties with temperature and the effect of the caliper angle can be also incorporated. It is important that a more accurate method of calculating the surface temperature be found, probably by treating the flow into the disc as a transient flow of heat

through a solid, rather than assuming a temperature gradient through the disc. The prediction would then be applicable to all rates of energy input and not limited to low ones.

The programme can be modified to predict the disc temperature during acceleration and steady speed cooling conditions; a normal road cycle of accelerate, cruise, brake, and accelerate again could then be studied.

Ultimately, it is intended that this temperature prediction should form the basis for lining wear rate calculations.

Chapter 6

CONCLUSIONS AND FURTHER WORK

The object of the investigation was to measure the heat transfer from a rotating disc with emphasis on the effects of disturbing the boundary layer. The methods of producing these disturbances were linked with the environment of real disc brakes. The effect of vehicle motion was simulated by imposing a crossflow of air on the experimental disc; and a brake caliper by masking a sector of the disc. As it was desirable to increase the heat transfer coefficient in order to improve disc cooling, further experiments were made with boundary layer trips and air jets directed onto the disc surface.

The first set of experiments reproduced previous work on the heat transfer from a rotating disc in still air in an attempt to rationalize the differing results of earlier publications. In the region of natural convection and laminar flow, at rotational Reynolds numbers below 2×10^4 for the first, and below 2.4×10^5 for the second, it was found that the measurements followed the equations presented by Richardson and Saunders,

$$Nu_o = 0.4 \, (Gr_o + Re_o^{\,2})^{\frac{1}{4}} \qquad (6.01)$$

except when the disc was stationary, when a higher heat transfer was recorded. It was concluded that this discrepancy was due to a non-isothermal disc surface rather than an inaccuracy in equation (6.01). Ambient temperature measurements showed a large recirculation of air inside the enclosure, raising the ambient temperature by 22% with a disc to ambient temperature difference of $50^{\circ}C$. Measurements of the laminar flow tangential profile agreed closely with the prediction of Cochran, and the experimental data of Gregory, Stuart and Walker, but the

yawmeter proved too insensitive to measure the angle of yaw to determine the radial profile. The onset of turbulence came at a Reynolds number of 2.3×10^5 and measurements of the heat transfer in the region of turbulent flow indicated a heat transfer for the whole of the disc under turbulent flow as

$$Nu_o = 0.015\, Re_o^{0.8} \qquad (6.02)$$

in agreement with the experimental data of Cobb & Saunders. It may appear strange that the present laminar and turbulent results agree with those found by different previous authors, both of whom used the same apparatus as used in the present work, but this occurred because Cobb & Saunders made an error in their measurement of the ambient temperature. This affected the laminar measurements only as the ambient thermocouple was probably situated in the more disturbed turbulent recirculation stream but not in the laminar one. Richardson & Saunders discovered this error and rectified it to give the result already described by equation (6.01).

The heat transfer in the transition zone was predicted within 15% by the equation

$$Nu_o = \frac{0.4\, Re_{cr}}{\sqrt{Re_o}} + 0.015 \left[Re_o^{0.8} - Re_{cr}^{0.8} \sqrt{\frac{Re_{cr}}{Re_o}} \right] \qquad (6.03)$$

The turbulent tangential velocity profile again agreed well with that of Gregory, Stuart & Walker.

The heat transfer from a rotating disc in still air has now been exhaustively investigated and all the recent papers were concerned with non-isothermal surfaces, nearby planes, axial forced flow and fluid injection through the surface. However, the heat transfer at Prandtl numbers other than 0.7 has hardly been investigated experimentally, the only successful work was by Kreith, Taylor & Chong at Pr = 2.4 using a mass transfer technique. Sparrow & Gregg have predicted the heat transfer in the laminar region for the full range of Prandtl number,

but in the turbulent region of flow results around a Prandtl number of one only have been found. No theoretical temperature profile has been evaluated as the Navier-Stokes continuity and energy equations have not been solved directly for turbulent flow, integral methods being used instead.

The brake caliper was represented by masking a sector of the disc with a plywood model. Tests showed that the width of the caliper did not affect the heat transfer and was adequately simulated by plywood of thickness 13mm, provided that at small angles of sector the air was not allowed to recirculate over the sector. It is doubtful if air could recirculate over a caliper as it is much wider than the plywood sector and the air would be deflected well away from the disc. In addition, calipers usually cover about a 40°-60° sector of the disc and experiments showed that in this range only a small recirculation occurred at low rotational speeds.

When certain sectors of the disc, from 0 to 360°, were masked off, not only was that area of convective heat transfer lost but the flow in the region of the sector was considerably disturbed. It was not possible to produce a theoretical correlation to the effects of these disturbances due to the complexity of the flow patterns, but an empirical relation was found which agreed to within 5% of experimental data in the laminar region but deviated much more, by up to 200%, in the turbulent region. This assumed that the disturbance effect was independent of caliper angle and equal to the difference in heat transfer between that for a free disc and for a disc with a scraper touching the surface. The scraper caused the airflow to be disturbed in the same way as occurred on the leading edge of a sector but masked a negligible area of the disc surface. The empirical relation was

$$Nu = \frac{360 - \phi}{360} Nu_{free} + (Nu_{scraper} - Nu_{free}) \qquad (6.04)$$

The experimental data (figure 4.17) covered an adequate range of sector angles and rotational Reynolds numbers for all existing disc brake designs, but should a higher rotational Reynolds number be needed the graphs show that the lines through the experimental data have settled to the usual Reynolds number to the 0.8 index and therefore can be extrapolated with confidence.

No detailed measurements of the complex behaviour of the flow were made, only a flow visualization technique being used, and a more complete understanding of the behaviour would be available if a detailed velocity survey were made in these areas. In particular the indication that a laminar layer behind a sector is extended into the region that would be turbulent on a free disc needs verification, either by velocity profile measurement or by flow visualization in a tank of fluid using air bubbles in water, which shows the pattern of flow much more clearly than can be seen by smoke visualization.

When a disc brake is fitted to a vehicle it is necessarily subjected to a forced crossflow of air with the vehicle in motion. This was reproduced by installing the experimental disc in a wind tunnel. It was found that the square edge of the disc caused separation of the flow over an initial length of the surface and turbulent flow thereafter, causing the heat transfer to be 33% higher than predicted by stationary surface forced convection theories. Few previous investigations exist on separation at sharp leading edges at subsonic speeds and its effect on the heat transfer, and a considerable amount of further work is needed into the effect of the leading edge radius and width. All previous heat transfer investigations on a stationary surface were made outside the leading edge region and with a well tapered nose in order to prevent the very disturbance that is of most interest here.

Heat transfer experiments were made with an adequate range of rotational speeds but it is possible that higher crossflow velocities

will be encountered. The lines of heat transfer tend to converge at high crossflow velocities showing that rotation was having little effect, so extrapolation for higher crossflow velocities would be easy to make, the line for zero rotation being merely extended to the required value of crossflow Reynolds number.

A semi-empirical theoretical correlation was developed which agreed with the experimental data for rotational and crossflow existing simultaneously, to within 5%. This was based on experimental measurements of the heat transfer from a rotating disc in an air crossflow. Local heat transfer coefficients deduced from best equations through the data were vectorially added, to find the resultant local coefficients, which were then used to calculate the mean heat transfer. This method of prediction used the novel technique of assigning directions to the heat transfer coefficients so that they could be added vectorially to determine the resultant one, similar to the theory of superposition of flows.

For the experimental disc the ratio of width to diameter was fixed and the separation effect was nearly constant for the full range of crossflow velocities. The disc also had a guard rim giving a heated initial length before the test section was reached. Neither of these conditions exist on brake discs, where the width to diameter ratio varies from 3% to 8%, whilst on the experimental disc this was 6.3%. Due to the small range of this ratio it was assumed that the effect of separation remained constant for brake discs at 33% above that predicted from stationary surface theories. A theoretical prediction of the heat transfer from a stationary disc in a crossflow without a guard rim was easily made by measuring the characteristic length direct from the leading edge and not from the edge of the guard rim, as was done for the experimental disc. However, this did not allow for the main disc having a higher percentage of area in the region of separated flow so

the heat transfer would be higher than predicted, but the magnitude of this deviation is not known. This emphasises the need for further information on the effect of a sharp leading edge on the heat transfer.

A data sheet based on the above assumptions was prepared for rotational Reynolds numbers up to 2.5×10^6 and crossflow Reynolds numbers up to 10^6 (figure 4.28).

A more realistic set of conditions were applied when tests were made with the disc rotating in a wind tunnel with sectors of the disc masked off. This reproduced the most common configuration of a disc brake on a vehicle. It does, however, neglect the effect of disturbances to the airflow caused by surrounding bodies, for example, the wheel, vehicle wing, axle and road springs. Road tests have shown that these tend to reduce the volume and velocity of air flowing across the disc, but further measurements are needed from vehicle tests to assess the effective crossflow velocity on the disc for a range of vehicle speeds. Alternatively this effective velocity could be found by calculation of the heat transfer coefficients from cooling curve measurements on vehicle tests and comparing these with heat transfer coefficients found with the present experiments.

Tests with a simulated caliper on the disc in different positions relative to the direction of crossflow showed little change in the heat transfer. With the masking sector in the trailing position it was found that, for the range of crossflow and rotational speeds tested, the ratio of Nusselt number to the Nusselt number found with a free disc followed a single line, plotted against sector angle, to within 13% (figure 4.32). By ignoring the area of the sector of disc masked off in the method of prediction used for a rotating disc in a crossflow good correlation was achieved with the experimental data, except at low rotational speeds when separation of the flow at the leading edge had a more significant effect on the heat transfer.

Experiments to trip the boundary layer were made more as an exercise to compare the results with those from a scraper rather than as an attempt to significantly increase the heat transfer from the disc. The trip wire gave a different pattern of flow to that found with a scraper on the disc. The scraper had increased the heat transfer by creating a swirl of air, with little recirculation to the other side, but the wire did not hinder the flow, only tripped it from laminar to turbulent flow, causing an increase in heat transfer of 10% in the laminar region but none in the turbulent region. With a radially mounted wire the whole of the surface was not affected as the airflow followed a spiral path to leave the disc at the rim. Tests with a larger number of wires taped to the surface of the disc further increased the heat transfer to a value beyond the line for all the disc under turbulent flow, indicating that some separation of flow probably occurred behind the wires, which has already been shown to give a large increase in the local rate of heat transfer.

A very interesting result was found with a circle of wire taped to the disc surface; this should have given 89% of the disc under turbulent flow, but when the experimental data was compared with values for discs with their surfaces under all laminar and all turbulent flow it was found that only 75% of the disc was under turbulent flow. This suggests that the axial inflow of air might damp the turbulent disturbances and eventually cause the flow to revert to laminar type. This supports evidence from other sources who found that mass addition to a boundary layer causes the flow to be more stable and inhibits the formation of turbulent flow.

With a thin jet of air blowing onto the disc surface, mounted on a radius and extending over the full radius of the disc, the best angle of inclination to the surface was 80°, blowing against the direction of rotation. Further tests were made with the jet at right angles to the

surface as this would give the same effect with the disc rotating in both directions. In the range of tests the distance between the nozzle exit and the disc surface had little effect on the heat transfer. The heat transfer was increased more with the nozzle mounted radially than when it was mounted in a side-on position, indicating that the interaction with the rotational flow was more effective with the nozzle in the former position.

Since the mass supply of air needs to be as small as possible with the unit on a vehicle, a plot of volume flow against Nusselt number was produced (figure 4.42), which indicated that the smallest opening was the most effective. However, the velocity of supply from this nozzle was limited by the higher static pressure causing the nozzle to vibrate, but this could be overcome by strengthening or altering the design of the nozzle.

Calculations using a reasonable supply for a commercial vehicle show that the Nusselt number could be increased to twice that for a free disc at Re_o = 200000, equivalent to a 0.4 m (15.5 in.) disc rotating at 200 r.p.m. Measurements at other rotational speeds show that the air jet has more effect on the heat transfer as the speed decreases so the improvement on that for a free disc would be correspondingly larger. These results indicate that a useful gain in the heat transfer coefficient is to be had from air jet cooling of a disc brake in a dirt shield but a more realistic comparison can only be made by evaluating the effect on a disc brake operating temperature for a typical vehicle duty. Further work needs to be done with the brake temperature prediction method outlined in Chapter five to calculate this effect.

A considerable amount of further work needs to be done on the application of the measurements of the heat transfer coefficients that have been made during the present work. Newcomb {66}has published

the results of many measurements of the cooling rate (b_v values) of disc brakes mounted on vehicles travelling at various speeds. From these cooling rates can be calculated the average heat transfer coefficient to allow comparison with those measured here at the same rotational and crossflow speeds, and with the same caliper angle. Any differences will then be directly attributable to the disturbed airflow and the shielding around the disc. By analysis of many such sets of experimental data it may be possible to establish a range of "vehicle factors" dependent on the installation conditions and vehicle usage.

Once such "vehicle factors" have been developed they can be supplemented into the method of disc brake temperature prediction outlined in Chapter five, and further comparisons made with measured disc brake temperatures.

Even further ahead, it is envisaged that the wear life characteristics of friction pads, highly dependent on disc temperature, can be used with the calculated operating temperature to find the wear life. Present methods of wear life calculation average the road duty and calculate a typical temperature and wear life pattern but this can lead to considerable discrepancies through insufficient accuracy in the averaging technique. By utilising the speed of a computer the wear life could be calculated for each brake application of a braking duty taken from actual road measurements and a much closer prediction of the brake wear life should result.

Summarising then, a number of experiments are needed to improve the range, applicability and dependability of the present measurements, but by far the largest amount of work lies in developing the application of these results.

APPENDIX 1

HEAT TRANSFER FROM A ROTATING DISC IN STILL AIR

LAMINAR FLOW REGION

THEORETICAL ANALYSIS OF WAGNER {13} AND KREITH, TAYLOR & CHONG {34} .

The theoretical analysis described in these two papers are identical in derivation, but they are used to give results for different Prandtl numbers in each . Here the theory is derived in full and the numerical work done on an Elliot 903 computer.

The heat flow equation is derived from the steady state equation, the axial velocity profile according to Karman {3} is substituted and integration yields the heat transfer coefficient. This is a common method used for many heat transfer systems where the boundary layer velocity profiles are known and is usually called the INTEGRAL METHOD.

In cylindrical co-ordinates the steady state equation for heat transfer to or from a rotating plate is

$$\alpha \left(\frac{\partial^2 \theta}{\partial R^2} + \frac{1}{R} \frac{\partial \theta}{\partial R} + \frac{\partial^2 \theta}{\partial z^2} \right) - u_r \frac{\partial \theta}{\partial R} - u_z \frac{\partial \theta}{\partial z} = 0 \qquad \text{(A1.01)}$$

when viscous dissipation is neglected and fluid properties are uniform, and where $\theta = (T - T_\infty)$.

The boundary conditions are for uniform surface temperature and

at $z = 0$ $\qquad \theta = \theta_w = (T_w - T_\infty)$

at $z = \infty$ $\qquad \theta = 0$

Now, as proposed by Karman, the boundary layer thickness δ is independent of the radius R, and hence the temperature difference θ is independent of R, giving, from (A1.01)

$$\alpha\left(\frac{d^2\theta}{dz^2}\right) - u_z\left(\frac{d\theta}{dz}\right) = 0 \qquad (A1.02)$$

Integrating this once, assuming that the solution is $\frac{d\theta}{dz} = e^{f(z)}$ then $\frac{d^2\theta}{dz^2} = f'(z)e^{f(z)} = f'(z)\frac{d\theta}{dz}$, compared with $\frac{d^2\theta}{dz^2} = \frac{u_z}{\alpha}\frac{d\theta}{dz}$

$$\therefore \quad f'(z) = \frac{u_z}{\alpha}$$

$$\therefore \quad \frac{d\theta}{dz} = e^{\int_o^z \frac{u_z}{\alpha}\,dz} \qquad (A1.03)$$

Integrating again $\int_o^\theta \frac{d\theta}{dz}\,dz = \theta = \int_\infty^z \exp\left(\frac{1}{\alpha}\int_o^z u_z dz\right)dz$

giving $\theta = -\int_z^\infty \exp\left(\frac{1}{\alpha}\int_o^z u_z dz\right)dz \qquad (A1.04)$

Dividing (A1.03) by (A1.04)

$$\frac{d\theta}{dz}\frac{1}{\theta} = \frac{\exp\frac{1}{\alpha}\int_o^z u_z dz}{-\int_z^\infty \left(\exp\frac{1}{\alpha}\int_o^z u_z dz\right)dz} \qquad (A1.05)$$

$$\frac{d\theta}{dz} = -\frac{\theta \exp\frac{1}{\alpha}\int_o^z u_z\,dz}{\int_z^\infty \left(\exp\frac{1}{\alpha}\int_o^z u_z dz\right)dz} \qquad (A1.06)$$

Now when $\theta = \theta_w$, $z = 0$

$$\therefore \quad \frac{d\theta}{dz} = -\frac{\theta_w \exp\frac{1}{\alpha}\int_o^z u_z dz}{\int_o^\infty \left(\exp\frac{1}{\alpha}\int_o^z u_z dz\right)dz} \qquad (A1.07)$$

and $$h = \frac{1}{\theta_w}\left[-k\left(\frac{\partial\theta}{\partial z}\right)_{z=o}\right]$$

$$= -\frac{k}{\theta_w}\left[\frac{\exp\frac{1}{\alpha}\int_o^o u_z\,dz\,(-\theta_w)}{\int_o^\infty \left(\exp\frac{1}{\alpha}\int_o^z u_z dz\right)dz}\right]$$

$$= k \frac{1}{\int_o^\infty (\exp \frac{1}{\alpha} \int_o^z u_z \, dz) \, dz} \qquad (A1.08)$$

$$Nu = \frac{hR}{k} = \frac{R}{\int_o^\infty (\exp \frac{1}{\alpha} \int_o^z u_z \, d_z) \, dz} \qquad (A1.09)$$

At this point the velocity profile for u_z is obtained from Karman {3},

viz. for $z \leq \delta$

$$u_z = -2\omega \int_o^z \left[1.026 \left(\frac{z}{\delta}\right)\left(1-\frac{z}{\delta}\right)^2\left(1+\frac{2z}{\delta}\right) - \frac{1}{2}\left(\frac{z}{\delta}\right)^2\left(1-\frac{z}{\delta}\right)^2\right] dz$$

$$= -2\omega z \left[0.31\left(\frac{z}{\delta}\right)^4 - 0.52\left(\frac{z}{\delta}\right)^3 - 0.17\left(\frac{z}{\delta}\right)^2 + 0.51\left(\frac{z}{\delta}\right)\right] \qquad (A1.10)$$

for $z > \delta$ $\qquad u_z = -0.708\sqrt{\nu\omega}$ $\qquad (A1.11)$

Now $$Nu = \frac{R}{\int_o^\delta \exp\left(\frac{1}{\alpha}\int_o^z u_z dz\right)dz + \int_\delta^\infty \exp\left(\frac{1}{\alpha}\int_o^z u_z dz\right) dz} \qquad (A1.12)$$

Let $$A = \int_o^\delta \exp\left(\frac{1}{\alpha}\int_o^z u_z dz\right)dz \qquad (A1.13)$$

and $$B = \int_\delta^\infty \exp\left(\frac{1}{\alpha}\int_o^z u_z dz\right)dz \qquad (A1.14)$$

<u>To determine A</u>

$$\frac{1}{\alpha}\int_o^z u_z dz = -\frac{2\omega}{\alpha}\left[\frac{0.31}{6}\frac{z^6}{\delta^4} - \frac{0.52}{5}\frac{z^5}{\delta^3} - \frac{0.17}{4}\frac{z^4}{\delta^2} + \frac{0.51}{3}\frac{z^3}{\delta}\right]$$

$$\therefore \quad A = \int_o^\delta \exp\left[\frac{-2\omega}{\alpha}\left(0.171\frac{z^3}{\delta} - 0.0415\frac{z^4}{\delta^2} - 0.1026\frac{z^5}{\delta^3} + 0.0517\frac{z^6}{\delta^4}\right)\right]dz$$

Let $X = \frac{z}{\delta}$

then $$A = \delta \int_o^1 \exp\left[-2Pr\xi\delta^2(0.171X^3 - 0.0415X^4 - 0.1026X^5 + 0.0517X^6)\right]dX$$

$$= \xi_\delta \sqrt{\frac{\nu}{\omega}} \int_o^1 \exp\left[2Pr\xi_\delta{}^2(-0.171X^3+0.0415X^4 + 0.1026X^5-0.0517X^6)\right] dX$$

(A1.15)

To determine B

$$B = \int_\delta^\infty \exp\left[\frac{-0.708\omega^{\frac{1}{2}} z\ Pr}{\nu^{\frac{1}{2}}}\right] dz$$

$$B = \exp\left[-0.708\ z\sqrt{\frac{\omega}{\nu}}\ Pr\right]_\delta^\infty \left(\frac{1}{-0.708\sqrt{\frac{\omega}{\nu}}\ Pr}\right)$$

$$= \left\{0 - \exp\left[-0.708\ \delta\sqrt{\frac{\omega}{\nu}}\ Pr\right]\right\}\left(-\sqrt{\frac{\nu}{\omega}}\ \frac{1}{0.708\ Pr}\right)$$

$$= \sqrt{\frac{\nu}{\omega}}\ \frac{1}{0.708\ Pr \exp\ (0.708\xi_\delta\ Pr)} \qquad \text{(A1.16)}$$

Putting the expression for A and B back into equation (A1.12) we obtain

$$Nu = \frac{R\sqrt{\frac{\omega}{\nu}}}{\left[\xi_\delta \int_o^1 \exp\left[2\ Pr\ \xi_\delta{}^2(-\ 0.171X^3 + 0.0415X^4 + 0.1026X^5 - 0.0517X^6)\right]dX + \frac{1}{0.708\ Pr \exp\ (0.708\ \xi_\delta\ Pr)}\right]}$$

..... (A1.17)

The expression (A1.17) was evaluated for Pr = 0.74 and 2.4 on an Elliot 903 computer, with the computer programme shown in figure 1 in this appendix.

Pr = 0.74 (Wagner)
Data $\xi_\delta = 2.58.$

$$Nu = 0.388\ R\sqrt{\frac{\omega}{\nu}} = 0.388\ Re^{\frac{1}{2}}$$

Pr = 2.4 (Kreith, Taylor & Chong)
Data $\xi_\delta = 2.58.$

$$Nu = 0.665\ Re^{\frac{1}{2}}$$

APPENDIX 1 FIGURE 1

Computer Programme to calculate Equation (A1.17)

Integration evaluated by Simpsons procedure

```
CVAE09;


"BEGIN" "REAL" EO,PR,X,AA,BB,Z;
"REAL" "PROCEDURE" F;
F:=(EXP(2*PR*EO↑2*(-.171*X↑3+.0417*X↑4+.1039*X↑5-.0517*X↑6)));
"REAL""PROCEDURE" SIMPS(X,A,B,DELTA,V);
"VALUE" A,B,DELTA,V;
"REAL" X,A,B,DELTA,V;
"BEGIN"  "INTEGER" N,K;
"REAL" H,J,I;
"SWITCH" S:=J1;
V:=(B-A)*V;
N:=1;
H:=(B-A)/2;
X:=A;
J:=F;
X:=B;
J:=(J+F)*H;
J1:
B:=0;
"FOR" K:=1 "STEP" 1 "UNTIL" N "DO"
"BEGIN" X:=(2*K-1)*H+A;
B:=B+F;
"END";
I:=4*H*B+J;
"IF" (ABS(V)*DELTA) < ABS(I-V) "THEN"
"BEGIN" V:=I;
J:=(I+J)/4;
N:=2*N;
H:=H/2;
"GOTO" J1;
"END";
SIMPS:=I/3;
"END" SIMPS;
"READ" EO,PR;
AA:=EO*SIMPS(X,0,1,.001,3);
BB:=1/(.708*PR*EXP(.708*EO*PR));
Z:=1/(AA+BB);
"PRINT" ALIGNED(1,4),EO,PR,AA,BB,Z;
"END";
```

APPENDIX 2

INTEGRAL METHOD OF EVALUATION OF LAMINAR HEAT TRANSFER FROM A ROTATING DISC IN STILL AIR, USING THE VELOCITY PROFILES DERIVED BY COCHRAN {4}

This analysis was made prior to the discovery that Young had made the same approach to the problem, but he did not evaluate the heat transfer for all values of the Prandtl number, which has been done here.

Wagner {13} used the velocity profiles of Karman {3} in his theoretical analysis (shown in appendix 1) of the heat transfer coefficient. Cochran {4} then rectified the work of Karman and therefore it would be reasonable to expect a more accurate result if Cochran's profiles were used in the analysis of appendix 1. In addition, the heat transfer is calculated at all values of the Prandtl number to compare with the theoretical data of Sparrow & Gregg {17} and others.

From appendix 1, we have equation (A1.09).

$$Nu = \frac{R}{\int_0^{\infty} \left(\exp \frac{1}{\alpha} \int_0^z u_z dz\right) dz}$$

Cochran gives the velocity profile

$$F = a_1 \left(1 - \frac{\xi}{\xi_\delta}\right)^2 \left(\xi + \frac{2}{\xi_\delta}\right) - \frac{\xi^2}{2} \left(1 - \frac{\xi}{\xi_\delta}\right)^2 \qquad \text{(A2.01)}$$

where $a_1 = a\xi_\delta = 0.19466\xi_\delta$ and $\xi_\delta = 2.79$ (A2.02)

$$\therefore \quad H = \int_0^{\xi} -2 \left[a\xi_\delta \left(1 - \frac{\xi}{\xi_\delta}\right)^2 \left(\xi + \frac{2}{\xi_\delta}\right) - \frac{\xi^2}{2} \left(1 - \frac{\xi}{\xi_\delta}\right)^2 \right] d\xi$$

$$= -\left[a\xi_\delta \xi^2 - \frac{\xi^3}{3} + \frac{1}{2} \frac{\xi^4}{\xi_\delta} (1 - 3a) + \frac{2}{5} \frac{\xi^5}{\xi_\delta^2} \left(2a - \frac{1}{2}\right) \right]$$

As $H = \frac{u_z}{\sqrt{\nu\omega}}$ we have

for $z \leq \delta$ $\quad u_z = -\sqrt{\nu\omega}\left[a\xi_\delta\xi^2 - \frac{\xi^3}{3} + \frac{1}{2}\frac{\xi^4}{\xi_\delta}(1-3a) + \frac{2}{5}\frac{\xi^5}{\xi_\delta^2}\left(2a-\frac{1}{2}\right)\right]$

.....(A2.03)

for $z > \delta$ $\quad u_z = -0.55\sqrt{\nu\omega}$ (A2.04)

As before, equation (A1.09) gives

$$Nu = \frac{R}{\int_o^\delta (\exp \frac{1}{\alpha}\int_o^z u_z dz)dz + \int_\delta^\infty (\exp \frac{1}{\alpha}\int_o^z u_z dz)\, dz}$$

Let $A = \int_o^\delta (\exp \frac{1}{\alpha}\int_o^z u_z dz)\, dz$ (A2.05)

and $B = \int_\delta^\infty (\exp \frac{1}{\alpha}\int_o^z u_z dz)\, dz$ (A2.06)

To determine A

$$\frac{1}{\alpha}\int_o^z u_z dz = \frac{1}{\alpha}\int_o^z -\sqrt{\nu\omega}\left[a\,\xi_\delta\xi^2 - \frac{\xi^3}{3} + \frac{1}{2}\frac{\xi^4}{\xi_\delta}(1-3a) + \frac{2}{5}\frac{\xi^5}{\xi_\delta^2}\left(2a-\frac{1}{2}\right)\right] dz$$

$$= -\,Pr\int_0^\xi \left[a\xi_\delta\xi^2 - \frac{\xi^3}{3} + \frac{1}{2}\frac{\xi^4}{\xi_\delta}(1-3a) + \frac{2}{5}\frac{\xi^5}{\xi_\delta^2}\left(2a-\frac{1}{2}\right)\right] d\xi$$

$$= -\,Pr\left[\frac{a}{3}\xi_\delta\xi^3 - \frac{\xi^4}{12} + \frac{\xi^5}{10\xi_\delta}(1-3a) + \frac{\xi^6}{15\xi_\delta^2}\left(2a-\frac{1}{2}\right)\right]$$

Now $\frac{\xi}{\xi_\delta} = \frac{z}{\delta}$ giving

$$\frac{1}{\alpha}\int_o^z u_z dz = -Pr\,\xi_\delta{}^4\left[\frac{a}{3}\left(\frac{z}{\delta}\right)^3 - \frac{1}{12}\left(\frac{z}{\delta}\right)^4 + \frac{1}{10}\left(\frac{z}{\delta}\right)^5(1-3a) + \frac{1}{15}\left(\frac{z}{\delta}\right)^6\left(2a-\frac{1}{2}\right)\right]$$

Therefore

$$A = \int_0^{\delta} \exp \left\{ Pr\ \xi_\delta^4 \left[-\frac{a}{3}\left(\frac{z}{\delta}\right)^3 + \frac{1}{12}\left(\frac{z}{\delta}\right)^4 - \frac{1}{10}\left(\frac{z}{\delta}\right)^5 (1-3a) - \frac{1}{15}\left(\frac{z}{\delta}\right)^6 \left(2a - \frac{1}{2}\right) \right] \right\} dz$$

$$A = \int_0^{1} \exp \left\{ Pr\ \xi_\delta^4 \left[-\frac{a}{3}\left(\frac{z}{\delta}\right)^3 + \frac{1}{12}\left(\frac{z}{\delta}\right)^4 - \frac{1}{10}\left(\frac{z}{\delta}\right)^5 (1-3a) - \frac{1}{15}\left(\frac{z}{\delta}\right)^6 \left(2a - \frac{1}{2}\right) \right] \right\} \xi_\delta \sqrt{\frac{\nu}{\omega}}\, d\left(\frac{z}{\delta}\right)$$

Let $X = \frac{z}{\delta}$

$$A = \xi_\delta \sqrt{\frac{\nu}{\omega}} \int_0^{1} \exp \left\{ Pr\ \xi_\delta^4 \left[-\frac{a}{3}X^3 + \frac{1}{12}X^4 - \frac{X^5}{10}(1-3a) - \frac{X^6}{15}\left(2a - \frac{1}{2}\right) \right] \right\} dX \quad \ldots(A2.07)$$

To determine B

$$B = \int_\delta^{\infty} \exp\left(\frac{1}{\alpha} \int_0^{z} - 0.55 \sqrt{\nu\omega}\, dz \right) dz$$

$$= \int_\delta^{\infty} \exp\left(\frac{-0.55 \sqrt{\nu\omega}\ z}{\alpha} \right) dz$$

$$= \left[\exp\left(\frac{-0.55 \sqrt{\nu\omega}\ z}{\alpha} \right) \frac{\alpha}{-0.55 \sqrt{\nu\omega}} \right]_\delta^{\infty}$$

$$= \exp\left(\frac{-0.55 \sqrt{\nu\omega}\ \delta}{\alpha} \right) \frac{\alpha}{0.55 \sqrt{\nu\omega}}$$

where $\delta = 2.79 \sqrt{\frac{\nu}{\omega}}$

$$\therefore \quad B = \exp\left(-1.533 \frac{\nu}{\alpha}\right) \frac{\alpha}{0.55 \sqrt{\nu\omega}}$$

$$= \frac{\exp\left(-1.533\ Pr\right)}{0.55\ Pr} \sqrt{\frac{\nu}{\omega}} \qquad (A2.08)$$

A and B were calculated by Elliot 903 computer, using the programme shown in figure 1 of this appendix, for various values of Pr as follows.

For the equation $Nu = C\ Re^{\frac{1}{2}}$, the table gives the value of C.

Pr	A	B	C
0.1	2.701	15.595	0.0547
0.7	2.263	0.887	0.318
0.74	2.231	0.790	0.3312
1	2.096	0.392	0.402
10	0.863	0	1.159
100	0.363	0	2.755

APPENDIX 2 FIGURE 1

Computer Programme to calculate Equations (A2.07) & (A2.08)

Integration evaluated by Simpsons procedure

```
CVAL05;

"BEGIN" "REAL" EO,PR,A1,Y,X,A2,AA,BB;
"REAL""PROCEDURE" YY;
YY:=(EXP(EO↑3*PR*(-A2/3*X↑3+EO/12*X↑4-0.1*(EO-3*A2)*X↑5-1/15*
(2*A2-EO/2)*X↑6)));

"REAL" "PROCEDURE" SIMPS(X,A,B,DELTA,V);
"VALUE" A,B,DELTA,V;
"REAL" X,A,B,DELTA,V;
"BEGIN" "INTEGER" N,K;
"REAL" H,J,I;
"SWITCH" S:=J1;
V:=(B-A)*V;
N:=1;
H:=(B-A)/2;
X:=A;  J:=YY;  X:=B;  J:=(J+YY)*H;
J1:
B:=0;
"FOR" K:=1 "STEP" 1 "UNTIL" N "DO"
"BEGIN" X:=(2*K-1)*H+A;
B:=B+YY;
"END";
I:=4*H*B+J;
"IF" (ABS(V)*DELTA) < ABS(I-V) "THEN"
"BEGIN" V:=I;  J:=(I+J)/4;  N:=2*N;
H:=H/2;
"GOTO" J1;
"END";
SIMPS:=I/3;
"END" SIMPS;
"READ" EO,PR,A1;
A2:=A1*EO;
Y:=SIMPS(X,0,1,0.001,3);
AA:=Y*EO;
BB:=1/(EXP(.55*EO*PR)*.55*PR);
Y:=1/(AA+BB);
"PRINT" ALIGNED(2,4),EO,PR,AA,BB,Y;
"END";
```

APPENDIX 3

CALCULATION OF WHIRLING SPEED OF DISC AND SHAFT

Shaft

The shaft with the disc mounted on it has a hole down the centre to carry the thermocouple wires.

outside diameter $d_o = 3.18$ cm

inside diameter $d_i = 0.635$ cm

length between bearings $l = 34.3$ cm

mass per unit length $w = 60.1$ g/cm

moment of inertia $I_s = 5.04$ cm^4

modulus of elasticity $E_s = 20.6 \times 10^6$ N/cm^2

shaft whirling speed $w_s = \frac{\pi^2}{l^2} \sqrt{\frac{gEI}{w}}$

$= 3.5 \times 10^3 \ \frac{\text{rad}}{\text{s}}$

$= 33\,400$ r.p.m.

Disc

mass of disc $W = 13.05$ kg

whirling speed due to disc only

$$w_d = \sqrt{\frac{48 \ E \ I \ g}{W l^3}}$$

$= 969 \ \frac{\text{rad}}{\text{s}}$

$= 9250$ r.p.m.

Dunkerley's formula

$$\frac{1}{w^2} = \frac{1}{w_s{}^2} + \frac{1}{w_d{}^2}$$

giving $w = 8910$ r.p.m.

Disc out of balance

Obviously the disc and the shaft cannot be perfectly balanced, and an accuracy of balance of 36 g cm was achieved.

Neglect the shaft, as the previous calculations have shown its effect on the whirling speed to be small compared to that of the disc.

Out of balance puts effective centre of gravity at a distance e = 0.00276 cm from the axis of rotation, and the maximum allowable stress in the shaft is 100 N/mm^2.

This stress would be caused by a static force of

$$W_s = \frac{4 I \sigma}{\frac{d}{2} l} = 3700 \text{ N}$$

giving a deflection of

$$y = \frac{W_s}{\mu} \quad \text{where} \quad \mu = \frac{48 E I}{l^3} = 122\,500 \frac{N}{cm}$$

$$\therefore \quad y = 0.0302 \text{ cm.}$$

Now the corresponding rotational speed is given by

$$w^2 = \frac{\mu g}{W} \frac{y}{y \pm e}$$

$$= \frac{122\,500 \times 100}{13.05} \left[\frac{0.0302}{0.0302 \pm 0.00276} \right] \frac{rad^2}{s^2}$$

$$w_{min}^2 = 94 \times \frac{0.0302}{0.03296} = 862\,000 \quad \left(\frac{rad}{s}\right)^2$$

$$\therefore \quad w_{min} = 930 \frac{rad}{s} = 8870 \text{ rev / min}$$

So the out of balance effect is negligible, and the whirling speed is well above the maximum operating speed of 3000 r.p.m.

APPENDIX 4

MANUFACTURERS OF EQUIPMENT

Components of Rig

Bearings	S.K.F. self-aligning bearings with taper lock fitting.
Belt Drive	Fenner Spacesaver Drive Alpha Section.
Motor & Control Unit	Goodyear Transformers Ltd.
Slip Rings	Star Electro Carbons Ltd.
Heater Wire	Wiggin Brightray Alloy C.
Rheostats	Zenith Type TNE and TS slidewire.

Instrumentation

Temperature	Pye thermocouple test set. Cat.No. 7556.
Electrical Meters	Ernest Turner Ltd. and Weston Ltd.
Speed	Hasler Tachometer
Pressure (boundary layer)	I.R.D. Micromanometer type MDC., manufactured by Hilger & Watt Ltd., supplied by Furness Controls Ltd., lent by the University of Aston.
Line pressure gauge	Smith & Sons Ltd.

Auxiliary Equipment

Wind Tunnel	Plint & Partners Ltd., 18 in. blower tunnel, lent by the University of Aston.
Pressure valve and filter	Enots Ltd.
Paraffin Smoke Generator	Airscrew Co.Ltd. & Jicwood Ltd., lent by the University of Aston.

APPENDIX 5

POWER REQUIREMENT OF ELECTRIC HEATERS IN DISC

These were calculated with the convective heat transfer coefficients for a disc and a cylinder, found by previous workers.

Main disc heater

The convective heat transfer from an isolated rotating disc in the turbulent region of flow was found by Cobb & Saunders {32} as

$$Nu_o = 0.015\ Re_o^{0.8}$$

With the experimental disc of 0.4 m diameter and 3000 r.p.m. the maximum Reynolds number is 8×10^5.

$$\therefore \quad Nu_o = 794 = \frac{h_m R_o}{k}$$

$$\therefore \quad h_m = \frac{794 \times 0.00927}{0.202} \quad \frac{J}{m^2\ s\ {}^oK} \qquad \text{at } 77^oC$$

$$= 36.4 \quad \frac{J}{m^2\ s\ {}^oK}$$

Area of the main disc (two sides) $= 2\pi\ 0.2^2 \quad m^2$

$$= 0.256 \quad m^2$$

At the maximum speed a temperature difference of 50°K would be sufficient.

$$\therefore \quad \text{Power to heater} = 36.4 \times 0.256 \times 50 \quad \text{Watt}$$

$$= \underline{470 \quad \text{Watt}}$$

Guard rim heater

From sides $Nu_r = 0.0197\ Re_r^{0.8}$

for $R_r = \frac{20.2 + 22.6}{2} = 21.4$ cm

$Re_r = 9 \times 10^5$

$\therefore \quad Nu_r = 1140$

$\therefore \quad h = 52.2 \frac{J}{m^2\ s\ ^oC}$

area of two sides of guard ring

$= 2\pi(0.226^2 - 0.202^2)\ m^2$

$= 0.0641\ m^2$

For a temperature difference of 50°C.

Power loss $= 52.2 \times 0.0641 \times 50$ Watt

$= 168$ Watt

From rim

convective heat transfer from a cylinder according to Anderson & Saunders {38} (neglecting effects of thin cylinder)

$Nu = 0.10\ Re^{\frac{2}{3}}$ where $Nu = \frac{h_d}{k}$

and $Re = \frac{2\omega R^2}{\nu}$

at $Re = 2 \times 10^6$

$Nu = 1589$

$\therefore\ h = \frac{1589 \times 0.00927}{2 \times 0.226} = 32.6 \frac{J}{m^2\ s\ ^oK}$

area of rim $= 2\pi 0.226 \times 0.0285\ m^2$

$= 0.0405\ m^2$

$\therefore$ power loss from rim $= 32.6 \times 0.0405 \times 50$ Watt

$= 66$ Watt.

Total loss from guard heater = 168 + 66 = 234 Watt

Ratio of main to guard heaters $= \frac{470}{234} = 2 : 1$

Current through main heater $= \sqrt{\frac{470}{120}} = 1.98$ A

Current through guard heater $= \sqrt{\frac{234}{23}} = 3.19$ A

Lowest powers

At 30 r.p.m. , $Re_o = 8000$

and the laminar heat transfer, according to Richardson & Saunders {35} is

$$Nu_o = 0.4\ Re_o^{0.5} = 35.8 .$$

Ratio of maximum Nu_o to minimum = $\frac{35.8}{794} = 0.045$

$\therefore$ minimum power main = 21.1 Watt
minimum power guard = 10.5 Watt
} at 30 r.p.m. and 50°C.

$\therefore$ minimum current $_{main}$ = 0.419 A

minimum current $_{guard}$ = 0.675 A

With the equipment available the chosen maximum and minimum currents were

Main	2 A	to	0.39 A	continuously variable
Guard	4 A	to	0.46 A	continuously variable.

APPENDIX 6

THE NATURAL CONVECTION HEAT TRANSFER FROM A CIRCULAR FLAT PLATE

Ostrach {55} gives the natural convection heat transfer from a vertical flat plate, with a uniform wall temperature and laminar flow as

$$Nu_x = 0.388\ (Gr_x\ Pr)^{\frac{1}{4}} \qquad (A6.01)$$

For air of Prandtl number 0.714 we have

$$Nu_x = 0.36\ Gr_x^{\frac{1}{4}} \qquad (A6.02)$$

$$\text{i.e. } h_x = 0.36\ k\left(\frac{g\theta}{T_o\nu^2}\right)^{\frac{1}{4}} \frac{1}{x^{\frac{1}{4}}} \qquad (A6.03)$$

Assuming that the flow lines are exactly vertical gives the distance x as that from the point being considered to the leading edge below it. This was verified by flow visualization using titanium tetrachloride smoke induced into the airstream below the disc.

For any plate with temperature difference dθ and varying heat transfer coefficient we have

$$Q = h_m A \frac{d\theta}{dt} = h_1A_1 \frac{d\theta}{dt} + h_2A_2 \frac{d\theta}{dt} + h_3A_3 \frac{d\theta}{dt} + \ldots \qquad (A6.04)$$

$$\text{So } h_mA = h_1A_1 + h_2A_2 + h_3A_3 + \ldots \qquad (A6.05)$$

$$h_m = \frac{1}{A}\sum_{n=1}^{n=\infty} h_nA_n \qquad (A6.06)$$

Evaluated numerically for the experimental disc, allowing for the guard heater rim

$$\frac{1}{A}\sum_{x=o}^{x=2R_o} \frac{A}{x^{0.25}} = 0.4982\ \frac{1}{cm^{\frac{1}{4}}} \qquad (A6.07)$$

Now, using equation 03,

$$\frac{h_m R_o}{k} = \frac{R_o}{k} \sum h_x = R_o \; 0.36 \left(\frac{g\theta}{T_o \nu^2}\right)^{\frac{1}{4}} \sum \frac{1}{x^{\frac{1}{4}}} \qquad \text{(A6.08)}$$

Putting 07 into 08

$$\frac{h_m R_o}{k} = 0.36 \quad Ro \left(\frac{g\,\theta}{T_o \nu^2}\right)^{\frac{1}{4}} \quad 0.4982 \quad \frac{1}{cm^{\frac{1}{4}}} \qquad \text{(A6.09)}$$

For the experimental disc R_o = 20.16 cm.

giving $Nu_o = 0.36 \times 0.4982 \times 2.12 \, (Gr_o)^{\frac{1}{4}}$ (A6.10)

i.e. $\underline{Nu_o = 0.38 \, (Gr_o)^{\frac{1}{4}}}$

APPENDIX 7

SURVEY OF THE AIRFLOW IN THE ENTRANCE TO THE TEST SECTION OF THE WIND TUNNEL

The mean stream velocity in the entrance to the test section was found by following British Standard 848, Part I, 1963. This instructs that velocities be taken at the points shown in figure 1 of this appendix. This was done with a British Standard combined total and static Pitot tube, and readings were taken on an inclined manometer. The results are shown in figure 2, together with the average velocities and the mean tunnel velocity.

The velocities varied by + 5 % , - 10 % from the mean tunnel velocity, whilst the centre point velocity differed by only + 1.6 % from the mean tunnel velocity.

APPENDIX 7 FIGURE 1

Pitot Positions for Wind Tunnel Flow Measurement

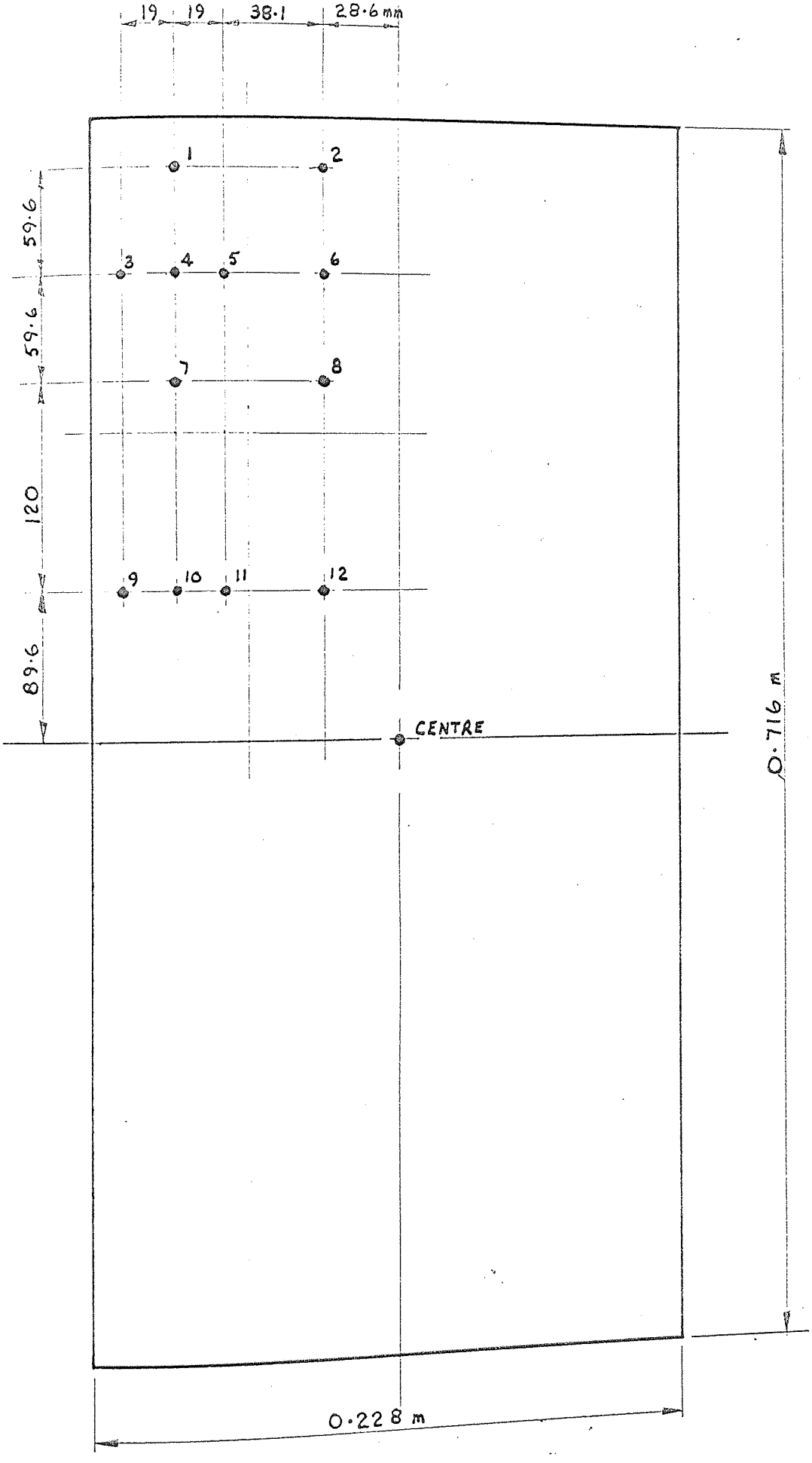

APPENDIX 7 FIGURE 2

Exploration of Airflow at Entrance to Wind Tunnel

Velocity Measurements metre/sec.

	1 32·5		2 28·0	29·3		30·95	
3 31·45	4 32·75	5 32·75	6 32·0	30·95	31·75	32·4	31·9
	7 32·4		8 32·5	32·4		32·5	
9 31·75	10 32·0	11 32·0	12 32·0	31·9	32·0	32·0	28·3
			31·8				
28·5	32·0	32·0	31·9	31·9	31·9	31·9	26·6
	32·4		32·4	32·4		32·4	
31·2	32·5	32·5	31·6	32·0	32·75	32·75	29·6
	30·7		28·6	28·1		32·4	

Average Velocities Calculated to BS 848

32·12	30·83	30·88	31·58
31·92	32·0	31·9	30·77
30·83	31·9	31·9	29·47
31·45	30·87	30·83	31·48

Mean tunnel velocity = 31·3 m/s.

Difference between mean and centre readings = 1·6 %

BIBLIOGRAPHY

ROTATING DISC

1. Dorfman, L.A., 1963. "Hydrodynamic Resistance and the Heat Loss of Rotating Solids". (Oliver & Boyd, London).

2. Kreith, F. "Convection Heat Transfer in Rotating Systems", Advances in Heat Transfer, 1968, 5 (Academic Press).

Fluid Mechanics - Theoretical Investigations

3. Karman, T. von. "Uber Laminare und Turbulente Reibung" (in German) Z. angew Math. Mech., 1921, 1 244-252.

4. Cochran, W.G. "The Flow due to a Rotating Disc" Proc. Camb. Phil. Soc., 1934, 30 365.

5. Goldstein, S. "On the Resistance to the Rotation of a Disc Immersed in a Fluid" Proc. Camb. Phil. Soc., 1935, 31 232-241.

6. Hannah, D.M. "Forced Flow Against a Rotating Disc" British Aero. Res. Comm. Rep. & Memo. No. 2772, 1947.

7. Bachelor, G.K. "Notes on a Class of Solutions of the Navier Stokes Equations Representing Steady Rotationally-Symetric Flow". Q. J. Mech. Appl. Math., March 1951, 4 (1) 29-41.

8. Schlichting, H. and Truckenbrodt, E. "The Flow Around a Rotating Disc in a Uniform Stream". Readers Forum, J. Aero. Sci., 1951, 18 639.

9. Tifford, A.N. and Chu, S.T. "On the Flow Around a Rotating Disc in a Uniform Stream". J. Aero. Sci., 1952, 19 284-285.

Fluid Mechanics-Experimental Investigations

10. Theodorsen, T. and Regier, A. "Experiments on Drag of Revolving Discs, Cylinders and Streamline Rods at High Speeds". N.A.C.A. Tech. Rep. No. 793, 1944.

11. Gregory, N., Stuart, J.T. and Walker, W.S. "On the Stability of Three Dimensional Boundary Layers with Application to Flow due to a Rotating Disc". Phil. Trans. 1956, 248 155

12. Hanold, R.J. and Moszynski, J.R. "Secondary Flows Associated with Slowly Oscillating and Rotating Discs". J. Heat Transfer, 1967, 89 (2), 177-184.

Heat Transfer - Theoretical Investigations

13. Wagner, C. "Heat Transfer from a Rotating Disc to Ambient Air". J. Appl. Phys., 1948, 19 837-841.

14. Tifford, A.N. Note on "Heat Transfer by Laminar Flow from a Rotating Plate". J. Aero. Sci., 1951, 18 567.

15. Millsaps, K. and Pohlhausen, K. "Heat Transfer by Laminar Flow from a Rotating Plate". J. Aero. Sci., 1952,19 120-126

16. Davies, D.R. "On the Calculation of Eddy Viscosity and Heat Transfer in a Turbulent Boundary Layer near a Rapidly Rotating Disc". Q. J. Mech. Appl. Math., May 1959, 12 (2) 211-221.

17. Sparrow, E.M. & Gregg, J.L. "Heat Transfer from a Rotating Disc to Fluids of any Prandtl Number". J. Heat Transfer, Aug. 1959, 249-251.

18. Sparrow, E.M. and Gregg, J.L. "Mass Transfer, Flow and Heat Transfer about a Rotating Disc". Trans. A.S.M.E. Series C., Nov. 1960, 294-302.

19. Yamaga, J. "On the Heat Transfer from Rotating Disc Normal to Uniform Flow". Proc. 10th Japan Nat. Congr. Appl. Mech., 1960, 279-282.

20. Cess, R.D. & Sparrow, E.M. "Unsteady Heat Transfer from a Rotating Disc and at a Stagnation Point". U.S.A. Part II International Developments in Heat Transfer A.S.M.E. Int. Heat Transfer Conf., 1961.

21. Kreith, F., Doughman, E. and Kozlowski, H. "Mass and Heat Transfer from an Enclosed Rotating Disc with and without Source Flow". J. Heat Transfer., May 1963, 153-163.

22. Kapinos, V.M. "Heat Exchange of the Flow in the Clearance Between Two Rotating Discs" (reference only). A.E.I. Tech. News Bull. 2 October 1964, (1980) abstra. 69437.

23. Tien, C.L. and Tsuji, J. "Heat Transfer by Laminar Forced Flow Against a Non-Isothermal Rotating Disc". Int. J. Heat & Mass Transfer, Feb 1964, 7 (2) 247-252.

24. Riley, N. "The Heat Transfer from a Rotating Disc". Q.J. Mech. Appl. Math., August 1964, 17 (3), 331-349.

25. Kapinos, V.M. "Heat Exchange of the Flow in the Clearance Between Two Rotating Discs". (in Russian). Izv. Akad. Nauk. S.S.S.R., Otd. Tekh. Nauk. Energi. i. Transp., July-Aug. 1964, 511-521.

26. Kreith, F. and Viviand, H. "Heat Transfer in Laminar Source Flow Between a Stationary and a Rotating Disc". 3rd Int. Heat Transfer Conf. Aug.7-12, 1966, Mon. Aug. 8. Papers 1-40, Vol.I. 293-298.

27. Dorfman, L.A. "Heat Transfer During Flow of Viscous Fluid Between a Stationary Screen and Rotating Disc Subjected to Blowing". Teplofiz. vys. temp., 1966, 4 (5) 683-688 (summary only).

28. Sharma, S.K. and Agarwal, R.S. "Heat Transfer from an Enclosed Rotating Disc". Appl. Sci. Res. A., 1966, 16 (3) 204-214.

29. Mabuchi, I., Tanaka, T. and Sakakibara, Y. "The Convective Heat Transfer from a Rotating Disc I. The Effect of Dissipative Energy on the Laminar Heat Transfer from a Disc Rotating in Uniform Forced Stream". Bull. J.S.M.E., 1967, 10 (37) 104-112.

30. Yoh, J.C.Y. and Price, J.F. "Non-Similar Boundary Layer Heat Transfer of a Rotating Cone in Forced Flow". J. Heat Transfer, May 1967, 139-145.

Heat Transfer - Experimental Investigations

31. Young, R.L. "Heat Transfer from a Rotating Plate". A.S.M.E., 1954, 54-5A-51, 1163-1168.

32. Cobb, E.C. and Saunders, O.A. "Heat Transfer from a Rotating Disc". Proc. R. Soc., A, 1956, 236 343-351.

33. Richardson, P.D. "Some Studies of the Flow and Heat Transfer Associated with a Rotating Disc". Ph.D. Thesis, University of London, 1958.

34. Kreith, F., Taylor, J.H. and Chong, J.P. "Heat and Mass Transfer from a Rotating Disc". Trans. A.S.M.E., Sec. C. Vol. 00, May 1959, 95-105.

35. Richardson, P.D. and Saunders, O.A. "Studies of Flow and Heat Transfer Associated with a Rotating Disc". J. Mech. Engng. Sci. 1963, 5 (4) 336-342.

36. Lee, M.H. "Effect of Boundary Layer Control on Heat Transfer from a Rotating Disc". Ph.D. Thesis, University of London, 1966.

37. Iguchi, A. and Maki, T. "Heat and Mass Transfer from a Rotating Disc in an Open Environment". Mem. Fac. Engng. Nagoya University, 1967, 19 (1) 144

OTHER ROTATING BODIES

38. Anderson, J.T. and Saunders, O.A. "Convection from an Isolated Heated Horizontal Cylinder Rotating About its Axis". Proc. R. Soc. 1953, (A217), 555.

39. Kays, W.M. and Bjorklund, I.S. "Heat Transfer from a Rotating Cylinder with and without Crossflow". A.S.M.E., Jan. 1958, Paper No. 56-A-71.

40. Nordlie, R.L. and Kreith, F. "Convection Heat Transfer from a Rotating Sphere". International Developments in Heat Transfer". 1961, Int. Heat Transfer. Conf. Part II.

41. Löblich, K.R. "The Significance to Heat and Mass Transfer of Re-circulation Zones Behind Bodies in a Field of Flow". Chemie-Ing-Technik 39, 1967, No. 7.

FLAT PLATE PARALLEL TO STREAM

Forced Convection

42. Lighthill, M.J. "Contributions to the Theory of Heat Transfer Through a Laminar Boundary Layer". Proc. R. Soc. A.202, 1950, 359.

43. Tribus, M. and Klein, J. "Forced Convection from Non-Isothermal Surfaces". Heat Transfer Symposium, University of Michigan, 1953, 211.

44. Furber, B.N. "Some Heat and Mass Transfer Experiments on Humid Air in Turbulent Flow Over a Plane Containing an Isolated Cooled Region". Proc. Instn. Mech. Engrs., 1954, 168, 847.

45. Davies, D.R. and Bourne, D.E. "On the Calculation of Heat and Mass Transfer in Laminar and Turbulent Boundary Layers". Q.J. Mech. Appl. Math., Dec. 1956, Vol IX, Part 4, 457-488.

46. Edwards, A. and Furber, B.N. "The Influence of Free-Stream Turbulence on Heat Transfer by Convection from an Isolated Region of a Plane Surface in Parallel Air Flow". Proc. Instn. Mech. Engrs., 1956, 170 (28).

47. Persh, J. and Sherwood, A.W. "An Experimental Investigation of the Boundary Layer Flow on a Flat Plate". J. Aero. Sci., July 1956, 23 703.

48, Ede, A.J. and Saunders, O.A. "Heat Transfer from a Flat Surface to a Parallel Stream of Water". Proc. Instn. Mech. Engrs, 1958, 172 (23) 743.

49. Bourne, D.E. "A Note on the Approximate Calculation of the Temperature Distribution in an Incompressible Laminar Boundary Layer over a Heated Plane Surface". Q.J. Mech. Appl. Math., Aug. 1959, Vol XII, Part 3, 337-339.

50. Granville, R.A. and Boxall, G. "Measurement of Convective Heat Transfer by Means of the Reynolds Analogy". Brit.J.Appl. Phys., Oct. 1960, 11 (10), 471-475.

51. Hanna, O.T. and Myers, J.E. "An Analogy Between Heat and Momentum Transfer for the Turbulent Boundary Layer on a Flat Plate". J.A.I.Ch.E., 1961, 7, 532-533.

52. Tendeland, T., Nielson, H.L. and Fohrman, M.J. "The Flow Field Over Blunted Flat Plates and its Effects on Turbulent Boundary Layer Growth and Heat Transfer at a Mach Number of 4.7". N.A.S.A., T.N. D-689, Washington, Feb. 1961.

Natural Convection

53. Ede, A.J. "Advances in Free Convection". Advances in Heat Transfer, 1967, 4 (Academic Press).

54. Ostrach, S. "An Analysis of Laminar Free-Convection Flow and Heat Transfer About a Flat Plate Parallel to the Direction of the Generating Body Force". 1952, N.A.C.A. TN 2635; 1953, N.A.C.A. Rept. 1111.

55. Griffiths, E. and Davis, A.H. "The Transmission of Heat by Radiation and Convection". D.S.I.R. Food Invest. Board Spec. Rept. 9, 1922, 1931.

56. Colburn, A.P. and Hougen, O.A. "Studies in Heat Transmission: 1. Measurement of Fluid and Surface Temperatures". 1930, Ind. & Eng. Chem. 5 (22) 522.

57. Eckert, E.R.G. and Jackson, T. "Analysis of Turbulent Free Convection Boundary Layer on Flat Plates". 1950, N.A.C.A. TN 2207.

58. Hara, T. "Heat Transfer by Laminar Free Convection About a Vertical Flat Plate with Large Temperature Difference". J.S.M.E., 1958, 1 (3) 251-254.

59. Hara, T. "Free Convection Flow About a Heated Vertical Plate in Air". Trans. J.S.M.E., 1954, 20 (96), 517.

SEPARATED FLOWS

60. Chilcott, R.E. "A Review of Separated and Reattaching Flows with Heat Transfer". Int. J. Heat and Mass Transfer, June 1967, 10 783-797.

61. Richardson, P.D. "Heat and Mass Transfer in Turbulent Separated Flows". Chem.Eng.Sci. 1963, 18 149-155.

EQUIPMENT

62. Moffat, R.J. "Designing Thermocouples for Response Rate". Trans. A.S.M.E. Feb. 1958, 257-262.

63. Watson, C.G. "A Survey of Techniques for Measuring Surface Temperature". N.E.L. Rept. No. 153, June 1964.

64. Drew, D. "Sliprings - a Review". Strain - J. British Soc. Strain Measurement. Oct. 1966 2 (4). 35-41.

65. Baker. "Temperature Measurement in Engineering" Vol. 1. (Chapman & Hall).

DISC BRAKES

66. Newcomb, T.P. "Cooling Rates of Brake Drums and Discs". Proc. Instn. Mech. Engrs. 1965-66, 180, Part 2A.

67. Newcomb, T.P. "Temperatures Reached in Disc Brakes". J. Mech Engng. Sci. 1960, 2 (3), 167-177.

68. Evans, D.J. and Newcomb, T.P. "Temperatures Reached in Braking when the Thermal Properties of Drum or Disc Vary with Temperature". J. Mech. Engng. Sci. 1961, 3 (4), 315-317.

69. Newcomb, T.P. "Transient Temperatures Attained in Disc Brakes". British J. Appl. Phys., July 1959, 10, 339-340.

GENERAL TEXTS

70. Kaye, G.W.C. and Laby, T.H. "Tables of Physical and Chemical Constants". 1966, (Longmans, Green & Co.).

71 Eckert, E.R.G. and Gross, J.F. "Introduction to Heat and Mass Transfer". 1963 (McGraw-Hill, New York).

72. Kreith, F. "Principles of Heat Transfer". 2nd Ed., 1965 (International Text Book Co.).

73. Fishenden, M. and Saunders, O.A. "An Introduction to Heat Transfer". 1950 (Clarendon Press).

74. Schlichting, H. "Boundary Layer Theory". 1968 (McGraw-Hill).